Influence of Fluid Pressure and Effective Stress on Quartz Cementation in Clastic Reservoirs

OLAKUNLE JOSEPH OYE

Influence of Fluid Pressure and Effective Stress on Quartz Cementation in Clastic Reservoirs

Olakunle Joseph Oye

This thesis is submitted in partial fulfilment of the requirements for the degree of Doctor of Philosophy at Durham University

Department of Earth Sciences

Durham University

2019

Declaration

I hereby certify that the work described in this thesis is my own, except where otherwise acknowledged, and that it has not been submitted previously for a degree at this or any other university.

February 2019

Olakunle Joseph Oye

Acknowledgement

My greatest thanks go to the Almighty God, the Creator of the universe, and the Possessor of the heavens and the earth for sparing my life and providing all resources required for making this feat a reality.

I would also like to express my sincere gratitude to my excellent supervisory team: Andrew Aplin, Stuart Jones, and Jon Gluyas for their continuous support throughout my PhD programme. Andy was very supportive throughout this study. His guidance helped me in all the time of research and writing of this thesis. His invaluable advice helped improve me as a researcher and scientist. I could not have imagined having a better supervisor and mentor for my PhD study. Andy, thank you very much and God bless you.

I would like to thank my wonderful wife Bukola and my precious daughter Ayanfeoluwa for their love, patience and understanding throughout the entire span of the programme. I love you guys. My sincere gratitude also goes to my father Joshua Olanipekun Oye (God rest his soul) for pointing me in the right direction very early in life. I would also like to thank my mother Mrs Dorcas Oye for supporting morally and prayerfully, and to my siblings Funmilola, Oyindamola, and Olatunde for their advice and prayers. God bless you all.

Special appreciation goes to the Government of the Federal Republic of Nigeria and Petroleum Development Technology Fund (PTDF) Nigeria for providing the funds for this research project.

My appreciation also goes to Ian Chaplin for the preparation of numerous rock and thin sections, and Leon Bowen for his excellent support and time at the scanning electron microscope. My appreciation also goes to the team at the University of Wisconsin-Madison SIMS (WiscSIMS) laboratory, especially Ian Orland and John Valley. You guys made my time at the WiscSIMS laboratory worthwhile.

I would also like to thank everyone in the Department of Earth Sciences at Durham University that has contributed in any form to making this PhD programme a success; from the students to the administrative and finance offices. Thank you all!

Abstract

It is well established that the development of shallow overpressure within sedimentary basins reduces vertical effective stress (VES) and inhibits mechanical compaction, thus preserving porosity. However, the influence of vertical effective stress on chemical compaction/pressure dissolution and related quartz cementation in sandstones has been under-appreciated in many clastic reservoir studies that have favoured temperature as the key control on quartz cementation. These models suppose that quartz cementation is controlled by temperature-related precipitation kinetics and that the supply of silica is largely irrelevant. However, it is commonly considered that the main source of silica for quartz cement is from intergranular pressure solution, the rate of which is influenced by VES. This study integrates quantitative petrographic data, high spatial resolution oxygen isotope analyses of quartz cement, basin modelling, and a kinetic model for quartz cementation to understand the relevance of VES to quartz cementation by investigating clay-poor sandstones of the Upper Jurassic Fulmar Formation from Clyde, Elgin and Fulmar fields in the UK Central Graben and Paleocene-Eocene Wilcox Group from Lake Creek and Rotherwood fields in the Texas Gulf Coast. These sandstones have distinctly different histories of vertical effective stress (VES) and temperature. The study not only shows that most or all the silica for quartz cement can be derived from intergranular pressure dissolution, but that the extent of intergranular pressure dissolution and related quartz cementation correlated strongly with VES and poorly with temperature. Oxygen isotope data obtained from the quartz cements yield temperature ranges for quartz precipitation which are taken to indicate that the rate of quartz cementation is more strongly related to the history of VES rather than the history of temperature. This analysis suggests that it is the vertical effective stress history, rather than the temperature history, that exerts the greatest influence on quartz cementation. This work has significant implications for understanding how overpressure and VES influence porosity preservation in high pressure, high temperature (HPHT) reservoirs, and would also aid the development of better reservoir quality predictive models for prospective HPHT reservoirs.

Table of Contents

Glossary

BSE – Backscattered Electron

CL – Cathodoluminescence

CNS – Central North Sea

EDS – Energy Dispersive X-ray Spectroscopy

GOM – Gulf of Mexico

IPD – Intergranular Pressure Dissolution

SEM - Scanning Electron Microscope

SIMS – Secondary Ion Mass Spectrometry

UWQ – University of Wisconsin Quartz Standard

VES – Vertical Effective Stress

1. General Introduction

1.1 Background

In recent times, the oil and gas industry has been exploring for deeper hydrocarbon targets. Such environments are characterised by High Pressure and High Temperature (HPHT), and pose a great concern to operating companies in terms of delineating quality reservoir formation with economically viable hydrocarbon accumulation. More importantly, the accurate prediction of highly porous and permeable reservoir ahead of the drill-bit is central to the success of any exploration programme (Primmer et al., 1997; Bloch et al., 2002; Taylor et al., 2010; Worden et al., 2018a). During field development, the prediction of field-wide reservoir quality is very important for appraisal, development and subsequent hydrocarbon production, given the heterogeneous nature of porosity and permeability that exist within petroleum reservoirs (Primmer et al., 1997; Worden et al., 1998; Storvoll et al., 2002; Gier et al., 2008; Morad et al., 2010; Taylor et al., 2010; Tobin et al., 2010; Stricker et al., 2016b; Worden et al., 2018a; Worden et al., 2018b).

The successful prediction of reservoir quality in clastic sandstone reservoirs requires understanding of geological processes that control the evolution of porosity and permeability in such lithologies. The identified principal controls include: depositional processes (provenance, transport and depositional environment) which determine primary sedimentary texture, composition, porosity and permeability (Stewart, 1986; Ajdukiewicz and Lander, 2010; Morad et al., 2010; Bjørlykke, 2014), early diagenesis which occurs at shallow depth(< 2000m) where sediment is in contact with seawater and/or ground water (Gier et al., 2008; Ajdukiewicz and Lander, 2010; Bjørlykke, 2014), and deep diagenesis during which diagenetic pathways are influenced by the combination of depositional and early diagenetic processes (Ajdukiewicz and Lander, 2010; Morad et al., 2010).

In general, compaction, dissolution and precipitation are processes common to both early and late diagenesis (Gier et al., 2008; Ajdukiewicz and Lander, 2010). While the first phase of compaction (mechanical compaction) is the main reservoir quality-reducing process in sandstone during early diagenesis as porosity and permeability reduce due to grain rearrangement (Houseknecht, 1987; Houseknecht, 1989; Ehrenberg, 1990; Lundegard, 1992; Osborne and Swarbrick, 1997b; Paxton et al., 2002), chemical compaction dominates the late phase by introducing diagenetic cement from grain mineral dissolution and precipitation into the system as burial progresses (Osborne and

Swarbrick, 1997b; Morad et al., 2010; Bjørlykke, 2014). Nonetheless, the creation of secondary porosity from dissolved mineral grains (e.g. feldspars) and calcite cement, even though minor, can have positive diagenetic effect on reservoir quality in deeply buried sandstone (Wilkinson et al., 1997; Lasocki et al., 1999; Osborne and Swarbrick, 1999; Dutton and Loucks, 2010; Oye et al., 2018).

Pore fluid pressure, and thus related vertical effective stress (VES), has been appraised as a possible mechanism for reservoir quality preservation in sandstones in many studies (Ehrenberg, 1990; Walderhaug, 1994a; Walderhaug, 1994b; Osborne and Swarbrick, 1997a; Osborne and Swarbrick, 1997b; Bjørkum et al., 1998; Osborne and Swarbrick, 1999; Bloch et al., 2002; Taylor et al., 2010; Bjørlykke, 2014). High pore fluid pressure (overpressure) is a subsurface phenomenon whereby pore fluid pressure exceeds the hydrostatic gradient in sedimentary rocks, and the direct consequence of this process is that the fluid acts to reduce the pressure exerted by the overburden, the effective stress, on rock grains (Osborne and Swarbrick, 1997b; Bloch et al., 2002). There is a consensus that shallow overpressure development can reduce the effect of mechanical compaction on sand grains (e.g. Osborne and Swarbrick, 1999; Stricker et al., 2016b). At greater depth, chemical compaction becomes active and reduces porosity independent of effective stress (Walderhaug, 1994a; Walderhaug, 1994b; Bjørlykke, 2014). Porosity is lost during mechanical compaction through stress-induced, sand grain rearrangement, and chemical compaction through chemically-induced cementation (Paxton et al., 2002; Ehrenberg et al., 2008). While previous studies (Ehrenberg, 1990; Osborne and Swarbrick, 1997b; Osborne and Swarbrick, 1999) have suggested that the occurrence of low VES due to early shallow development of overpressure could impede chemical compaction and related quartz cementation and preserve porosity, others (Bjørkum et al., 1998; Bloch et al., 2002; Bjørlykke, 2014) have argued that the effect of overpressure on chemical compaction is almost negligible since quartz cementation will proceed, with or without high pore fluid pressure, as temperature increases with burial.

Understanding the relevance of pore fluid pressure and vertical effective stress to quartz cementation during sandstone diagenesis, and the accurate assessment and quantification of the diagenetic effects on sandstone reservoir is imperative for better reservoir quality prediction and effective de-risking of hydrocarbon prospects during exploration and production programmes (Worden et al., 2018a).

1.2 Quartz Cementation in Sandstone

Quartz cement is a major porosity and permeability "degrader" and the most volumetrically important of the major diagenetic cement (i.e. silica and carbonate) in deeply buried sandstone reservoirs (McBride, 1989; Ehrenberg, 1990; Bjorlykke and Egeberg, 1993; Walderhaug, 1996; Worden et al., 1998; Gier et al., 2008; Worden et al., 2018b). Quartz cementation in sandstones is controlled by the following three geochemical processes; rate of supply of silica from the source, transportation of aqueous silica, and precipitation of silica from aqueous solution (Oelkers et al., 1996; Bjørkum et al., 1998; Worden and Morad, 2000; Bloch et al., 2002; Taylor et al., 2010; Bjørlykke, 2014).

1.2.1 Potential Controls on Quartz Cementation in Sandstone

The schematic illustration for the various controls on quartz cementation in sandstones is represented in Figure 1.1. Worden and Morad (2000) categorized the sources of silica for quartz cementation into those sourced locally within sandstone of interest and those derived from external sources (i.e. adjacent shale or sand bodies) outside the sandstone reservoir of interest. Different opinions exist regarding the internal sources of silica for quartz cementation (McBride, 1989). Even though recent development (Ehrenberg, 1990; Walderhaug, 1994a; Walderhaug, 1994b; Bjorkum, 1996; Walderhaug, 1996; Sheldon et al., 2003; Harwood et al., 2013) favour silica sourced locally by dissolution along stylolites and grain contacts, the mechanism that controls the formation of this pore occluding cement is still contentious. While some studies (Weyl, 1959; Rutter and Elliott, 1976; De Boer et al., 1977; Robin, 1978; Tada et al., 1987; Tada and Siever, 1989; Ehrenberg, 1990; Elias and Hajash, 1992; Shimizu, 1995; Renard et al., 1997; Osborne and Swarbrick, 1999; Renard et al., 1999; Sheldon et al., 2003; Gratier et al., 2005; van Noort et al., 2008; Nenna and Aydin, 2011) support VES-driven dissolution process, others (Bjorkum, 1996; Oelkers et al., 1996; Walderhaug, 1996; Bjørkum et al., 1998; Lander and Walderhaug, 1999) claimed that the process is "stress-insensitive" and catalysed by sheet silicates (clays and micas) at the right temperature conditions.

Apart from VES-driven pressure dissolution sourced silica, other potential internal and external sources were comprehensively discussed in Worden and Morad (2000). Internal sources of silica include localised feldspar dissolution, clay mineral reactions, and biogenic silica dissolution. Silica from biogenic sources has been linked to precipitation of microcrystalline quartz cement, and this has significant implications for reservoir quality evolution in sandstones (Bloch et al., 2002; Morad et al., 2010; Taylor

et al., 2010). Silica may be sourced externally from adjacent or more deeply buried mudrocks and/or sandstones(e.g. Gluyas and Cade, 1997). However, remotely sourced silica remains controversial due to the large scale transportation (metres to kilometres) that is required to mobilise them to precipitation sites (Worden and Morad, 2000).

The various mechanisms of silica transportation examined in previous studies (McBride, 1989; Bjorlykke and Egeberg, 1993; Aplin and Warren, 1994; Giles et al., 2000) include: meteoric recharge, fluid-flow by advection, thermal convection, and diffusion. While meteoric recharge is possible in shallow buried or substantially uplifted sandstones (Wilkinson et al., 2006; Harwood, 2011), thermal convection may be important locally around hydrothermal intrusions and salt domes (Bjorlykke and Egeberg, 1993). Also, Aplin and Warren (1994) have shown that mass-transport of silica by advection is unlikely, since this would require large-scale water movement which is difficult to achieve in deeply buried sandstones. Hence, diffusive transport and/or small-scale convection is deemed to be the most important process of silica transportation in deeply buried sandstones (Aplin and Warren, 1994). However, the diffusive mechanism is unlikely to be able to transport silica from long-distance sources (Bjorlykke and Egeberg, 1993).

Many studies (Heald and Larese, 1974; Aase et al., 1996; Osborne and Swarbrick, 1999; Bloch et al., 2002; Storvoll et al., 2002; Taylor et al., 2004; Ajdukiewicz et al., 2010; French et al., 2012; Worden et al., 2012; Dutton et al., 2016; Stricker et al., 2016b; Oye et al., 2018) have linked the presence of low volume of diagenetic quartz cement in deeply buried quartz-rich sandstone reservoirs to the presence of grain coats on detrital quartz grain surfaces. These workers have shown that the presence of effective clay and/or well-developed micro quartz grain coats on quartz grains in deeply buried sandstones inhibit chemical compaction and related quartz cementation by making potential quartz cement precipitation sites unavailable, thus preserving economic reservoir quality.

The presence of carbonate cement can also have an inhibitive effect on the precipitation of quartz cement (Lander and Walderhaug, 1999; Lasocki et al., 1999). The early precipitation of carbonate cement would not only occlude pore spaces, but also reduce the available surface area for quartz precipitation (Lander and Walderhaug, 1999). In addition, Bjorlykke and Egeberg (1993) pointed out that the presence of carbonate

cement is likely to limit diffusive transportation of silica from source to precipitation sites thus reducing the volume of precipitated quartz cement.

Although contentious, some studies (Gluyas et al., 1993; Worden et al., 1998; Marchand et al., 2000; Worden and Morad, 2000; Marchand et al., 2001; Wilkinson and Haszeldine, 2011; Worden et al., 2018b) have related the observation of low volume of quartz cement and economic reservoir quality in some sandstone reservoirs to early hydrocarbon charge. Others (Walderhaug, 1994a, Walderhaug, 1994b, Worden et al., 1998, Maast et al., 2011) suggested that quartz precipitation would proceed in the presence of hydrocarbon as long as water remains the wetting phase in sandstone reservoirs. However, emerging thoughts from field-based (Worden et al., 1998; Marchand et al., 2002; Worden et al., 2018b) and experimental (Sathar et al., 2012) observations have shown that silica diffusion and precipitation would be stalled at high hydrocarbon saturation.

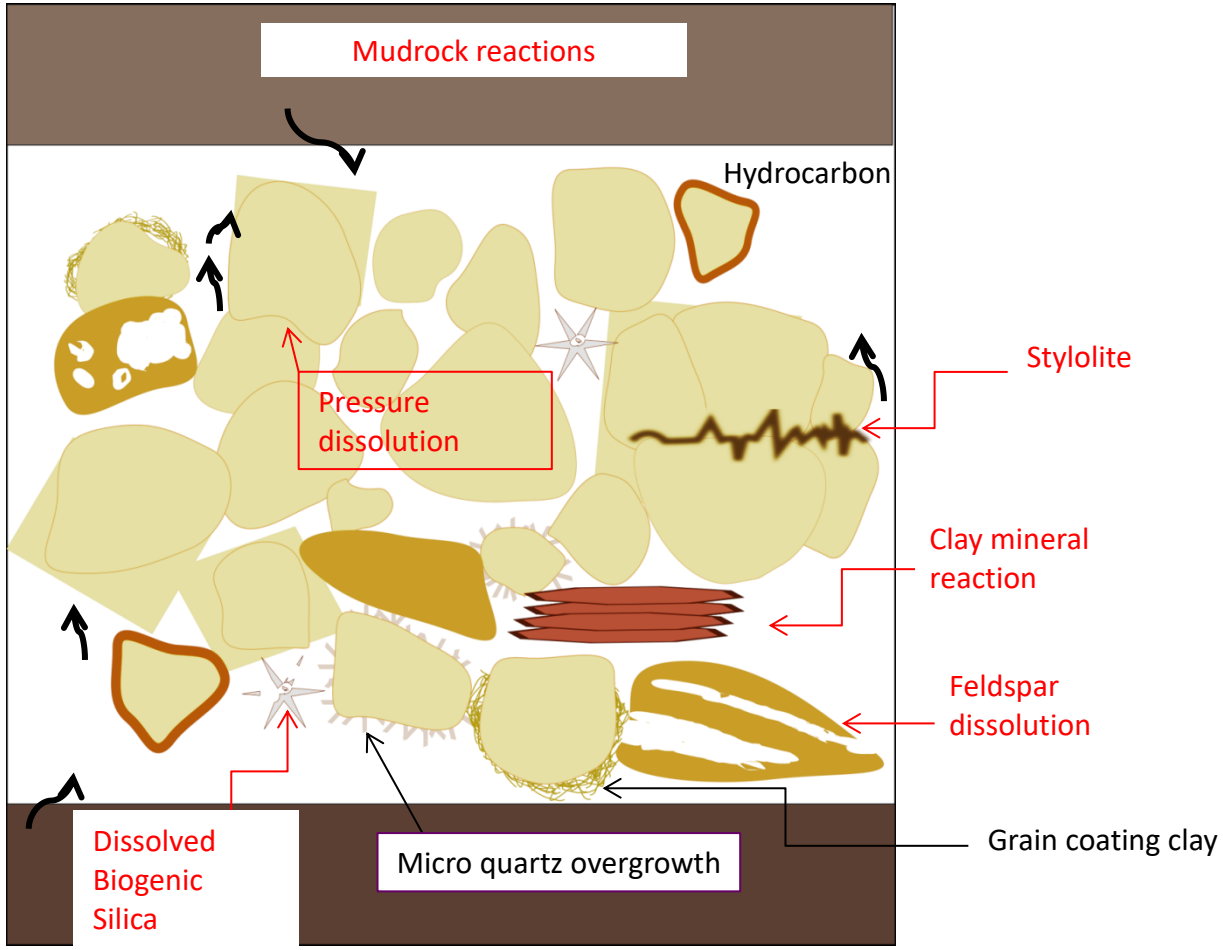

Figure 1.1. Schematic diagram for potential controls on quartz cementation in sandstones. The red labels are silica sources, and the blacks are quartz cement inhibitors (adapted from Worden and Morad (2000))

1.3 Quartz Cementation and Vertical Effective Stress

In highly pressured (overpressure) environments, the development of shallow overpressure (a subsurface phenomenon whereby pore fluid pressure exceeds hydrostatic gradient) within sedimentary basins reduces VES and inhibits mechanical compaction (Osborne and Swarbrick, 1999; Bloch et al., 2002; Sathar and Jones, 2016), thus preserving porosity and economic reservoir quality. A schematic diagram illustrating the development of overpressure and different pressure-depth profiles is shown in Figure 1.2. The assumption is that the process is maintained beyond shallow burial (> 2500m) to depth and temperature where quartz cementation is frequently observed. Such effect halts the supply of silica by preventing VES-driven pressure dissolution, a presumed source of quartz cement for chemical compaction, and preserve reservoir quality in deeply buried sandstones (Osborne and Swarbrick, 1999). Indeed, numerous studies (Thomson, 1959; Weyl, 1959; Rutter and Elliott, 1976; De Boer et al., 1977; Robin, 1978; Tada et al., 1987; Tada and Siever, 1989; Dewers and Ortoleva, 1990; Dewers and Ortoleva, 1991; Elias and Hajash, 1992; Shimizu, 1995; Renard et al., 1997; Renard et al., 1999; Sheldon et al., 2003; Gratier et al., 2005; van Noort et al., 2008; Nenna and Aydin, 2011) have shown that pressure dissolution in sandstones is driven by VES. Theoretical (Sheldon et al., 2003), experimental (Elias and Hajash, 1992; Gratier et al., 2005; van Noort et al., 2008) and field based (Thomson, 1959; Houseknecht, 1988) evidence has shown that this process occurs in response to the development of anisotropic stress.

The influence of VES on chemical compaction (pressure dissolution) and related quartz cementation in sandstones has been underplayed in several clastic reservoir studies, e.g. (Bjorkum, 1996; Walderhaug, 1996; Bjørkum et al., 1998), that have favoured temperature as the key control on quartz cementation. Quartz cementation and chemical compaction has been described as the result of VES-insensitive thermodynamically and kinetically controlled processes such as: clay and mica catalysed dissolution along stylolites and grain contacts, transportation of aqueous silica by diffusion, and precipitation of silica as cement on quartz grains (Oelkers et al., 1996; Bjørkum et al., 1998; Bjørlykke, 2014). As suggested by Walderhaug (1994b) and Walderhaug et al. (2009), quartz precipitation rate increases exponentially with temperature and time. This rate has been assumed to be the slowest and the rate limiting step for quartz cementation (Walderhaug, 1994b; Bjorkum, 1996; Walderhaug, 1996; Walderhaug et al., 2009). Hence, models of quartz cementation have been developed that incorporate

temperature-controlled precipitation kinetics without the need for the main source of silica – VES-driven pressure dissolution.

1.4 Research Aim and Hypotheses

The role of vertical effective stress as a driver for pressure dissolution along quartz grains contact and stylolites, and as an eventual controller of the supply of silica for quartz cementation in sandstone remains a subject of controversy in many clastic reservoir studies (e.g. Sheldon et al., 2003; Taylor et al., 2010; Stricker et al., 2016b; Worden et al., 2018a) . In particular, vertical effective stress-driven pressure dissolution was not incorporated in the algorithm of recently-developed quartz cementation models (e.g. Walderhaug, 1996; Lander and Walderhaug, 1999; Walderhaug, 2000). These models suppose that quartz cementation is purely a function of temperature and that supply through dissolution of quartz at grain contacts, driven by vertical effective stress, is largely irrelevant. Precipitation of quartz cement has been adjudged the rate controlling step in these models and not dissolution (i.e. silica source), and the rate of quartz precipitation has been described to be influenced by temperature, time, grain sizes, grain coats and available quartz surface area. Consequently, an attempt will be made in this research by integrating improved high-resolution rock analysing tools and computer modelling to study how vertical effective stress (VES) controls quartz cementation in sandstone. In particular, the following hypotheses will be tested in this study:

- Vertical effective stress is a control on quartz cementation
- evaluate the effect of microquartz and clay coatings and hydrocarbon charge on quartz cementation.

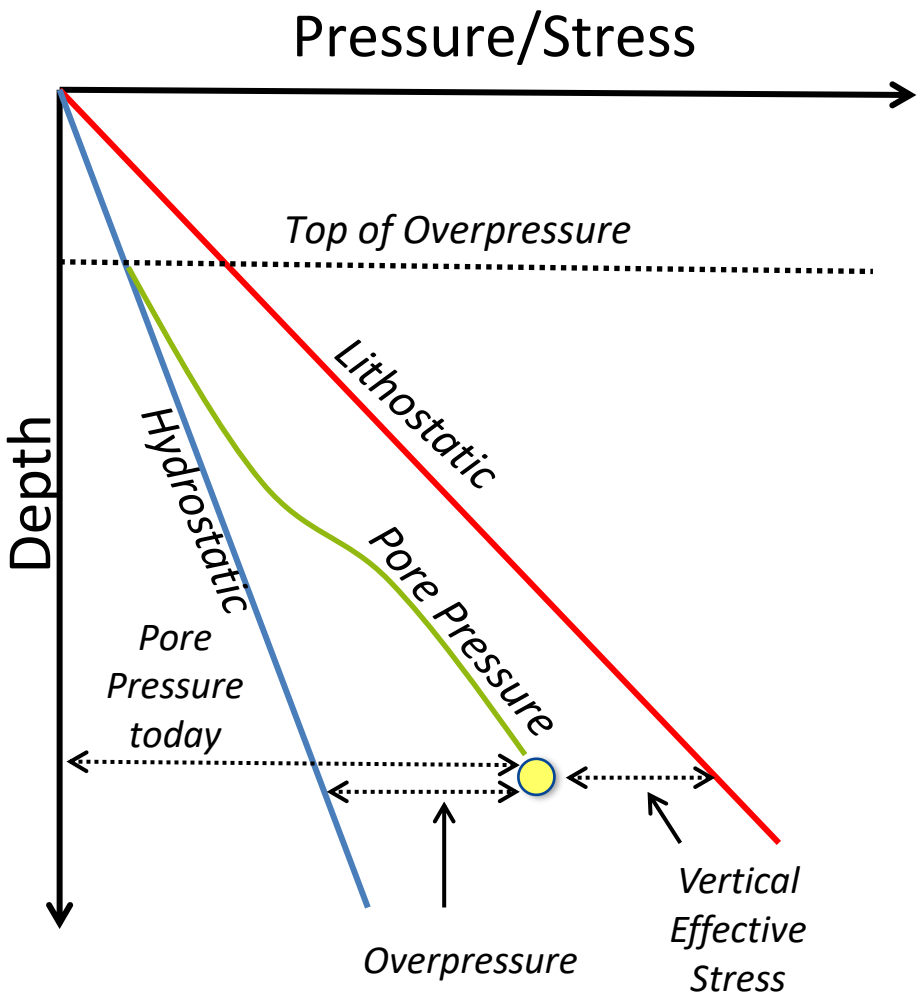

Figure 1.2. Diagram illustrating pressure-depth profiles in overpressured sandstones. In this hypothetical example, effective stress is acting perpendicular to bedding (vertical effective stress).

1.5 Thesis Structure

This thesis is made up of six chapters.

- The current chapter gives a general background for the intended research based on previous studies, and emphasized the main ideas, including the research aim and hypothesis.
- Chapter two gives a detailed description of a set of high resolution analytical and modelling techniques designed to achieve the aim of this study.
- Chapter three focuses on diagenesis in the Upper Jurassic Fulmar Formation sandstones from Clyde, Elgin and Fulmar fields in the Central North Sea.
- Chapter four is a detailed study on vertical effective stress as the main control on quartz cementation in the Fulmar Formation sandstones from Elgin field.
- Chapter five compares the relative effect of vertical effective stress and temperature histories on the rate of quartz cement in the Upper Jurassic Fulmar Formation sandstones from the Central North Sea and the Paleocene-Eocene Wilcox Group sandstones from the Gulf of Mexico.
- Chapter six integrates the key findings on the role of temperature and vertical effective stress on quartz cementation in sandstones.

2. Methodology

2.1. Sampling Strategy

This research was aimed at understanding the role of vertical effective stress (VES) and temperature on quartz cementation in sandstones. Hence, reservoir sandstones were selected across a range of present-day VES and temperature regimes from multiple wells in two locations:

Location 1: Upper Jurassic Fulmar Formation sandstones from the Central North Sea, UK. Previous studies on the Fulmar Formation show these sandstones have fairly uniform character and variable VES and temperature regimes across several geographical locality within the Central North Sea (Gowland, 1996; Osborne and Swarbrick, 1999; Wilkinson and Haszeldine, 2011). A large number of oil fields with wells that penetrated the Fulmar Formation reservoir were selected based on well log data obtained from the Information Handling Service (IHS) website and other information available in the public domain (e.g. Fraser et al., 2003; Gluyas and Hichens, 2003). The number of fields was reduced to three based on their present-day VES and temperature (Table 2.1). Core examination and core sampling was performed at the British Geological Survey (BGS) Keyworth. Sandstone samples were obtained from core sections from three wells, one well from each of the oil fields. In all, sixty samples were collected at approximately one metre intervals (Table 2.2). The sampled intervals were chosen to target the Upper Jurassic Fulmar Formation sandstone facies with the best reservoir quality, the upper shoreface sandstones, based on facies characteristics described by Gowland (1996). The Fulmar Formation reservoirs are probably at their maximum burial depth, with maximum formation pressure and temperature conditions.

Location 2: Paleocene-Eocene Wilcox Group sandstones from the Gulf of Mexico (GOM), USA. Two wells that penetrated the Wilcox Group sandstones were selected based on the study carried out by Harwood (2011). These wells, from Lake Creek and Rotherwood Fields in Montgomery and Harris counties in the Gulf of Mexico, have varying present-day VES and temperatures (Table 2.1). The selected Wilcox Group sandstones are most probably at or close to their maximum burial depth with maximum formation pressure and temperature conditions. It is also note-worthy that temperatures of the Wilcox Group sandstones across different location is not strictly a function of burial depth, but varying geothermal gradients (Day-Stirrat et al., 2010; Dutton and Loucks, 2010)

Table 2.1. Present-day VES and temperature matrix for the selected Fulmar Formation and Wilcox Group sandstones from selected oil fields from the UK Central North Sea and US Gulf Coast

Location	Fields	Group/ Formation	Present-day Temp. (°C)	Present-day VES (MPa)
Central North Sea, UK	Fulmar	Fulmar	130	31.0
Central North Sea, UK	Clyde	Fulmar	147	40.0
Central North Sea, UK	Elgin	Fulmar	189	12.5
Gulf of Mexico, USA	Lake Creek	Wilcox	143	33.4
Gulf of Mexico, USA	Rotherwood	Wilcox	185	23.9

2.2. Petrographic Analyses

Petrographic analyses are useful for classification of rock and description of texture, fabrics, composition, mineralogy and diagenetic state of the sandstone samples. This research was partly designed to investigate and quantify quartz cement in reservoir sandstones. Hence, petrographic analyses were carried out on rock chips and thin sections prepared form core samples using optical microscopy, and combined scanning electron microscopy and cathodoluminescence (SEM-CL) microscopy.

2.2.1. Sample Preparation

The microscopy work involves the use of two types of sample preparation methods. First, a set of thin sections were prepared from the available sample sets by sawing off a slice (slab-like) of each of the rock samples. The slabs were impregnated with blue epoxy dye to ease the identification of pore spaces in thin section, and subsequently glued to a glass slide prior to grinding down to a standard thickness of ~ 30 microns. The thin sections were finally made ready for analysis by applying aluminium or diamond polish depending on the nature of analytical work to be carried out. The second method involved the preparation of rock chips mainly for examination under scanning electron microscope. Rock chips of specific samples were obtained, mounted on electron microscope pins and coated with a thin film of gold (about 30nm) using a Cressington Sputter Coater 108.

2.2.2. Standard Petrography

The standard petrography work used a Leica DM 2500P microscope fitted with a light-emitting diode (LED) illumination source to enhance light transmission through thin sections. This technique was used to determine the nature of the framework grains and their relationship with pore matrix in thin sections (Nichols, 2009). The optical properties of the mineral grains were assessed in the transmission mode. A Conwy Valley Systems Limited Petrog digital petrography system was integrated with the Leica microscope for quantification works. The system features a digitally-controlled precision stepping stage mounted on the microscope stage. The setup allows systematic calculation of the proportion of grain types, grain contacts, grain coats, matrix and cement by making not less than 300 point count in thin section slides and expressing the result in percentage (Nichols, 2009).

2.2.3. Cathodoluminescence Petrography

For many years, cathodoluminescence (CL) petrography has been an indispensable tool for qualitative and quantitative diagenetic studies of sandstones (Sibley and Blatt,

1976a; Houseknecht, 1984; Houseknecht, 1987; Houseknecht, 1991; Evans et al., 1994; Reed and Milliken, 2003). Because this technique eases the discrimination of detrital and authigenic quartz in sandstones, some petrographers favour the technique for analysing compaction and quartz cementation. Although, the use of CL for quantification of quartz cements in sandstones has evolved over time (e.g. Houseknecht, 1991; Evans et al., 1994) most analyses are still being carried out over small sample areas. Secondly, the reliance on the use of backscattered electron (BSE) grey level image segmentation (Evans et al., 1994) for mineral identification during previous CL petrographic works is sometimes associated with uncertainties. For example, minerals like albite that have the same average atomic mass as quartz are not discriminated by BSE (Evans et al., 1994).

In this study, we developed an improved CL petrographic technique for quantifying compaction and quartz cementation in sandstones. This new approach is simple, eliminates uncertainties associated with atomic masses, and allows routine quantification over predefined large representative sample area. The detailed description of this new technique is presented in the next section.

2.2.3.1. Instrumentation

CL petrography and chemical analyses of thin-sections were carried out at the GJ Russell Microscopy Facility in Durham University. The CL imaging was performed using a Gatan mono-CL3 detector connected to a Hitachi Analytical SU-70 UHR Schottky Emission Scanning Electron Microscope (SEM). The mono-CL3 system collects, disperses, measures and records cathodoluminescence signals, and uses a retractable parabolic mirror. An Oxford Instruments energy dispersive X-ray (EDX) system (X-MaxN 50 Silicon Drift Detector) was used for the chemical analytical work. The EDX utilises integrated Aztec Energy Acquisition and Energy Dispersive Spectrum Analysis software for ease of characterisation. The CL and EDX detectors were both integrated with the SEM, and the capability of the integrated system ensures that automated large area CL imaging, chemical mapping and phase analyses of thin-sections are routinely possible.

2.2.3.2. CL Sample Selection

Fulmar Formation sample selection for CL petrography was based on the petrographic information obtained from modal analysis of sixty thin sections from optical microscopy. This selection procedure was carried out for the purpose of choosing the

most appropriate samples for investigation of quartz cementation. First, samples with pervasive carbonate cement were removed to ensure uniformity of analysed samples, thus removing bias that may be introduced by carbonate cement during quantification, and also eliminates imaging problems usually associated with carbonate luminescence. A total of thirty carbonate-screened thin sections were then chosen for cathodoluminescence (CL) petrography (Table 2.2) representing the full range of quartz cement content. In the case of the Wilcox Group sandstones, data were obtained from Harwood (2011).

2.2.3.3. Imaging

The SEM was operated at 12 Kev with analytical working distance range of 16.9mm – 17.1mm. The selected CL petrography sample sets were primed for analysis by diamond-polishing each section and applying a thin film of carbon coat (about 30nm) on the samples. The SEM was configured to acquire CL images in panchromatic mode from a pre-defined large area (9 mm^2) from each thin section. This was done to incorporate a minimum of 300 mineral grains at x300 magnification, 1024 by 1024 resolution, and 40µs dwell time. At this condition, a mosaic of about 70 frames of CL images representing the 9 mm^2 area is acquired in one hour. The CL mirror is then retracted to allow for EDX map acquisition over the same area. Apart from the dwell time that is increased to 300µs to improve the quality of acquired EDX data, all prevailing acquisition conditions are left constant. The automated system is left unattended at this stage, and a complete suite of CL and EDX data set are available for processing in seven hours. A schematic of the entire acquisition process is provided on Figure 2.1.

2.2.3.4. Processing

The procedure adopted for the processing of acquired CL and EDX data sets is the same for all the analysed samples. The process was carried out using Aztec software. Even though the data were automatically aligned during acquisition, a manual alignment procedure was performed on the data for best result. The aligned data were subsequently montaged to form two single large maps, one each for CL and EDX. While the CL map data are converted to image (Figure 2.2) for the purpose of quantification, the EDX map data are converted to phase map data. Since the composition of interest is mainly quartz, the silica phase map is calculated and the phase image (Figure 2.2) is generated to complement the CL quantification work.

2.2.3.5. Quantification

Two different techniques were initially considered for quantification work. The first, image analysis techniques; similar to that of Evans et al. (1994) , but with the use of the EDX phase map instead of BSE image for mineral identification. However, the nature of the work to be carried out, which includes quantifying dissolution along grain-to-grain contacts, cannot be achieved using this technique. Also, different quartz grains and overgrowths exhibit varying CL intensities, based on their environment of formation. Hence, the use of image analysis (Evans et al., 1994) involving image subtraction and grey level segmentation of CL images would most likely lead to large underestimation or overestimation of quartz cementation.

As a consequence, the technique adopted for the quantification work is an improvement on pre-existing methods (e.g. Sibley and Blatt, 1976a; Houseknecht, 1991) of estimating petrographic variables from CL data. The CL image was used primarily for the quantification, while the silica phase image serves as the mineral identification control (Figure 2.2). The investigated samples are essentially arkosic - subarkosic sandstone, and the colour contrast between the pure silica phase (quartz) and other silicate minerals (e.g. feldspar) facilitated easy discrimination. A grid of 1600 (40x40) square boxes was created from an excel worksheet and used for the quantification procedure. The grid was placed on the CL image on a PowerPoint slide and adjusted to fit. The petrographic features of interest (quartz cement and points of quartz to quartz grain dissolution) that coincide with the centre of each box are counted and assigned a point each. This procedure is like the usual point counting operation during optical microscopy, where the centre point of the microscope cross hairs is used for measurement. The only exception is that a more statistically robust data are generated at a scale of 1600 point counts per sample.

Table 2.2. Overview of the Upper Jurassic Fulmar Formation sandstones from Clyde, Elgin and Fulmar fields showing the various depths and the corresponding petrographic procedures for each sample. Detailed petrographic data are reported in Appendix 1 and Appendix 2

TVDSS (m)	Depth (m)	Depth	Field	Optical Microscopy	CL Petrography
3245.3	3269.1	10725.3	Fulmar	X	X
3246.4	3270.1	10728.8	Fulmar	X	
3247.0	3270.8	10730.9	Fulmar	X	
3247.6	3271.4	10733.0	Fulmar	X	
3248.7	3272.5	10736.5	Fulmar	X	X
3249.2	3273.0	10738.1	Fulmar	X	X
3249.7	3273.5	10739.8	Fulmar	X	
3260.7	3284.5	10775.9	Fulmar	X	X
3261.4	3285.1	10778.0	Fulmar	X	X
3262.0	3285.7	10780.0	Fulmar	X	
3262.6	3286.4	10782.0	Fulmar	X	
3264.1	3287.9	10787.0	Fulmar	X	
3264.4	3288.2	10788.1	Fulmar	X	X
3268.8	3292.6	10802.5	Fulmar	X	
3270.1	3293.9	10806.6	Fulmar	X	X
3270.7	3294.5	10808.7	Fulmar	X	
3271.2	3294.9	10810.1	Fulmar	X	X
3272.4	3296.2	10814.3	Fulmar	X	X
3273.1	3296.8	10816.4	Fulmar	X	
3274.8	3298.5	10822.0	Fulmar	X	
3275.7	3299.5	10825.1	Fulmar	X	
3276.2	3300.0	10826.7	Fulmar	X	X
3770.8	3795.8	12453.3	Clyde	X	
3772.2	3797.2	12457.9	Clyde	X	
3773.0	3798.0	12460.8	Clyde	X	X
3773.7	3798.7	12462.8	Clyde	X	
3774.5	3799.5	12465.7	Clyde	X	X
3776.4	3801.4	12471.8	Clyde	X	
3777.4	3802.4	12475.2	Clyde	X	X
3778.2	3803.2	12477.8	Clyde	X	X
3779.0	3804.0	12480.2	Clyde	X	
3780.6	3805.6	12485.5	Clyde	X	X
3781.1	3806.1	12487.3	Clyde	X	X
3781.8	3806.8	12489.5	Clyde	X	X
3782.9	3807.9	12493.2	Clyde	X	
3783.6	3808.6	12495.4	Clyde	X	
3784.2	3809.2	12497.5	Clyde	X	X
3785.1	3810.1	12500.2	Clyde	X	X
3785.7	3810.7	12502.3	Clyde	X	
3786.3	3811.3	12504.3	Clyde	x	

3787.5	3812.5	12508.2	Clyde	x	X
5413.3	5602.4	18380.6	Elgin	x	
5414.3	5603.4	18383.9	Elgin	x	
5415.5	5604.6	18387.8	Elgin	x	
5416.0	5605.1	18389.4	Elgin	x	X
5417.1	5606.2	18392.9	Elgin	x	X
5418.4	5607.5	18397.3	Elgin	x	
5418.9	5608.0	18399.0	Elgin	x	
5420.5	5609.6	18404.2	Elgin	x	
5422.4	5611.5	18410.4	Elgin	x	
5424.8	5613.9	18418.3	Elgin	x	X
5427.2	5616.3	18426.2	Elgin	x	X
5428.6	5617.7	18430.8	Elgin	x	X
5429.3	5618.4	18433.1	Elgin	x	X
5430.3	5619.4	18436.2	Elgin	x	X
5431.5	5620.6	18440.1	Elgin	x	X
5432.2	5621.3	18442.6	Elgin	x	
5433.1	5622.2	18445.5	Elgin	x	X
5434.6	5623.7	18450.5	Elgin	x	
5435.3	5624.4	18452.8	Elgin	x	X

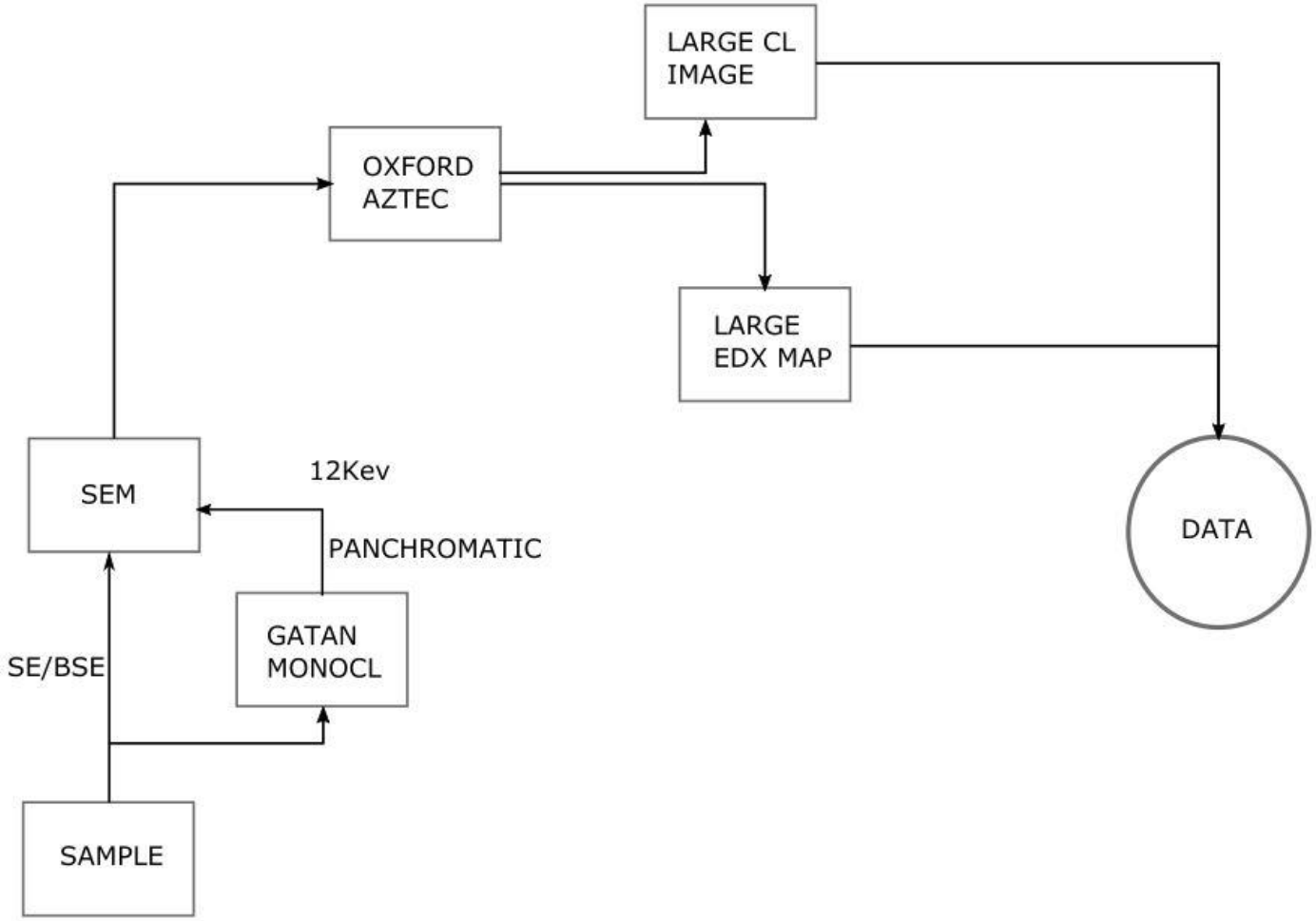

Figure 2.1 Schematic of the CL Petrography data acquisition

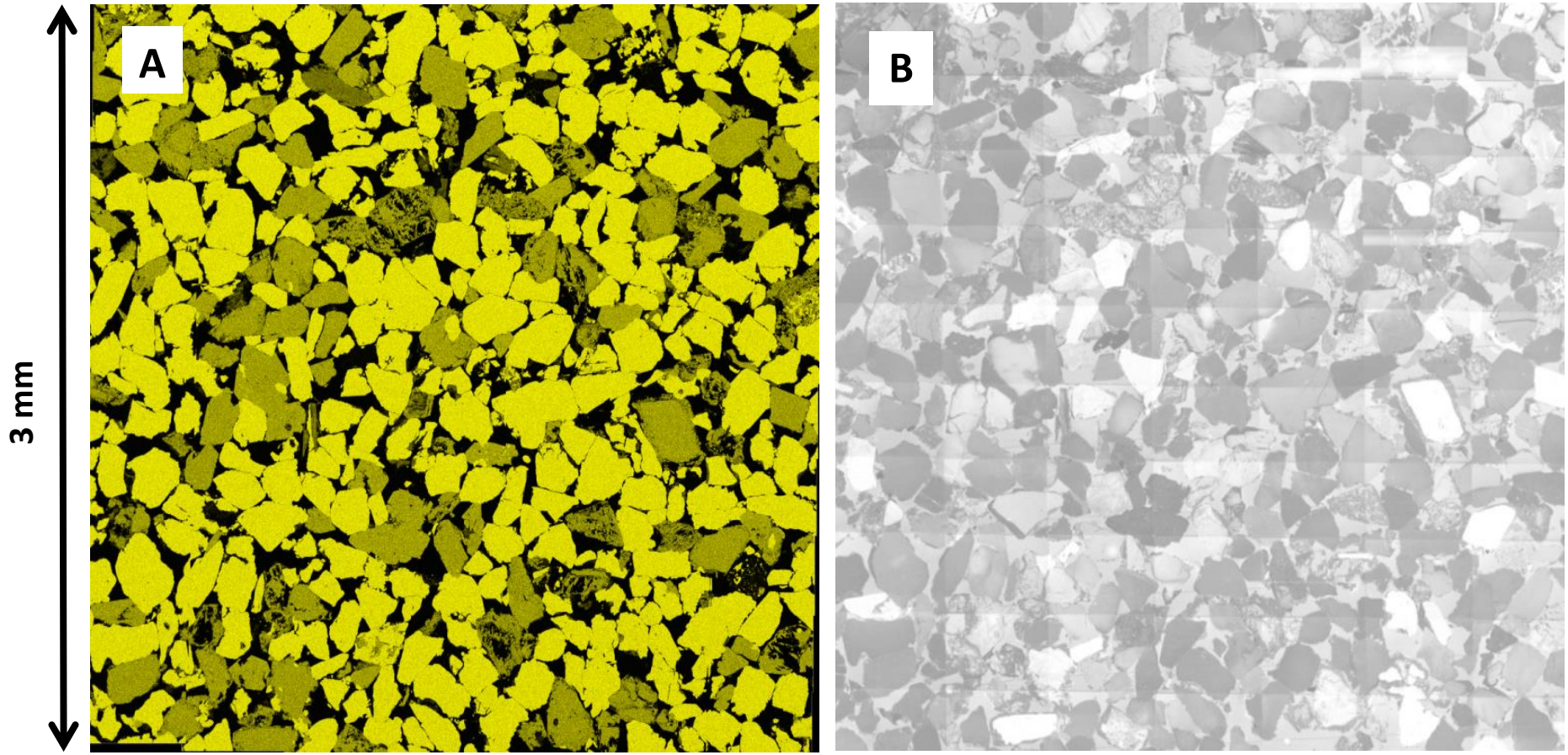

Figure 2.2. Sample large area petrographic maps (300 grains minimum coverage) used for quartz cementation and pressure dissolution quantification. A) Silica map from energy dispersive x-ray (EDX) with the quartz grains in bright yellow. B) CL map for detrital and authigenic quartz discrimination

2.3. Basin Modelling

The evolution of sedimentary basins and hydrocarbon reservoirs through time can be reconstructed using basin modelling software. One-dimensional basin modelling approach was adopted in the current study to provide insight on how temperature and effective stress in the Fulmar Formation and Wilcox Group sandstone reservoirs evolved through time in Clyde, Elgin, Fulmar, Lake Creek and Rotherwood fields. Though the technique is limited in its ability to model overpressure generation from the effect of lateral flow and hydrocarbon charge, overpressure generation from compaction disequilibrium can be effectively simulated. The one-dimensional modelling work was carried out using Schlumberger's PetroMod Petroleum Systems modelling software (Version 2014.1). The software uses a back-stripping and forward modelling approach to reconstruct the burial histories of sedimentary basins.

2.3.1. Geological Inputs

The main inputs for the basin models include: sedimentary layers, layer thicknesses, lithologies (Table 2.5, Table 2.6 and Table 2.7), erosion and depositional events, and source rock properties. While the geological data used for the modelling the histories of the GOM fields were obtained from Ruarri Day-stirrat in Shell Oil, Houston and other literature sources (e.g.…), the data used for the Central North Sea fields were obtained from well composite logs, geological well reports, core analysis, and core description reports sourced mainly from IHS and other credible published data available online and print form (e.g. Millenium Atlas). Geological ages (Table 2.5, Table 2.6 and Table 2.7) derived from the Millenium Atlas (Gluyas and Hichens, 2003) were used to set the model. Stratigraphic layers and layers thicknesses were derived from well composite logs, while geologic ages of each layers, erosional events, and estimates for eroded thicknesses were established from the Millennium Atlas (Gluyas and Hichens, 2003). The geological evolution of the Fulmar field, as reviewed from Stockbridge and Gray (1991), reveals the area experienced extensive erosion in the Mid and Late Cimmerian. A similar burial history path was assumed for the Clyde field due to its proximity to the Fulmar field. However, the eroded layers for all three fields were estimated from the information available in the Millennium Atlas (Gluyas and Hichens, 2003). This was achieved by comparing the thicknesses of eroded layers from individual fields to that of similar but well-preserved layers in adjacent fields.

2.3.2.Boundary Conditions

There are three types of boundary conditions defined for model input in the PetroMod software. These are palaeowater depth, sediment water interface temperature, and heat flow conditions. The palaeowater depths for Elgin field were defined by combining information obtained from the public domain (Tipsword et al., 1966; Gennaro, 2011) and Total UK Limited unpublished biostratigraphy report. Palaeowater depths for Clyde and Fulmar fields were inferred using facies and likely depositional environments for the different lithologies. Sediment water interface temperature trend was assigned to each model automatically using the in-built PetroMod calculator. The heat flow model input parameters adopted for each of the three fields (Table 2.3) were defined after Allen and Allen (2005), with the highest heat flow values (Table 2.4) recorded at the peaks of the Permo-Triassic and Upper Jurassic paleo-rifting events recorded in North Sea geology.

Table 2.3. Boundary Conditions and Heat Flow model input parameter for Clyde, Elgin and Fulmar Fields. Stretching factors (beta) were inferred from White and Latin (1993)

Heat Flow Model Parameter								
Field	Well	Rifting Event 1	Rifting Event 2	Beta Crust	Beta Mantle	Crustal Thickness (km)	Mantle Thickness (km)	Crust Basal Temperature (ºC)
Clyde	30/17B-2	Permo-Triassic	Upper Jurassic	1.7	1.9	30	90	1333
Elgin	22/30C-G4	Permo-Triassic	Upper Jurassic	1.7	1.9	30	90	1333
Fulmar	30/16-7	Permo-Triassic	Upper Jurassic	1.8	2.0	30	90	1333

2.3.3.Thermal Calibration

The thermal models were calibrated using measured temperature, and vitrinite reflectance (%Ro) data. Drill Stem Test (DST) temperature data for Clyde field and corrected bottom-hole temperature (BHT) data for Elgin field were obtained from the Total UK Limited unpublished well report. In the case of the Fulmar field, temperature and %Ro data were obtained from Mehenni and Roodenburg (1990). Because Fulmar and Clyde are adjacent fields, their thermal histories should not differ significantly. Hence, Fulmar field %Ro data were incorporated in the Clyde field model. In the case of Elgin, %Ro data were obtained from the Total UK Limited unpublished

geochemistry report. The heat flow models were adjusted several times until an optimum fit was achieved between the measured and modelled (temperature and %Ro) data.

Table 2.4. Measured data types and heat flow peaks used for thermal calibration of Clyde, Elgin and Fulmar models

Thermal Calibration and Heat Flow					
Field	Well	Measured data		Optimal Heat Flow Peaks (mW/m2)	
				Permo-Triassic	Upper Jurassic
Clyde	30/17B-2	Temperature	Vitrinite Reflectance	69.7	89.6
Elgin	22/30C-G4	Temperature	Vitrinite Reflectance	69.7	89.4
Fulmar	30/16-7	Temperature	Vitrinite Reflectance	69.7	86.4

2.3.4.Pore Pressure and Effective Stress Modelling

Pore pressure data obtained from field measurements were used to constrain the pore pressure model for reconstruction of stress histories for the three fields. Terzaghi (1925) expression:

Vertical effective stress (σ^1) = Lithostatic stress (σ) – Pore pressure (Pp),

was used during the pressure modelling to calculate present-day vertical effective stress from the present-day measured pore pressure data, and the vertical effective stress histories using the same relation. In order to model compaction, Fulmar Formation porosities from routine core analysis were incorporated in the model. Since porosity is a function of lithology, tighter constraints were placed on the model by modifying PetroMod's default lithologies to match those observed on the field. These lithologies were defined using well composite logs and, core analysis and description reports. Based on this study, the Chalk Group and the Pre-Cretaceous shales (Kimmeridge Clay and Heather Formations) are very important for modelling the observed pore pressure in the Fulmar Formation. The default chalk and shale permeabilities in PetroMod were modified after Swarbrick et al. (2000), to lower values for the Chalk Group and the Pre-

Cretaceous shales until modelled pore pressure matches Present-day formation pressures.

2.4. Kinetic Modelling of Quartz Cementation

Quartz cementation models have been developed for routine simulation of diagenesis and reservoir quality in sandstone. In recent times, widely commercial diagenetic modelling software has been developed. These packages use a precipitation algorithm premised on the precipitation kinetics developed empirically by Walderhaug (1994a) and Walderhaug (1994b). The precipitation model assumes that barriers to quartz precipitation kinetics are overcome at temperatures around 80^{o}C, and the reaction progresses exponentially with increasing temperature (Walderhaug, 1994a; Walderhaug, 1994b; Walderhaug, 1996; Walderhaug, 2000). This quartz cementation threshold temperature corresponds to burial depths of about 2500m which is often designated as the onset of chemical compaction (Taylor et al., 2010; Bjørlykke, 2014). At this depth, Intergranular volume (IGV) has been reduced to about 26% of bulk rock volume by mechanical compaction. This IGV is assumed to be the porosity at the start of quartz cementation (Houseknecht, 1987; Ajdukiewicz and Lander, 2010), assuming hydrostatic pore pressure.

2.4.1. Model Kinetics

The model developed by Walderhaug (1994b) uses mathematically simple precipitation kinetics for modelling quartz cementation. According to Walderhaug (1996), when temperature is fixed in a 1cm^3 volume of sandstone with a quartz surface area, A (cm^2), the volume of quartz cement, V_q (cm^3) precipitated during a time t (s) can be calculated as:

$$V_q = MrAt/\rho$$

Equation 2.1

Where M, r and ρ are molar mass of quartz (60.09 g/mol), rate of quartz precipitation (moles/cm^{2}s) and density of quartz (2.65g/cm^3) respectively. The rate (r) can further be expressed as logarithm function of temperature (Walderhaug, 1994a; Walderhaug, 1996):

$$r = a10^{bT}$$

Equation 2.2

Where T is temperature (°C), and a and b are constants with units of mol/cm^2 and 1/°C respectively. Since time and temperature are linked by linear functions, T can be expressed a linear function of time (t) and Equation 2.2 can be replaced by

$$r = a10^{b\,(ct+d)}$$

Equation 2.3

Where *c* is the heating rate (°C/s), d is the initial temperature (°C).

Subsequently, Walderhaug (1996) combined Equation 2.1 and Equation 2.3 to derive an expression for predicting the volume (V_q) of quartz cement precipitated on a unit volume of sandstone as a series of linear time temperature segments:

$$V_{q2} = \phi_o - (\phi_o - V_{q1}) \exp - MaA_o/\rho\phi_o bc\ln 10\,(10^{bT2} - 10^{bT1})$$

Equation 2.4

Where V_{q1} is the amount of quartz cement present at time T_1 and V_{q2} is the amount of quartz cement precipitated from time T_1 and T_2 and A_o (cm^2) is initial quartz surface area. Equation 2.4 is Walderhaug (1996) quartz cementation model.

Based on the work of Lasaga (1984), A_o is calculated as the cumulative surface area of spheres with a diameter, D, equal to the grain size and with a total volume equal to the fraction of detrital quartz, f, in a unit volume, v, of the sandstone. Hence, A_o can be expressed as:

$$A_o = 6fv/D$$

Equation 2.5

Since the quartz surface area changes as quartz cement precipitation progresses. The changes in quartz surface area are considered to be proportional to porosity loss caused

by quartz cement precipitation. The quartz surface area after precipitation is expressed as:

$$A = A_o (\phi_o - V_q)/\phi_o$$

Equation 2.6

Where ϕ_O is the porosity at the start of precipitation

Walderhaug's (1996) equation for quartz cementation (Equation 2.4) was used to simulate the growth of quartz cement in the Fulmar sandstone samples from Clyde, Elgin and Fulmar fields. Although there are other sophisticated Arrhenius-based models in which the rate of cementation can be adjusted by changing the activation energy (Walderhaug, 2000), these were not available for this study. The studied sandstones are arkosic - subarkosic in composition; hence the model is only applicable to the quartz fraction of the bulk rocks.

2.4.2.Model Input Parameters

The kinetic model was run using Walderhaug (1996) standard parameters. This involved the use of 1cm3 of sandstone and a starting porosity of 26% (approximate porosity at the onset of quartz cementation). Detrital quartz fractions and grain sizes were estimated from CL petrographic analysis of thin sections. Heating rates were calculated from time-temperature histories generated from basin models constructed using PetroMod version 2014.1.

Walderhaug (1996) calculated the amount of quartz precipitated as a sum of series of time steps from the threshold temperature (80°C) to maximum burial temperature because time-temperature curves usually have variable gradients at intervals. The changing time steps imply the values of c and d are not constant throughout the burial history (Walderhaug 1996). Secondly, the quartz surface area changes with the precipitation of additional cement. Hence, the surface area must be adjusted to accommodate the addition prior to usage in the next time step (Walderhaug, 1996). The Walderhaug (1996) method was adopted in this study to calculate cement volume after every one million years' time step.

2.5. Secondary-ion Mass Spectrometry (SIMS)

SIMS analysis allows oxygen isotope ratios to be measured on quartz overgrowth from selected samples, and consequently help to constrain the history of quartz cementation (Harwood et al., 2013). This high precision SIMS technique was used to investigate quartz cement growth histories in the Fulmar Formation sandstones from Clyde, Elgin and Fulmar fields. Oxygen isotopes are stable isotopes, and their abundance are measured as differences in the isotopic ratio of the related isotopes. The principle of oxygen isotope geochemistry based on Emery and Robinson (1993) is briefly described in this section. Stable isotope data are reported using δ (del) notation, and the ratios are always expressed as deviation in parts per thousand (‰), from the same ratio in an internationally accepted standard. For example, the accepted standard for oxygen isotope measurements is V-SMOW (Vienna Standard Mean Ocean Water).

$$\delta_A = ([R_A - R_{stnd}]/R_{stnd}).10^3$$

Equation 2.7

Where R_A is the ratio of heavy to light oxygen isotopes ($^{18}O/^{16}O$)

In the case of two phases, A and B, the stable isotope fractionation factor is given as:

$$\alpha_{A - B} = R_A/R_B$$

Equation 2.8

For example, if A is quartz and B is water, equation 2.8 can be written as:

$$\alpha^{O}_{quartz - water} = (^{18}O/^{16}O)_{quartz}/(^{18}O/^{16}O)_{water}$$

Equation 2.9

Since the fractionation factor is a function of the δ values of the two phases,

$$\alpha_{A-B} = (1 + \delta_A/1000)/(1 + \delta_B/1000) = (1000 + \delta_A)/(1000 + \delta_B)$$

Equation 2.10

In addition, the isotopic difference between two phases can be denoted as Δ (delta). Therefore,

$$\Delta_{A-B} = \delta_A - \delta_B$$

Equation 2.11

Equation 2.11 can be related to α by manipulating Equation 2.7 to Equation 2.9 to give:

$$\Delta_{A-B} = \delta_A - \delta_B \sim 10^3 \ln \alpha_{A-B}$$

Equation 2.12

Equation 2.12 is useful only when Δ is < 10‰, and assuming that phases A and B formed in equilibrium. Hence, α_{A-B} can simply be calculated by subtracting the measured isotopic composition of the phases (Emery and Robinson, 1993).

2.5.1. Oxygen Isotope Geothermometry

The use of stable isotopes (e.g. oxygen isotopes) as geothermometers is premised on the fact that equilibrium isotope fractionation factor of an isotope exchange reaction is temperature dependent (Emery and Robinson, 1993). In most mineral-mineral or mineral-water (e.g. quartz-water) systems, at temperatures above 0°C, $10^3 \ln \alpha$ varies as an approximate linear function of $1/T^2$, where T is temperature in kelvin. Assuming A and B are constants for a particular system:

$$10^3 \ln \alpha = A\,(10^6/T^2) + B$$

Equation 2.13

The value of $10^3 \ln \alpha$ decreases as temperature increases.

The equilibrium isotope effect of oxygen isotopes is controlled by the varying thermodynamic properties of ^{16}O, ^{17}O and ^{18}O (Emery and Robinson, 1993). In essence, the fractionation of ^{18}O between oxygen containing phases (e.g. quartz and water) is a function of temperature and thermodynamic properties of ^{16}O, ^{17}O and ^{18}O isotopes. This forms the basis for oxygen isotope geothermometry. The experiments performed by Clayton et al. (1972) for oxygen isotope fractionation in two phase systems at low (200 – 500°C) and high (500 – 750°C) temperatures resulted in the development of equations that are appropriate for plotting isotopic fractionation against temperature. Because diagenetic conditions like quartz precipitation occurs at lower temperature, it was considered most appropriate to use Clayton et al. (1972) low temperature expression (Equation 2.14) to calculate oxygen isotope fractionation between quartz and water in this study. The extrapolation of this equation down to very low temperature (ca. 10°C) has been shown to yield good agreement with Labeyrie (1974) empirical estimates on diatoms (Kelly et al., 2007). It is noteworthy to point out that oxygen isotopic composition of quartz is a dual function of temperature and $\delta^{18}O$ of water (Emery and Robinson, 1993). Hence, oxygen isotope data cannot generate a unique temperature record of quartz precipitation.

$$10^3 \ln \alpha_{quartz\text{-}water} = 3.38 (10^6/T^2) - 3.40$$

Equation 2.14

2.5.2. SIMS Sample Selection

The data and images obtained from standard and CL petrographic analyses provided a guide for the selection of appropriate samples for SIMS analysis. Three sandstone samples, one from each of the CNS locations (Clyde, Elgin and Fulmar fields) were selected. The petrographic examination of representative thin sections from the selected sandstone samples shows that they have well-developed macroquartz overgrowths with sizes in the region of 30µm and above. These growth sizes are important selection criteria, as larger overgrowths offer more spots for SIMS data acquisition.

2.5.3.Sample Preparation and Overgrowth Selection

This section gives a brief description of SIMS sample preparation procedure. A more detailed preparation procedure is provided in Kelly et al. (2007) and Kita et al. (2009).

The three selected sandstone samples were cut into slabs to make ~15mm diameter rock section. The rock sections were embedded in epoxy to make a round sample mount with diameters and thicknesses less than 25mm and 5mm respectively. Grains (2 – 3) of University of Wisconsin quartz standard (UWQ-1), pre-analysed using laser fluorination (Kelly et al., 2007), with $\delta^{18}O$ value of 12.33 ± 0.07‰ were mounted at the centre of each rock section (Appendix 3). The rock sections were first polished with diamond, and later with colloidal silica to achieve a smooth relief of < 3µm to minimize the effect of sample topography on the precision and accuracy of the SIMS analysis (Kita et al., 2009). Samples were then gold-coated to compensate for surface charges during SIMS analysis. The rock sections were subjected to pre-SIMS-analysis imaging using SEM-BSE and SEM-CL to identify and select the best overgrowths. The acquisition and processing of each set of images (SEM-BSE and SEM-CL) for the various rock sections lasted for about 20 hours each. The domain of overgrowth selection was restricted to within 4mm radius of the UWQ-1 standard. In all, three overgrowths per rock section were selected for SIMS analysis.

2.5.4.SIMS Analysis

The SIMS analysis was performed at the WiscSIMS Laboratory at the University of Wisconsin-Madison using a CAMECA IMS-1280 ion microprobe. In situ oxygen isotope analyses was used to create micro scale $\delta^{18}O$ profiles across nine selected quartz overgrowths from three rock sections during a SIMS session carried out between 5th and 7th April 2017. Data were collected using a $^{133}Cs^{+}$ primary ion beam with an intensity of 21 to 23pA focused to form analysis spot sizes of approximately 3µm diameter. General conditions of analysis are similar to those reported by Kozdon et al. (2009). During the session, four consecutive analyses were made on the UWQ-1 standard before and after 5 - 15 sample measurements. This was necessary to ensure correction of instrument bias during analysis (Kita et al., 2009). A more detailed SIMS analysis procedure is described in Kelly et al. (2007), Page et al. (2007), Kita et al. (2009), Valley and Kita (2009) and Pollington et al. (2011).

2.5.5.SIMS Pits Characterisation

The pre-SIMS-analysis images (SEM-CL and SEM-BSE) were used to target ion microprobe spots during analysis. Because sectoral zoning was obvious on most of the selected overgrowth (e.g. Figure 2.3), analysis spots were designed to follow the zone

trajectories from the detrital-authigenic quartz boundaries to the outermost edge of the overgrowths. Each SIMS pit (analysed spot) was examined post-analysis using SEM-CL to determine if it falls on holes, cracks, fluid inclusions, authigenic quartz, detrital quartz or mixed authigenic-detrital quartz. All data points that fall on irregular features were deemed to have been compromised and were subsequently discarded from the dataset. Measurements were later made across the overgrowths to calculate the width of the overgrowths and the relative distance of each SIMS pit to the edge of the detrital quartz using the method shown on Figure 2.3.

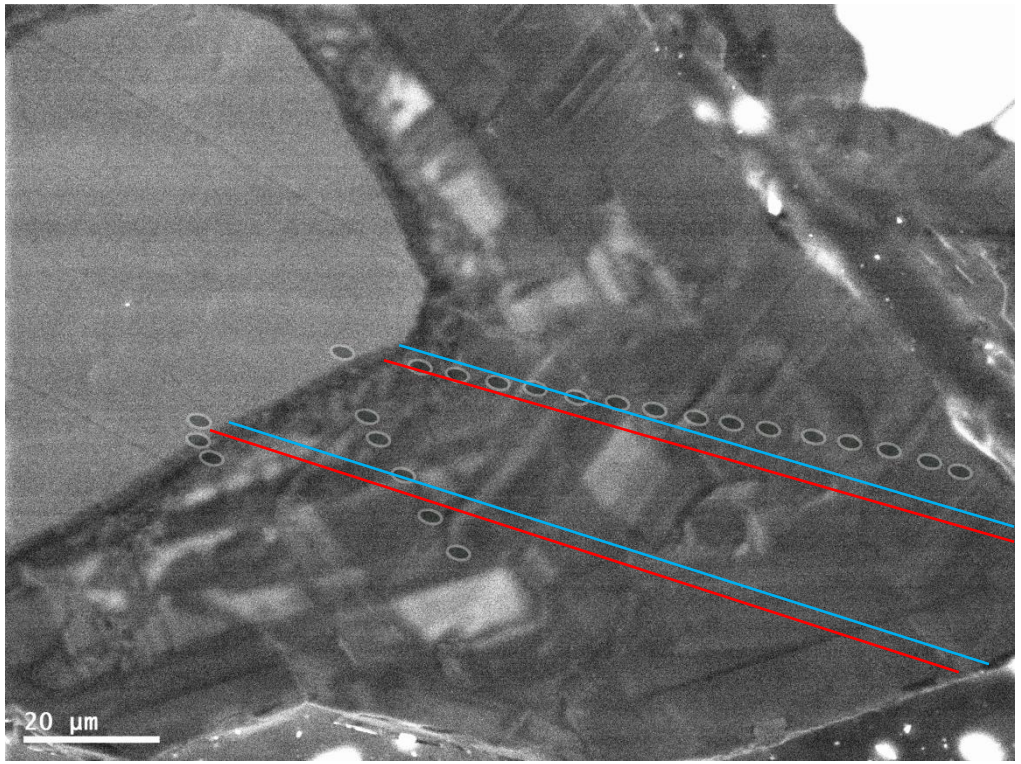

Figure 2.3. SEM-CL image showing mosaic-style zoning in quartz overgrowths, and the technique used to measure the distance of each analysis spot away from the detrital quartz grain. Analysis spots were oriented to follow growth trajectory. Blue line represents distance to each analysis spot, while red represents total width of overgrowth

Table 2.5. Formation thicknesses and Lithotypes used for Elgin Field (22/30c-G4) burial history modelling. Percentage values shows mix ratio for interbedded Formations.

System	Series	Group	Age (Ma)	Formation	Lithology	Thickness (m)
Neogene	Miocene -Pleistocene	Nordland Group (Undiff.)	13	Nordland Group (Undiff.)	Shale	1416
Paleogene	Eocene - Miocene	Hordaland Group (undiff.)	54	Hordaland Group (undiff.)	Shale	1579
Paleogene	Eocene	Rogaland	54.3	Balder Fm	Silty Shale 95% tuff 5%	30
Paleogene	Paleocene	Rogaland	56	Sele Fm	Shale 65% Sandstone 35%	48
Paleogene	Paleocene	Montrose	57.8	Lista Fm	Shale	79
Paleogene	Paleocene	Montrose	58.3	Lista Fm (Andrew Member)	Shale 65% Limestone 35%	63
Paleogene	Paleocene	Montrose	62.5	Maureen Fm	Shaly Limestone 90% Marl 10%	130
Paleogene	Paleocene	Chalk	65	Ekofisk Fm	Chalk 85% Silt 5% Clay 5% Marl 5%	102
Cretaceous	Upper	Chalk	72	Tor Fm	Chalk	502
Cretaceous	Upper	Chalk	91	Hod Fm	Chalk 90% Marl 10%	718
Cretaceous	Upper	Chalk	93	Herring Fm	Chalk	144
Cretaceous	Upper	Chalk	94	Plenus Marl Fm	Shale	2
Cretaceous	Upper	Chalk	99	Hidra Fm	Chalk	85
Cretaceous	Lower	Cromer Knoll	107	Rodby Fm	Shale 65% Limestone 30% Marl 5%	15
Cretaceous	Lower	Cromer Knoll	128.5	Valhall	Shale 60% Marl 40%	49
Jurassic	Upper	Humber	153	Kimmeridge C. Fm.	Shale (black)	103
Jurassic	Upper	Humber	156	Heather Fm	Shale (organic rich, typical)	334
Jurassic	Upper	Humber	158.4	Fulmar Sands	Sandstone (arkose, quartz rich)	160
Jurassic	Middle	Fladen	166	Pentland Sand	Sandstone (clay rich)	164
Jurassic	Middle	Fladen	170	Pentland Shale	Shale (organic rich, typical)	110

Table 2.6. Formation thicknesses and Lithotypes used for Clyde Field (30/17B-2) burial history modelling. Percentage values shows mix ratio for interbedded Formations.

System	Series	Group	Age (Ma)	Formation	Lithology	Thickness (m)
Neogene	Miocene -Pleistocene	Nordland Group (Undiff.)	13	Nordland Group (Undiff.)	Shale (organic lean, typical)	1441
Paleogene	Eocene - Miocene	Hordaland Group (undiff.)	54	Hordaland Group (undiff.)	Shale 70% Silt 30%	1375
Paleogene	Eocene	Rogaland	54.3	Balder Fm	Shale 70% Silt 30%	14
Paleogene	Paleocene	Rogaland	56	Sele Fm	Shale70% Silt 30%	45
Paleogene	Paleocene	Montrose	58.3	Lista Fm	Shale 70% Sand 30%	109
Paleogene	Paleocene	Montrose	62.5	Maureen Fm	Marl 85% silt 10% Clay 5%	23
Paleogene	Paleocene	Chalk	65	Ekofisk Fm	Chalk 80% Clay 10% Limestone 10%	67
Cretaceous	Upper	Chalk	72	Tor Fm	Chalk 90% Silt 5% Clay 5%	327
Cretaceous	Upper	Chalk	91	Hod Fm	Chalk 85% Silt 5% Clay 5% Marl 5%	120
Cretaceous	Lower	Cromer Knoll	128.5	Cromer Knoll	Marl	5
Jurassic	Upper	Humber	149.5	Kimmeridge C. Fm.	Shale (8% TOC) 80% Silt 20%	68
Jurassic	Upper	Humber	158.4	Fulmar Sands	Sandstone (arkose, quartz rich)	217
Triassic	Lower	Heron	248.2	Smith Bank Fm	Shale (organic lean, sandy)	81

Table 2.7. Formation thicknesses and Lithotypes used for Fulmar Field (30/16-7) burial history modelling. Percentage values shows mix ratio for interbedded Formations.

System	Series	Group	Formation	Age (Ma)	Lithology	Thickness (m)
Paleogene	Eocene - Miocene	Hordaland Group (undiff.)	Nord/Hord	54	Shale (typical)	2687
Paleogene	Eocene	Rogaland	Balder Fm	56	Shale (silty)95% tuff 5%	14
Paleogene	Paleocene	Montrose	Lista Fm	62.5	Shale70% Silt 30%	160
Cretaceous		Chalk	Chalk grp	91	Chalk90% Mar l10%	67
Jurassic	Upper	Humber	Kimmeridge C. Fm.	150.7	Shale (8% TOC) 90% silt 10%	156
Jurassic	Upper	Humber	Kimm/Ribble Sand	151.38	Sandstone (typical)	43
Jurassic	Upper	Humber	Kimm/Avon Sh	152.06	Shale80% (8% TOC) silt 20%	29
Jurassic	Upper	Humber	Fulmar Sands	158.4	Sandstone (arkose, quartz rich)	277
Triassic	Lower	Heron	Smith Bank Fm	248.2	Shale (organic lean, sandy)	142

3. Diagenesis and Quartz Cementation in the Fulmar Formation

3.1. Summary

This study assessed and compared the state of diagenesis, quartz cement distribution, and the temperature and timing of quartz cementation in the Upper Jurassic Fulmar Formation sandstones from Clyde, Elgin and Fulmar fields by using a multidisciplinary approach comprising petrographic analysis, high spatial resolution oxygen isotope analysis, basin modelling, and quartz cementation modelling. It was revealed that post-depositional processes such as: mechanical and chemical compaction, mineral grain dissolution, mineral precipitations are the attendant diagenetic processes that have interplayed to alter the original Fulmar Formation sands into sandstones. It was also discovered that macroquartz cements are uniformly distributed but occur in low volumes (< 5 %) in all sample sets. Quartz cement volume in Elgin field at 189°C is comparable to that of Fulmar and Clyde at 130°C and 147°C. This suggests that quartz cementation is controlled by factors other than burial depth and temperature in the studied Fulmar Formation sandstones. Further studies would be required to elucidate the key controls on quartz cementation in these sandstones.

3.2. Introduction

Diagenesis refers to the post-depositional physico-chemical processes such as: compaction, chemical alteration, dissolution and precipitation, that combine to transform sediment into sedimentary rocks (Worden and Burley, 2003; Bjørlykke, 2014). In deeply-buried sandstones, diagenetic study is important for understanding reservoir quality (porosity and permeability) evolution. Recent development has also seen the inclusion of diagenetic studies as a key part of petroleum exploration and production for the assessment and prediction of reservoir quality prior to drilling operations (Worden et al., 2018a).

Sands undergo mechanical grain rearrangement (compaction) at shallow depth due to vertical effective stress from increasing overburden. Depending on depositional facies, chemical processes at shallow burial depth can lead to early precipitation of carbonate or silica during near-surface diagenesis (Morad et al., 2000; Morad et al., 2010; Bjørlykke, 2014). Early carbonate or silica cement would occlude porosity and permeability, but may also lead to the formation of a rigid framework that could restrict further mechanical compaction (Lasocki et al., 1999; Taylor et al., 2015). Post-depositional influx of meteoric water may also lead to feldspar dissolution and precipitation of kaolinitic clay cement (Bjørlykke et al., 1979; Walderhaug, 2000; Worden and Morad, 2000; Morad et al., 2010).

Beyond shallow burial (> 2500m), mechanical compaction becomes less important and sands begin to lose porosity under the influence of chemical drivers. This process reduces reservoir quality through intergranular dissolution and precipitation of minerals (Bjørlykke, 2014). For example, dissolution of quartz at intergranular contacts in quartz-rich sandstones releases silica that precipitates as authigenic quartz cement on free quartz surfaces and occludes available pore spaces. Partial or whole mineral grain dissolution (e.g. feldspar dissolution) may also feature during mid to late burial diagenesis, thus leading to the formation of moldic pores termed “secondary porosity” and precipitation of new products like authigenic illite clays (Worden and Morad, 2000). Minerals may also be altered chemically such that textural evidence of previous phases are preserved or completely changed so that new crystal shapes and sizes are formed (Worden and Burley, 2003).

Many studies have described the diagenesis of the Upper Jurassic Fulmar Formation sandstones (Stewart, 1986; Wilkinson and Haszeldine, 1996; Wilkinson et al., 1997;

Haszeldine et al., 1999; Lasocki et al., 1999; Osborne and Swarbrick, 1999; Hendry et al., 2000; Kuhn et al., 2003; Lee and Parsons, 2003; Wilkinson et al., 2006; Wilkinson and Haszeldine, 2011; Taylor et al., 2015). Two types of authigenic quartz cements have been reported in the Fulmar Formation: microquartz and macroquartz overgrowths (Osborne and Swarbrick, 1999; Taylor et al., 2015). Macroquartz cement is a commonly cited reservoir quality degrader (McBride, 1989; Worden and Morad, 2000). In contrast, microquartz overgrowths are known for their grain-coating effect that help to preserve porosity (Aase et al., 1996; French et al., 2012; Worden et al., 2012; French and Worden, 2013). However, excessive precipitation of microquartz cement can also be deleterious to reservoir quality due to its pore-occluding nature (McBride, 1989).

Apart from authigenic quartz cements, studies have shown that dolomite (Kuhn et al., 2003), and ankerite (Hendry et al., 2000) are the other commonly observed pore-occluding diagenetic cements in the Fulmar Formation. Partially and/or completely dissolved K-feldspar grains and associated authigenic illite clays have also been reported as key diagenetic features in the Fulmar Formation (Wilkinson and Haszeldine, 1996; Wilkinson et al., 1997; Osborne and Swarbrick, 1999; Taylor et al., 2015).

In addition, previous studies that evaluated the temperature and timing of macroquartz cementation in the Fulmar Formation used fluid inclusion analysis (Osborne and Swarbrick, 1999). The limitation of this technique is that fluid inclusions are usually restricted to regions close to the boundary between detrital quartz grains and overgrowths (Walderhaug, 1994a).

This chapter presents the assessment and comparison of diagenesis in the Upper Jurassic Fulmar Formation sandstones from the Clyde, Elgin and Fulmar fields. The Fulmar Formation sandstones have fairly-uniform character but exhibit variable present-day effective stress and temperature regimes across these three fields. Focus was placed on the quartz cement distribution, and the temperature and timing of quartz cementation across these fields. A multidisciplinary approach, comprising petrographic analysis, high spatial resolution oxygen isotope analysis, basin modelling, and quartz cementation modelling, was adopted for this study to answer the following questions,
(a) Which diagenetic processes have interplayed to transform the Fulmar Formation from sand to sandstone?
(b) How is quartz cement distributed within the Fulmar Formation sandstones?

(c) What is the temperature and timing of quartz cementation in the Fulmar Formation sandstones?

Subsequent chapters evaluate the controls, and especially the role played by fluid pressure and vertical effective stress, on quartz cementation in the Upper Jurassic Fulmar Formation.

3.3. Geological Setting

The Central Graben, Moray Firth, and Viking Graben are the main structural elements of the North Sea rift system that were formed principally in response to east-west extensional forces during Callovian to early Kimmeridgian times (Isaksen, 2004). This rift system initiation, together with other successive events including (a) northeast-southwest extensional phase from Kimmeridgian to Volgian (Erratt, 1993), and (b) graben sagging phase leading to the accumulation of thick sediment during the Cretaceous and Tertiary (Isaksen, 2004), have all shaped the geology of the North Sea. The Central Graben is the main trough in the Central North Sea and has a prolific petroleum system. The depositional sequences in the Central Graben have been divided into pre-rift, syn-rift and post-rift sequences. The syn-rift sequences are the Triassic and Jurassic siliciclastic deposits with approximate thickness of 2000m, while the post-rift sequences encompasses around 4500m thick Cretaceous to Holocene sediment (Glennie, 2009).

This study is focussed on the Upper Jurassic Fulmar Formation reservoirs from Clyde, Elgin, and Fulmar fields of the Central Graben in the UK Quadrants 22 and 30 (Figure 3.1). The Fulmar forms the lower part of the Humber group that onlaps the Triassic and Zechstein salt, with age spanning from Oxfordian to late Kimmeridgian (Stewart, 1986). The Fulmar Formation was chosen because: (1) it is the principal reservoir in the Central North Sea (2) it is fairly homogenous across several locations within the Central Graben and (3) the formation captures variable pressure and temperature regimes from the edge of the basin to the centre where the Fulmar thickness is up to 300m (Fraser et al., 2003).

3.3.1. Clyde Field

Clyde is an oil-producing field situated about 290km south east of Aberdeen (Figure 3.1). The field lies in block 30/17B in the UK sector of the Central North Sea, marked by a NW-SE trending parallel–subparallel faulting system, and flanked by the Central Graben to the east and the Auk Ridge to the west. The field experienced two crustal

extension events: Permian-Early Triassic crustal extension and the Late Jurassic crustal extension (Stevens and Wallis, 1991). These two rift phases exerted great influence on the sediment deposition in the Clyde area. The depositional sequences have been divided into the syn-rift and the post-rift sequences (Stevens and Wallis, 1991). The syn-rift sequences in the order of succession are: Devonian Continental Deposits, Permian Rotliegende Sands, Zechstein Evaporites, Triassic Red Beds, Late Jurassic Fulmar Sands, Kimmeridge Clay Formation and the Early Cretaceous Cromer Knoll Group (Stevens and Wallis, 1991) , and the post-rift sequence in successive order are: Late Cretaceous Chalk and the Tertiary Marine Claystones (Stevens and Wallis, 1991). The main petroleum systems elements in the Clyde area include the Kimmeridge Clay Formation, which doubles as a source and seal lithology, and the Late Jurassic shallow marine Fulmar sands (Turner, 1993). The average pore pressure, vertical effective stress, and temperature of the Fulmar reservoir in the Clyde area stands at 45MPa, 40MPa and 147°C respectively at a subsea depth of 3750m (Stevens and Wallis, 1991).

3.3.2.Elgin Field

Elgin field lies in the UK sector of the Central Graben, about 240km east of Aberdeen (Figure 3.1). This gas condensate-bearing field straddles Blocks 22/30c, 22/30b and 29/5b of the Central North Sea. The Elgin area experienced extension events in the Triassic and the Late Jurassic/Early Cretaceous prior minor compression phases that spans through Late Tertiary (Eggink et al., 1996; Lasocki et al., 1999). Structurally, the field is an anticline bounded by sub-vertical faults, and also traversed and compartmentalised by sealing NW-SE trending minor normal faults (Lasocki et al., 1999). The general structure of the field has been significantly influenced by halokinesis. The main reservoir in the Elgin area is the Upper Jurassic shallow marine Fulmar sandstone with an average thickness of about 300m, charged with gas condensate mainly from two different sources: the Kimmeridge Clay Formation and the Heather Formation. The Tertiary in the Elgin area was marked by accumulation of thick deposits of the Nordland and Hordaland shales which together with the tight Chalk Group impeded fluid flow, initiated and maintained high formation pressures in the reservoir sands (Darby et al., 1996). The Fulmar Formation reservoir in Elgin field, with an average formation pressure, vertical effective stress, and temperature of 111Mpa, 12.5MPa and 189°C respectively at a subsea depth of 5364m (Lasocki et al., 1999) , is one of the deepest and hottest in the Central North Sea.

3.3.3.Fulmar Field

The Fulmar field is in the UK sector of the Central North Sea, about 275km southeast of Aberdeen (Figure 3.1). The field straddles block 30/16 and 30/11B, but mostly situated in the former. The Fulmar is a triangulated anticlinal dome flanked by the Auk Terrace to the west and the Central Graben to the east (Spaak et al., 1999; Kuhn et al., 2003). The field had experienced three main tectonic activities: halokinesis, basement fault reactivation, and syn – post depositional fault movement (Kuhn et al., 2003). These events have significantly influenced depositional sequences in the Fulmar area. Three distinct faulting systems based on orientation have been recognised in the Fulmar field. These include: a set of NW-SE trending faults, ENE-WSW trending fault, and E-W trending fault (Stockbridge and Gray, 1991; Kuhn et al., 2003). The Late Jurassic shallow marine Fulmar Formation is the main reservoir in the Fulmar area. These reservoir sands are fine-medium grained, moderately- to well sorted, bioturbated arkosic sandstone with localised cross-bedding and ripples (Kuhn et al., 2003). The Fulmar reservoir has an average formation pressure, vertical effective stress, and temperature of 39MPa, 31MPa and 127°C respectively at a subsea depth of 3200m (Mehenni and Roodenburg, 1990). The Kimmeridge Clay Formation is the main source rock, and also forms a seal lithology jointly with the Upper Cretaceous Chalk in the Fulmar area (Kuhn et al., 2003). The Ribble sand and the Avon shale are two members delineated in the lower part of the Kimmeridge Clay Formation in the South Western part of Fulmar field (Mehenni and Roodenburg, 1990; Stockbridge and Gray, 1991; Spaak et al., 1999; Kuhn et al., 2003; Lee and Parsons, 2003).

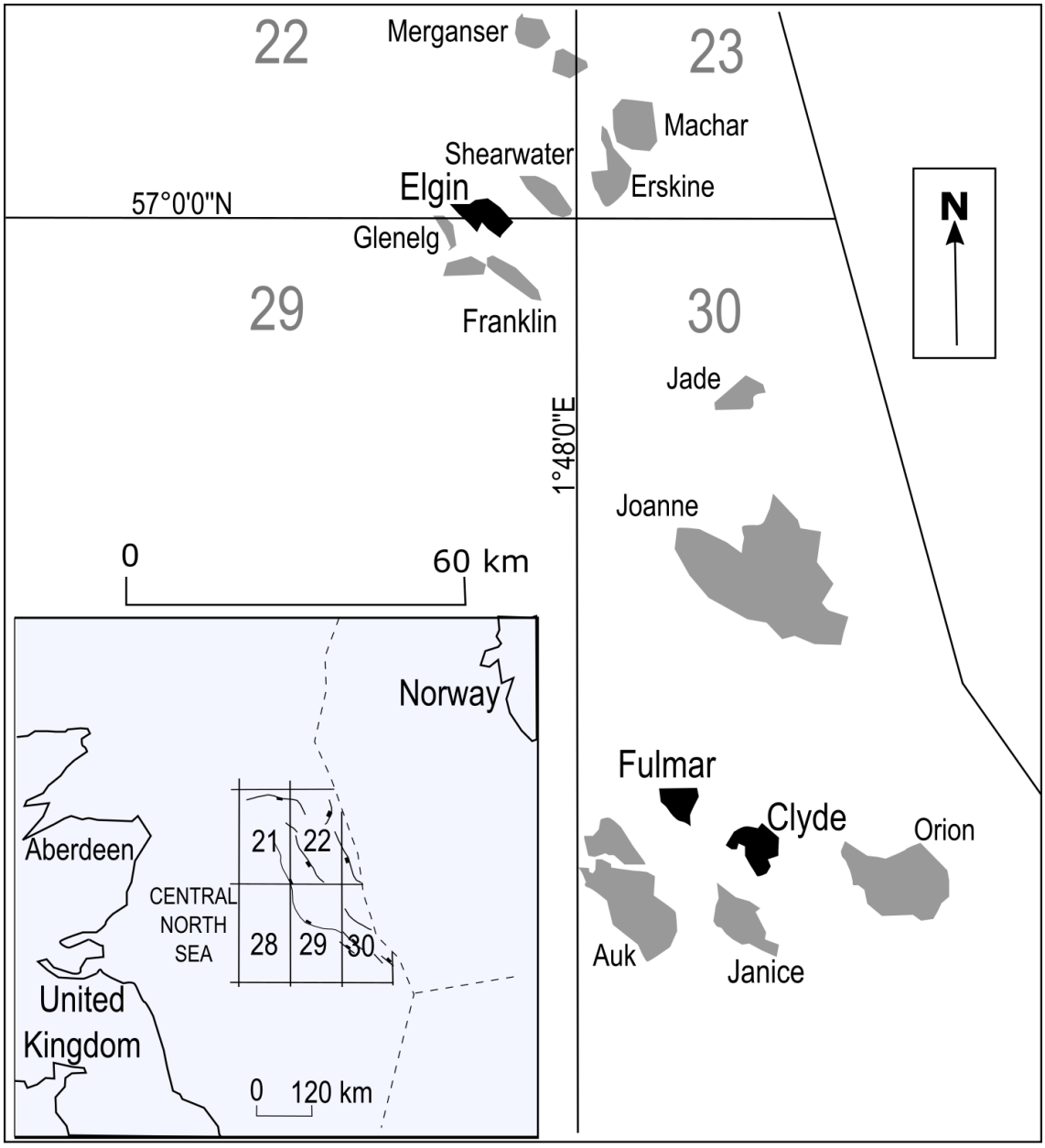

Figure 3.1. Map of the Central North Sea showing the three study locations: Clyde, Elgin and Fulmar fields, and other surrounding hydrocarbon fields

3.3.4. Upper Jurassic Fulmar Formation Sedimentology

The Upper Jurassic Fulmar Formation is the primary hydrocarbon-producing reservoir in many oil fields in the UK sector of the Central Graben. Apart from the northwest of the Elgin field where the Base Cretaceous unconformity (BCU) eroded down to the Fulmar level, the formation (Figure 3.2) is overlain conformably by the Heather and the Kimmeridge Clay Formations (Lasocki et al., 1999).The Pentland Formation underlying the Fulmar is also virtually conformable in the axial part of the Central Graben (Lasocki et al., 1999). The Upper Jurassic Fulmar Formation is a highly bioturbated heterolithic, shallow marine sand-silt deposit (Gowland, 1996), and typically occurs as coarsening-upward succession grading from siltstones into very fine-medium-grained sandstone (Gowland, 1996, Hendry et al., 2000, Lasocki et al., 1999, Taylor et al., 2015, Stewart, 1986).Localised fining-upward successions have also been delineated (Gowland, 1996, Lasocki et al., 1999). The dearth of sedimentary structures due to intense bioturbation, and the influence of syn-sedimentary tectonism and halokinesis created a complicated facies pattern within the Fulmar sandstone (Gowland, 1996, Hendry et al., 2000). Hence, facies characterisation of these sandstones typically requires a more detailed study of lithology, grain sizes, sedimentary structures (where present), and ichnofabrics like *Teichicnus* and *Ophiomorpha* (Gowland, 1996, Taylor and Gawthorpe, 1993). The occurrence of abundant rock-forming siliceous sponge spicules, of the genus *Rhaxella*, have been reported in some intervals within the Fulmar Formation (Gowland, 1996). Gowland (1996) and Taylor et al. (2015) described these *Rhaxella* sponge spicules as the likely source of grain-coating microcrystalline quartz in the Fulmar sandstone. Helium porosities of up to 30% in some deeply buried clean facies indicate that these sandstones are anomalously porous relative to other North Sea sandstones for their depth of burial (Osborne and Swarbrick, 1999).

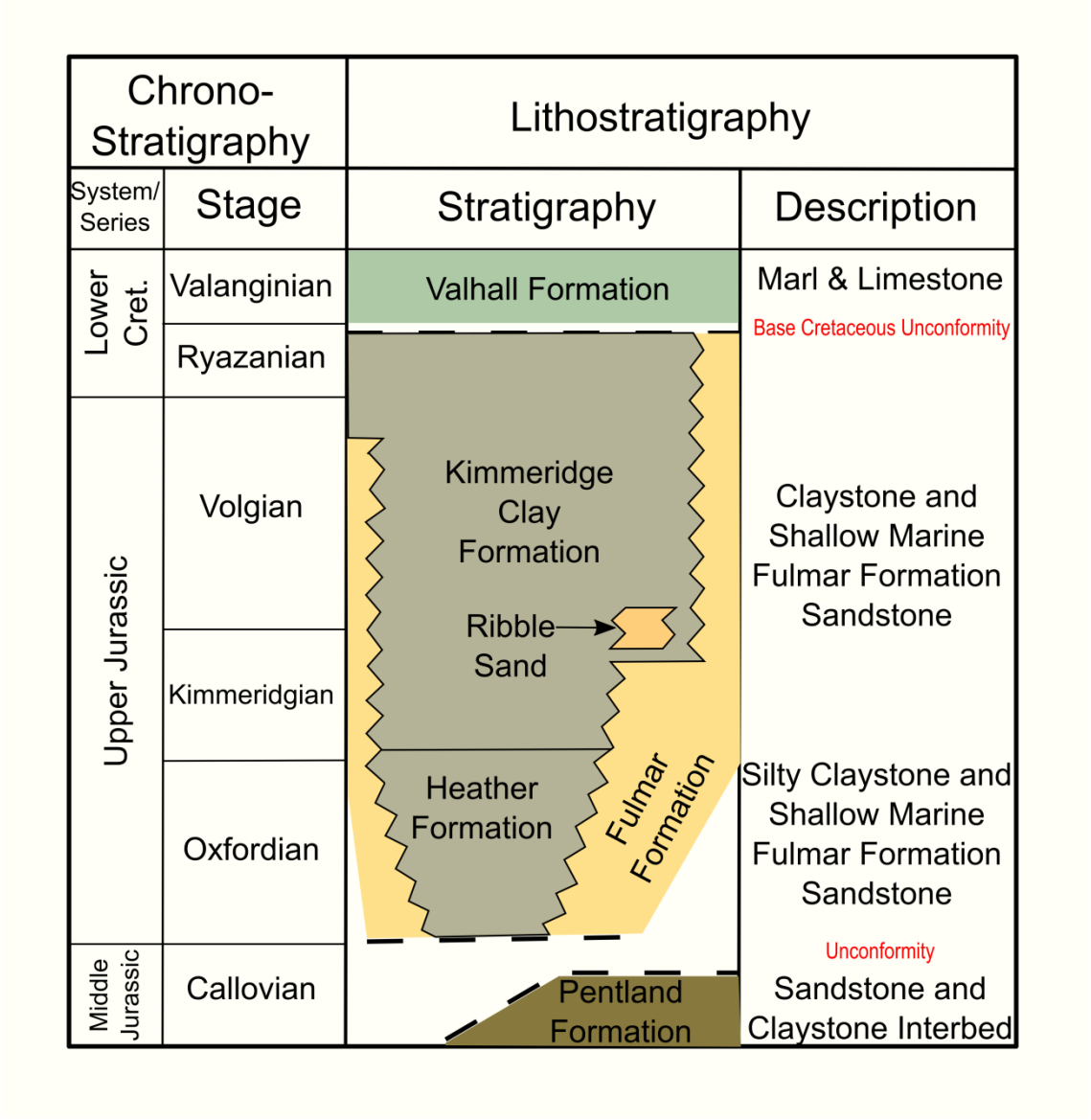

Figure 3.2. Regional Stratigraphy of the Central North Sea from Middle Jurassic to Lower Cretaceous (adapted from Graham et al., 2003).

3.4. Methodology

3.4.1. Sampling

This study was carried out using 60 Fulmar Formation sandstones samples and thin sections from Clyde (well 30/17B-2), Elgin (well 22/30C-G4), and Fulmar (well 30/16-7) fields. 19 samples each were chosen from Clyde and Elgin fields at regular intervals between 3770 to 3790 m true vertical depth subsea (TVDSS) and 5410 and 5440 m TVDSS, and 22 samples were chosen from Fulmar field between 3240 and 3280 m TVDSS. All samples were collected from intervals with the best reservoir quality: the upper shoreface sandstone facies (Figure 3.3, Figure 3.4 and Figure 3.5).

3.4.2. Petrography

Quantitative and qualitative petrographic analyses were carried out on the Fulmar Formation samples and thin sections using both optical and scanning electron microscopy. The optical properties and the nature of framework grains, and their relationship with pore matrix and/or diagenetic cements were assessed under plane and cross polarised light in transmission mode. A Conwy Valley Systems Limited Petrog digital petrography system was integrated with the microscope for quantification works. The setup was used for systematic quantification of the proportion of grain types, grain contacts, grain coats, matrix and cement by making not less than 300 point-count in thin section slides and expressing the result in percentage. The resulting data wer used to select samples for electron microscopy. Since quantification of quartz cement is a major part of the petrographic study, CL petrographic analysis was carried out on 30 carbonate-poor thin sections (10 from each field) representing all range of quartz cements quantified in the studied sandstones during optical microscopy. The CL petrography involved the acquisition of Si element and CL maps (Figure 2.2) over the same areas (3mm x 3mm) for each of the thirty thin sections using energy dispersive X-ray (EDX) and SEM-CL. A grid of 1600 (40x40) square boxes generated from excel was superimposed on the CL map, while the EDX map was used as a control for the identification of mineral grains. Modal analysis was then performed by manual point-counting of both detrital quartz, dissolved quartz and authigenic quartz using the grids to generate 1600 data points per thin section.

3.4.3. Basin Modelling

One –dimensional basin modelling was used to provide insight on how temperature evolved through time in Clyde, Elgin and Fulmar fields. The basin modelling was performed using Petromod software (version 2014.1). This software reconstructs basin

evolution using a forward modelling approach. The geological data used for the modelling were obtained from well composite logs, geological well report, core analysis, and core description reports. The heat flow model input parameters adopted for each of the three fields were defined after Allen and Allen (2005), with the highest heat flow values (Table 2.4) recorded at the peaks of the Permo-Triassic and Upper Jurassic paleo-rifting events recorded in Central North Sea geology. The thermal models were calibrated using measured temperature, and vitrinite reflectance data as paleothermometer (Figure 3.6, Figure 3.7 and Figure 3.8). The time-temperature histories for each of the three fields were subsequently generated for comparison, and for use in quartz cementation modelling.

3.4.4. Quartz Cementation Modelling

Quartz cementation models for Clyde, Elgin, and Fulmar fields sandstones were built using Walderhaug's (1996) quartz precipitation kinetics standard parameters. This involved the use of $1cm^3$ of sandstone and a starting porosity of 26% (approximate porosity at the onset of quartz cementation) . Detrital quartz fractions and grain sizes were estimated from CL petrographic analysis of thin sections. Heating rates were calculated from time-temperature histories generated from basin models constructed using PetroMod (version 2014.1). A more detailed description of the quartz cementation modelling is provided in section 2.4

3.4.5. Oxygen Isotope Analysis

High resolution secondary ion mass spectrometry (SIMS) analysis performed at the WiscSIMS Laboratory in the University of Wisconsin-Madison using a CAMECA ims-1280 ion microprobe (Kita et al., 2009), was used to create profiles of oxygen isotope ratios ($\delta^{18}O$) on quartz overgrowths in three sandstone samples each from Clyde Elgin and Fulmar sample sets. Nine distinct overgrowths, three from each sandstone sample, with thicknesses between 30 and 100 µm were chosen for *in situ* oxygen isotope analysis. Prior analysis, each sample was embedded in a polished epoxy mount alongside grains of University of Wisconsin quartz standard UWQ-1 (Kita et al., 2009). Micro profiles of $\delta^{18}O$ were then measured across each overgrowth using a 3µm spot diameter on the ion microprobe. Bracketing analyses were performed on the quartz standards within the mounts to enable correction of measured $\delta^{18}O$ values to the Vienna Standard Mean Ocean Water (VSMOW) scale and monitor instrumental drift (Kita et al., 2009; Valley and Kita, 2009). A more detailed SIMS analytical procedure is

described in Kelly et al. (2007), Page et al. (2007), Kita et al. (2009), Valley and Kita (2009) and Pollington et al. (2011).

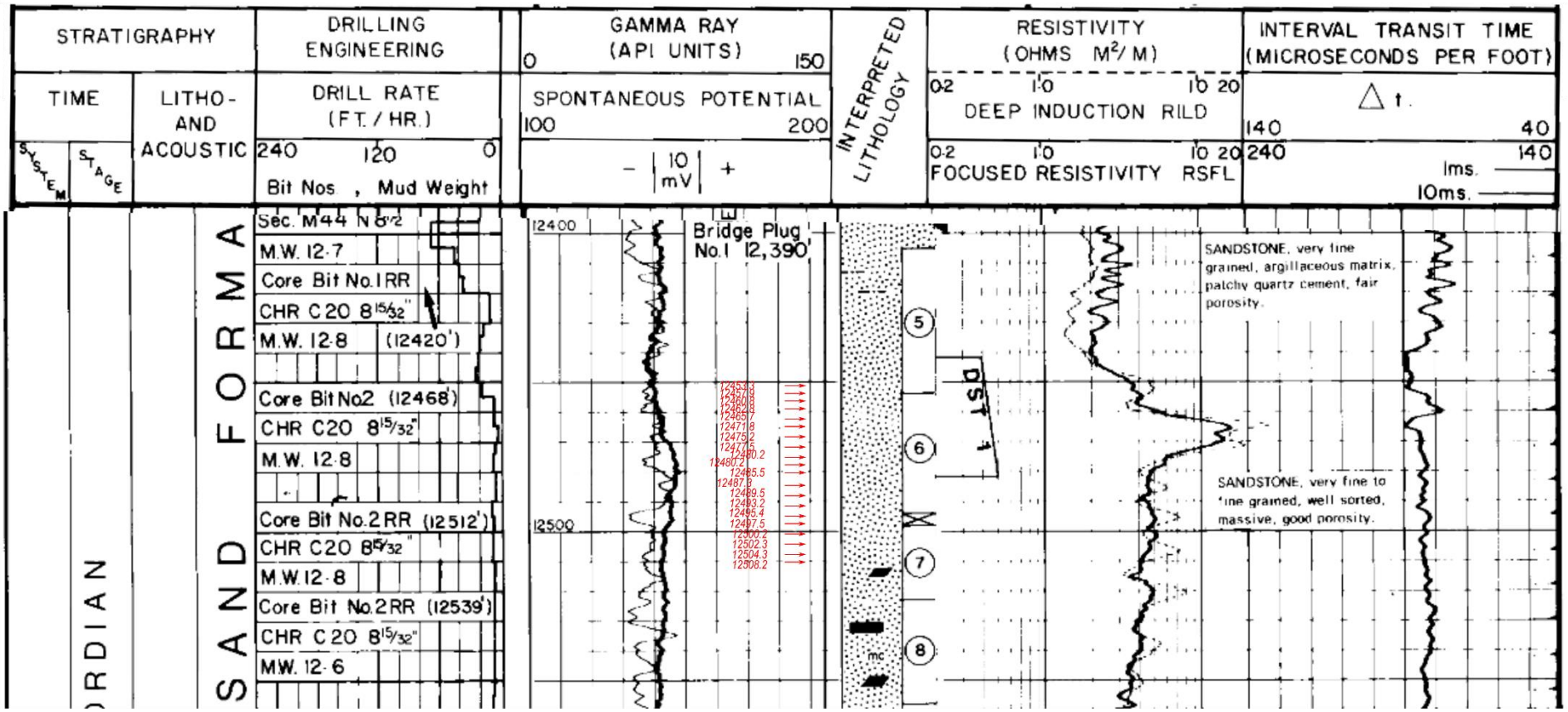

Figure 3.3. Clyde Field (30/17B-2) depth section showing reservoir intervals (red arrows) sampled for analysis

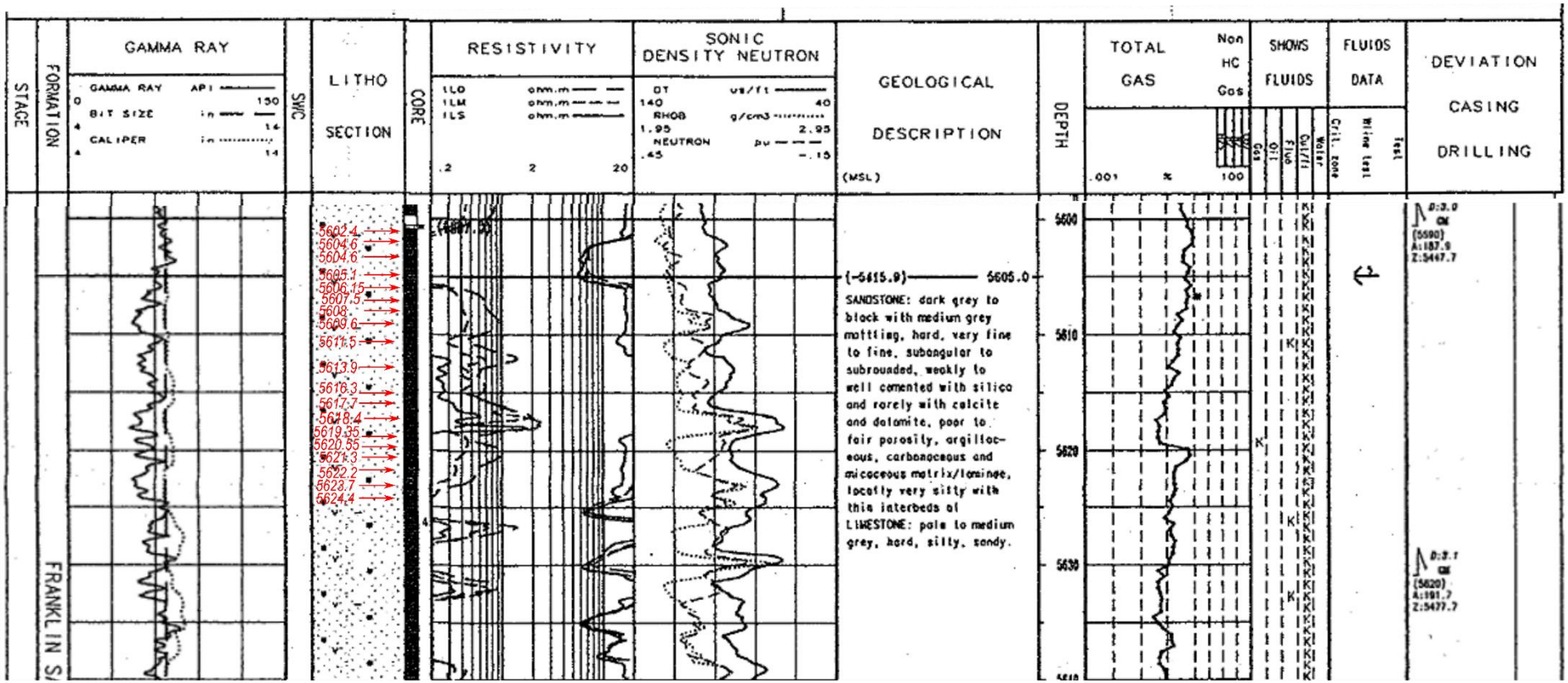

Figure 3.4.Elgin Field (22/30C-G4) depth section showing reservoir intervals (red arrows) sampled for analysis

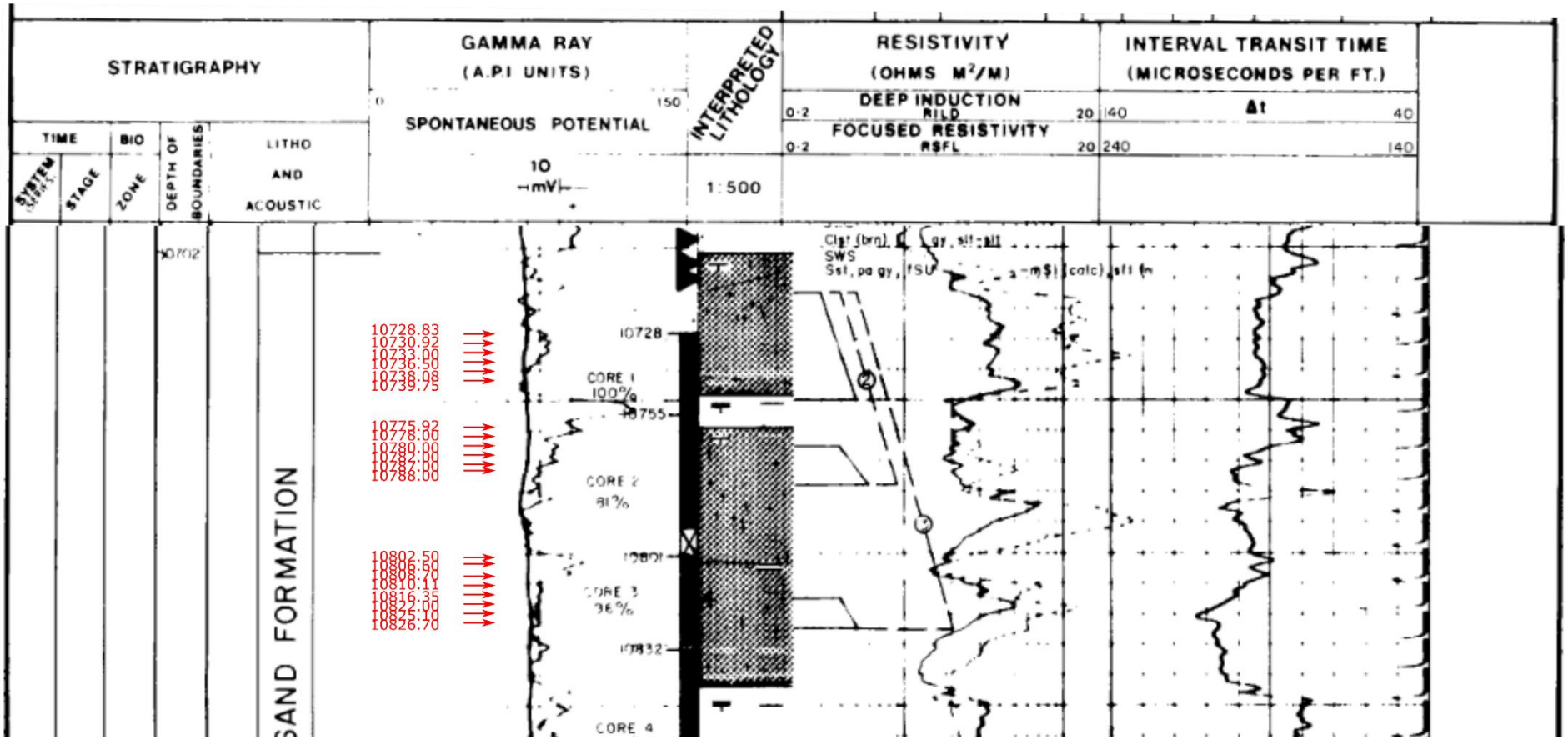

Figure 3.5. Fulmar Field (30/16-7) depth section showing reservoir intervals (red arrows) sampled for analysis

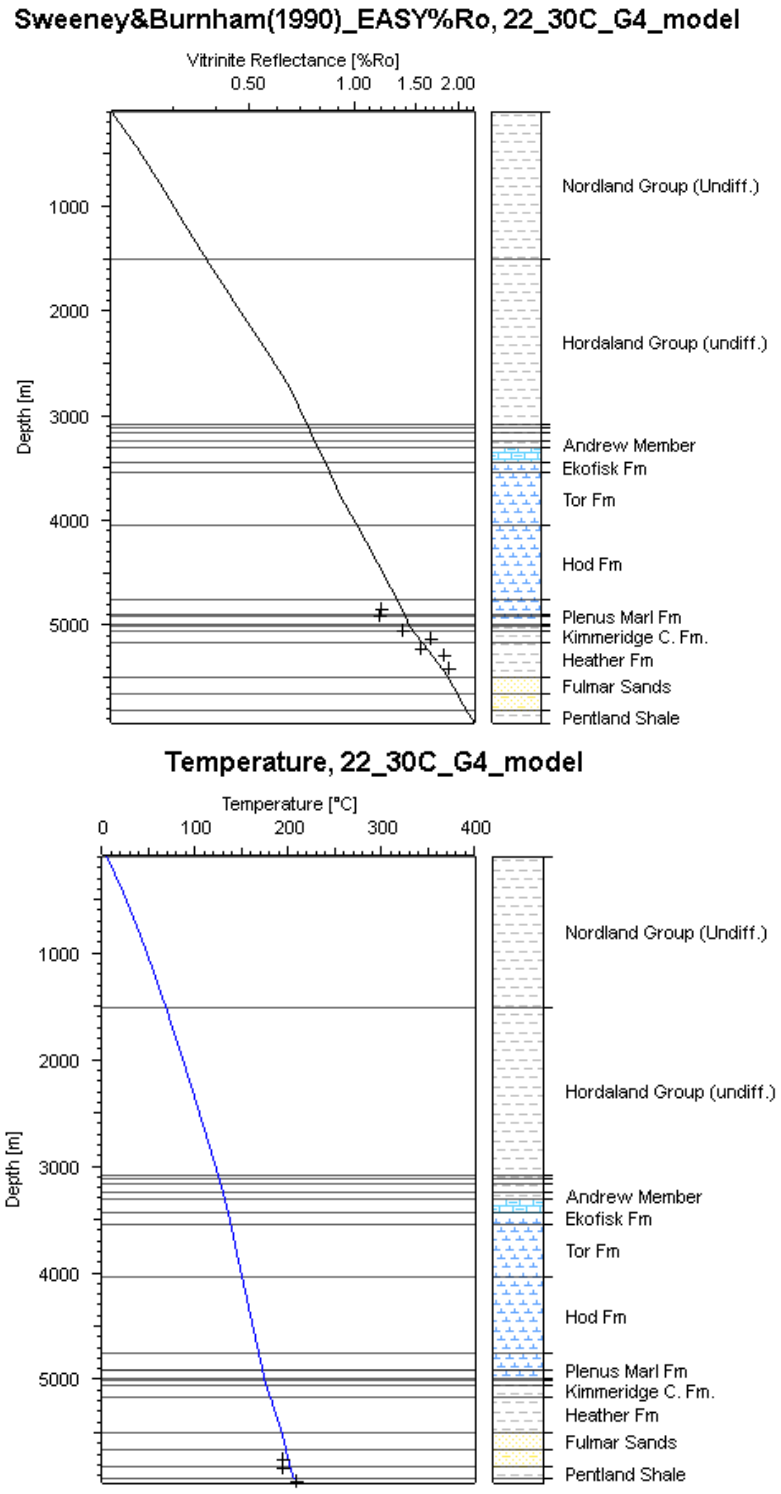

Figure 3.6. Stratigraphic log and temperature calibration for well 22/30C-G4 from Elgin field. Measured temperature and vitrinite reflectance data show good fits to the model curves.

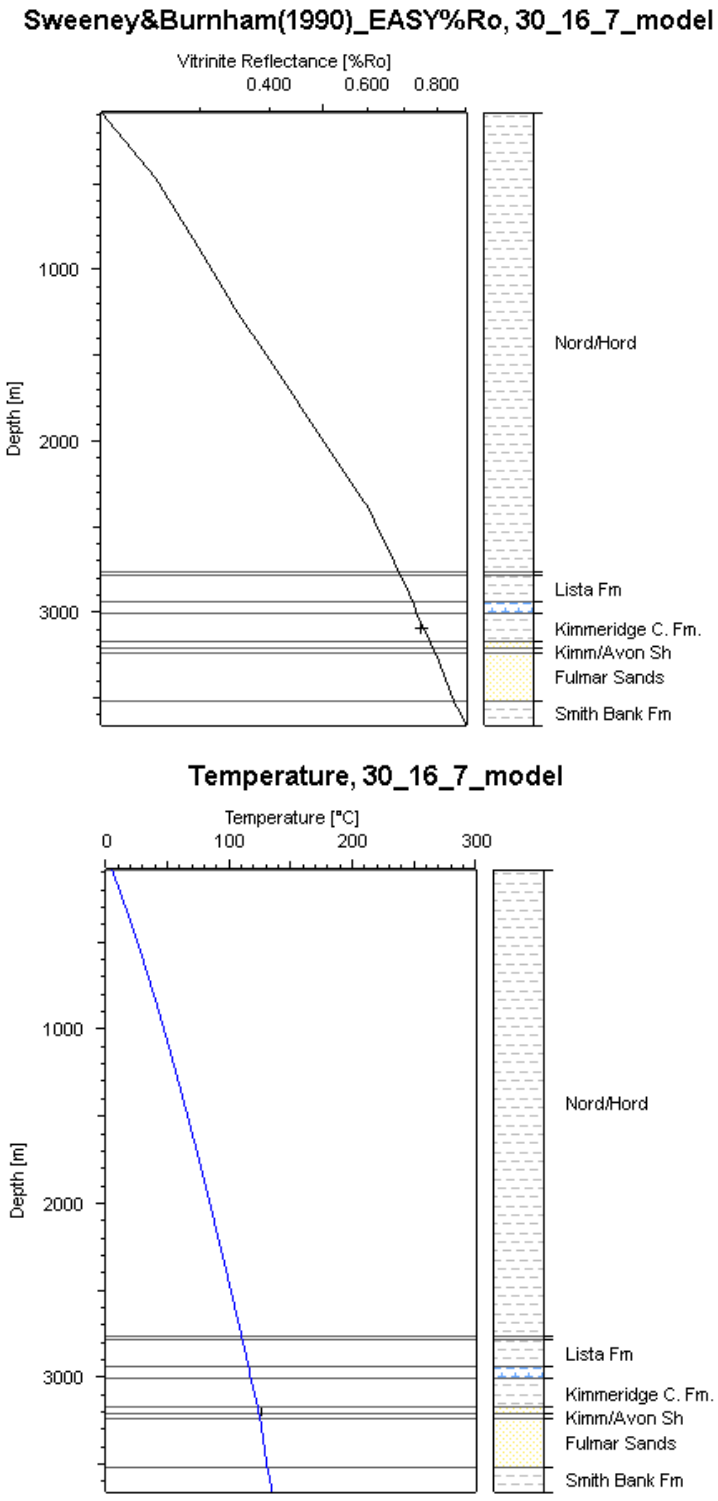

Figure 3.7. Stratigraphic log and temperature calibration for well 30/16-7 from Fulmar field. Measured temperature and vitrinite reflectance data obtained from Mehenni and Roodenburg (1990) show good fits to the model curves.

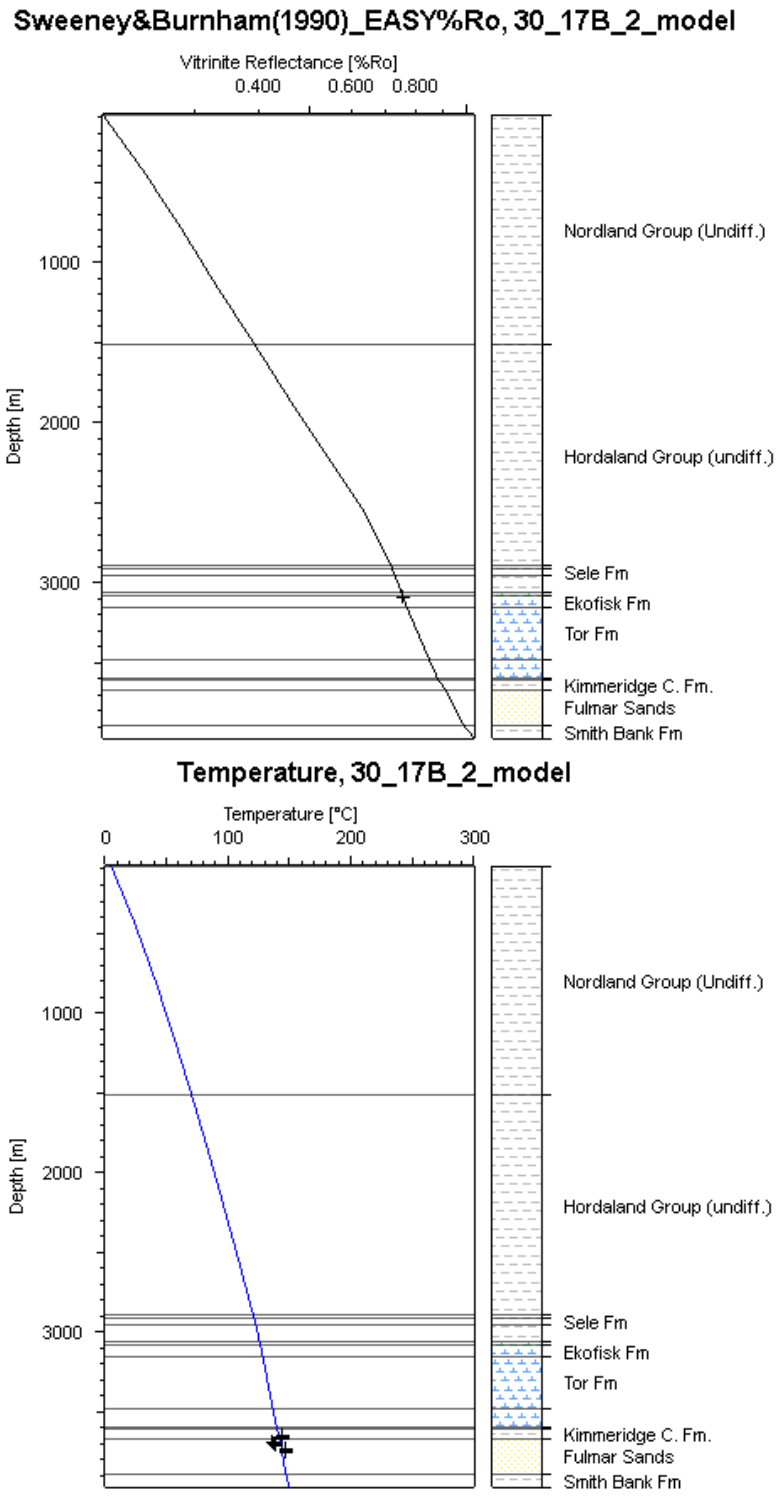

Figure 3.8. Stratigraphic log and temperature calibration for well 30/17B-2 from Clyde field. Measured temperature data show good fits to the model curves. Fulmar field vitrinite reflectance data was adopted for Clyde field.

3.5. Petrographic Observation

3.5.1. Rock Classification and Grain Size Analysis

The ternary plots constructed using data generated from standard petrographic analysis of sixty Upper Jurassic Fulmar sandstone thin sections from Clyde, Elgin and Fulmar fields summarise the bulk percentage compositions of their three main mineral grains; quartz, feldspar and lithic fragments. Data from all locations plot in the sub-arkosic to arkosic region (Figure 3.9) indicating these sandstones are mineralogically immature. The average feldspar contents for these samples are above 20% of the bulk samples, and lithic fragment fractions are low to negligible. These sandstones have sub-angular to sub-rounded grain shapes and well sorted. Initial grain sizes (original grain sizes at deposition) measured from CL petrographic data ranges from 0.062 – 0.411 mm (average 0.180 mm) for Clyde, 0.063 - 0.360 mm (average 0.156 mm) for Elgin, and 0.046 – 0.530 mm (average 0.207 mm) for Fulmar. The limited grain size variability of these sandstones is obvious on the grain size graph (Figure 3.10) with most sandstones being fine grained.

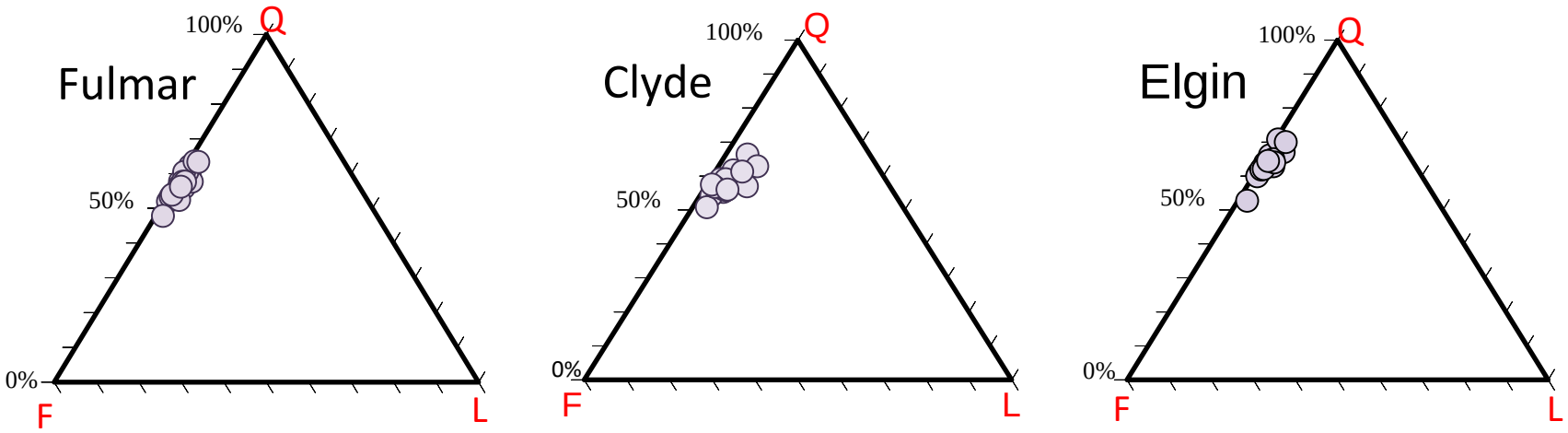

Figure 3.9. Quartz, Feldspar & Lithic fragment (QFL) ternary plot for the analysed Upper Jurassic Fulmar Formation samples from Clyde, Elgin, and Fulmar fields showing that samples are arkosic sandstones. Feldspar fraction represents only present-day composition, as dissolved feldspars (intragranular porosity) were not considered

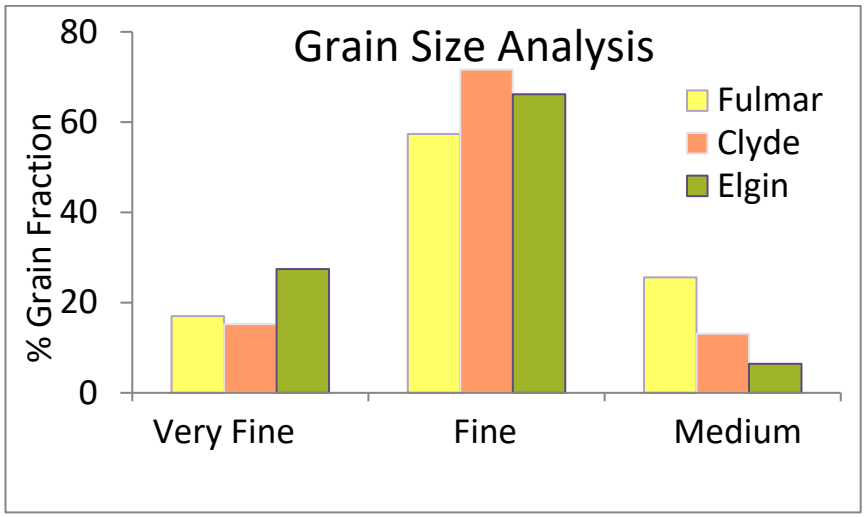

Figure 3.10. Grain size plot for the Upper Jurassic Fulmar sandstones from Clyde, Elgin and Fulmar field, showing most grains plotting in the fine-grained band

3.5.2. Porosity, CoPL, and CePL

Petrographically quantified porosities in analysed Upper Jurassic Fulmar Formation sample sets are of two types: intergranular and intragranular porosities. The total optical and intergranular porosities (Figure 3.11) average 13.8 and 12.9% in Clyde samples; 14.3 and 11% in Elgin samples; and 18.6 and 18.5% in Fulmar samples. Intragranular porosities were estimated as visible porosities within partially or wholly dissolved mineral grains (e.g. feldspars) during quantitative petrographic analysis. Intragranular porosity averages 3.3 % of bulk samples in the Fulmar sandstones from Elgin field compared with the 0.9 % in Clyde and 0.1 % Fulmar fields, thus suggesting that feldspar dissolution may be higher with burial depth and temperature in the Fulmar Formation (Wilkinson and Haszeldine, 1996). The wider range of porosity in the Elgin sample set, compared to Clyde and Fulmar sample sets (Figure 3.11), is a reflection of the influence of carbonate cementation (low end) and feldspar dissolution (high end) on porosities in these sandstones. Helium porosity in these sandstones also average 24% for Clyde, 22% for Elgin, and 30% for Fulmar. Comparison of these data with Ramm et al. (1997) porosity-depth trend for normally compacted sands shows that the studied sandstones have anomalously high porosity for their current burial depths (Figure 3.12).

Compaction and cementation are the two main porosity-reducing processes during diagenesis. Lundegard's (1992) method for comparing compactional porosity loss (CoPL) and cementational porosity loss (CePL) was used to determine the dominant porosity-reducing process in the analysed sandstones (Figure 3.13). The uncertainties associated with this method include the assumption of initial porosities (45%) and underestimation of compaction due to grain dissolution during burial (Lundegard, 1992). Most data on the graph (Figure 3.13) plots in CoPL zone suggesting that porosity loss in the samples is due mainly to mechanical compaction. Petrographic observations show compaction features such as bent and broken mica flakes and concavo-convex contacts (Figure 3.14). Examination of the few Clyde and Elgin samples plotting in the CePL zone shows the influence of carbonate cement.

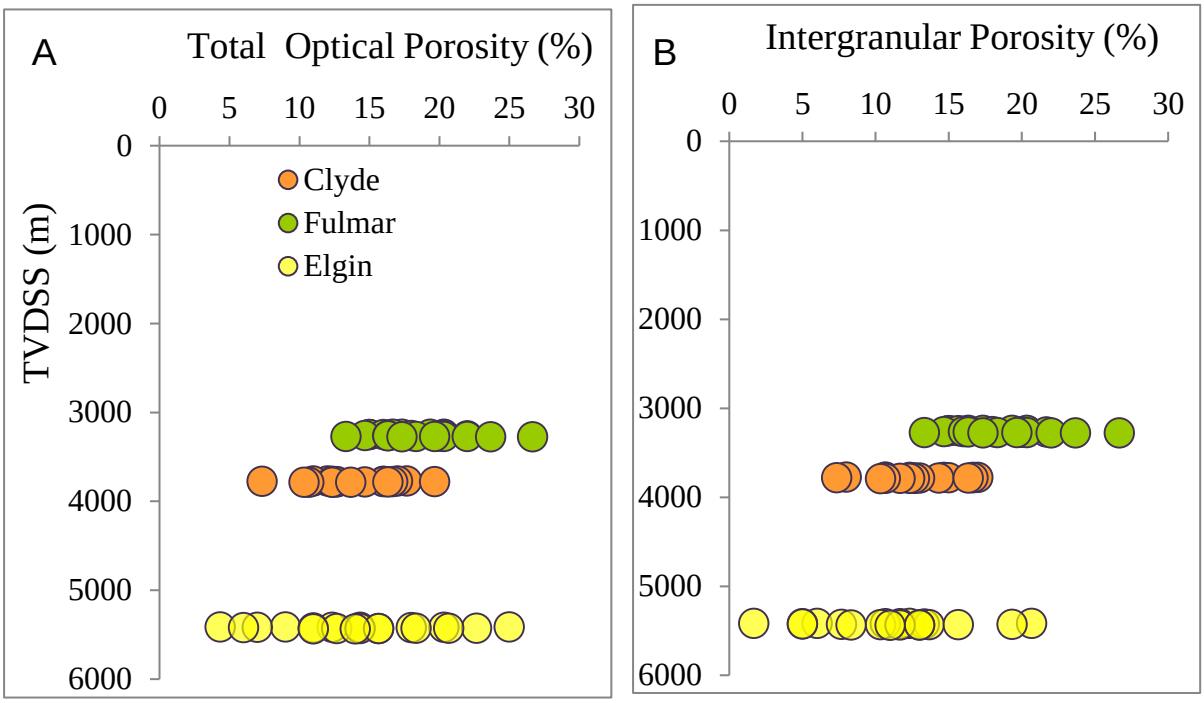

Figure 3.11. Total optical (A) and intergranular (B) porosities for the Upper Jurassic Fulmar Formation sandstones from Clyde, Elgin, and Fulmar fields. The influence of carbonate cementation and feldspar dissolution is seen in the wider range of porosities for the Elgin sample set compared with Clyde and Fulmar sample sets.

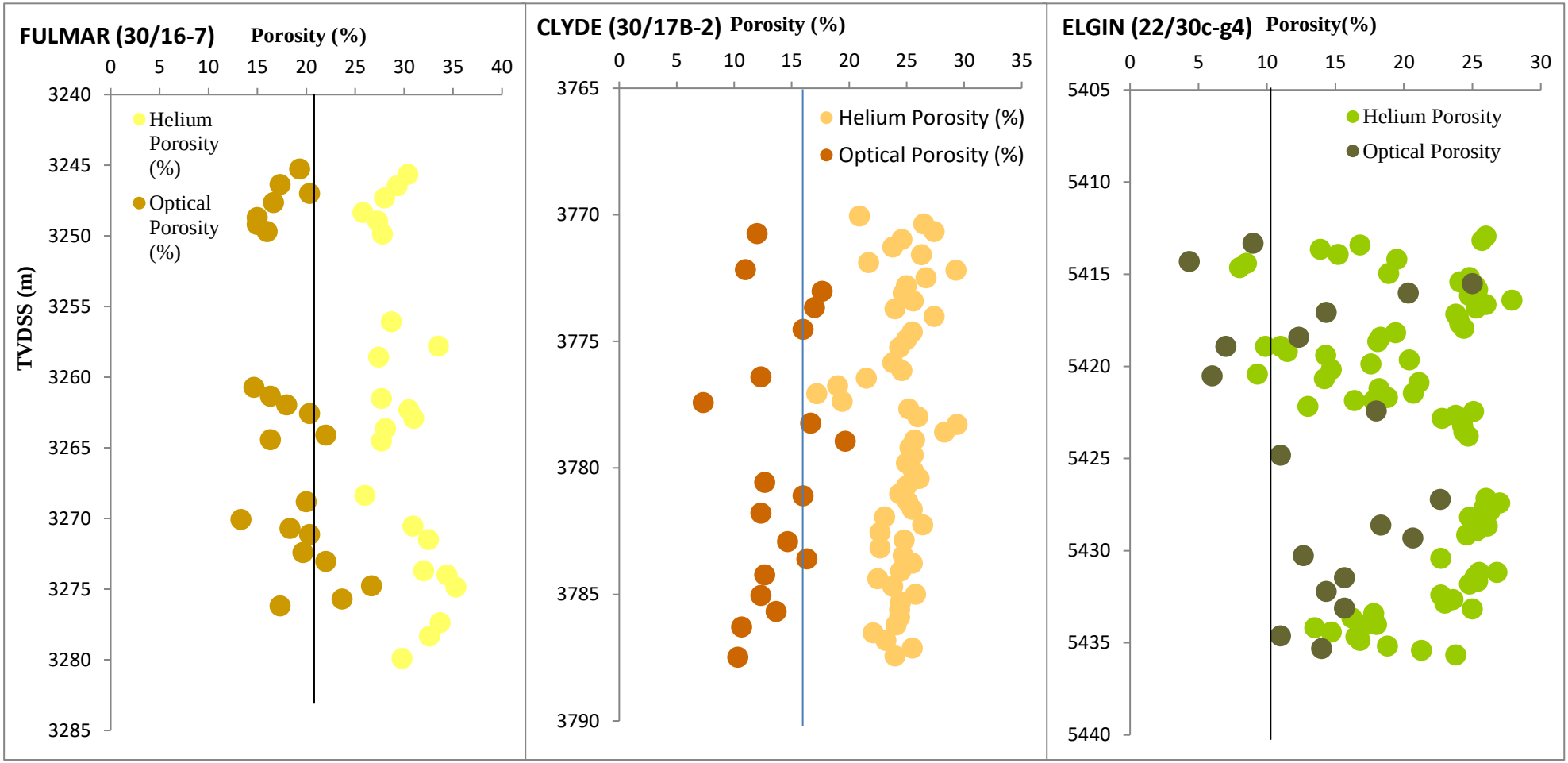

Figure 3.12. Optical and Helium (core) porosity of Clyde, Elgin and Fulmar Fields sample sets with depth relationship to normally compacted sandstones (Ramm et al., 1997) . Plots show that porosity in these sandstones is higher than would be expected relative to depth and normal compaction behaviour of sandstones.

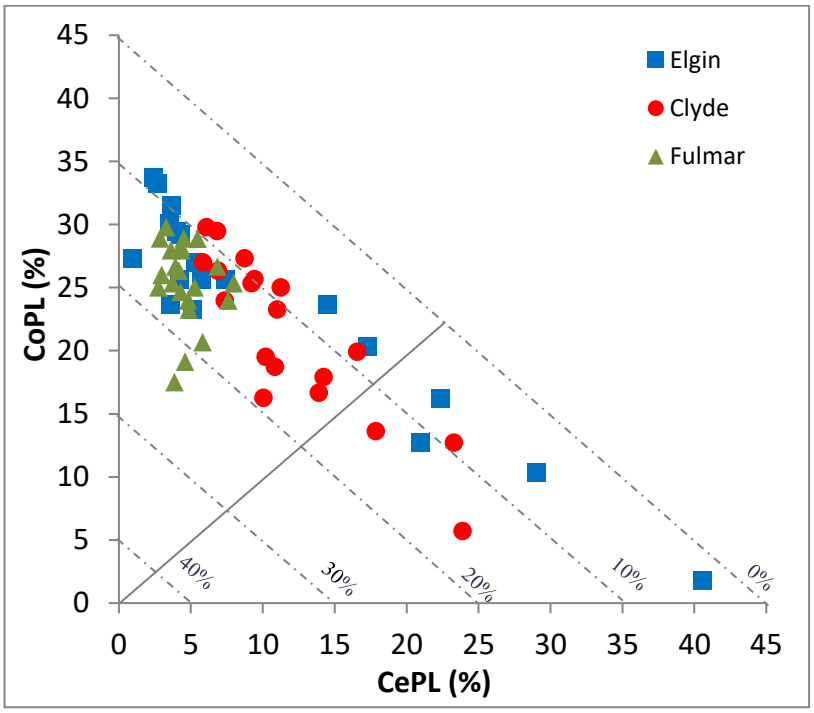

Figure 3.13. Compactional porosity loss (CoPL) versus cementational porosity loss (CePL) for the Upper Jurassic Fulmar Formation sandstone samples from Clyde, Elgin, and Fulmar fields calculated using the method of Lundegard (1992). The diagonal lines represent line of equal porosity loss by compaction and cementation. Porosity loss in the samples is due mainly to compaction. The wide spread observed for Clyde and Elgin data sets is due to the influence of carbonate cement.

3.5.3. Quartz cement

Quartz cementation is the most important diagenetic cement in the analysed sandstones from Clyde, Elgin and Fulmar fields. Standard and cathodoluminescence petrography were used to quantitatively analyse the volume of quartz cement in all sample sets. Two types of quartz overgrowths, microquartz and macroquartz, were observed in all samples. However, their abundance varies across the three sample sets. Microquartz overgrowths in this study refers to thin, randomly oriented, microcrystalline quartz overgrowths with lengths ranging from 1 to 10µm (Aase et al., 1996; French and Worden, 2013). While microquartz overgrowths are commonly well-developed in Clyde and Fulmar sandstone samples, they are nearly absent and poorly developed in the Elgin sample set (Figure 3.15). The microquartz overgrowths are known to behave like grain-coating clays by limiting surface area of detrital quartz available for precipitation of

macroquartz overgrowths (Aase et al., 1996; French et al., 2012; Worden et al., 2012; French and Worden, 2013).

On the other hand, macroquartz overgrowths (interchanged with quartz overgrowth for the purpose of this study) are syntaxial, blocky and in optical continuity with their detrital host grain. Quantitative petrographic analysis from optical microscopy measured low volume of macroquartz cement for the samples from Clyde (3.6%), Elgin (2.0%), and Fulmar (2.8%) fields (Table 3.1). It was difficult discriminating some of the detrital grains and their overgrowths by standard petrography because (1) some mineral grains in the Elgin sample set were coated with bitumen and (2) the clay rims at the boundaries between some detrital quartz and their overgrowths are not well resolved. Also, optical microscopy showed that some samples contain carbonate cement, and these were removed from the sample set since early carbonate can significantly occlude porosity and thus bias quartz cement results. A total of thirty samples, ten from each field, were then chosen for cathodoluminescence (CL) petrography, representing the full range of quartz cement contents. The CL allows discrimination of the detrital quartz from the quartz overgrowths, and also reveals zonation within some of the overgrowths (Figure 3.16). The cross plots of normalised quartz cement volume quantified from CL petrography versus sample depth and temperature are shown in Figure 3.17. The result shows that the average volume of normalised quartz cement, 0.15 in the Clyde sample set, is more than 0.11 and 0.12 in the Fulmar and Elgin sample set respectively.

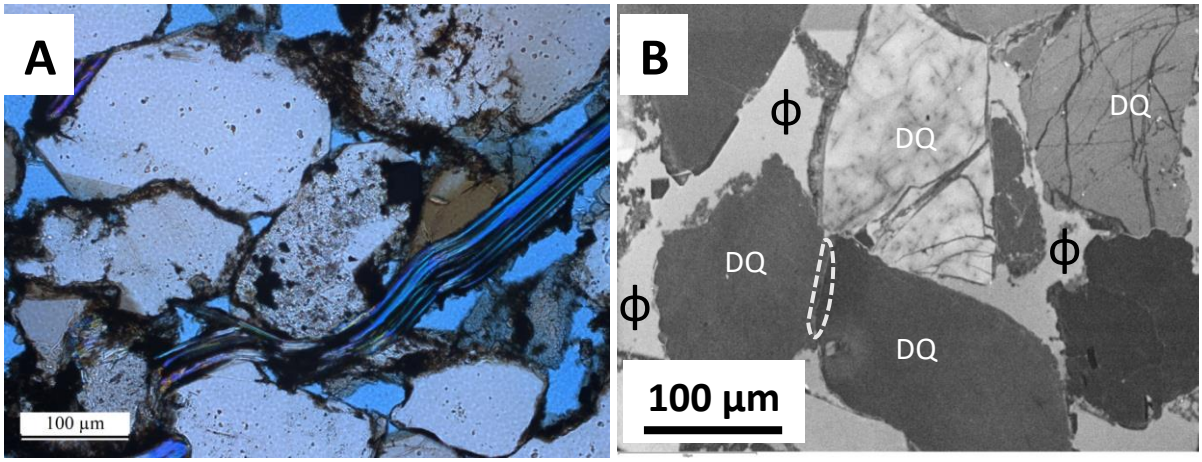

Figure 3.14. Photomicrographs showing compaction and pressure dissolution features in the Upper Jurassic Fulmar Formation A) Compacted sandstone with bent and broken mica flake. B) Dashed outline defining a concavo-convex contact.

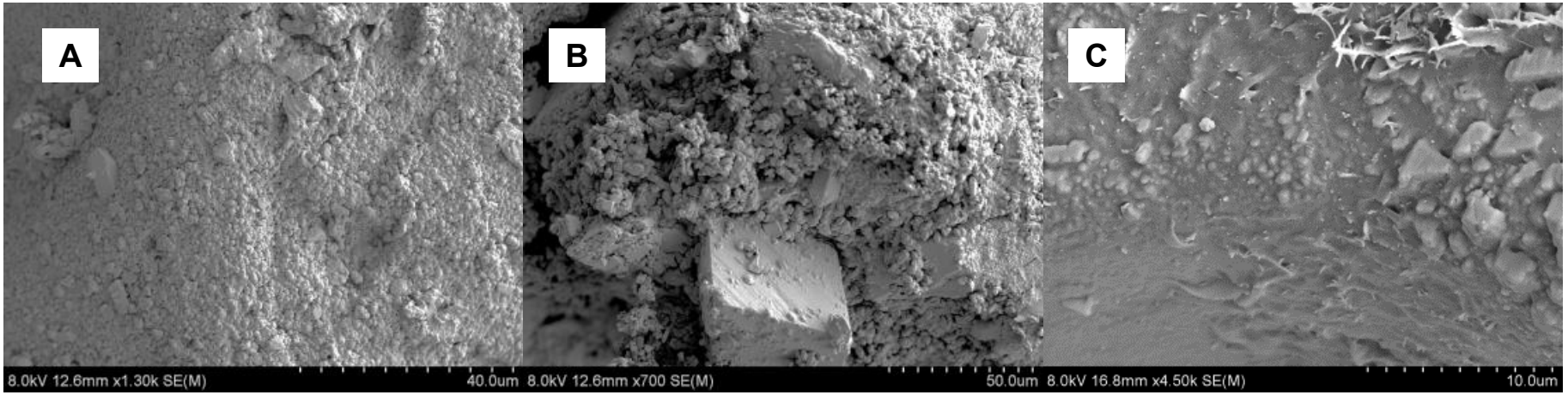

Figure 3.15. SEM images of Upper Jurassic Fulmar Formation sandstones showing microquartz overgrowths in samples from Clyde (A), Fulmar (B) and Elgin (C) fields. Microquartz overgrowths are almost absent and poorly developed in Elgin field.

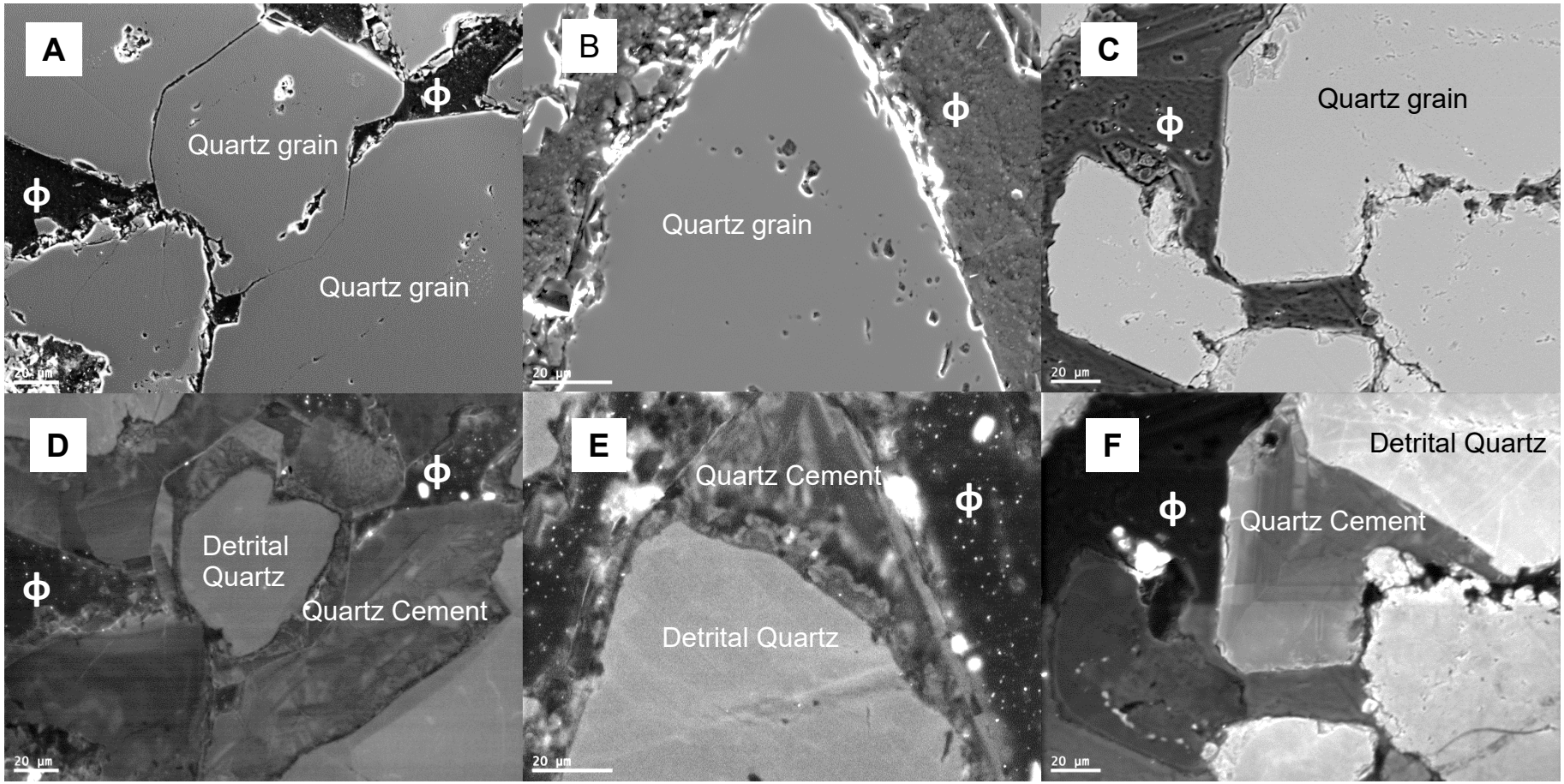

Figure 3.16. Micrographs of Upper Jurassic Fulmar Formation sandstone samples. The pairs AD, B E, and C F shows BSE and corresponding CL images of sample from Clyde, Fulmar, and Elgin fields. Apart from clearly discriminating detrital quartz and quartz cement, some of the CL images also reveal zoning within the quartz overgrowths.

Table 3.1. Summary of petrographic data for the Upper Jurassic Fulmar Formation sandstones from Clyde, Elgin, and Fulmar fields. Sampled population is the same for Clyde and Elgin fields.

	Clyde					Elgin				Fulmar				
	No of samples	Mean	Stan. Dev..	Min	Max	Mean	Stan. Dev.	Min	Max	No of samples	Mean	Stan. Dev.	Min.	Max.
Detrital grain size (mm)	10	0.18	0.06	0.06	0.41	0.16	0.05	0.06	0.36	10	0.21	0.08	0.05	0.53
Quartz (%)	19	38.1	3.9	30.3	44.3	44.2	5.6	32.3	55.7	22	40.5	3.2	34.7	46.7
Feldspar (%)	19	27.3	3.3	19.7	32.7	23.5	3.4	17.3	29.7	22	30.0	3.4	23.7	36.7
Lithic Fragments (%)	19	1.2	0.5	0.0	2.3	1.1	0.7	0.0	2.7	22	1.2	0.6	0.0	2.7
Quartz cement - standard petrography (%)	19	3.6	1.6	0.7	7.0	2.0	1.4	0.3	6.3	22	2.8	1.7	0.0	6.3
Quartz cement - CL petrography (%)	10	4.4	1.1	2.7	5.9	4.6	1.2	2.1	6.4	10	3.71	2.14	0.9	6.9
Quartz cement normalised to detrital quartz	10	0.15	0.03	0.10	0.20	0.12	0.03	0.05	0.15	10	0.11	0.06	0.03	0.21
Carbonate cement (%)	19	8.7	5.1	1.3	21	9.4	12.3	0.0	40	22	1.0	0.5	0.0	1.7
Intergranular porosity (%)	19	13.7	3.0	7.3	19.7	11.0	4.6	1.7	20.7	22	18.5	3.1	14.7	26.7
Intragranular porosity (%)	19	0.9	1.0	0.0	3.0	3.3	1.5	1.0	8.0	22	0.1	0.1	0.0	0.3
Total optical porosity	19	13.8	3.0	7.3	19.7	14.3	5.6	4.3	25	22	18.6	3.2	13.3	26.7
Core Porosity (%)	33	24.4	2.1	17.2	29.4	22.0	5.2	8.5	27.9	23	30.0	2.7	25.8	35.3
Clay matrix (%)	19	2.3	1.4	0.3	5.3	2.8	2.3	0.7	9.3	22	1.4	0.9	0.3	4.3
Intergranular Volume (%)	19	30.5	5.4	21.7	41.7	25.7	7.4	16.0	43.3	22	26.1	3.0	21.7	33.3

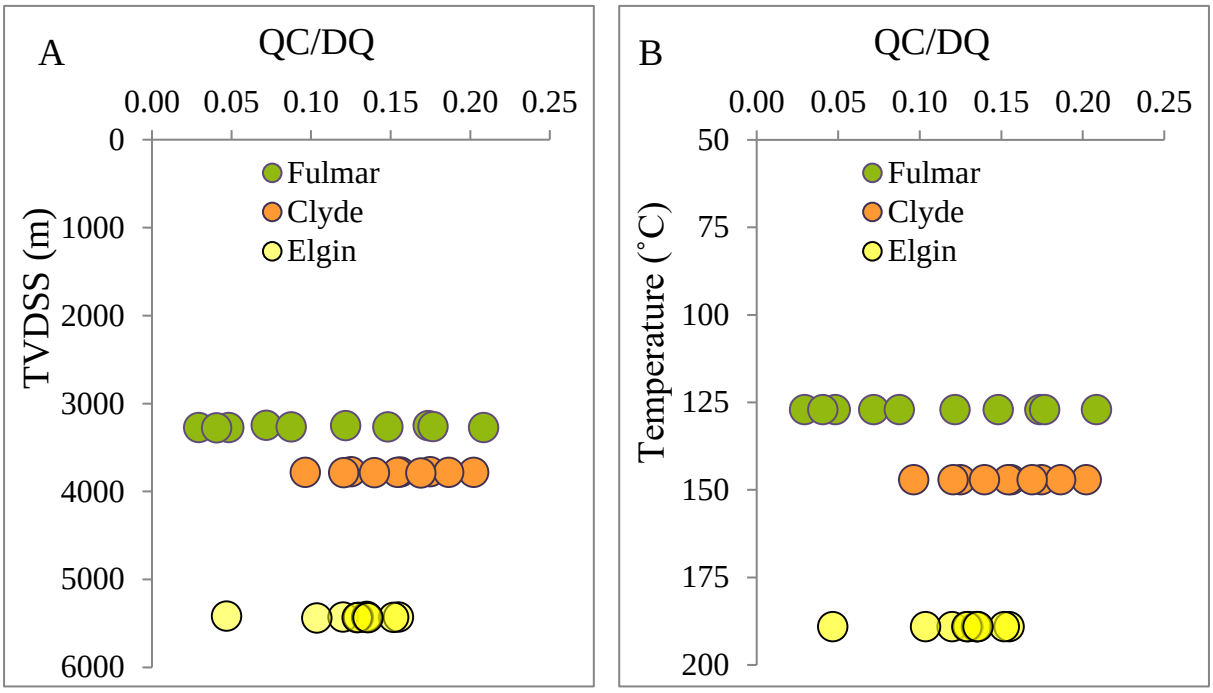

Figure 3.17. Cross plot of quartz cement against depth (A) and temperature (B) for the Upper Jurassic Fulmar sandstones from Clyde, Elgin, and Fulmar fields. The great depth and high temperature experienced by Fulmar Formation sandstones from Elgin field does not translate to larger volume of quartz cement. The volumes of quartz cement (QC) have been normalised to detrital quartz (DQ) content to eliminate bias that may arise from variability of detrital quartz fractions among analysed samples *(see* Houseknecht, 1984; Houseknecht, 1988; Houseknecht, 1991). The wider range of quartz cement volume in Fulmar field sample set is influenced by microquartz grain coat.

3.5.4. Feldspars and Feldspar Dissolution

The samples from Clyde, Elgin and Fulmar fields have high feldspar contents, especially K-feldspar and its polymorphs; microcline and sanidine, and minor plagioclase. Feldspar intergrowths, perthitite, are common in Clyde and Fulmar samples (Lee and Parsons, 2003). Partially or completely dissolved feldspars with initial shapes preserved by clay rims (Figure 3.18) or overgrowths are features common in Elgin, moderate in Clyde, and scarce in Fulmar. Feldspar dissolution is a "mesodiagenetic" process (Morad et al., 2010) that improves reservoir quality by increasing porosity. These features were represented by intragranular porosities during modal analysis of thin sections. Analysis reveals that intragranular porosity from feldspar dissolution makes up about 3.3% of bulk rock volume (23 % of total porosity) in Elgin sample set. The values are much less in Clyde and Fulmar fields where dissolved feldspars only make up 0.9 % and 0.1 % of bulk rock volume respectively. However, it is noteworthy that the volume of porosity from feldspar dissolution may not equal net porosity gain as part of the porosities are offset by products of the reaction; such as neo-formed illite, which may be deposited within the dissolved feldspars or in adjacent intergranular spaces (Taylor et al., 2015), and silica (Osborne and Swarbrick, 1999; Worden and Morad, 2000), which may precipitate as cement on detrital nuclei. Elgin sample set are clay mineral cement-starved despite the volume of dissolved ions from feldspars. Wilkinson and Haszeldine (1996) reported abundant intragranular porosities from feldspar dissolution elsewhere in the Fulmar Formation and attributed this occurrence to an effect of change in bulk chemistry during burial that liberated aluminium and other ions (e.g. potassium), and which were subsequently exported from the system. The general lack of abundant authigenic illite in the Fulmar Formation, also observed in this study, has been attributed to the possible use of the liberated aluminium and potassium ions for smectite illitization in adjacent shale formations (Osborne and Swarbrick, 1999). Pore-reducing authigenic feldspars were observed on clay-free surfaces of some detrital feldspar across all three fields (Figure 3.18). These are orthoclase feldspar overgrowths, and are especially common in the Fulmar field sample sets where they are up to 50microns thick (Lee and Parsons, 2003) and up to 5.7% of bulk rock volume.

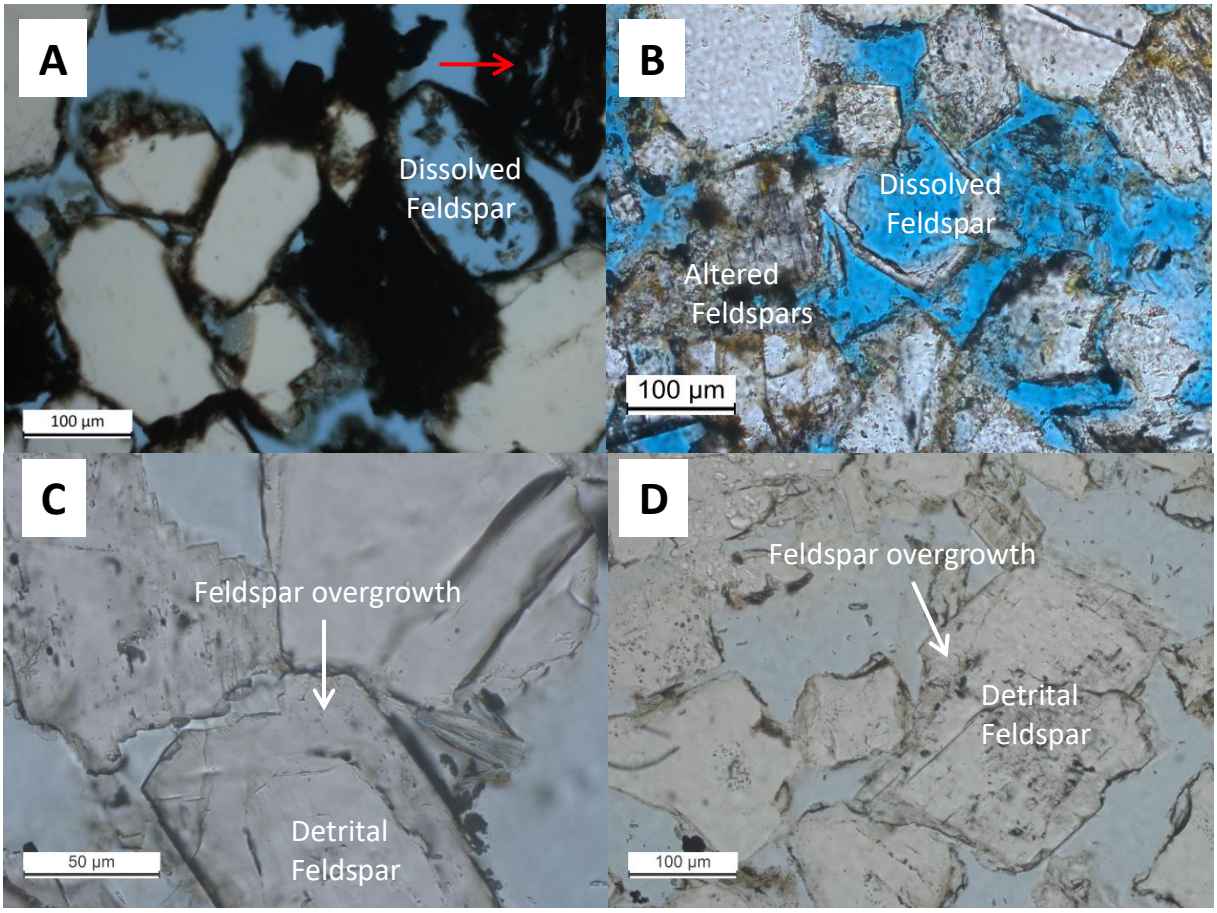

Figure 3.18. Photomicrographs of Upper Jurassic Fulmar Formation sandstone. A) Elgin field sample showing bitumen impregnated clay rim preserving the shape of completely dissolved feldspar and the red arrow point at partially dissolved feldspar impregnated with bitumen. B) Clyde field sample showing altered feldspars, and preserved feldspar overgrowth outlining the shape of dissolved feldspar. C and D show feldspar overgrowths on detrital feldspars in Fulmar field samples.

3.5.5. Clay and matrix contents

The analysed sample sets from Clyde, Elgin and Fulmar are generally clean sands, due to facies screening of samples during selection (i.e. upper shoreface sandstones). Quantitative petrographic analysis (Table 3.1) shows these sample sets have very low clay contents (< 3% of bulk rock volume) occurring in various forms such as: matrix content, pore-lining clays, and grain coats. Pore-lining and grain-coating clays are mainly bitumen-impregnated illite in the Elgin samples. Grain coating illite is the dominant type of grain coatings in the Elgin sample set and is locally found engulfed at the boundary between authigenic and detrital quartz (Figure 3.19). Clyde and Fulmar sample sets, however, have abundant grain-coating microquartz beside illitic clays

(Figure 3.19). Numerous studies have identified illite as the most important grain-coating clay in the Upper Jurassic Fulmar Formation (Wilkinson and Haszeldine, 1996; Darby et al., 1997; Wilkinson et al., 1997; Haszeldine et al., 1999; Lasocki et al., 1999; Osborne and Swarbrick, 1999; Wilkinson and Haszeldine, 2011). This contrasts with some other Mesozoic sandstones in the Central North Sea, like the Triassic Skagerrak Formation, which contain prominent grain-coating chlorite (McKie et al., 2010; Grant et al., 2014; Taylor et al., 2015; Stricker et al., 2016b).

The matrix compositions observed from all three fields' sample sets are mostly illitic clays. Unlike in Elgin field where the illite clays are bitumen-impregnated (Figure 3.19) and locally associated with pyrite, the clay minerals observed in the Fulmar field sample set through SEM-BSE (Figure 3.19) are mixed with mud size micas, carbonate fragments and frambroidal pyrite. Distinct associations were seen in the Clyde sample set where pore-occluding microquartz exhibits sporadic mixing with carbonate fragments and frambroidal pyrite (Figure 3.19). Standard petrographic observations also reveal the presence of minor replacive authigenic brownish (illite) and greenish (chlorite?) clay within intragranular pore spaces in partially dissolved feldspars from Fulmar field samples (Figure 3.19). The occurrence of illite clays in the Upper Jurassic Fulmar Formation has been reported to be the products of smectite-illitization and/or feldspar dissolution (Osborne and Swabrick 1999). The presence of degraded glauconites (Figure 3.19) in the Clyde and Fulmar field samples suggests that some of their clay minerals might have been sourced from this mineral (Stewart 1986).

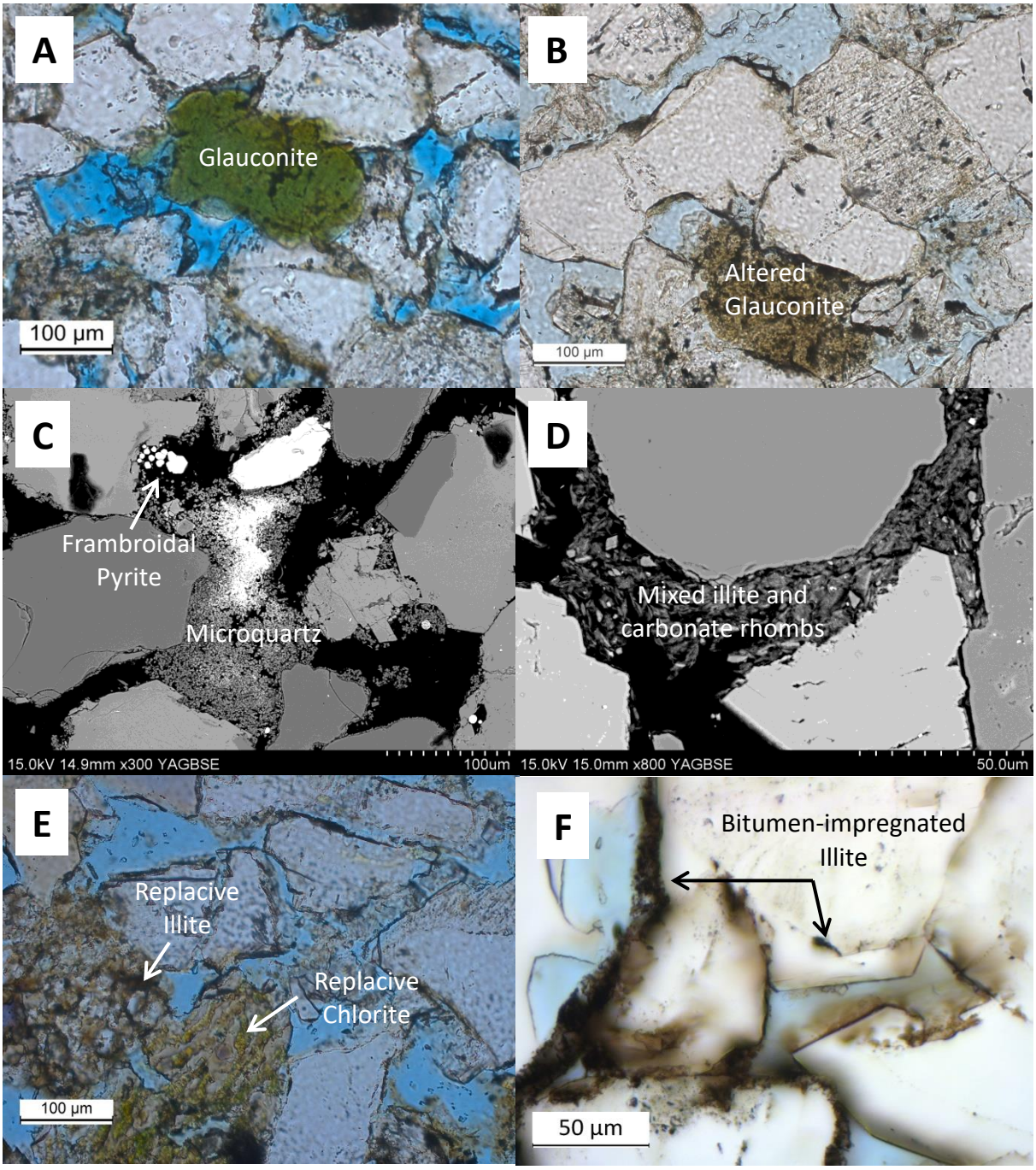

Figure 3.19. Photomicrographs of Upper Jurassic Fulmar Formation sandstones. Clyde and Fulmar fields' samples show presence of glauconite in thin sections (plate A and B). The glauconite in plate B is probably altered. Plate C shows pore-filling microquartz and frambroidal pyrite in Clyde field sample. Plate D shows clay mixed with carbonate fragments in Fulmar field sample. Plate E shows illite and chlorite replacing feldspars in Fulmar field sample. Plate F show some bitumen impregnated illite lining pores, and some other engulfed at the boundary between detrital and authigenic quartz.

3.5.6. Carbonate Cement

Carbonate cement in the analysed sample sets exists in various forms and has compositions that have probably evolved with time and temperature in the study areas. Quantitative petrographic analysis data shows that these cements are scarce and localised in the Fulmar field, less than 1% of sample, but average ~9% in each of the Clyde and Elgin fields. The data also show that carbonate cement are more evenly distributed in samples from Clyde than Elgin. The carbonate cements occur discretely as dolomite or ferroan dolomite and zoned "species" (dolomite core surrounded by ferroan dolomite) in Clyde and Fulmar fields. The forms of these carbonates are similar to those observed by Stewart (1986): as isolated rhombohedral crystals within available pore spaces; as replacive crystals within intragranular pores; as intergranular pore-occluding crystals that partially or completely enclose adjacent grains. Intergranular pore-filling carbonate fragment/mud species were also observed locally in samples from Fulmar field; where they are also associated with moldic porosities that are likely a product of carbonate grain dissolution (Figure 3.20). Carbonate cement seen in samples from high temperature Elgin field vary moderately when compared with those from Clyde and Fulmar fields. A detailed study on the Elgin field carbonate cement was carried out by Hendry et al. (2000). Apart from dolomite and ferroan dolomite, two series of ankerite cements, (Fe-series) and (Fe+Mn-series), were observed in the Elgin samples. In this study, the Fe-series is distinguished from ferroan dolomite based on their Fe/Mg ratios. These cements generally exhibit characteristic carbonate cleavages, and their main textural characteristics and compositions revealed from SEM-BSE and EDX include: irregular mosaic of multi-coloured crystals (colour influenced by compositional variation) of dolomite; ferroan dolomite and ankerite (Figure 3.20); ankerite micro-concretions with concentric euhedral overgrowths displaying colour contrasting regular alternations of ferroan dolomite and ankerite, and terminating outwardly in euhedral calcite overgrowth (Figure 3.20); mottled texture ankerite with colour variation (Figure 3.20) depicting subtle compositional variations (Hendry et al., 2000); and rhombohedral (Fe) ankerite crystals with light coloured planar overgrowth of (Fe+Mn) ankerite (Figure 3.20). These carbonates are either in isolation within available pore spaces or as pore occluding cement completely destroying macro-porosity across large area, and replacing partially assimilated adjacent grains and intragranular pores within partially or completely dissolved detrital grains (Figure 3.21).

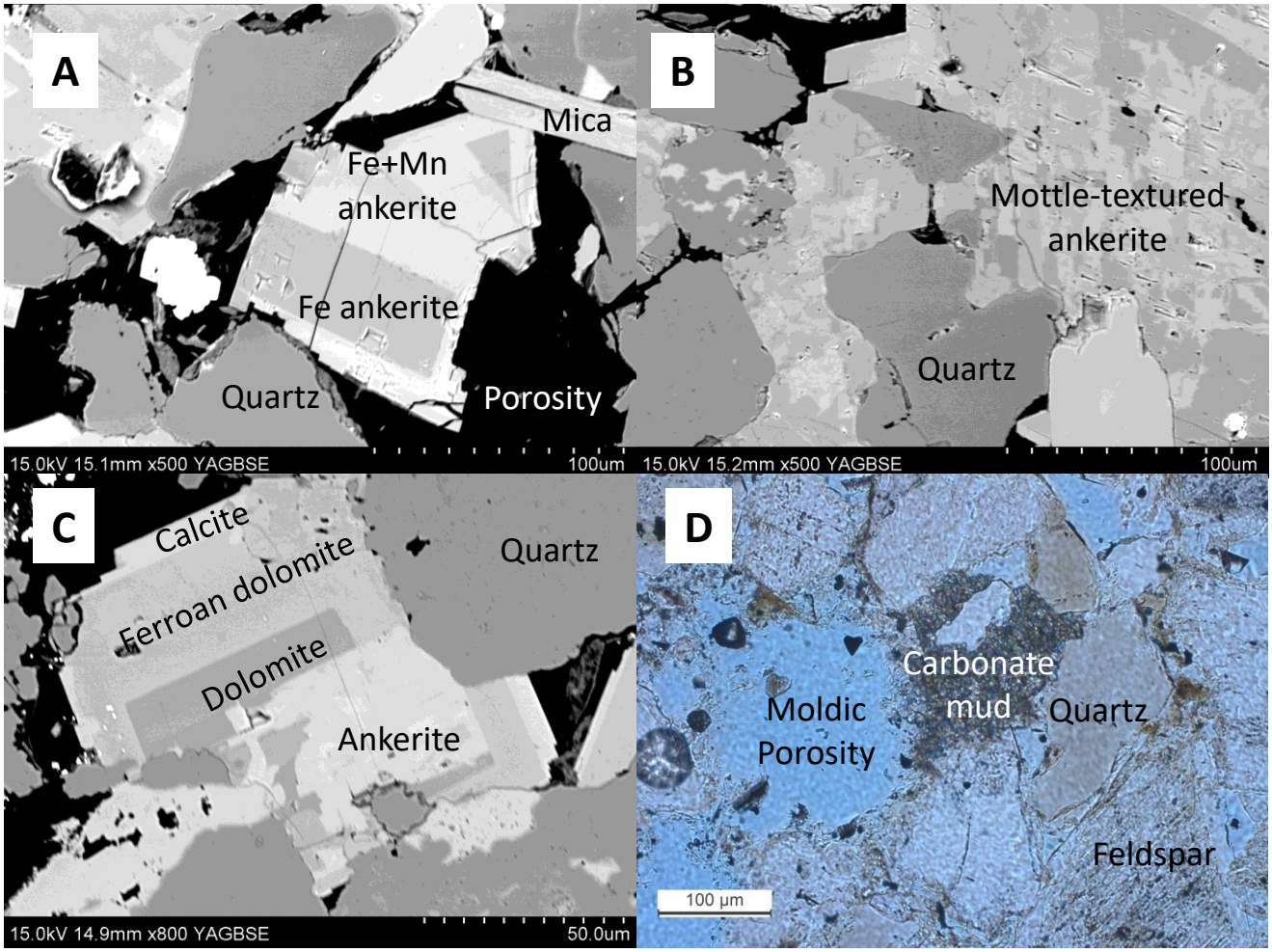

Figure 3.20. Photomicrograph of Upper Jurassic Fulmar formation sandstones. A) BSE image of Elgin field sample showing zoned ankerite occupying intergranular pore space. B) BSE image of Elgin field sample showing mottle-textured ankerite completely occluding macro-porosity. C) BSE image showing of Elgin field sample ankerite overgrown by zoned carbonates with euhedral terminations. D) Optical petrographic image of Fulmar field sample showing carbonate mud/fragment adjacent to a secondary moldic porosity which is probably the product of carbonate dissolution.

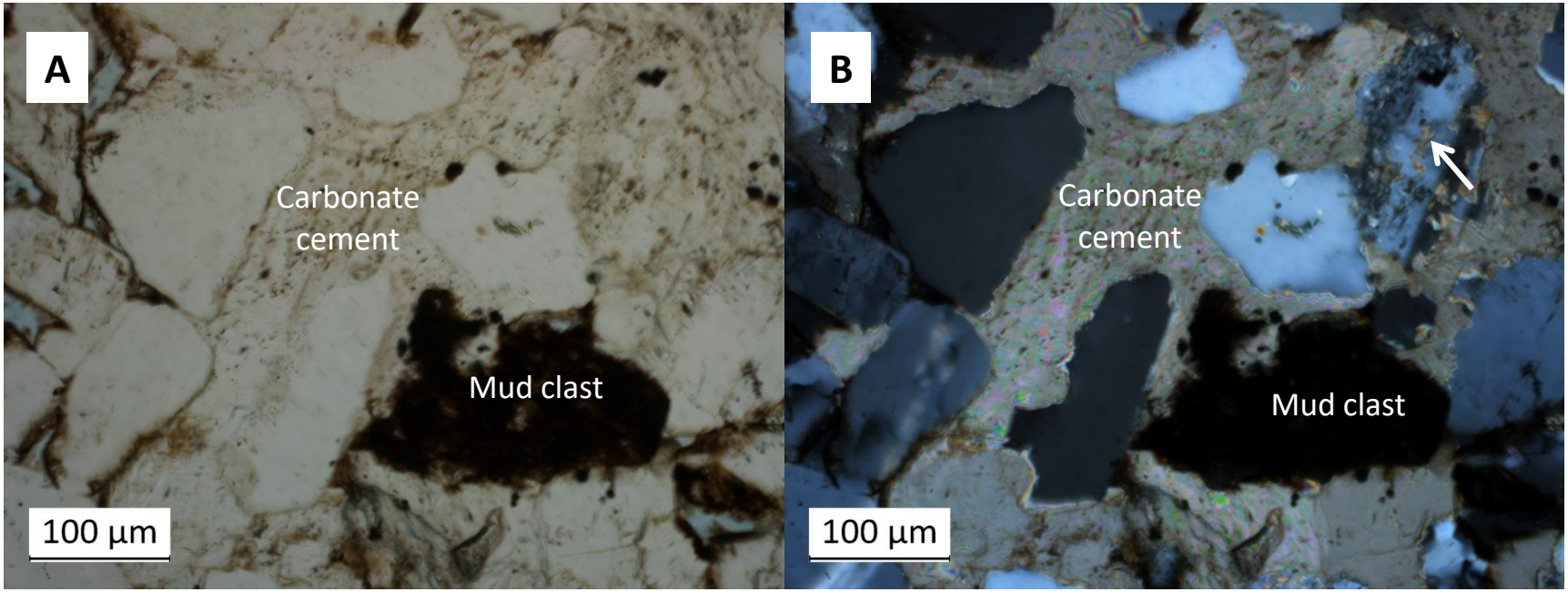

Figure 3.21. Plane (A) and crossed (B) polarised light photomicrograph of Upper Jurassic Fulmar Formation sandstones from Elgin field showing porosity destruction by carbonate (Ankerite?) cement. Carbonate can be seen replacing partially dissolved plagioclase feldspar (white arrow in plate B)

3.6. Time - Temperature Histories and Cementation Models

Thermal history modelling for the Upper Jurassic Fulmar Formation sandstones from Clyde, Elgin, and Fulmar fields (Figure 3.22) show that sandstones from Elgin experienced temperatures above 80˚C (classic quartz cementation threshold) for over 90My compared with the 46My and 43My for Clyde and Fulmar fields. The heating rates and time-temperature segments calculated from the thermal history for each field (Table 3.2) were incorporated into the quartz cementation model using Walderhaug (1996) precipitation kinetics. The model output (Figure 3.23) predicted 26% quartz cement volume for Elgin, 16.4% for Clyde, and 14% for Fulmar. These models consider only the detrital quartz fraction of the sandstones; and assumed a relatively clean quartz surface area.

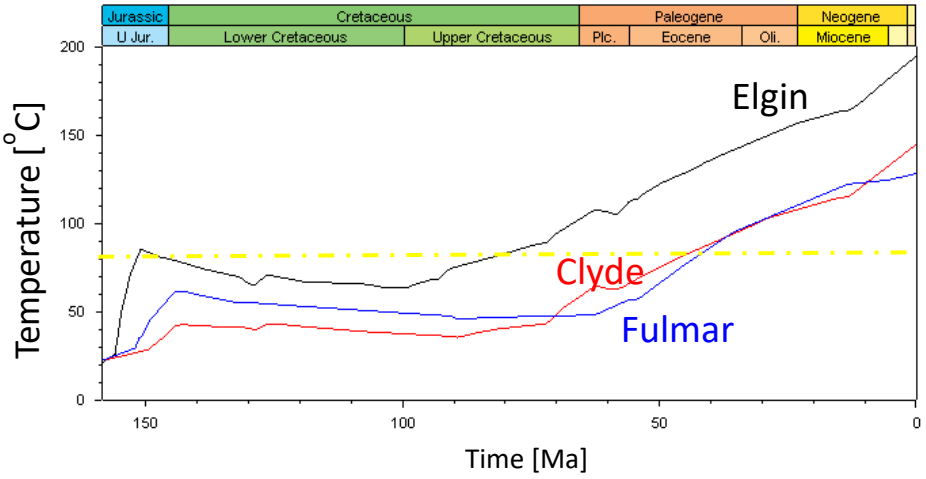

Figure 3.22. Temperature history reconstructions for the Upper Jurassic Fulmar Formation from Clyde, Elgin, and Fulmar fields using Petromod (version 2014.1). Yellow dashed line is showing quartz cementation threshold temperature at 80ºC

Table 3.2. Calculated heating rates and linear time-temperature segments from 80˚C threshold temperature to Present-day for the Upper Jurassic Fulmar Sandstones from Clyde, Elgin, and Fulmar fields

Time Segment	Clyde Time (My)	Heating rate (˚C/My)	Fulmar Time (My)	Heating rate (˚C/My)	Elgin Time (My)	Heating rate (˚C/My)
S1	-	-	-	-	1.0	6.9
S2	-	-	-	-	3.0	-1.2
S3	-	-	-	-	1.0	-1.0
S4	-	-	-	-	1.0	-0.7
S5	-	-	-	-	4.0	0.8
S6	-	-	-	-	5.0	0.9
S7	-	-	-	-	3.0	0.6
S8	-	-	-	-	1.0	2.6
S9	-	-	-	-	1.0	2.4
S10	-	-	-	-	7.0	1.8
S11	-	-	-	-	1.0	0.5
S12	-	-	-	-	2.0	-0.6
S13	-	-	-	-	1.0	-1.0
S14	-	-	-	-	1.0	0.1
S15	-	-	-	-	1.0	3.2
S16	-	-	-	-	1.0	3.4
S17	-	-	-	-	1.0	1.3
S18	-	-	-	-	1.0	1.1
S19	-	-	-	-	1.0	2.5
S20	-	-	-	-	1.0	1.8
S21	-	-	-	-	2.0	1.7
S22	-	-	-	-	1.0	1.5
S23	-	-	-	-	2.0	1.3
S24	-	-	-	-	2.0	1.2
S25	-	-	-	-	1.0	1.3
S26	-	-	-	-	3.0	1.5
S27	-	-	-	-	1.0	1.4
S28	-	-	-	-	2.0	1.3
S29	-	-	7.0	2.0	7.0	1.2
S30	2.0	1.4	1.0	1.9	8.0	1.1
S31	12.0	1.3	2.0	1.4	8.0	0.8
S32	4.0	1.4	20.0	1.2	1.0	0.6
S33	13.0	0.8	1.0	0.9	1.0	0.2
S34	1.0	0.6	7.0	0.3	2.0	2.0
S35	2.0	0.5	1.0	0.4	4.0	2.5
S36	13.0	2.3	5.0	0.7	7.0	2.4

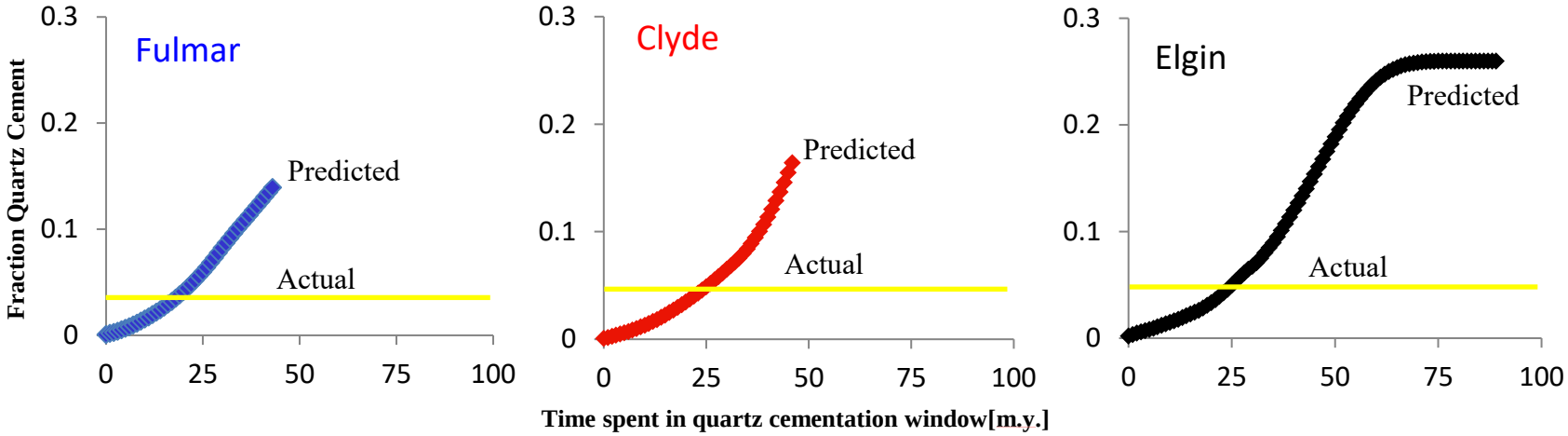

Figure 3.23. Quartz cementation models showing Fraction quartz cement versus time for the Upper Jurassic Fulmar Formation sandstones from Clyde, Elgin, and Fulmar fields using the temperature history in **Error! Reference source not found.**. These models predict samples from high temperature Elgin should be completely cemented at present day, assuming a clean surface area for the quartz fractions of the sandstones. The yellow line marks the actual quartz cement volume measured in the sandstones during CL petrography.

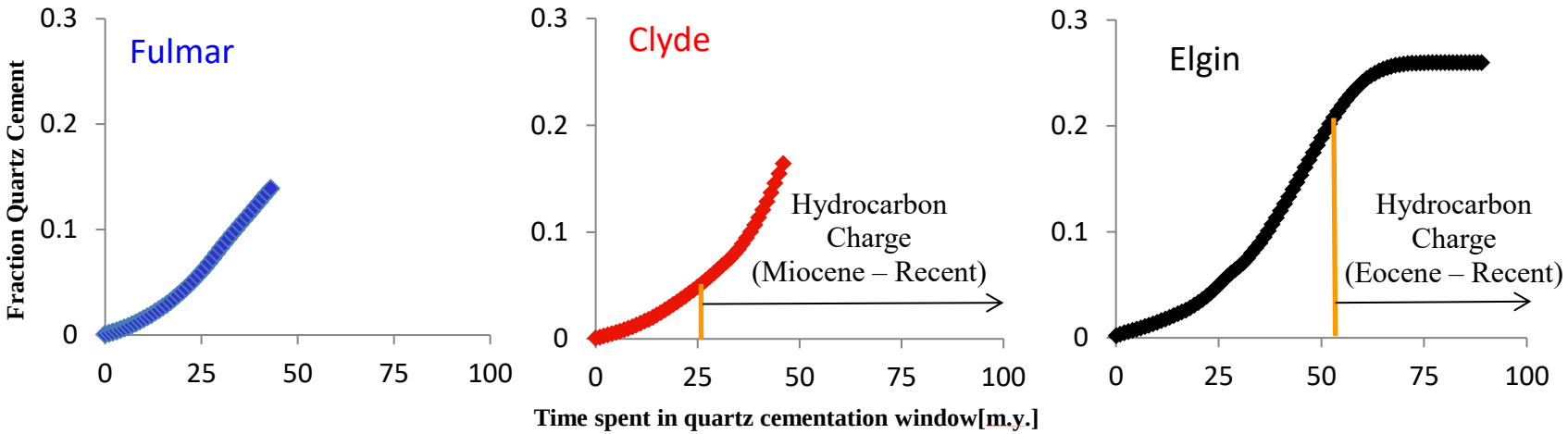

Figure 3.24. Quartz cementation model with projected time of hydrocarbon emplacement in Clyde and Elgin fields based on Stevens and Wallis (1991), Rudkiewicz et al. (2000), and this study. Fulmar field samples are from a non-hydrocarbon bearing zone

3.7. Oxygen Isotope Analysis (SIMS)

Three Fulmar Formation sandstone samples from Clyde, Elgin and Fulmar sample sets with well-developed macroquartz overgrowths with sizes in the region of 30 microns and above were selected for oxygen isotope analysis. The oxygen isotope analyses was performed at WiscSIMS Laboratory in the University of Wisconsin-Madison in two 12-hour sessions from 6th to 7th April 2017. A total of 167 measurements, 58 on University of Wisconsin quartz standard (UWQ-1) and 109 on pre-selected detrital quartz grains and associated overgrowths, were made on the selected Fulmar Formation sandstone samples from Clyde, Elgin, and Fulmar.

3.7.1. Internal Quartz Standard (UWQ-1) Analysis

The internal quartz standards or UWQ-1 analysis is important for calculating external precision and instrument bias. This method was well described by Kita et al. (2009). The $\delta^{18}O$ value of homogenous UWQ-1 grains, as analysed from laser fluorination technique, is 12.33 ± 0.07‰ (1SD, n= 29; 1SE = ±0.01‰; (Kelly et al., 2007)). The UWQ-1 quartz standards were embedded within each of the three Fulmar Formation sandstone samples cast in epoxy mount. Four analyses of the UWQ-1 standards were performed before and after every 5 to 15 sample measurements to form bracket of 8 UWQ-1 standard analyses. The external precision and instrument bias are then calculated by using the spot to spot reproducibility of each bracket of UWQ-1 standard analyses. The reproducibility (Table 3.3 and Figure 3.25) looks good during the two sessions of the SIMS analyses, despite a number of sample changes within each session. According to Kita et al. (2009), instrument bias is typically introduced during measurements due to the following reasons: 1) Individual isotopes have varying ionisation efficiency when transmitting through the mass spectrometer. 2) Individual detectors also have varying efficiencies. The effect of these is that measured ratios will always differ from true values, and must be corrected to V-SMOW scale (Harwood, 2011). When the laser fluorination value is compared to standard measurements, the deviation can be used to calculate true values (Kelly et al., 2007).

Table 3.3. Summary of measurements made on UWQ-1 grains (quartz standards embedded in thin sections) during the SIMS analyses performed on the three Fulmar Formation sandstone samples from Clyde, Elgin and Fulmar fields.

Sample	Session	Spot size (µm)	no	Average $\delta^{18}O$ measured (‰)	Min $\delta^{18}O$ measured (‰)	Max $\delta^{18}O$ measured (‰)	Mass bias (‰)
Clyde	6th April 2017	3	16	-8.50 ± 0.70 (2SD)	-8.80	-8.01	-20.57
Elgin	6th April 2017	3	12	-8.27 ± 0.75 (2SD)	-8.95	-7.86	-20.34
Elgin	7th April 2017	3	12	-9.16 ± 0.89 (2SD)	-9.78	-8.40	-21.23
Fulmar	7th April 2017	3	12	-9.36 ± 0.65 (2SD)	-9.72	-8.78	-21.42
Clyde	7th April 2017	3	6	-9.23 ± 0.78 (2SD)	-9.62	-8.77	-21.30

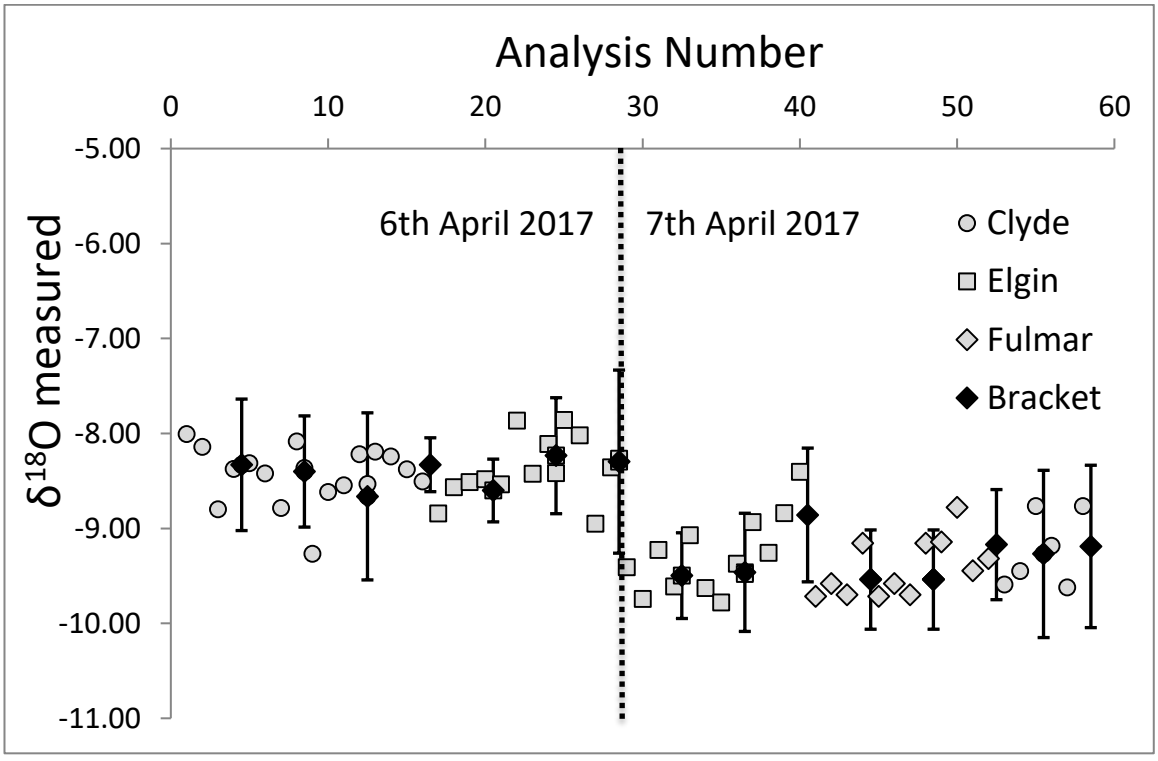

Figure 3.25. Plot of UWQ-1 grains (quartz standards embedded in thin sections) measurements for Clyde, Elgin and Fulmar fields. Brackets represent the average of 8 individual measurements (apart from the last two brackets that represent 6 measurements) made before and after each set of sample measurements. The error bars are the average error of each set of bracket analyses.

3.7.2.SIMS Analysis of Quartz Overgrowths

Post-analysis SIMS pits examination was carried out on the three analysed Fulmar Formation sandstone samples using Backscattered (BSE) and Cathodoluminescence (SEM-CL) microscopy. Nine SIMS pits from Elgin and Fulmar samples compromised by the occurrence of fluid inclusions, detrital quartz input, or any other forms of breach were excluded from further analysis (Table 3.4 and Appendix 3). The distance of each SIMS pit from the detrital quartz boundary was measured by taking a straight line across the quartz overgrowths from the detrital grain boundary to each SIMS pit. The plots in Figure 3.26 illustrate how $\delta^{18}O_{(quartz\ cement)}$ of all samples, except Elgin's samples, evolve to less positive values from the detrital quartz boundary to the outer edge of the overgrowth.

Table 3.4. Summary of $\delta^{18}O_{(quartz\ cement)}$ measurements made on pre-selected quartz overgrowths in the Fulmar Formation sandstone samples from Clyde, Elgin and Fulmar fields. Compromised analysis spots are measurements affected by fluid inclusions, detrital inputs, cracks, and other irregularities

Sample	TVDss (m)	Spot size (µm)	No of analysis spots	Quartz Cement Analysis			
				No of compromised analysis spots	Min $\delta^{18}O$ VSMOW (‰)	Max $\delta^{18}O$ VSMOW (‰)	Precision (±2SD)
Fulmar	3249	3	21	5	+24.2	+27.9	0.8
Clyde	3775	3	37	0	+22.7	+26.8	0.7
Elgin	5417	3	35	4	+19.7	+22.4	0.7
			93	9			

3.7.3.SIMS Analysis of Detrital Quartz

Sixteen SIMS measurements were made on nine detrital quartz grains from the analysed Fulmar Formation samples from Clyde, Elgin and Fulmar fields. The $\delta^{18}O$ range of +5.7 to +15.2‰ for the detrital quartz grains strongly contrast the +19.7 to 27.9‰ for the quartz overgrowths (Table 3.5 and Figure 3.27).

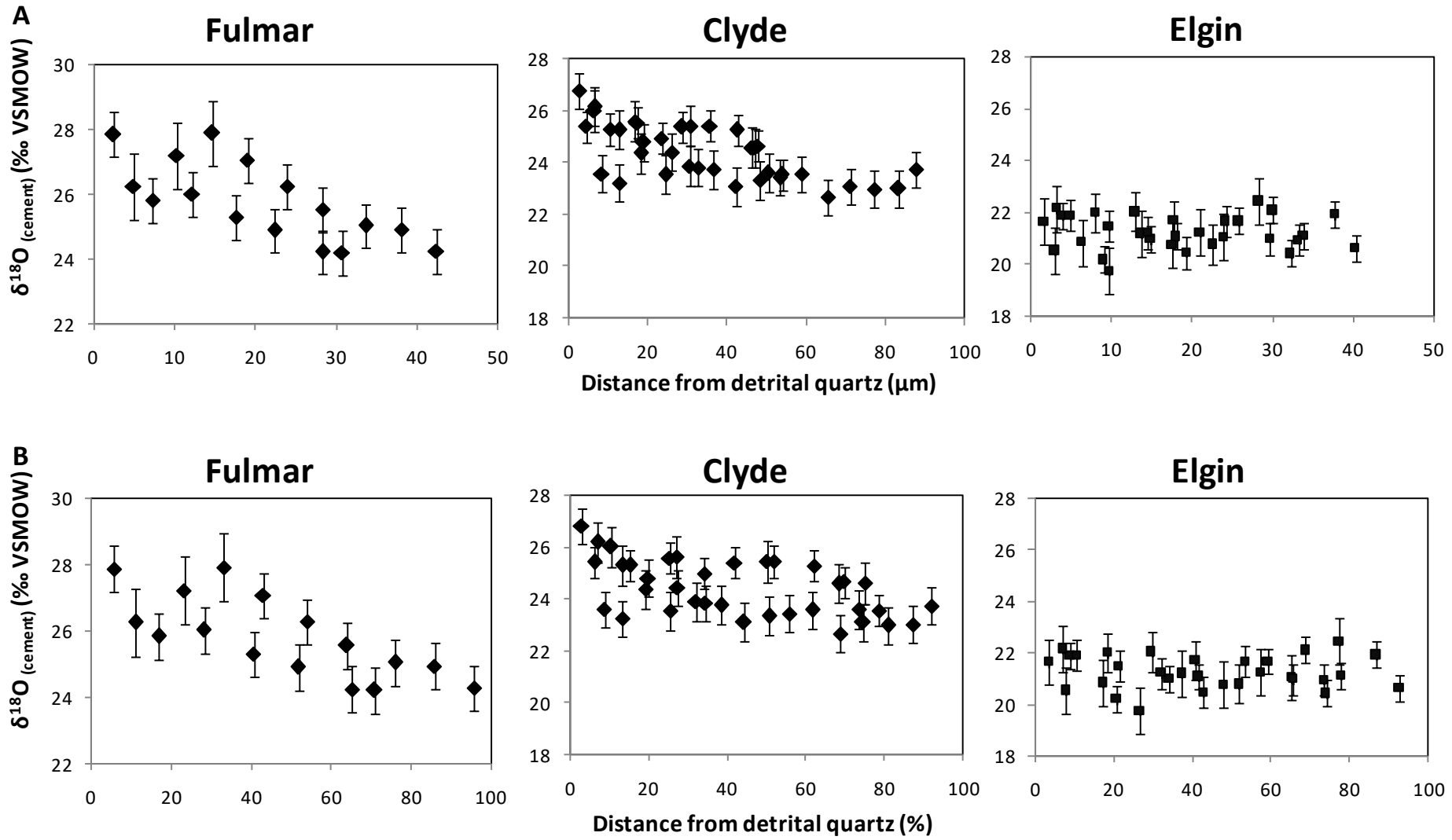

Figure 3.26. SIMS analysis plots for the Upper Jurassic Fulmar sandstones from Clyde, Elgin, and Fulmar fields using 3 µm spots. A) Plot of $\delta^{18}0_{(cement)}$ versus distance in microns (µm) from detrital quartz boundaries. B) Same plot with distance in percentage (%).

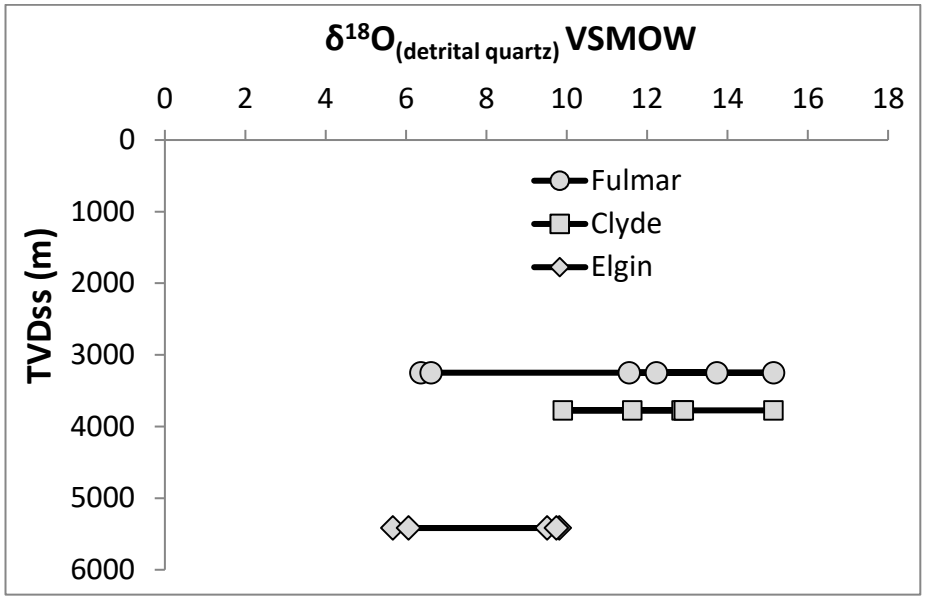

Figure 3.27. Graph illustrating variation in range of $\delta^{18}O_{(detrital)}$ measurements for the Fulmar Formation samples from Clyde, Elgin, and Fulmar fields.

Table 3.5. Summary of the detrital quartz SIMS measurements for the analysed Fulmar Formation samples from Clyde, Elgin and Fulmar fields.

Sample	TVDss (m)	Spot size (µm)	Detrital Quartz Analysis		
			Population	Min $\delta^{18}O$ VSMOW (‰)	Max $\delta^{18}O$ VSMOW (‰)
Fulmar	3249	3	6	+6.4	+15.2
Clyde	3775	3	5	+9.9	+15.2
Elgin	5417	3	5	+5.7	+9.8
Total			16		

3.8. Discussion

The detrital compositions and diagenesis of the studied sandstones from Clyde, Elgin, and Fulmar fields are consistent with those documented in previous studies on the Upper Jurassic Fulmar Formation (Stewart, 1986; Wilkinson et al., 1997; Haszeldine et al., 1999; Osborne and Swarbrick, 1999; Hendry et al., 2000; Burns et al., 2005; Wilkinson and Haszeldine, 2011; Taylor et al., 2015). The Fulmar sandstones are clean, moderately to well sorted, fine-grained arkosic - subarkosic sandstones (Figure 3.9 and Figure 3.10). These sandstones are most likely at their maximum burial depth, with average present-day temperatures are 130°C for Fulmar sample sets; 147°C for Clyde sample sets; and 189°C for Elgin sample sets. Quartz (mainly monocrystalline), feldspars (mainly K-feldspars), and lithic fragments are the main detrital compositions in these sandstones. Quartz cement, carbonate cement, microquartz cements, authigenic illite, and dissolved feldspars are the most significant diagenetic phases. Others are pyrite, K-feldspar overgrowths, and hydrocarbon.

3.8.1. Porosity and Porosity-Loss in the Fulmar Formation

Porosities in the analysed sandstones are high (Figure 3.12 and Table 3.1) for their current burial depths. Other studies (e.g. Osborne and Swarbrick, 1999; Wilkinson and Haszeldine, 2011) have also identified this exceptional character in the Fulmar Formation compared to other sandstones at equivalent depth worldwide. Analysis from CoPL and CePL plots shows that compaction is the main control on intergranular-porosity loss in these sandstones (Figure 3.13). The degree of compaction is, however, moderate as petrographic observations of all sample sets, including the deeply buried sandstone samples from Elgin field, reveal lack of intense compaction or pressure dissolution features such as: sutured contacts and stylolites. The lack of intense mechanical compaction features are commonly reported in the Upper Jurassic Fulmar Formation of the Central North Sea, and has been linked to the reducing effect of fluid overpressure on overburden stress (Lasocki et al., 1999; Osborne and Swarbrick, 1999). Petrographic observation of preserved moldic intragranular porosities (~ 3.3 % of bulk samples), mostly from K-feldspar dissolution, seems to corroborate the inhibitive effect of overpressure on compaction in the Fulmar sandstones. However, some authors (e.g. Taylor et al., 2015) concluded that porosities are maintained due to rigidity and lithification of the framework grains of the Fulmar Formation sandstones. The presence of intergranular pressure dissolution features in the studied sandstones (e.g. Figure 3.14) seems to contradict such claim.

Along with porosity-loss by compaction, cementation has also contributed variably to porosity-reduction in the analysed Upper Jurassic Fulmar sandstones. Although quartz cement is the diagenetic cement of interest in this study, the localised destruction of large pore spaces by carbonate cement observed in some samples from Clyde and Elgin fields shows their significant influence on reservoir quality in these sandstones (Figure 3.21). The suggestion by some workers (e.g. Lasocki et al., 1999) that the development of rigid framework by early formation of authigenic carbonate may be responsible for reduction of compaction in the Upper Jurassic Fulmar Formation may not true, as qualitative data from petrographic analysis reveal that the carbonate cements are heterogeneously distributed in the analysed samples. The observation of moldic porosities suspected to be sites of dissolved carbonates in some Fulmar field thin sections (Figure 3.20) tends to support the idea that later dissolution of carbonate cement may generate secondary porosities during diagenesis (Lasocki et al., 1999). Carbonate dissolution may result at greater depth due the release of substantial amount of organic acids during source rock maturation or the generation of higher acidity due to silica equilibria (Giles and Marshall, 1986; Smith and Ehrenberg, 1989; Hutcheon and Abercrombie, 1990). However, Kuhn et al. (2003) gave an alternative description of the moldic porosities observed in some Fulmar Formation sandstones as sites of sponge spicule dissolution. Hendry et al. (2000) also reported that petrographic analysis of some deeply buried Fulmar Formation sandstones from the Central North Sea suggested only minor dissolution of early carbonate cements.

3.8.2. Carbonate Diagenesis

Overall assessment of carbonate cement types in the studied sandstones from all three study locations suggests mineral replacement or precipitation of new phases with temperature. The development most likely initiated with the transformation of early-formed bioclast-sourced calcite to dolomite through incorporation of Mg^{2+}, followed by minor enrichment of dolomite with Fe^{2+} to form Fe-dolomite, and concludes with major enrichment of Fe-dolomite with more Fe^{2+} Mg^{2+} and Mn^{2+} to form ankerite. The above description seems to match the different stages of carbonate cement evolution observed across the three study fields; with Fulmar having predominantly calcite and dolomite cements; Clyde having dolomite and ferroan dolomite cements; and Elgin, the hottest field, having ankerite and dolomite as the main carbonate cements. Indeed, Hendry et al. (2000) revealed that ankerite is an insignificant phase in Central North Sea Fulmar Formation reservoirs that have never been buried beyond 3.5 km. Calcite formation in

the Fulmar Formation reservoirs occurred during early phase of diagenesis from calcitic bioclasts, most likely before compaction (Stewart, 1986). As burial depth and temperature increases, dolomite precipitated from pore fluid derived from seawater enriched in cations (Fe^{2+} and Mg^{2+}) and dissolved bioclastic carbonates; and later, ankerite formed from combination of dissolved carbon reservoir derived from marine bioclastic carbonate and organic matter in the presence of pore fluids that have been further enriched with Fe^{2+} and Mg^{2+} (Hendry et al., 2000). These supplementary cation enrichments may have been released during thermal breakdown of organic matter and/or smectite illitization in adjacent Heather and Kimmeridge Clay Formations (Stewart, 1986; Hendry et al., 2000). Indeed, similar photoluminescent and isotope character have been observed between ankerite cement in Fulmar and Heather Formations that suggests a link between processes occurring in these sandstones and mudstones (Hendry et al., 2000). Hendry et al. (2000) also concluded that precipitation of ankerite and macroquartz cement probably occurred simultaneously in the Fulmar Formation sandstones from Elgin field.

3.8.3. Illite and Chlorite Clays

Petrographic observations in this study are in agreement with previous studies (Wilkinson and Haszeldine, 1996; Darby et al., 1997; Wilkinson et al., 1997; Osborne and Swarbrick, 1999; Wilkinson and Haszeldine, 2011; Taylor et al., 2015) that illitic clays are the most important diagenetic clay type in the Upper Jurassic Fulmar Formation. Illitic clays were observed in the analysed sandstones (a) engulfed between some corresponding detrital and authigenic quartz species (b) filling both intergranular and intragranular pores (c) coating the surfaces of some detrital and authigenic minerals and (d) as replacive minerals outlining shapes of completely dissolved grains (Figure 3.18 and Figure 3.19).

Clay mineral transformation processes such as: kaolinite illitization and smectite illitization are some of the processes through which authigenic illite are formed in sandstones (Osborne and Swarbrick, 1999). Kaolinitic clays, or evidence of prior existence of kaolinite, were not recorded in the Fulmar Formation sandstones analysed in this study. The possibility of kaolinite transformation as the source of illite in the Fulmar Formation sandstones has been dispelled by Osborne and Swarbrick (1999); since kaolinite is likely a product of feldspar dissolution in meteoric water, and no such reactions have been reported for the Fulmar Formation in the Central North Sea. The only reported feldspar dissolution event in the Fulmar Formation, as discussed in

previous section, is the mid-late diagenesis-related dissolution that is known to directly generate authigenic illite (Wilkinson et al., 1997; Lasocki et al., 1999). Smectite illitization is, thus, favoured as the most likely clay transformation process related to illite formation in the Fulmar Formation (Osborne and Swarbrick, 1999). It is difficult to distinguish the illitic clays sourced from clay mineral transformation from those sourced directly from feldspar dissolution in the samples from Elgin field, since they are all bitumen-impregnated and recrystallized under the influence of temperature (Wilkinson and Haszeldine, 2011). This problem could be resolved by examining their position relative to other minerals within the samples. Based on this premise, the illitic clays observed coating detrital grains in the studied samples are likely to have detrital origin, and those coating authigenic cements or replacing other detrital grains would most likely be authigenic (Figure 3.18 and Figure 3.19). Besides illite formation, the clay mineral transformation and feldspar dissolution processes described above are also known to release silica, which could subsequently precipitate as authigenic cement on detrital quartz (Osborne and Swarbrick, 1999; Worden and Morad, 2000).

Although the timing of illite formation in the analysed sandstones is not known; previous work by Darby et al. (1997) using K-Ar dating for some Fulmar Formation sandstones from elsewhere in the Central Graben has revealed that illite ages range from 85-58 Ma on the graben margins, and 33-30 Ma in the graben centre. The implication is that the temperature of illite formation varied across geographic location in the Central North Sea, and this could be applicable in the case of the Fulmar Formation sample sets from the three locations in this study. The position of illite relative to other minerals (e.g. quartz) as observed during petrographic analysis suggests that the timing of illite formation not only varied locally but also occur over a wide window. While illitic clays engulfed in between detrital and authigenic clays or coating detrital grains formed prior to quartz cementation, illite coating detrital grains most likely formed later in the diagenetic history.

Apart from illite, minor chlorite was observed only in the samples from Fulmar field. Chloritic clays are important because of their grain-coating effect that enhances porosity preservation in reservoir sandstones (Ehrenberg, 1993; Aagaard et al., 2000; Bloch et al., 2002; Morad et al., 2002; Stricker et al., 2016b). However, the chlorite clays observed in the Fulmar field sample set were found replacing partially dissolved feldspars (Figure 3.19). Although the paucity of grain-coating chlorite in the studied

sandstones suggests depositional facies effect (Bloch et al., 2002), previous studies have shown that grain-coating chlorite can develop in sandstones deposited in a shallow marine environment (Ehrenberg, 1993; Morad et al., 2002). Because chlorites are Fe-rich clay sourced from Fe-rich precursor minerals, it is possible that these clays have a diagenetic link with the glauconites observed (Figure 3.19) in the sandstone samples from Fulmar field (Stewart, 1986). However, berthierine and /or smectite are the most commonly cited precursor of chlorite in reservoir sandstones (Aagaard et al., 2000; Worden and Morad, 2000; Bloch et al., 2002; Morad et al., 2010).

3.8.4.Pyrite

Pyrite occurs as a minor authigenic phases in the studied sandstones as frambroidal aggregates (Figure 3.19). The frambroidal pyrites are probably the earliest formed diagenetic cement in these samples, as they typically precipitate at shallow depth, and are thought to be associated with organic matter (Berner, 1970; Stewart, 1986).

3.8.5.Dissolved Feldspars and Feldspar Overgrowths

Although average sandstone compositions are similar in the studied sample sets, comparison of quantitative petrographic data shows that Elgin sample set has the highest average quartz fraction of all three sample sets (Figure 3.9, Table 3.1 and Appendix 1). This is likely due to the occurrence of more dissolved K-feldspars in Elgin samples compare with Clyde and Fulmar samples, as revealed by the fraction of intragranular porosities during quantitative petrography. Elgin sandstones are at the highest present-day burial depths (around 5500 mTVDSS) and temperature of the three sample sets. Petrographic observation of the feldspars not only shows that they are at various stages of dissolution in the analysed samples, but that the magnitude of dissolution varies across the three sample sets, with just ~ 0.1 dissolution volume % recorded in the shallowest samples from around 3200 mTVDSS. The greater degree of feldspar dissolution encountered in the sandstone samples from Elgin field compare to Clyde and Fulmar fields' samples (Table 3.1) seems to support previous conclusion by Wilkinson and Haszeldine (1996), that the volume of dissolved feldspars increases with burial depth in the Upper Jurassic Fulmar Formation. The above description strictly suggests that feldspar dissolution in the Fulmar Formation in the Central Graben is a product of mid-late diagenesis (Wilkinson et al., 1997; Lasocki et al., 1999). Feldspar dissolution may have supplied some of the authigenic illite and quartz present in these sandstones, because the ions liberated during the dissolution process would eventually enrich the formation water with materials that would later precipitate as illite and quartz

cement (Osborne and Swarbrick, 1999; Worden and Morad, 2000). The model reaction for this process as expressed by Osborne and Swarbrick (1999) is:

1.0 K-feldspar + $0.174H_2O$ + 0.522 H^+ + 0.109 Mg^{2+} = 0.739 K+ + 0.435 illite + 1.478 quartz.

The exact mechanism driving the process of feldspar dissolution in the Fulmar Formation remains unclear. The process has been reported to be related to organic acid enrichment of pore water linked to hydrocarbon maturation and compaction of adjacent mudrock (e.g. Lasocki et al., 1999). However, Giles and Marshall (1986) suggested that organic-acid-driven feldspar dissolution in deeply buried reservoirs is highly unlikely because the acid generated during maturation would tend to react in the source rock, and only volumetrically insignificant quantities would escape into adjacent sandstones.

Feldspar overgrowth in the upper Jurassic Fulmar Formation are mainly K-feldspar and minor albite (Stewart, 1986; Lee and Parsons, 2003). Because K-feldspar overgrowths precipitate at low diagenetic temperatures in the Fulmar Formation (Lee and Parsons, 2003), they tend to be more stable than high-temperature detrital K-feldspar. In this study, K-feldspar overgrowths exhibit variable abundance across the three sample sets. Fulmar field sample set have the most K-feldspar overgrowths, followed by Clyde, and Elgin with the least (Appendix 1 and Figure 3.18). The overgrowths in Clyde sample sets are locally enclose partially or completely dissolved detrital grains. Feldspar overgrowths are rare in Elgin sample sets, as they have mostly been altered or replaced by clay rims (Figure 3.18). These observations suggest that the stability of K-feldspar overgrowth reduces with increasing temperature and/or burial depth. The process that led to the replacement of K-feldspar overgrowths by authigenic illite in the Elgin sample set would have also released silica for quartz cementation in these sandstones (Worden and Morad, 2000).

3.8.6.Microquartz

Microquartz cement is common diagenetic phase in the studied sandstones, except for the Elgin sample set (Figure 3.15c). They were found within specific intervals either as pore-occluding chalcedonic cements (Figure 3.19), or randomly-oriented tiny polycrystalline overgrowths on detrital quartz; with lengths generally less than 5µm. Microquartz cements are rare in the studied Fulmar Formation sandstones from Elgin field. Similar observation have also been reported in other Fulmar Formations sandstones within the HPHT cluster in the Central North Sea (Osborne and Swarbrick,

1999; Taylor et al., 2015). Previous studies (Aase et al., 1996; Gowland, 1996; Osborne and Swarbrick, 1999) have linked the occurrence of microquartz cements to biogenic silica derived from the dissolution of *Rhaxella* sponge spicules. The spicules are considered to be have been incorporated in the sediment during deposition due to strong open-marine influence (Gowland, 1996). Because sponge spicules have high solubility; they dissolve with increasing burial depth and temperature, and re-precipitate as microquartz cement (Aase et al., 1996). This transformation likely occurred in the Upper Jurassic Fulmar Formation sandstones at depths shallower than 2500 m (Lasocki et al., 1999; Osborne and Swarbrick, 1999). The presence of microquartz cement has dual implication for reservoir quality in the studied sandstones. While grain-coating microquartz may enhance reservoir quality by inhibiting macroquartz cementation, abundant pore-occluding microquartz cement would have a negative effect on porosity and permeability in sandstones.

3.8.7.Diagenetic Quartz and Controls on Cementation

Quartz cementation is a major diagenetic process that led to porosity- and permeability-loss in sandstone reservoirs (McBride, 1989). Although quartz cementation is a source-transport-precipitation controlled process, the rate-controlling step has been a controversial subject (e.g. Walderhaug, 1996; Worden and Morad, 2000; Sheldon et al., 2003). Some workers have hypothesized (e.g. Walderhaug, 1996; Lander and Walderhaug, 1999; Walderhaug, 2000) that temperature-controlled precipitation kinetics are the main control on quartz cementation, and that quartz precipitation increases exponentially with temperature once the kinetic barriers are broken at the cementation threshold (70 – 80 °C). However, precipitation sites must be free from inhibitors such as: clay coats and microquartz (Aase et al., 1996; Bloch et al., 2002). Other researchers (Osborne and Swarbrick, 1999; Sheldon et al., 2003) have pointed out that the supply of silica seems to be the overarching control on quartz cementation in sandstones. Worden and Morad (2000) broadly classified the sources of silica for quartz cementation in sandstones into: (a) those sourced locally within the sandstone and (b) those sourced externally from other mudrocks or sandstones. Because silica sourced from remote locations would require greater travel distances and large scale fluid movement (Worden and Morad, 2000); such conditions may not be feasible beyond shallow burial (Aplin and Warren, 1994). Hence, internally sourced silica seems to be important in deeply buried sandstones. Whilst intergranular pressure dissolution and the related process of stylolitization are commonly regarded as ubiquitous internal sources

of silica in sandstones, feldspar dissolution and clay mineral reactions are the other potential sources (Osborne and Swarbrick, 1999; Worden and Morad, 2000).

In the studied sample sets, higher temperature does not necessarily mean greater volume of quartz cement (Figure 3.17 and Table 3.1). Quantitative CL petrography shows that the average volume of quartz cement is generally low (< 5 %) in the studied sample sets (Table 3.1), despite the fact that these samples have experienced temperatures well above the expected quartz cementation threshold (70 - 80°C) (Walderhaug, 1996). This is well illustrated by the comparison of the petrographic result with quartz cementation model outputs, which shows that modelled quartz cement volumes far exceed measured volumes for all three sample sets (Figure 3.23). In particular, high temperature Elgin field samples have spent 90 Ma in the quartz cementation window (Figure 3.23) and still have low normalised average quartz cement volume (0.12) compared to Clyde (0.15) and Fulmar (0.11) field sample sets.

The occurrence of small volume of quartz cement in these sandstones could possibly mean these sandstones did not receive adequate supply of silica, or that free quartz surface areas (precipitation sites) were not available for quartz cementation. Previous study (Osborne and Swarbrick, 1999) on some Upper Jurassic Fulmar Formation sandstones from other locations in the Central North Sea attributed the presence of low volume of quartz cement to inadequate silica supply. The study reported that the sandstones are overpressured, and that this development slow-down vertical effective stress (VES) which in turn limited intergranular pressure dissolution – an internal source of silica for quartz cementation. This explanation could be applicable to the sample sets in the present study, as the different reservoirs have varying degree of overpressure and VES at present-day (Table 2.1). Elgin sample set with the highest temperature and lowest VES at present-day has very low quartz cement volume. This suggests that very low VES has an influence on quartz cementation in Fulmar sandstones. The SIMS analysis plots on Figure 3.26 seems to support this data, as Elgin Field samples have the narrowest range of $\delta^{18}O_{\text{quartz cement}}$ of all three sample sets.

The presence of compaction features like concave-convex contacts (e.g. Figure 3.14) is evidence that intergranular pressure dissolution may have supplied part of the silica for quartz cementation in the studied sandstones. However; contributions from intergranular pressure dissolution would most likely be moderate, since intense compaction/pressure dissolution features such stylolitic or sutured contacts are absent.

Stylolitic bands were also not observed in Fulmar Formation core samples. Previous studies (Osborne and Swarbrick, 1999; Taylor et al., 2015) have also reported the absence of these features in the Fulmar Formation from other locations. The lack of stylolitic or sutured contacts are probably linked to low VES history in these sandstones. Further investigation on the effect of overpressure and intergranular pressure dissolution in the studied Fulmar Formation sandstones would require the reconstruction of pore pressure and vertical effective stress histories, and the petrographic quantification of intergranular pressure dissolution.

Apart from silica sourced from pressure dissolution, contributions from other internal sources are also considered. Silica contribution from K-feldspar dissolution was inferred due to the presence of K-feldspar dissolution features (Figure 3.18). K-feldspar dissolution is most common in the Elgin field. Dissolution of K-feldspar has also been reported for the Upper Jurassic Fulmar Formation from other fields by other researchers (Wilkinson and Haszeldine, 1996; Wilkinson et al., 1997; Lasocki et al., 1999; Osborne and Swarbrick, 1999; Taylor et al., 2015). It is possible that silica was supplied by clay transformations (e.g. smectite illitisation) (Osborne and Swarbrick, 1999; Worden and Morad, 2000), as authigenic clays (mainly illite) were observed during petrographic analysis. Silica contribution from clay transformations may be volumetrically insignificant; as only minor clays are present in the samples (Table 3.1 and Appendix 1), and some of them might have come from feldspar dissolution.

Grain-coating clays and microquartz are well known inhibitors of quartz cementation in sandstones (Aase et al., 1996; Osborne and Swarbrick, 1999; Worden and Morad, 2000; Bloch et al., 2002; Stricker et al., 2016b). Petrographic analysis revealed the presence of grain-coating illite and microquartz (Figure 3.15 and Figure 3.19) in variable amounts in the studied sandstones. Grain-coating chlorites are the most effective and commonly reported grain-coats (Taylor et al., 2010), but were not observed in the studied sandstones. The only recorded presence of chlorites was in the Fulmar Field sample set, where they occur as replacive clay (Figure 3.19). The determination of the extent to which grain-coating illites and microquartz have limited quartz cementation in the studied samples would require the quantitative assessment of their coverage extent on detrital quartz fraction in the samples.

The effect of hydrocarbon emplacement on diagenesis, particularly quartz cementation, in sandstone reservoirs has been debated in many clastic reservoir studies (Saigal et al.,

1992; Gluyas et al., 1993; Walderhaug, 1994a; Walderhaug, 1994b; Marchand et al., 2000; Worden and Morad, 2000; Marchand et al., 2001; Marchand et al., 2002; Aase and Walderhaug, 2005; Taylor et al., 2010; Maast et al., 2011; Wilkinson and Haszeldine, 2011; Sathar et al., 2012; Taylor et al., 2015). There are two schools of thoughts on the effect of hydrocarbon emplacement. While some (Gluyas et al., 1993; Marchand et al., 2000; Marchand et al., 2001) suggested hydrocarbon emplacement would halt quartz cementation, others concluded the process would continue unhindered in the presence of hydrocarbon. The lack of appreciable difference between the volumes of quartz cement observed in oil and water bearing zones is one of the pieces of evidences usually cited to negate the effect of hydrocarbon emplacement (Walderhaug, 1994a; Walderhaug, 1994b; Marchand et al., 2001; Taylor et al., 2010). Recent studies (Maast et al., 2011; Sathar et al., 2012) have shown that it is possible for hydrocarbon emplacement to inhibit quartz cementation, if hydrocarbon saturation is very high and oil becomes the wetting phase in the reservoir.

The Fulmar Formation sandstones considered in this study were all obtained from hydrocarbon-bearing zones, with the exception of Fulmar field sample set. Logically, hydrocarbon has likely had no effect on diagenesis in the studied Fulmar Field sample set. In the case of the samples from Clyde and Elgin fields, hydrocarbon probably arrived in these reservoirs in the Miocene (Stevens and Wallis, 1991) and Eocene (Rudkiewicz et al., 2000) respectively (Figure 3.24). These timings are based on basin modelling results and need to be corroborated with hydrocarbon fluid inclusion and/or isotope data. However, fluid-inclusion analyses were not performed in this study. The integration of the reported timing of hydrocarbon charge with quartz precipitation models (Figure 3.23 and Figure 3.24) suggest that, barring other controls, quartz cementation would have occurred substantially in these sandstones before any hydrocarbon emplacement. The extent to which cementation has been affected after hydrocarbon emplacement is difficult to ascertain. This is because the facies of interest, the upper shoreface sandstones are restricted to the oil-bearing zone in these sandstones. Hence comparison with other facies from the water-leg would not be appropriate. It is however noteworthy that the greater burial temperatures (> 150 °C) experienced by samples from Elgin field probably led to in-reservoir cracking and formation of bitumen that can be seen staining some authigenic minerals (e.g. illite clays) in the studied sandstones (Figure 3.18 and Figure 3.19). The implication is that the formation of bitumen most likely postdates the precipitation of these authigenic minerals.

3.8.8. Timing of Quartz Cementation in the Fulmar Formation

The timing of quartz cementation in this study was constrained using high spatial resolution oxygen isotope ($\delta^{18}O$) data acquired during SIMS analysis. Based on the fractionation equation of Clayton et al. (1972) (Equation 2.14), the oxygen isotopic composition of quartz cement ($\delta^{18}O_{quartz\ cement}$) is a dual function of precipitation temperature and formation water ($\delta^{18}O_{water}$). Although unique cementation histories cannot be generated from isotope data, they can however, be integrated with known present-day $\delta^{18}O_{water}$ values to help place tighter constraint on cementation histories (Harwood et al., 2013).

Quartz cementation histories have been constrained using homogenisation temperatures from fluid inclusions in previous diagenetic studies (e.g. Walderhaug, 1994a; Walderhaug, 1994b). Fluid inclusions are often restricted to regions very close to the boundaries between detrital and authigenic quartz (Walderhaug, 1994b). This is challenging, as fluid inclusions could only constrain their temperature of formation (Harwood, 2011). The implication of this is that they bear no records for the earliest and later formed quartz cements. The integration of fluid inclusion data with oxygen isotope data could more likely produce better constraint on cementation histories. Since fluid inclusion analyses were not performed on the studied sandstones, I combined the $\delta^{18}O_{quartz\ cement}$ data and Upper Jurassic Fulmar Formation $\delta^{18}O_{water}$ (+ 4.5 ‰) with values for Jurassic Seawater (- 1 ‰) at deposition (Hendry et al., 2000) to calculate precipitation temperatures for the analysed samples (Figure 3.28). It is noteworthy that this $\delta^{18}O_{water}$ measurement was not taken from the Fulmar Formation in the Elgin area.

The temperature of quartz cementation calculated from the oxygen isotope equilibrium plot using the Jurassic Seawater (- 1 ‰) as a reference point (Figure 3.28), suggests that quartz cementation initiated around 50°C in Fulmar field, 55°C in Clyde field, and 80 °C in Elgin field. The calculated threshold cementation temperatures for Clyde and Fulmar fields sample sets are below the expected quartz cementation threshold (Walderhaug, 1994a). A threshold temperature of 80 °C for quartz cementation where $\delta^{18}O_{quartz\ cement}$ is +26.8 ‰ in Clyde and +27.9 ‰ in Fulmar would mean that precipitation was initiated in water with $\delta^{18}O_{water}$ of +2.94 ‰ in Clyde and +4.03 ‰ in Fulmar. These are very positive values compared to other North Sea water at 80 °C (Egeberg and Aagaard, 1989; Aplin and Warren, 1994; Warren et al., 1994; Harwood, 2011) and the likely $\delta^{18}O_{water}$ at deposition of the Fulmar Formation in the Upper Jurassic (- 1 ‰). Also, the closeness of these values to the present-day $\delta^{18}O_{water}$ (~ + 4.5

‰) in the Fulmar Formation would mean that formation water was nearly constant, especially in Fulmar field, throughout cementation history. These scenarios are unlikely because $\delta^{18}O_{water}$ tends to evolve to heavier values during burial diagenesis (Aplin and Warren, 1994; Warren et al., 1994). Hence, it is possible that precipitation initiated at temperatures lower than 80 °C in the Clyde and Fulmar fields samples. The contrasting case in Elgin field is likely due to the 1km of extremely rapid burial in the Upper Jurassic, as constrained from basin modelling. Quartz cementation threshold temperatures lower than 80 °C have also been reported in some other diagenetic studies (e.g. Vagle et al., 1994; Walderhaug, 1994b; Kelly et al., 2007; Harwood, 2011; Harwood et al., 2013).

The isotope data (Figure 3.28) also suggest that quartz cementation did not continue to present burial temperatures in the studied sandstones based on the $\delta^{18}O_{water}$ of ~ + 4.5 ‰ measured in the Fulmar Formation reservoir. This value contradicts the isotope model-based calculated values of ~ + 6.5 ‰ for both Clyde and Fulmar fields, and ~ + 7.0 ‰ for Elgin field, if quartz cementation were to continue to present burial temperature. Also, $\delta^{18}O_{water}$ values higher than + 4.5 ‰ are yet to be reported for any Upper Jurassic reservoirs in the Central North Sea (Warren et al., 1994). The $\delta^{18}O_{water}$ value (~ + 4.5 ‰) looks problematic and may be due to different reasons (Figure 3.28). For example, the data imply that quartz cementation halted around 110°C in Fulmar; 125°C in Clyde; and 150°C in Elgin. Basin modelling suggests that in the case of Clyde and Elgin fields, these were the likely Fulmar Formation temperatures when the reservoirs received substantial hydrocarbon charge from deeper source rocks. Could hydrocarbon charge have stalled quartz cementation in these sandstones? This is difficult to prove and would require supporting evidence from hydrocarbon fluid inclusion analyses. Also, the fact that hydrocarbon was not present in the Fulmar field sample set suggests that factors other than hydrocarbon charge (e.g. pore fluid overpressure) may be at play.

If quartz cementation thresholds are around 50 °C in Clyde and Fulmar fields sample sets as indicated by the SIMS data, it follows logically that silica for such early cementation came from sources other than pressure dissolution in chemical compaction zone, feldspar dissolution, and smectite illitization. This is because; these processes are mostly associated with burial temperatures around 70 - 80 °C to higher temperatures in the Upper Jurassic Fulmar Formation sandstones (Wilkinson and Haszeldine, 1996; Wilkinson et al., 1997; Osborne and Swarbrick, 1999; Hendry et al., 2000). Early quartz

cement might have been sourced from low temperature pressure dissolution (Bjorkum, 1996), and silica-supersaturated Jurassic seawater - similar to the mechanism described by Mackenzie and Gees (1971). Kaolinite formation from dissolved feldspar in meteoric water is another possible low temperature source of silica in sandstones (Osborne and Swarbrick, 1999). Silica contribution from kaolinite is highly unlikely in the studied Fulmar Formation sandstones, as no evidence for prior presence of kaolinites were observed during petrographic analysis. Also, feldspar dissolution is associated with deep burial (mid-late diagenesis) in the Upper Jurassic Fulmar Formation in the Central Graben (Wilkinson et al., 1997; Lasocki et al., 1999).

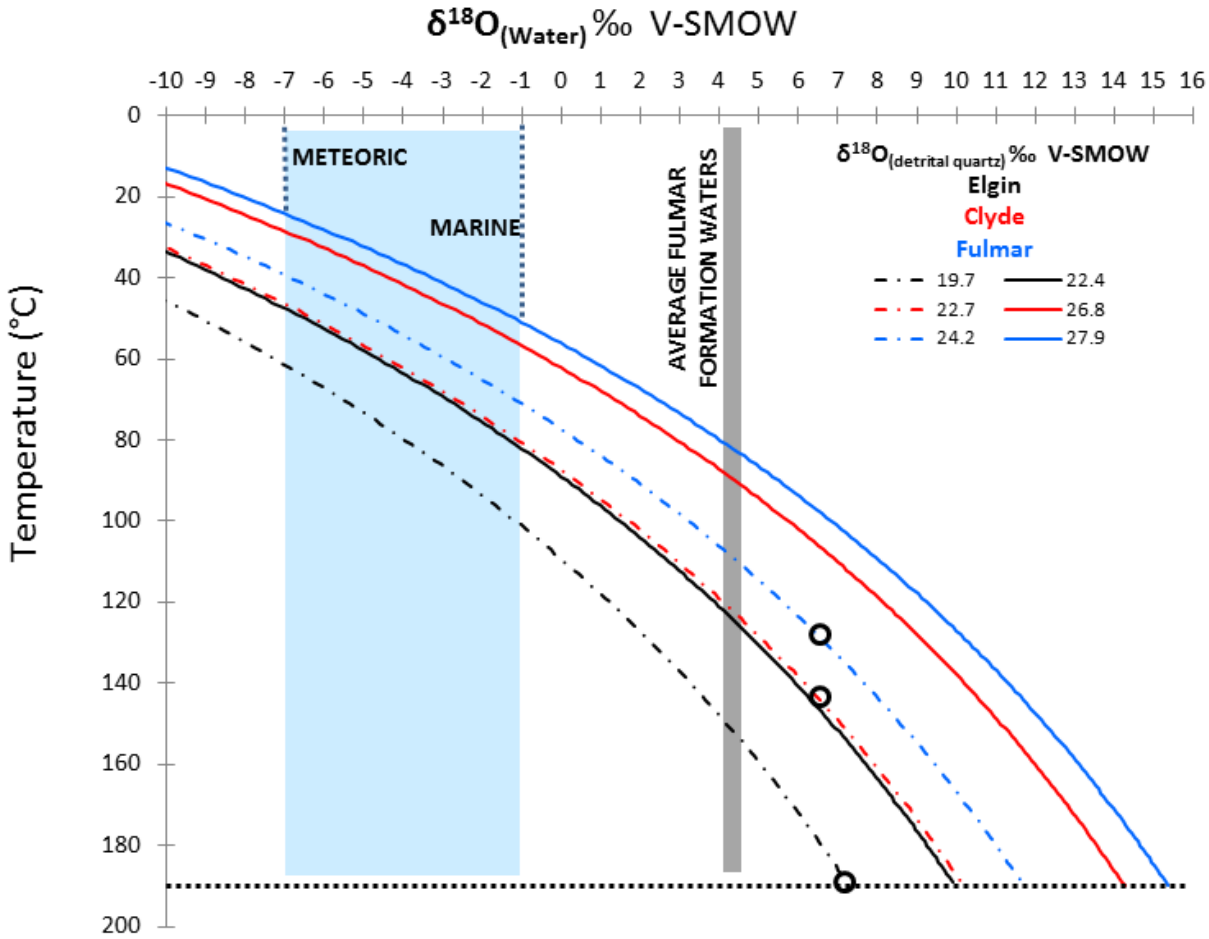

Figure 3.28. Plot of $\delta^{18}O_{water}$ in equilibrium with $\delta^{18}O_{quartz\ cement}$ (+27.9‰, + 26.8‰, +24.2‰, +22.7‰, +22.4‰ and +19.7‰) as a function of temperature for the Upper Jurassic Fulmar Formation from Clyde, Elgin and Fulmar fields. The grey bar indicates the measured $\delta^{18}O_{water}$ in the Fulmar Formation around 190°C. The black circles show the expected formation water conditions for the three fields based on the isotope model.

3.8.9. Paragenetic Sequence

This section described the post-depositional diagenetic alteration of Upper Jurassic Fulmar Formation sands into sandstones based on the studied samples from Clyde, Elgin and Fulmar fields. The paragenetic sequence (Figure 3.29) is developed based on the mineral grain and crystal growth relationships observed during petrographic analysis, basin modelling, and SIMS analyses. Since Fulmar field samples were obtained from non-hydrocarbon bearing interval, hydrocarbon charge was omitted from the attendant diagenetic process for the sample set (Figure 3.29).

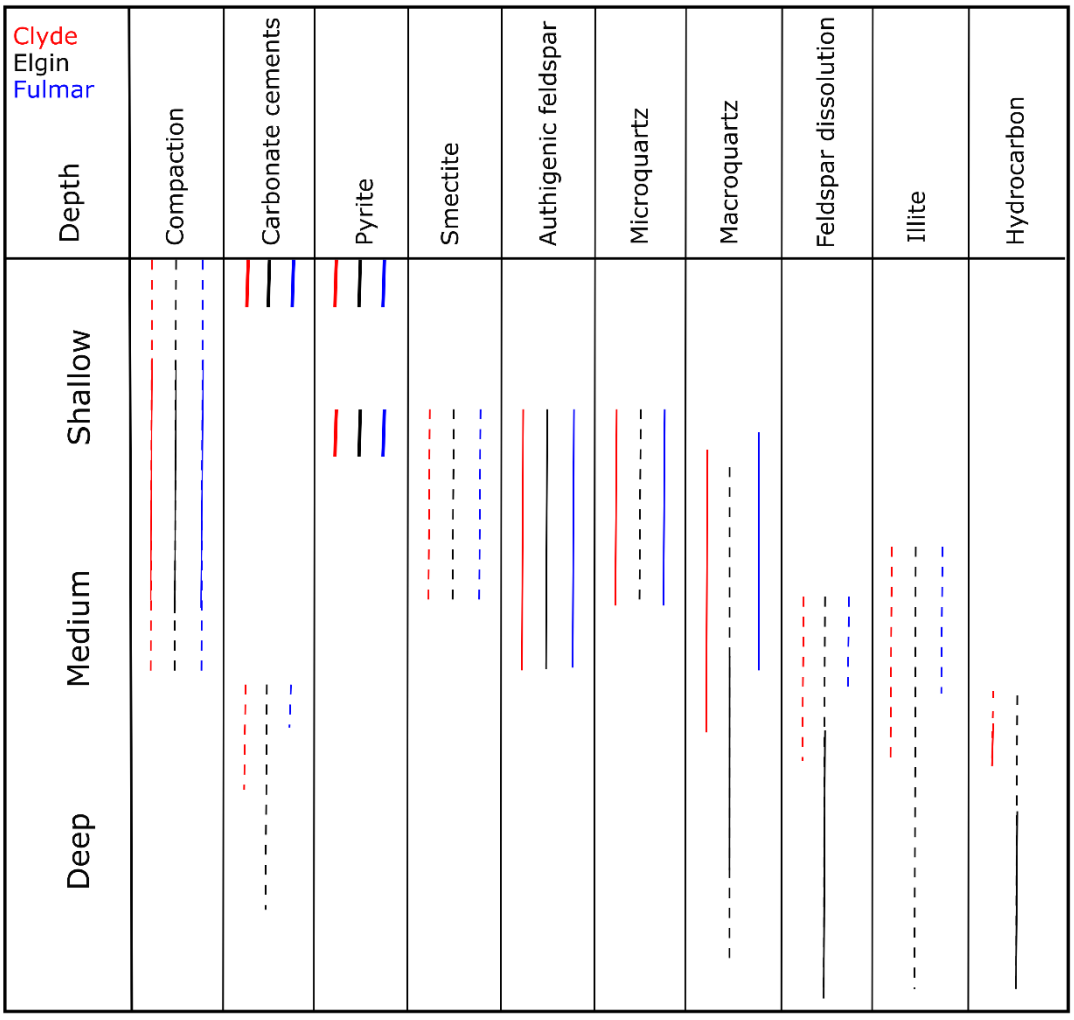

Figure 3.29. Paragenetic sequence of key diagenetic processes in the studied Upper Jurassic Fulmar Formation sandstones from Clyde, Elgin, and Fulmar fields

3.9. Conclusions

Diagenetic studies were carried out on the Upper Jurassic Fulmar Formation sample sets from Clyde, Elgin, and Fulmar fields. These studies show that post-depositional processes such as mechanical and chemical compaction, mineral grain dissolution, mineral precipitations are the attendant diagenetic processes that have interplayed to alter the original Fulmar Formation sands into sandstones.

Intergranular porosity-loss in these sandstones is driven mainly by mechanical compaction with moderate contributions from chemical compaction and pressure dissolution. The early precipitation of carbonates, which is about 9 % of bulk volume in Clyde and Elgin fields, has had localised reducing effect on mechanical compaction, due to their heterogeneous distribution in these sandstones. The chemical composition of carbonate varies with burial depth and temperature across the studied Upper Jurassic Fulmar Formation.

The dissolution of potassium feldspars led to the formation of intergranular porosity. Feldspar dissolution increased with burial depth and temperature in the Fulmar Formation. The dissolution process also produced authigenic illite and silica for quartz cementation. Illite clays are the main grain-coating and pore-filling authigenic clays in the studied sandstones.

Macroquartz and microquartz formed as authigenic cement during diagenesis in the Upper Jurassic Fulmar Formation sandstones. The microquartz cements exist as heterogeneously distributed overgrowths and pore-occluding cements with variable abundance in the sandstones. Macroquartz cements are uniformly distributed but occur in low volumes (< 5 %) in all sample sets. Quartz cement volume in Elgin field at 189°C is comparable to that of Fulmar and Clyde at 130°C and 147°C. This suggests that quartz cementation is controlled by factors other than burial depth and temperature in the studied Fulmar Formation sandstones. Further studies are required to elucidate the key controls on quartz cementation in these sandstones.

High resolution SIMS analyses suggest that macroquartz cement began to form in marine water around 50°C in Clyde and Fulmar fields. This contradicts the well-known classic quartz cementation threshold (70 - 80°C). The 80°C quartz cementation threshold observed in Elgin sample set is most likely associated with temperature increase due to Upper Jurassic rapid subsidence in the Elgin field.

4. Vertical effective stress as a control on quartz cementation in sandstones

This chapter has been accepted for publication in Marine and Petroleum Geology (14 September 2018).

OYE, O. J., APLIN, A. C., JONES, S. J., GLUYAS, J. G., BOWEN, L., ORLAND, I. J. & VALLEY, J. W. 2018. Vertical effective stress as a control on quartz cementation in sandstones. *Marine and Petroleum Geology*, 98**,** 640-652.

https://doi.org/10.1016/j.marpetgeo.2018.09.017

4.1. Summary

Temperature-controlled precipitation kinetics has become the overwhelmingly dominant hypothesis for the control of quartz cementation in sandstones. Here, I integrate quantitative petrographic data, high spatial resolution oxygen isotope analyses of quartz cement, basin modelling and a kinetic model for quartz precipitation to suggest that the supply of silica from stress-sensitive intergranular pressure dissolution at grain contacts is in fact a key control on quartz cementation in sandstones. I present data from highly overpressured sandstones in which, despite the current burial temperature of 190 °C, quartz cement occurs in low amounts (4.6 ± 1.2% of bulk volume). In situ oxygen isotope data across quartz overgrowths suggest that cementation occurred over 100 Ma and a temperature range of 80-150 °C, during which time high fluid overpressures resulted in consistently low vertical effective stress. I argue that the very low amounts of quartz cement can only be explained by the low vertical effective stress which occurred throughout the burial history and which restricted silica supply as a result of a low rate of intergranular pressure dissolution at grain contacts.

4.2. Introduction

During basin subsidence, sands become sandstones through the precipitation of macroquartz cement. Resultant changes in physical properties exert a primary control on the ability of sandstones to store and to transmit fluids: on a basin-scale as a control on the transfer of fluid pressure (Yardley and Swarbrick, 2000; Reilly and Flemings, 2010), and on a more local scale in the context of CO_2 storage, the development of low enthalpy geothermal energy resources and petroleum production. Given its importance as a geological process, many studies have examined the potentially multifaceted controls of macroquartz cementation and the underlying processes of supply, transport and precipitation of silica (Worden and Morad, 2000; Bloch et al., 2002; Taylor et al., 2010). Currently, the dominant hypothesis is that the rate-limiting step in macroquartz cementation is precipitation, such that the rate of macroquartz cementation is geologically negligible below 80 °C but then increases exponentially with temperature (Walderhaug, 1994a; Walderhaug, 1996; Ajdukiewicz and Lander, 2010). Grain coatings of microquartz and clay inhibit the precipitation of macroquartz cement (Heald and Larese, 1974; Aase et al., 1996; Osborne and Swarbrick, 1999; Worden and Morad, 2000; Bloch et al., 2002; Ajdukiewicz et al., 2010; Stricker et al., 2016b), and there is continuing debate about the extent to which petroleum acts as a brake on cementation by altering the wetting state of grains and/or increasing the tortuosity of diffusion pathways (Worden et al., 1998; Worden and Morad, 2000; Marchand et al., 2002; Sathar et al., 2012; Worden et al., 2018b). Predictive, computer-based models of macroquartz cementation incorporate these ideas and have become the dominant concepts for modelling both macroquartz cementation and the related loss of porosity and permeability (Walderhaug, 1996; Lander and Walderhaug, 1999; Ajdukiewicz and Lander, 2010).

Silica supply is not deemed to be important in current cementation models (Walderhaug, 1996; Lander and Walderhaug, 1999; Walderhaug, 2000). Intergranular pressure dissolution and the linked process of stylotization are known as key sources of silica but have fallen out of favour as a rate-controlling process. Intergranular pressure dissolution, or chemical compaction, occurs at grain contacts because the chemical potential of silica at stressed, grain-grain contacts is enhanced over that in the bulk solution (De Boer et al., 1977; Tada and Siever, 1989; Dewers and Ortoleva, 1990; Elias and Hajash, 1992; Shimizu, 1995; Renard et al., 1997; Sheldon et al., 2003; Gratier et al., 2005; van Noort et al., 2008). Silica is thus released at stressed interfaces

and precipitates on free quartz faces. Since the enhancement of chemical potential is a function of effective stress (Elias and Hajash, 1992; Sheldon et al., 2003), it is rational that the rate of intergranular pressure dissolution and thus of silica supply would be related to vertical effective stress (VES), and thus the history of VES through time. However, whilst some studies (Elias and Hajash, 1992; Osborne and Swarbrick, 1999; Sheldon et al., 2003; van Noort et al., 2008) support the idea that intergranular pressure dissolution in sandstones is related to maximum effective stress, others (Oelkers et al., 1996; Walderhaug, 1996; Bjørkum et al., 1998) reported that the process is "stress-insensitive" and catalysed by sheet silicates (clays and micas), with the rate being controlled mainly by temperature (Lander and Walderhaug, 1999; Walderhaug, 2000).

In order to test the role of vertical effective stress on macroquartz cementation, we report here the results of a study in which sandstones currently buried to 190 °C contain much lower amounts of macroquartz cement than is predicted by temperature-related macroquartz cementation models. Fluids within the sandstones are highly overpressured and the current vertical effective stress is low, suggesting that vertical effective stress may have limited macroquartz cementation due to a restriction in the rate of silica supply via intergranular pressure dissolution. However, other factors such as microquartz and clay coatings are known to influence quartz cementation and must be evaluated, and it is the *history* of vertical effective stress rather than the current vertical effective stress which would be expected to control the extent of silica supply via intergranular pressure dissolution.

Here, therefore, i integrate detailed quantitative petrographic analyses, high spatial resolution oxygen isotope analyses of macroquartz cement, basin modelling, and kinetic modelling of quartz precipitation in order to evaluate the hypothesis that it is the history of vertical effective stress, rather than that of temperature, that is a key control on macroquartz cementation. The following questions were also evaluated in this study:

(a) What is the role of grain coating clays and microquartz on quartz cementation in the Fulmar Formation sandstones from Elgin Field?
(b) Does hydrocarbon charge exert any influence on quartz cementation in the Fulmar Formation sandstones from Elgin Field?

4.3. Geological Setting

Elgin is part of the high pressure, high temperature (HPHT) area of the Central North Sea located in United Kingdom Quadrant 22, blocks 22, 24, 29 and 30, about 240km east of Aberdeen. It is surrounded by other producing fields including: Shearwater to the north east, Glenelg to the west, and Franklin to the south (Figure 4.1). The Elgin area experienced extensional events in the Triassic and the Late Jurassic/Early Cretaceous prior minor compression phases that spans through Neogene (Eggink et al., 1996; Lasocki et al., 1999). Structurally, the field is an anticline bounded by sub-vertical faults, and also traversed and compartmentalised by sealing NW-SE trending minor normal faults (Lasocki et al., 1999). The general structure of the field has been significantly influenced by halokinesis. Elgin field is a complex structural anticlinal trap (Lasocki et al., 1999) with the Upper Jurassic shallow marine Fulmar sandstone as the main reservoir and an average thickness of about 300 m. The reservoir is charged with gas condensate mainly from two sources: Upper Jurassic Kimmeridge Clay and Heather Formations (Lasocki et al., 1999; Isaksen, 2004). The Paleogene and Neogene in the Elgin area were marked by accumulation of thick deposits of the Nordland and Hordaland shales. These formations together with the tight Chalk group impeded fluid flow thus initiating and maintaining high formation pressures in the reservoir sandstones (Darby et al., 1996). The Upper Jurassic Fulmar sandstone in the Elgin field has experienced high pore fluid pressure around 110 MPa, and high temperature around 190 $^{\circ}$C. At these conditions, the Fulmar sandstone reservoir in the Elgin area is one of the deepest and hottest in the Central North Sea.

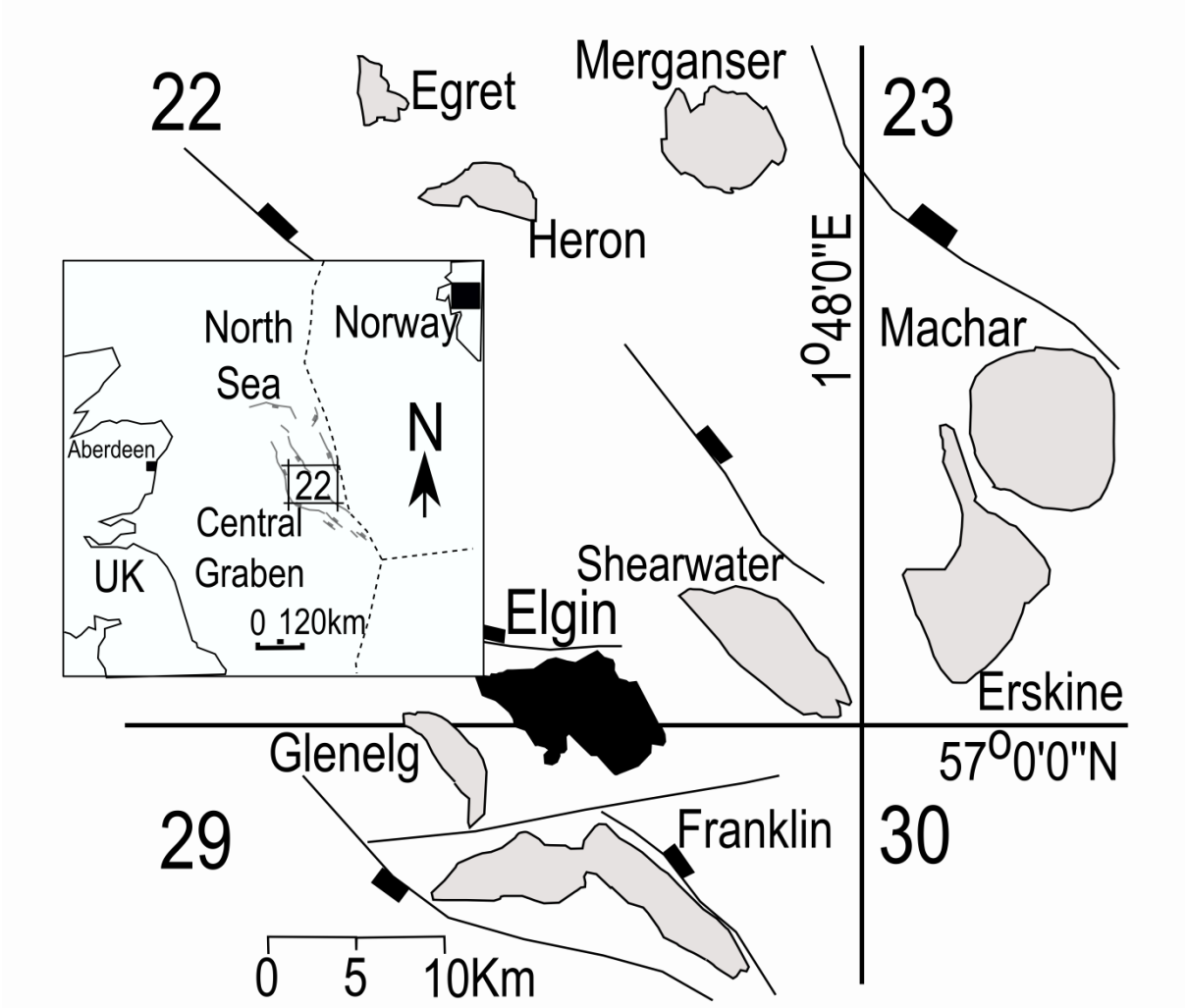

Figure 4.1. Map of the Central Graben in the UK North Sea showing Elgin field and other surrounding hydrocarbon fields

4.4. Fulmar Formation Sedimentology and Stratigraphy

The Upper Jurassic Fulmar Formation is the primary hydrocarbon producing reservoir in many oil fields in the UK sector of the Central Graben. Apart from the northwest of the Elgin field where the Base Cretaceous unconformity (BCU) erodes down to the Fulmar level, the formation (Figure 4.2) is overlain conformably by the Heather and the Kimmeridge Clay Formations (Lasocki et al., 1999). The Pentland Formation underlying the Fulmar is also perceived to be virtually conformable in the axial part of the Central Graben (Lasocki et al., 1999). The Upper Jurassic Fulmar Formation is a highly bioturbated heterolithic, shallow marine, sand-silt deposit (Gowland, 1996), and often occurs as coarsening-upward succession grading from siltstones into very fine-medium-grained sandstone (Stewart, 1986; Gowland, 1996; Lasocki et al., 1999; Hendry et al., 2000; Taylor et al., 2015). Occasional fining-upward successions have also been delineated locally (Gowland, 1996; Lasocki et al., 1999). The dearth of sedimentary structures due to intense bioturbation, and the influence of synsedimentary tectonism and halokinesis created a complicated facies pattern within the Fulmar sandstone (Gowland, 1996; Hendry et al., 2000). Hence, facies characterisation of these sandstones often requires a more detailed study of lithology, grain sizes, sedimentary structures (where present), and ichnofabrics like *Teichicnus* and *Ophiomorpha* (Taylor and Gawthorpe, 1993; Gowland, 1996).Depositional profile delineation using litho facies and ichnofabric description shows that the upper shoreface to offshore transition zones predominate in the Fulmar Formation of the Elgin field (Lasocki et al., 1999).The occurrence of abundant rock-forming siliceous sponge spicules, of the genus *Rhaxella*, has been reported in some intervals within the Fulmar Formation (Gowland, 1996). Gowland (1996) and Taylor et al. (2015) described these *Rhaxella* sponge spicules as the likely source of grain-coating microcrystalline quartz in the Fulmar sandstone. Helium porosities of up to 30 % in some deeply-buried clean facies indicate that these sandstones are anomalously porous relative to other North Sea sandstones (Osborne and Swarbrick, 1999).

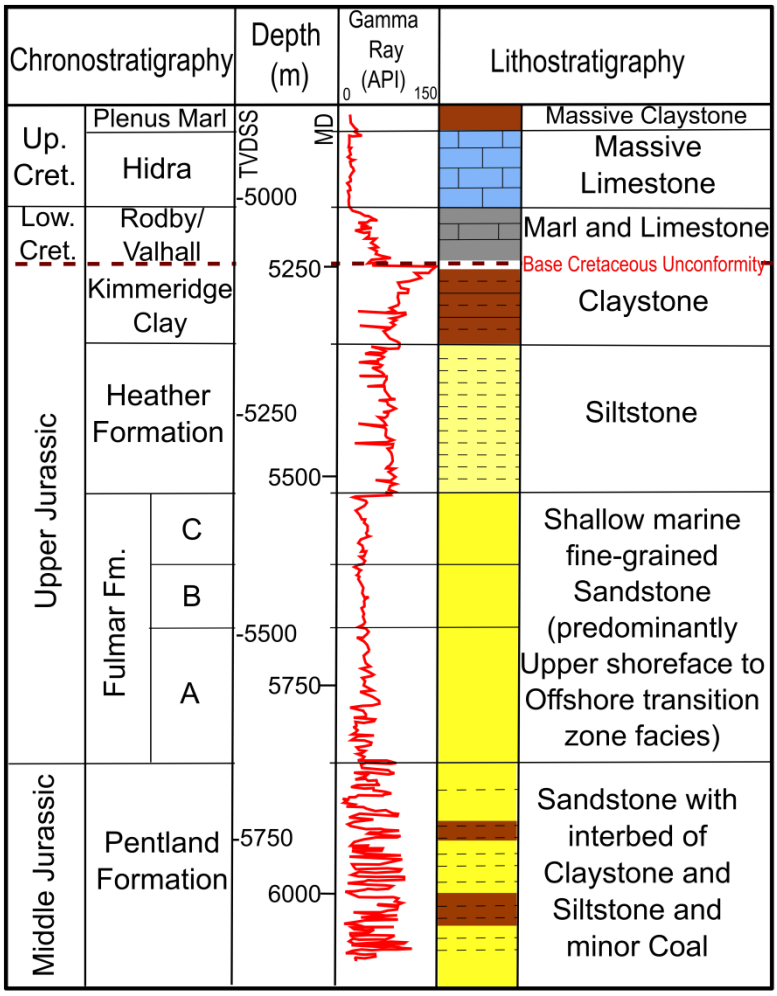

Figure 4.2. Stratigraphy of the Middle Jurassic to Upper Cretaceous in well 22/30C-G4 of the HPHT Elgin Field, Central North Sea, UK

4.5. Methodology

4.5.1. Sampling Strategy

Core samples investigated in this study were selected from Upper Jurassic Fulmar Formation in Elgin field (22/30C-G4) with present-day vertical effective stress and temperature of 12.5 MPa and 189 °C. The Fulmar sandstones in the Elgin field are most probably at their maximum burial depth with maximum formation pressure and temperature conditions. The sampled intervals were chosen to target the Fulmar sandstone facies with the best reservoir quality based on facies characteristics described by Gowland (1996), in order to limit the number of controlling variables. Hence, nineteen samples from clean upper shoreface sandstone facies, mainly the "B" sands (Figure 4.2), between 5400 and 5440 m true vertical depth sub-sea (TVDSS) were selected for analysis.

4.5.2. Petrography

Petrographic analyses were carried out on rock chips and thin sections prepared from core samples using optical microscopy, and combined scanning electron microscope and cathodoluminescence (SEM-CL) microscopy. The standard petrography work was conducted using a Leica DM 2500P microscope fitted with a light-emitting diode (LED) illumination source to enhance light transmission through thin sections. A Conwy Valley Systems Limited Petrog digital petrography system was integrated with the Leica microscope for quantification work. The system allowed systematic calculation of the proportion of grain types, grain contacts, grain coats, matrix and cement by making not less than 300 point counts in thin section slides and expressing the result in percentage (Nichols, 2009).

The analysed sample sets were carefully screened for carbonate cements, and optical microscopy revealed that these cements are heterogeneously distributed in the sample sets. We, therefore, deemed it fit to reject these carbonate-bearing samples; since early carbonate cement can significantly occlude porosity and thus bias quartz cement results. Overall, ten carbonate-free samples representing the full range of quartz cement contents were analysed during cathodoluminescence (CL) petrography.

Whilst based on well-established concepts (Sibley and Blatt, 1976a; Houseknecht, 1991; Evans et al., 1994), we developed an improved SEM methodology with which to quantify the amounts of overlap and authigenic quartz over statistically meaningful

sample areas. CL imaging used a Gatan mono-CL3 detector connected to a Hitachi SU-70 Analytical UHR Schottky Emission Scanning Electron Microscope. An Oxford Instruments' energy dispersive x-ray (EDX) system (X-MaxN 50 Silicon Drift Detector) was used to obtain the Si element map. Panchromatic CL images were obtained at x300 magnification, 1024 x 1024 resolutions, from predefined 3 mm x 3 mm areas from each thin section. A mosaic of about 70 frames of CL images representing the 9 mm^2 area was acquired in one hour. The CL mirror was then retracted to allow Si maps to be acquired over the same area, so that a complete CL and EDX data set was acquired in seven hours. Using the Si element map to identify quartz and the CL to identify quartz cement (Figure 2.2), we then manually point-counted both overlap quartz (points of quartz to quartz grain dissolution) and authigenic quartz using a grid of 1600 (40x40) square boxes superimposed on the CL image. The central point in each box is counted, generating 1600 data points per sample.

4.5.3. Effective Stress and Temperature Histories

The evolution of sedimentary basins and hydrocarbon reservoirs through time can be reconstructed using basin modelling software. The one-dimensional basin modelling approach was adopted in the current study to provide insight on how Fulmar Formation reservoir temperature and effective stress evolved through time in the Elgin field. Though the technique is limited by its inability to model fluid migration, lateral flow, and hydrocarbon charge, overpressure generation from compaction disequilibrium can be effectively simulated. Compaction disequilibrium is generally the most quantitatively important overpressure generation mechanism; if other processes, such as gas generation, also contributed to overpressure, this would act to reduce the effective stress through time. The one-dimensional modelling work was carried out using Schlumberger's PetroMod software (Version 2014.1). The software uses a forward modelling approach to reconstruct the burial histories of sedimentary basins. The present-day stratigraphic layers and thicknesses, lithology, and lithological description (Table 4.1) used for the modelling were obtained from well composite logs, geological well report, core analysis, and core description reports. Geological ages derived from the Millenium Atlas (Gluyas and Hichens, 2003) were used to set the model. Heat flow models were built after Allen and Allen (2005), with an average of 62 mW/m^2 throughout the basin's history. The highest heat flow values, 70 and 90 mW/m^2, were recorded consecutively at the peaks of the Permo-Triassic and Upper Jurassic paleo-

rifting events recorded in the North Sea geology. The thermal model was calibrated using corrected bottom-hole temperature obtained from operator's report, and vitrinite reflectance data as paleothermometer. In order to model compaction, Fulmar Formation porosities from routine core analysis were incorporated in the model. Since porosity is a function of lithology, tighter constraints were placed on the model by modifying PetroMod's default lithologies to match those observed on the field. These lithologies were defined using well composite logs and core analysis description. Base on this study, the Chalk Group and the Pre-Cretaceous shales (Kimmeridge Clay and Heather Formations) are very important for modelling the observed high pore pressure in the Fulmar Formation. The default chalk and shale permeabilities in PetroMod were modified after Swarbrick et al. (2000),to lower values for the Chalk Group and the Pre-Cretaceous shales until modelled pore pressure matches Present-day formation pressures.

4.5.4. Quartz Precipitation Kinetic Modelling

Walderhaug's (1996) quartz cementation model was used to model the growth of quartz cement in the HPHT Fulmar sandstone samples from Elgin field. This mathematically simple model uses a logarithmic function of temperature to calculate quartz cementation (Walderhaug, 1996; Walderhaug, 2000). Although there are other sophisticated Arrhenius-based models in which the rate of cementation can be adjusted by changing the activation energy, these were not available for this study. Walderhaug model is based on observations from reservoir sandstones from many oil fields and has been used extensively in the North Sea. For example; precipitation rates were calculated for some North Sea Brent Group sandstones using the logarithmic function, and the output was analogous to those calculated for the same set of sandstones using an Arrhenius-based function. (Walderhaug, 2000).

The Fulmar Formation sandstones from Elgin field are arkosic - subarkosic in composition; hence, the model was applied to only the quartz fraction of the bulk rock. The kinetic model was run using Walderhaug (1996) standard parameters This involved the use of $1cm^3$ of sandstone, 80°C threshold temperature and a starting porosity of 26 % (approximate porosity at the onset of quartz cementation) of bulk rock volume. The model also used pre-exponential a (1.98×10^{-22} moles/cm^2s) and exponential constant b (0.022°C) calculated by Walderhaug (1994b) for some North Sea sandstones. Detrital

quartz fractions and grain sizes were estimated from CL petrographic analysis of thin sections. The percentage of detrital quartz surface area with grain coats was calculated through visual inspection and manual quantification using CL, BSE and silica maps acquired over the same sample area. The method was adopted because BSE images usually facilitate easy identification of both grain-coating clays and microquartz in thin sections. Microquartz was, however, very rarely observed. The CL images also helped reveal if grain coatings are present on detrital or authigenic quartz. In order to incorporate grain-coat data into the model, the initial quartz surface area was reduced using the estimated grain coatings coverage area. This approach is similar to the method introduced by Walderhaug (2000). Heating rates were calculated from time-temperature histories generated from basin model constructed using PetroMod (version 2014.1).

4.5.5. Oxygen Isotope Analysis

Secondary Ion Mass Spectrometry (SIMS) analysis was performed at the WiscSIMS Laboratory at the University of Wisconsin-Madison. Three separate quartz grains with overgrowths thicknesses between 40 and 60 µm were chosen for *in situ* oxygen isotope analysis. Profiles of oxygen isotope ratios were measured using a 3 µm spot diameter on a CAMECA IMS 1280 ion microprobe (Kita et al., 2009). In order to correct measured $\delta^{18}O$ values to the Vienna Standard Mean Ocean Water (VSMOW) scale, bracketing standards were used to calculate the instrumental bias (Kita et al., 2009). Based on repeat analyses of the University of Wisconsin (UWQ-1,Kelly et al. (2007)) quartz standards embedded within samples cast in epoxy mount, the spot-to-spot external precision of all bracketing standards averaged 0.68 ‰ (2 SD) for the 3-µm spots. A more detailed SIMS analytical procedure is described in Page et al. (2007), Kita et al. (2009), Valley and Kita (2009) and Pollington et al. (2011). All data are reported in Appendix 3.

Table 4.1. Formation thicknesses and Lithotypes used for Elgin burial history modelling. Percentage values show mix ratio for interbedded Formations.

System	Series	Group	Age (Ma)	Formation	Lithology	Thickness (m)
Neogene	Miocene - Pleistocene	Nordland Group (Undiff.)	13	Nordland Group (Undiff.)	Shale	1416
Paleogene	Eocene - Miocene	Hordaland Group (undiff.)	54	Hordaland Group (undiff.)	Shale	1579
Paleogene	Eocene	Rogaland	54.3	Balder Fm	Silty Shale 95% tuff 5%	30
Paleogene	Paleocene	Rogaland	56	Sele Fm	Shale 65% Sandstone 35%	48
Paleogene	Paleocene	Montrose	57.8	Lista Fm	Shale	79
Paleogene	Paleocene	Montrose	58.3	Lista Fm (Andrew Member)	Shale 65% Limestone 35%	63
Paleogene	Paleocene	Montrose	62.5	Maureen Fm	Shaly Limestone 90% Marl 10%	130
Paleogene	Paleocene	Chalk	65	Ekofisk Fm	Chalk 85% Silt 5% Clay 5% Marl 5%	102
Cretaceous	Upper	Chalk	72	Tor Fm	Chalk	502
Cretaceous	Upper	Chalk	91	Hod Fm	Chalk 90% Marl 10%	718
Cretaceous	Upper	Chalk	93	Herring Fm	Chalk	144
Cretaceous	Upper	Chalk	94	Plenus Marl Fm	Shale	2
Cretaceous	Upper	Chalk	99	Hidra Fm	Chalk	85
Cretaceous	Lower	Cromer Knoll	107	Rodby Fm	Shale 65% Limestone 30% Marl 5%	15
Cretaceous	Lower	Cromer Knoll	128.5	Valhall	Shale 60% Marl 40%	49
Jurassic	Upper	Humber	153	Kimmeridge C. Fm.	Shale (black)	103
Jurassic	Upper	Humber	156	Heather Fm	Shale (organic rich, typical)	334
Jurassic	Upper	Humber	158.4	Fulmar Sands	Sandstone (arkose, quartz rich)	160
Jurassic	Middle	Fladen	166	Pentland Sand	Sandstone (clay rich)	164
Jurassic	Middle	Fladen	170	Pentland Shale	Shale (organic rich, typical)	110

4.6. Results

4.6.1. Burial, Thermal and VES Histories

The burial history of the Fulmar sands is characterised by (a) 1 km of rapid burial in the late Jurassic, (b) a period of very limited deposition in the early Cretaceous and (c) increased sedimentation rate of ~ 42 m/Myr from ca. 100 Ma to the present-day, with particularly rapid sedimentation rate of ~70 m/Myr in the last 12 Ma. The resulting temperature, pore pressure and effective stress histories are shown in Figure 4.3. With overpressure being generated from around 90 Ma, these constraints suggest that the vertical effective stress has been low throughout the entire burial history and has never been greater than the present-day value of 12.5 MPa. In terms of temperature, the Fulmar has resided within the classic > 70 - 80 °C quartz cementation window (Walderhaug, 1994a) for the last 90 Ma.

4.6.2. Petrographic Observations

The investigated Fulmar sandstones from Elgin field are clean upper shoreface facies. These sandstones are arkosic to sub-arkosic in composition with sub-angular to sub-rounded grain shapes. Initial grain sizes (original grain sizes at deposition) measured from CL petrographic data ranges from 0.063 - 0.36 mm, with an average of 0.156 mm. The limited grain size variability of these sandstones is shown on the grain-size graph with most sandstones being fine grained. The observed low clay (mainly illite) content, about 2.8 % of bulk volume, was expected as sample selection was originally designed to target clean upper shoreface sands. These clays are bitumen impregnated and are often found filling pores or coating detrital and authigenic quartz surfaces. Whole or partial dissolution of K-feldspars and their overgrowths are common features in these sandstones. Where the feldspars are wholly dissolved, a mouldic clay outline has preserved their original shapes. Pore-filling authigenic illites are sometimes found adjacent to these dissolved feldspars, suggesting their formation from the dissolution process. Other minor components observed are micas, pyrites and bitumen. Average optical and helium porosities in the Fulmar sandstones are 14.3 and 22 % (Table 4.2). All petrographic data are reported in Appendix 1. Carbonate and quartz make up the main diagenetic cements. The carbonate cements average ~9 % of bulk rock volume. Point count data from standard petrography and core examination shows these carbonate cements are unevenly distributed. A more detailed study on these cements was carried out by Hendry et al. (2000). Apart from dolomite and ferroan dolomites, syntaxial ankerite rims on dolomite nucleus were commonly observed in these samples.

Generally, these carbonate cements either occurs in isolation within available pore spaces or as pore occluding cement destroying porosity across large area. Evidence from fluid-inclusion analysis suggests the ankerite cements were precipitated at high temperatures (140 – 170 °C), and their formation immediately precedes hydrocarbon emplacement in the Elgin field (Hendry et al., 2000).

4.6.3. Quartz Cementation and Chemical Compaction

Two types of diagenetic quartz cements, macroquartz and microquartz, were identified in the analysed samples (Figure 4.4, Figure 4.5 and Figure 4.6). These cements occur as overgrowths on free detrital quartz surfaces. In this study, the term "microquartz overgrowth" is used to describe randomly oriented, thin, polycrystalline quartz overgrowths ranging from 1 to 10 µm in length. Microquartz overgrowths are predominantly absent in the analysed sandstones; with lengths around 1µm where present (Figure 4.5B). In contrast, the macroquartz overgrowths are syntaxial and blocky, and in optical continuity with detrital quartz when viewed under transmitted light. Apart from the fact that these quartz overgrowths are not continuous along grain boundaries, they also exhibit stunted growths by not growing fully across available pore spaces (Figure 4.4B). Another key observation is the engulfment of some of the early formed grain-coating illites by these quartz overgrowths.

Chemical compaction is a process of rock volume reduction by stress-sensitive pressure dissolution along grains or stylolitic contacts. The released materials (e.g. silica) are then re-precipitated locally on free detrital grain surfaces. The chemical compaction estimation method used by Sibley and Blatt (1976a) and Houseknecht (1991) was used to quantify the effect of intergranular pressure dissolution in the analysed sandstone samples. This quantification was performed on the same large area CL maps use for quartz cement quantification. Grain boundaries were projected along grain contacts where it appears dissolution has taken place (Figure 4.4B), and the inferred features were point-counted as percentage volumes of silica dissolved by intergranular pressure dissolution. Chemical compaction estimates from CL petrography (Figure 4.4B and Table 4.2) suggests an average of 2.7 ± 0.8 % of silica was released into the system by intergranular pressure dissolution. The textural maturity of the Fulmar sandstone was factored into the quantification process to reduce uncertainties.

4.6.4. Isotopic Composition of Quartz Cements

Similar to Harwood et al. (2013), we used high-spatial resolution SIMS to create 3-µm spot-size $\delta^{18}O$ profiles across three, 40-60 µm thick macroquartz overgrowths in one of the sandstone samples. Forty $\delta^{18}O$ measurements were made by SIMS on three different quartz grains, five from detrital quartz and thirty-five from their corresponding overgrowths, were taken during the entire analysis session. Four out of the thirty-five overgrowth measurements were compromised by the occurrence of fluid inclusions or included detrital quartz and discarded (Appendix 3). The remaining analyses are shown as a function of the distance from the detrital grain boundary in Figure 4.7. All $\delta^{18}O_{(quartz\ cement)}$ values fall within a 2.7 ‰ range, from +19.7 to +22.4 ‰ V-SMOW (Figure 4.7); the $\delta^{18}O$ values from all three overgrowths overlap and there is no trend from grain boundary to cement edge, and no relationship to concentric CL zonation.

Table 4.2. Petrographic analyses of the Upper Jurassic Fulmar Formation samples form Elgin Field, UK Central North Sea

	Mean	Standard deviation	Minimum	Maximum	Population
Detrital grain size (mm)	0.16	0.05	0.06	0.36	10
Quartz (%)	44.2	5.6	32.3	55.7	19
Feldspar (%)	23.5	3.4	17.3	29.7	19
Lithic Fragments (%)	1.1	0.7	0	2.7	19
Quartz cement - standard petrography (%)	2	1.4	0.3	6.3	19
Quartz cement - CL petrography (%)	4.6	1.2	2.1	6.4	10
Intergranular Pressure Dissolution - CL petrography (%)	2.7	0.8	1.4	3.8	10
Carbonate cement (%)	9.4	12.3	0	40	19
Intergranular porosity (%)	11	4.6	1.7	20.7	19
Intragranular porosity (%)	3.3	1.5	1	8	19
Core Porosity (%)	22	5.2	8.5	27.9	33
Total clay (%)	2.8	2.3	0.7	9.3	19

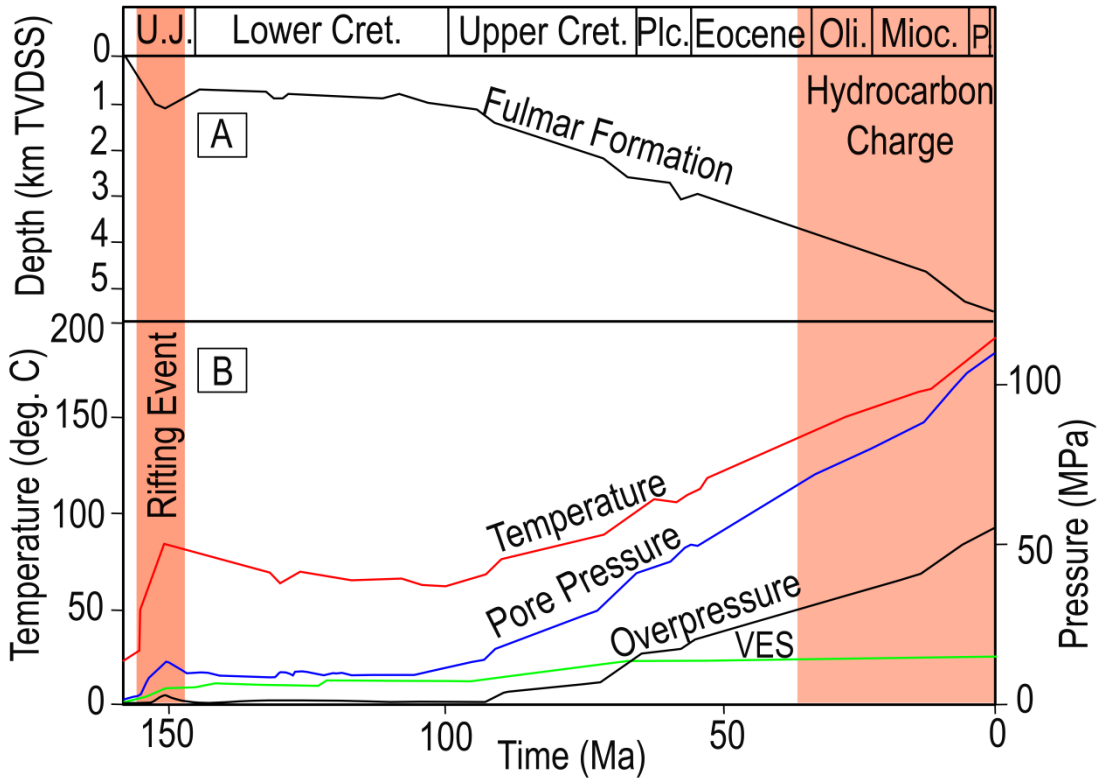

Figure 4.3. A) Modelled burial plot with depth in meters TVDSS (true vertical depth subsea). B) Modelled temperature, pore pressure, overpressure, and vertical effective stress (VES) histories for the Upper Jurassic Fulmar Formation of the HPHT Elgin field. These models were constructed by using a forward-modelling approach on PetroMod 1D version 2014.1. Overpressure was assumed to be due mainly to compaction disequilibrium and builds from ca. 90 Ma and Hydrocarbons were charged to the reservoir from ca. 40 Ma.

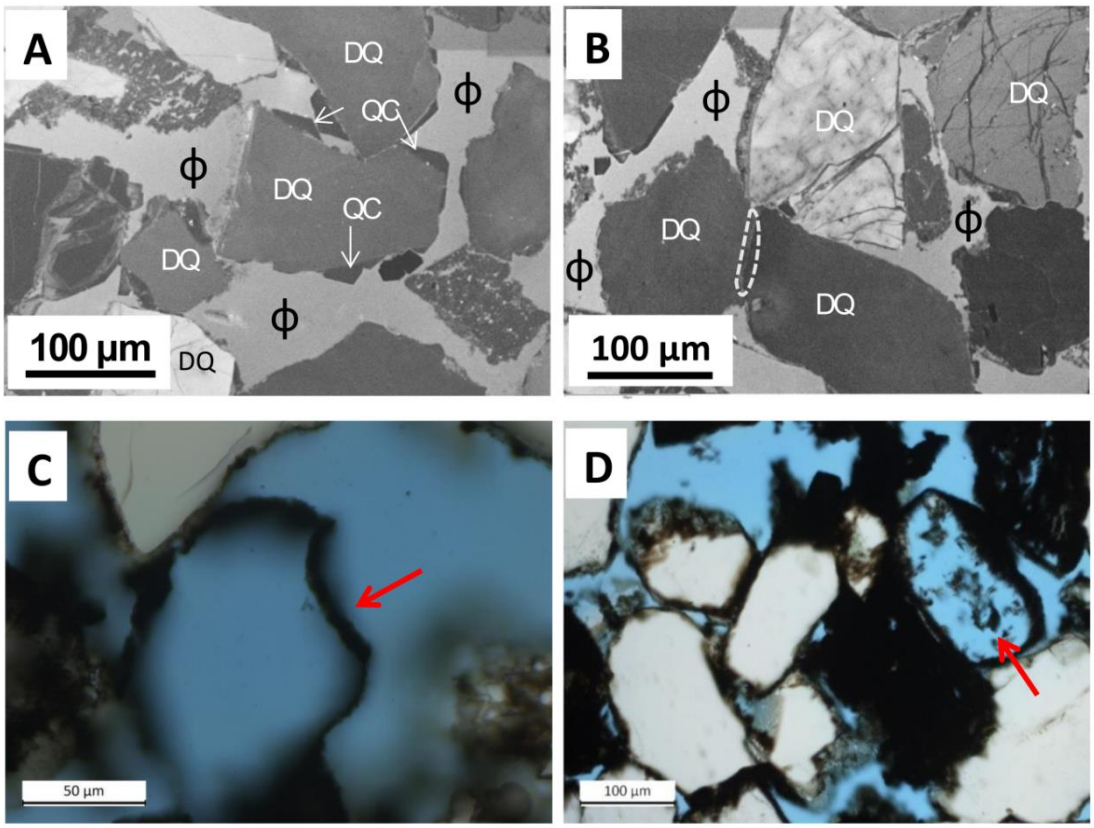

Figure 4.4. Photomicrographs of Fulmar Formation sandstones from HPHT Elgin field in the Central North Sea; A) CL image showing quartz cement (QC) on detrital quartz (DQ). Quartz cements are poorly developed despite significant porosity and very high present-day temperature (190 °C). B) CL image showing definition of overlap quartz (pressure dissolution) in dashed trace. Red arrows in plates C and D indicate intragranular porosity due to feldspar dissolution. Original grain shape is preserved as bitumen-impregnated clay rim.

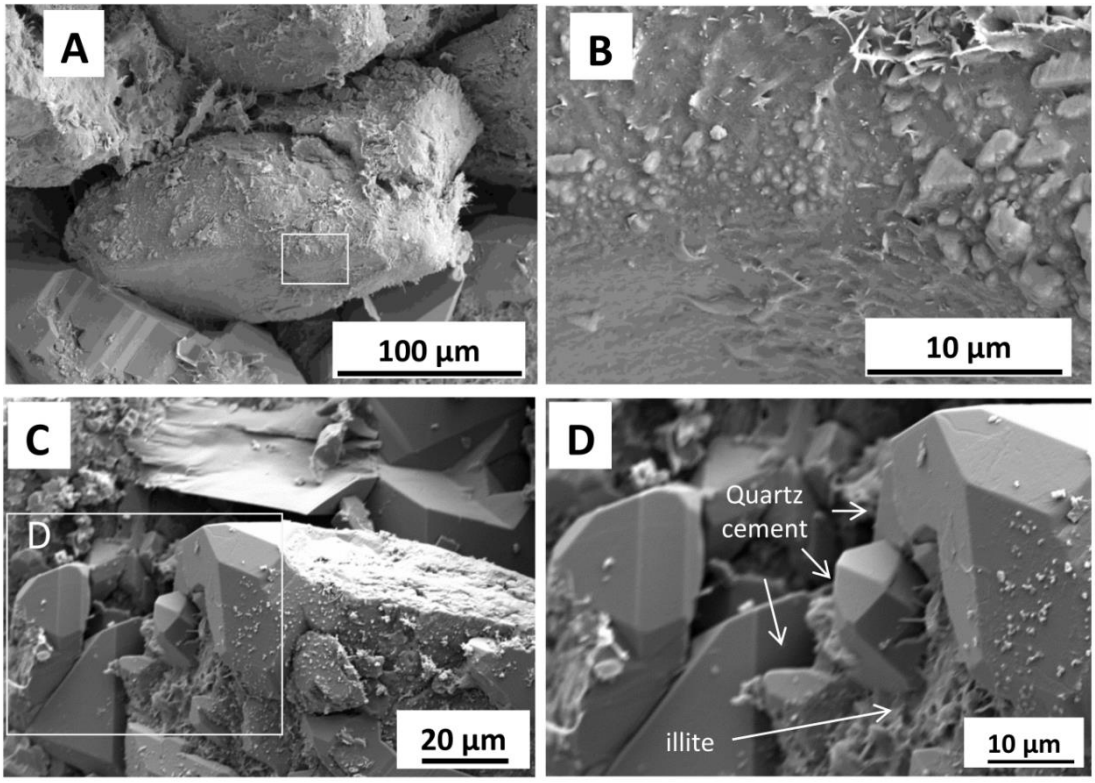

Figure 4.5. SEM images of Upper Jurassic Fulmar Formation sandstones from Elgin field. A) Low magnification of a quartz grain surface with limited clay and microquartz coatings. B) High magnification corresponding to the box in Plate A showing poorly developed microquartz overgrowth and clay coats. Microquartz overgrowths are very uncommon in this study. C) Low magnification SEM image of quartz grains with macroquartz cement. D) Higher magnification image corresponding to the box in Plate C showing that the presence of poorly-developed illite coatings did not prevent the growth of macroquartz

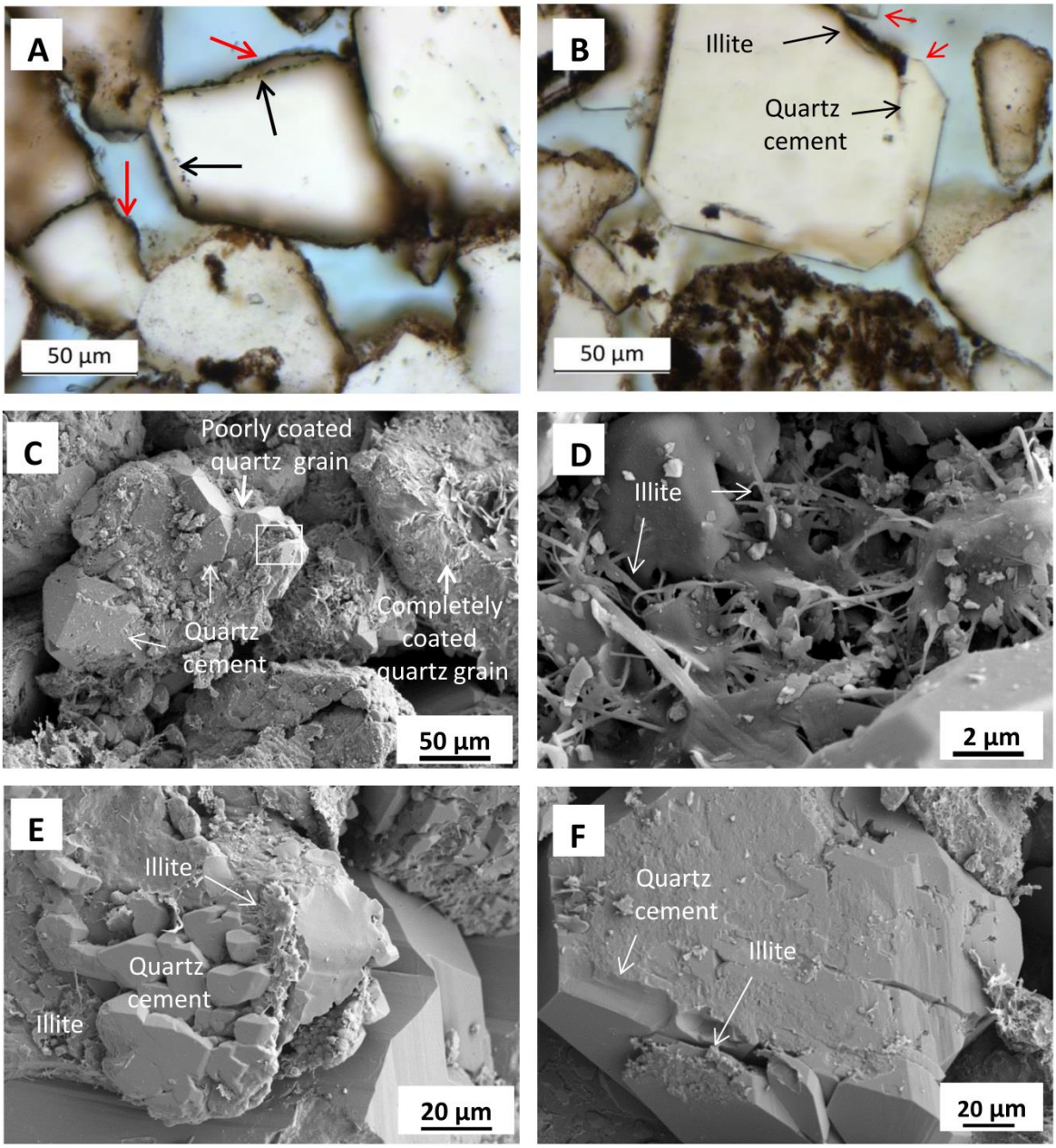

Figure 4.6. Micrographs of Upper Jurassic Fulmar Formation sandstones from Elgin field. A) Bitumen-stained illite with later quartz cement (black arrow); bitumen- impregnated authigenic illite (red arrows) coating earlier quartz cement surfaces. B) Quartz cements (red arrows) projecting over incomplete, bitumen-stained illite coatings. C) Quartz grain with quartz cement adjacent to another grain lacking quartz cement due to complete illite coatings. D) High magnification image corresponding to the box in Plate C. E) Quartz cement nucleation on detrital grain with poorly-developed illite coatings. F) Later illite formed on quartz cement.

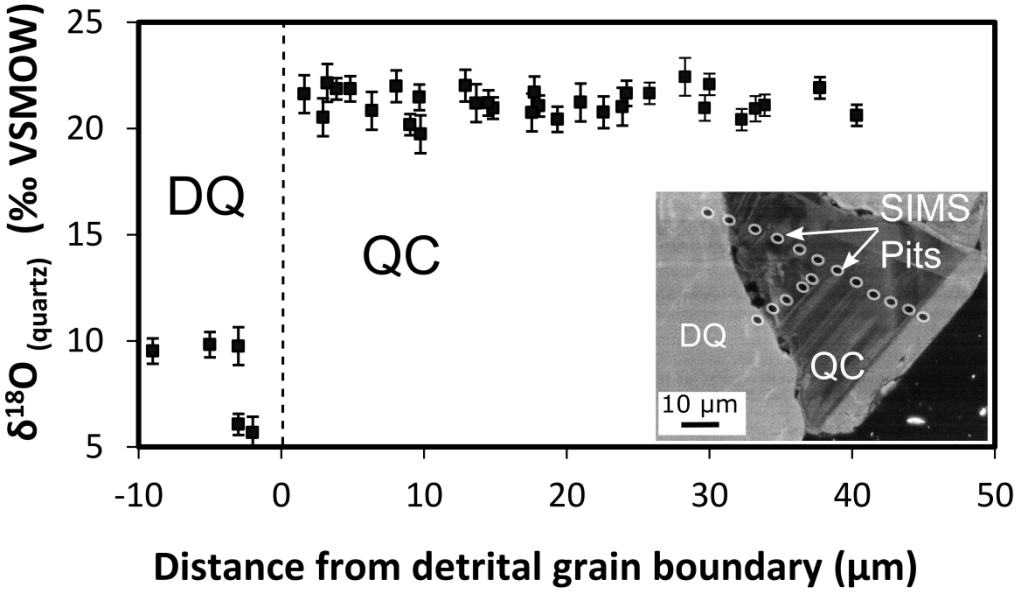

Figure 4.7. Plot of $\delta^{18}O$ of quartz cement (QC) and detrital quartz (DQ) against distance in microns from detrital grain boundary for three quartz overgrowths. The inset CL micrograph shows one of the three analysed overgrowths. The CL image shows 3µm diameter ion microprobe sampling spots (SIMS pits),

4.7. Controls on Quartz Cementation

It is commonly assumed that the rate-controlling step for quartz cementation of sandstones is the precipitation of silica (Walderhaug, 1994a; Walderhaug, 1996; Ajdukiewicz and Lander, 2010). In this scenario, the kinetic barriers which inhibit quartz precipitation are overcome, on geological timescales, at temperatures around 70 to 80 °C (McBride, 1989; Walderhaug, 1994a; Worden and Morad, 2000), above which rates of precipitation increase exponentially with temperature (Walderhaug, 1996). Models using these commonly-used precipitation kinetics predict that sandstones which, like those in Elgin, are buried to ca. 190 °C and have experienced temperatures greater than 80 °C for about 90 Myrs, would be very extensively cemented with quartz; however, samples in this study only have an average macroquartz cement content of 4.6 ± 1.2 vol. %. Previous studies (Osborne and Swarbrick, 1999; Taylor et al., 2015) have also reported the presence of low volumes of macroquartz cement in other Central North Sea HPHT sandstones. While Osborne and Swarbrick (1999) attributed the lack of quartz cement mainly to the effect of low VES induced by overpressure, Taylor et al. (2015) concluded that the effect of overpressure is insignificant, and that grain coatings are by far the most important factor. In this section, we provide a critical assessment of the controls on quartz cementation in these Fulmar sandstones and offer the best explanation for the occurrence of the small volumes of macroquartz cement.

4.7.1. Feldspar Dissolution

Sandstones in this study are rich in feldspar, especially K-feldspars and some plagioclase. Partially or completely dissolved feldspars with initial shape preserved as mouldic pores (Figure 4.4C and D) are common occurrence in the Upper Jurassic Fulmar sandstones (Wilkinson and Haszeldine, 1996; Osborne and Swarbrick, 1999; Taylor et al., 2015), and were also observed in this study. Feldspar dissolution as a mid to late diagenetic process in deeply buried Upper Jurassic Fulmar Formation has profound positive effect on reservoir quality (Wilkinson et al., 1997; Lasocki et al., 1999). However, volume of porosity from feldspar dissolution may not equal net porosity gain as part of the porosities are offset by products of the reaction: such as newly formed illite which may be deposited in adjacent intergranular pores (Giles, 1987; Taylor et al., 2015), and silica (Osborne and Swarbrick, 1999; Worden and Morad, 2000) which may precipitate as macroquartz cements on detrital nuclei. Petrographic data from modal analysis of thin sections reveals intragranular porosity from feldspar dissolution makes up about 3.3 % of bulk rock volume in the analysed

samples. These data could be used to estimate the volume of illite (Osborne and Swarbrick, 1999) and silica contributed to the system by dissolved feldspars. Elgin is a classic case of where silica contribution from feldspar dissolution could be adjudged as volumetrically significant, given the low volume of macroquartz cement observed in the Fulmar Formation. Writing the conversion of K-feldspar to illite as:

1.0 K-feldspar + 0.174H2O + 0.522 H+ + 0.109 Mg2+ = 0.739 K+ + 0.435 illite + 1.478 quartz,

and using the amount of illite (2.8%) observed in these samples as a reaction product, I estimate that dissolved feldspars supplied around 25 % silica for macroquartz cementation in the studied sandstones.

4.7.2. Grain-coating Microquartz

The occurrence of grain coating microquartz on the detrital quartz have been described as an effective inhibitor of macroquartz cementation in deeply buried sandstones (e.g. Aase et al. (1996)). As sandstones containing *Rhaxella* sponge spicules undergo increasing burial and temperature, the spicules dissolve to precipitate on clean detrital quartz surfaces as tiny microcrystalline quartz overgrowths (Aase et al., 1996; Osborne and Swarbrick, 1999). Various mechanisms have been proposed to explain how grain-coating microquartz inhibits the development of macroquartz cements: first, by inhibiting intergranular pressure solution through maintaining a higher equilibrium activity of dissolved silica as a result of the higher solubility of microquartz; and second, by arresting both mechanical and chemical compaction/pressure dissolution through the early formation of a rigid framework structure due to microquartz precipitation (Aase et al., 1996; Osborne and Swarbrick, 1999). Recent studies (French et al., 2012; Worden et al., 2012; French and Worden, 2013) have, however, identified an amorphous silica layer that usually exist between quartz grains and microcrystalline quartz overgrowths that not only give the overlying microcrystalline quartz their random orientation, but also insulates the host grain from macroquartz precipitation.

Several studies (Stewart, 1986; Aase et al., 1996; Gowland, 1996; Osborne and Swarbrick, 1999; Taylor et al., 2015) have documented the occurrence of sponge spicules and microquartz overgrowths within some stratigraphic intervals in the Upper Jurassic Fulmar and other Mesozoic sandstones in the Central North Sea. However,

detailed transmitted and SEM analysis shows that grain-coating microquartz cements are predominantly absent in our sample set (Figure 4.5A and B). Sparse and incomplete microquartz overgrowths were also reported by Taylor et al. (2015) in the Fulmar sandstones from Shearwater field, about 6km to the East of Elgin. Even though the present-day pore pressure in these reservoirs suggests the existence of a closed system; this seemingly rare and poorly-developed grain-coating by microquartz cements cannot be responsible for their low volume of macroquartz cement.

4.7.3. Grain-coating Clays

The grain coating effect of clay minerals as an inhibitor of macroquartz cementation has been well documented by several authors (Heald and Larese, 1974; Bloch et al., 2002; Berger et al., 2009; Morad et al., 2010; Nguyen et al., 2013; Stricker et al., 2016b). Authigenic chlorite-coat not only occurs more frequently than any other clay-coats, it is also the most important and effective inhibitor of macroquartz cementation (Taylor et al., 2010). The grain-coating ability of illite has also been reported, though less frequently than chlorite (Storvoll et al., 2002; Taylor et al., 2010). Numerous studies (Wilkinson and Haszeldine, 1996; Wilkinson et al., 1997; Osborne and Swarbrick, 1999; Wilkinson and Haszeldine, 2011; Taylor et al., 2015) have shown that illite is by-far the most common authigenic clay in the Upper Jurassic Fulmar Formation. Previous studies (e.g. Wilkinson and Haszeldine, 1996; Taylor et al., 2015) have shown that authigenic illite precipitates as one of the products of feldspar dissolution in the Upper Jurassic Fulmar Formation. If feldspar dissolution in the Upper Jurassic Fulmar Formation occurred during middle - late diagenesis (Haszeldine et al., 1999; Lasocki et al., 1999; Wilkinson and Haszeldine, 2011), it follows logically that dissolution-sourced authigenic illite first developed around same period. This contradicts observations made by Storvoll et al. (2002) in the Northern North Sea Garn Formation where authigenic illite precipitated at temperatures < 70 – 80 °C. Since the macroquartz cementation threshold is around 80 °C (e.g. Walderhaug, 1994a), some macroquartz cement would have precipitated on free detrital quartz surfaces in the Upper Jurassic Fulmar Formation prior to authigenic illite formation. Evidence from petrographic analysis (Figure 4.6A and F) confirms this assertion, as authigenic illite seen coating the surfaces of some macroquartz overgrowths suggests quartz cementation predates authigenic illite formation.

On the contrary, detrital grain-coating clays from bioturbation (Wilkinson and Haszeldine, 2011; Taylor et al., 2015) may exert some inhibitive effect on macroquartz cementation in the Fulmar Formation, although it is difficult to distinguish detrital illite from authigenic illite as a result of their diagenetic recrystallization (Wilkinson and Haszeldine, 2011). In this study, illite most commonly coats less than 30% of quartz surfaces (Figure 4.8). The effect of these poorly-developed grain-coats is that macroquartz cement often nucleates on the host detrital quartz due to breaks in coat continuity (Figure 4.5C and D, Figure 4.6). Quartz cements also engulf some grain-coating illite (Figure 4.6A). The implication is that discontinuous coats are not a very effective brake on quartz cementation. In order to test this claim, I incorporated clay coat data into the quartz cementation model used for this study. The model (Figure 4.9) suggests that 50% average clay coat coverage for the detrital quartz fraction in the studied sandstones would have little or no effect on quartz cementation. Similarly, comparison with Ajdukiewicz and Lander (2010) porosity-depth/temperature model, in which quartz cementation was modelled using an Arrhenius approach, suggests that sandstones at 190 °C should be completely cemented at the level of grain coat coverage observed in this study (Figure 4.10). The model was subsequently tested by varying the clay coat coverage values. The concurrence between measured and modelled quartz cement volume was achieved around 99 % clay coat coverage (Figure 4.9). A simplified interpretation for this data would mean that each detrital quartz grain in the studied sandstones must be almost completely coated (99 %) in order to limit the average volume of quartz cement to the observed value (4.6 %).

In addition, some studies (Harris, 2006; Fisher et al., 2009) have shown that detrital and authigenic illite at detrital quartz intergranular contacts behaves like other sheet silicates (e.g. micas) by promoting dissolution and subsequently increasing local supply of silica for macroquartz cementation. This silica-supply-enhancement ability of illite would most likely offset some of their restraining effect on macroquartz cementation.

Overall, grain-coating illite has undoubtedly had some influence on quartz cementation in the Fulmar Formation. Their limited distribution and dissolution-enhancing effects along quartz-quartz grain contacts shows these clay coats cannot significantly account for the low volume of quartz cement in the studied HPHT sandstones.

4.7.4.Hydrocarbon Emplacement

The role of hydrocarbon emplacement on macroquartz cementation in deeply buried sandstones has long been a subject of controversy. As a result, two schools of thought exist in the literature: those who suggest that early hydrocarbon emplacement can inhibit macroquartz cementation (Dixon et al., 1989; Saigal et al., 1992; Emery et al., 1993; Gluyas et al., 1993; Worden et al., 1998; Marchand et al., 2000; Marchand et al., 2001; Marchand et al., 2002; Haszeldine et al., 2003; Wilkinson and Haszeldine, 2011; Worden et al., 2018a; Worden et al., 2018b) and those who reported that hydrocarbon charge exerts no significant effect (Aase et al., 1996; Aase and Walderhaug, 2005; Molenaar et al., 2008). In general, field (Worden et al., 1998; Marchand et al., 2002; Maast et al., 2011; Worden et al., 2018b) and experimental (Sathar et al., 2012) observations suggest that early hydrocarbon charge, high hydrocarbon saturation and an oil-wet reservoir are required if hydrocarbons are to effectively halt the macroquartz cementation process.

Elgin is, of course, a hydrocarbon-filled reservoir and I can observe bitumen-impregnated illite coating some detrital quartz grains and overgrowths in the (Figure 4.6A and F). In the context of quartz cementation, it is therefore important to establish the timing of hydrocarbon charge. The reconstruction of the thermal history of the Elgin Horst structure shows that expulsion started from local source rocks in the Eocene. This result was however treated with caution because: (1) I used a one dimensional model that considers only the source rocks on the Elgin Horst structure and previous study (Rudkiewicz et al., 2000) has suggested that these sources contributed minor volume of hydrocarbon to the Fulmar Formation reservoir, and (2) organic geochemistry data suggests that the oil and condensates in the Fulmar Formation reservoir in Elgin are high maturity fluids that are mostly sourced from the Kimmeridge Clay and Heather Formations in the deeper part of the Central Graben (Isaksen, 2004). The hydrocarbon charge history as constrained by Rudkiewicz et al. (2000) using three-dimensional basin model incorporated the deeper source rocks also shows an Eocene arrival time (38 Ma). This implies that the Fulmar Formation in Elgin field would have been in the quartz cementation window for over 50 Myrs (Figure 4.3) prior to significant hydrocarbon charge, and substantial macroquartz cement should still have precipitated in the Fulmar Formation reservoir during burial between the onset of macroquartz cementation (80 °C) to the time of hydrocarbon charge (135 °C). Prior to

being charged, hydrocarbon saturation and wetting state are of course irrelevant as inhibitors of quartz cementation.

This result is consistent with Hendry et al. (2000) study that suggests hydrocarbon emplacement post-dates the precipitation of ankerite cements (140 – 170 °C) in the Elgin field. Oil-impregnation of illite grain-coats most probably formed at high temperatures and thus played little role in inhibiting macroquartz cementation.

4.7.5. Vertical Effective Stress

Vertical effective stress is the pressure exerted on a layer of rock by the weight of overlying sediment or overburden minus pore fluid pressure. The role of vertical effective stress as an effective driver of intergranular pressure dissolution and chemical compaction has been well documented in several studies (Thomson, 1959; Weyl, 1959; Rutter and Elliott, 1976; De Boer et al., 1977; Robin, 1978; Tada et al., 1987; Tada and Siever, 1989; Dewers and Ortoleva, 1990; Dewers and Ortoleva, 1991; Elias and Hajash, 1992; Shimizu, 1995; Renard et al., 1997; Renard et al., 1999; Sheldon et al., 2003; Gratier et al., 2005; van Noort et al., 2008; Nenna and Aydin, 2011). The magnitude of vertical effective stress in a sedimentary system is dependent on the prevalent pore pressure regime, such that an increase or decrease in pore pressure would produce corresponding decrease or increase in vertical effective stress (Osborne and Swarbrick, 1999). Theoretical (Sheldon et al., 2003), experimental (Elias and Hajash, 1992; Gratier et al., 2005; van Noort et al., 2008) and field based (Thomson, 1959; Houseknecht, 1988) evidence show that intergranular pressure dissolution occurs in response to the development of anisotropic stress in sandstones. The presence of sheet silicates only helps to catalyse the process by influencing the rate of dissolution and diffusion (Sheldon et al., 2003). Previous experimental studies on compaction in granular quartz (Rutter and Elliott, 1976; De Boer et al., 1977; Elias and Hajash, 1992; Niemeijer et al., 2002; Gratier et al., 2005; van Noort et al., 2008) revealed that the rate of chemical compaction of quartz-rich sandstones at greater depth (> 2500m) is indeed sensitive to temperature changes, but that the process is mainly controlled by stress-induced pressure dissolution. Since chemical compaction is stress-sensitive, the timely introduction of high pore fluid pressure in compacting sandstone would invariably arrest the driving force (vertical effective stress) for intergranular pressure dissolution and chemical compaction. Since macroquartz cementation is a dissolution-

transport-precipitation process, the inhibition of dissolution (silica source) should slowdown the entire cementation process (Ehrenberg, 1990; Osborne and Swarbrick, 1999; Sheldon et al., 2003; Stricker et al., 2016a) regardless of the prevailing temperature regime.

Basin modelling suggests that the initiation of a continuous phase of overpressure development in the Elgin area started in the early Upper Cretaceous (95 Ma) through to the present-day and that VES has never been greater than the present value of 12.5 MPa. The continuously low VES basin modelling result is consistent with petrographic observations such as the presence of uncollapsed, moldic pores (Figure 4.4C and D) and the absence of sutured or stylolitic grain contacts.

Whilst few dispute the role of intergranular pressure dissolution as a source of silica and thus of macroquartz cement in sandstones, the strong, current consensus is that the rate of macroquartz cementation in sandstones is a primary function of temperature-controlled quartz precipitation kinetics (Walderhaug, 1994b; Bjorkum, 1996; Taylor et al., 2015). An alternative view was proposed by Osborne and Swarbrick (1999), who argued that rates of intergranular pressure dissolution were influenced by vertical effective stress. Our data support that assertion, to the extent that we argue that vertical effective stress is the main control on macroquartz cementation in Elgin's Fulmar Formation sandstones. Vertical effective stress has never been more than ca. 12.5 MPa throughout the burial history of the Fulmar sands, so that despite the fact that (a) the present-day temperature is 190 °C and (b) the Fulmar sands have spent > 90 Ma in the >70-80 °C "quartz cementation window", the supply of silica at grain-grain contacts has been restricted by the continuing occurrence of high fluid pressures/low vertical effective stresses.

Notably, a lack of correlation between macroquartz cement volume and intergranular pressure dissolution has been cited elsewhere as evidence for non-suppression of macroquartz cementation by high fluid pressure/low vertical effective stress (e.g. Taylor et al., 2015). Because an overpressured system is essentially closed, diagenesis in such systems is limited to that possible within the realm of their indigenous fluid chemistry (Jeans, 1994; Stricker et al., 2016b). The implication is that the observed macroquartz cements in the studied sandstones were most likely sourced locally. CL petrography estimation shows intergranular pressure dissolution can source 60 – 70 % of the silica

for the observed macroquartz cement, and the rest was likely supplied by feldspar dissolution (Figure 4.11).

4.7.6. Quartz Cementation History

We now argue that *in situ* $\delta^{18}O_{quartz\ cement}$ profiles across individual overgrowths support our interpretation that macroquartz cement occurred over a wide temperature range, which in turn supports the interpretation that the rate of macroquartz cementation is controlled by the rate of silica supply, not precipitation. *In situ* oxygen isotopic profiles across three individual overgrowths exhibit a total range of 2.7 ‰, between 22.4 and 19.7 ‰ (Figure 4.7). Since the oxygen isotopic composition of quartz is a dual function of temperature and $\delta^{18}O_{H2O}$, the $\delta^{18}O_{quartz\ cement}$ data cannot generate a unique temperature record of macroquartz precipitation. We can however propose the most geologically realistic interpretation of the isotope data (Figure 4.12). We first reject the model that macroquartz precipitated from a water of constant $\delta^{18}O$ between 80 and 190 °C, since $\delta^{18}O_{quartz\ cement}$ would then exhibit a 12 ‰ range. Secondly, if macroquartz precipitation started at 80 °C with a $\delta^{18}O_{quartz\ cement}$ value of + 22.4 ‰, then it would have done so from a fluid similar to that of Jurassic seawater (-1 ‰). If all of the macroquartz precipitated from Jurassic seawater, then all cementation would have occurred between 80 and 100 °C, which is extremely unlikely given the many studies (e.g. Walderhaug, 1994a; Walderhaug, 1994b) which have shown that macroquartz cementation continues to much higher temperatures. Most likely, we suggest, is that because the present-day $\delta^{18}O_{H2O}$ in local Fulmar Formation sandstones is + 4.5 ‰ (Hendry et al., 2000), $\delta^{18}O_{H2O}$ evolved from -1 to + 4.5 ‰ during the period of macroquartz precipitation, giving a temperature window of 80 – 150 °C (Figure 4.12). The lack of isotopic record for temperatures beyond 150 °C was probably due to subsequent high degree of hydrocarbon saturation from substantial charging of the Fulmar Formation reservoir from the deeper source kitchen. We therefore suggest that this is the most reasonable explanation of the $\delta^{18}O_{quartz\ cement}$ data, being consistent with what is generally inferred about the onset of macroquartz cementation and also with what is known about the most probable diagenetic fluids in Elgin and the way that $\delta^{18}O_{H2O}$ tends to evolve, to heavier values, during burial diagenesis (Aplin and Warren, 1994; Warren et al., 1994). Using an 80 – 150 °C window for macroquartz cementation, the precipitation-kinetics model would predict 25 volume % macroquartz cement, compared with the actual 4.6 % (Figure 4.9 and Figure 4.10).

These data, combined with (a) the long history of low vertical effective stress and (b) the lack of any other factors which would inhibit quartz precipitation, strongly suggest that macroquartz cementation is controlled by the stress-related supply of silica at grain-grain contacts and *not* by precipitation kinetics at free quartz surfaces.

The lack of a volumetrically significant amount of macroquartz cement in the studied sandstones at their current burial depth and temperature (189 °C) contrasts with observations made for other deeply buried sandstones like the Garn Formation in the North Sea (Giles et al., 1992; Osborne and Swarbrick, 1999) and the Wilcox sandstones in the Gulf of Mexico (Dutton and Loucks, 2010), where large volumes of macroquartz cement are seen at high temperatures. This study has strong implications for the role of temperature and stress in the entire macroquartz cementation process. While temperature might be important for the precipitation kinetic process, substantial volume of macroquartz cement would not precipitate in the system if the supply of silica (source) is cut-off or greatly reduced.

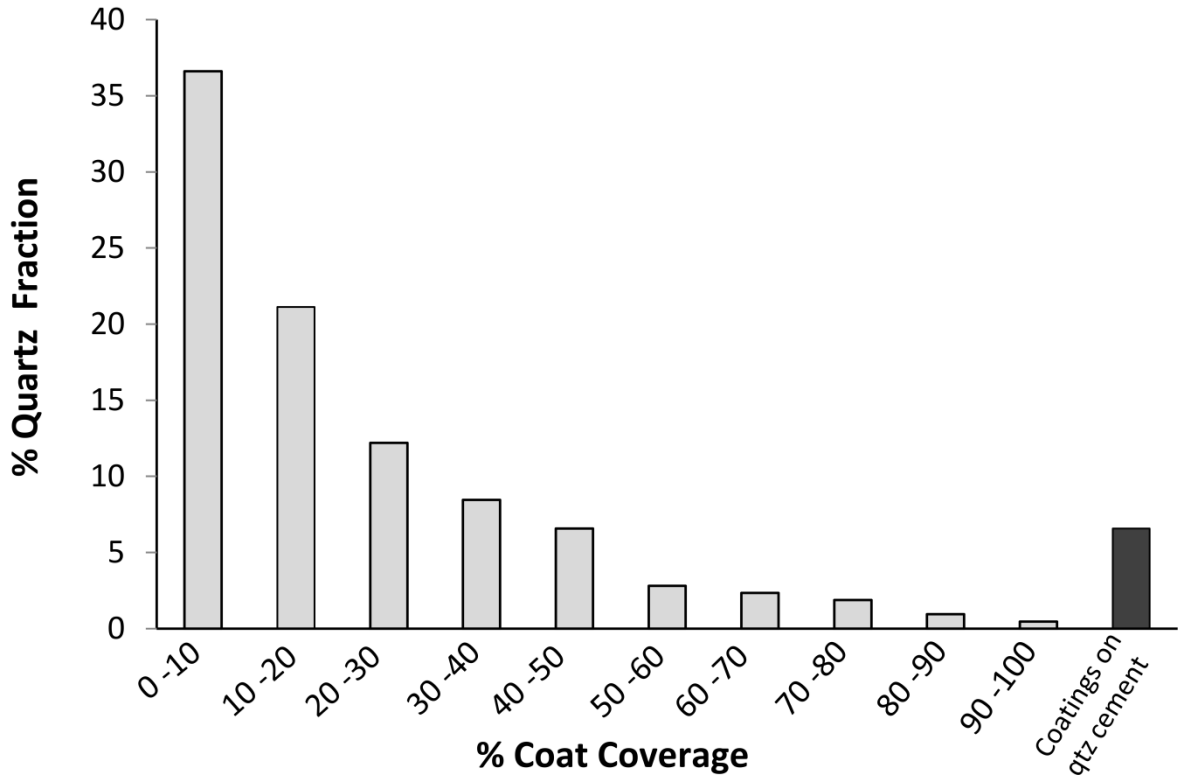

Figure 4.8. Percentage of quartz grains in analysed Fulmar Formation samples with their corresponding percentage grain-coating clay coverage. Black bar represents percentage of authigenic quartz (overgrowths) with clay coats.

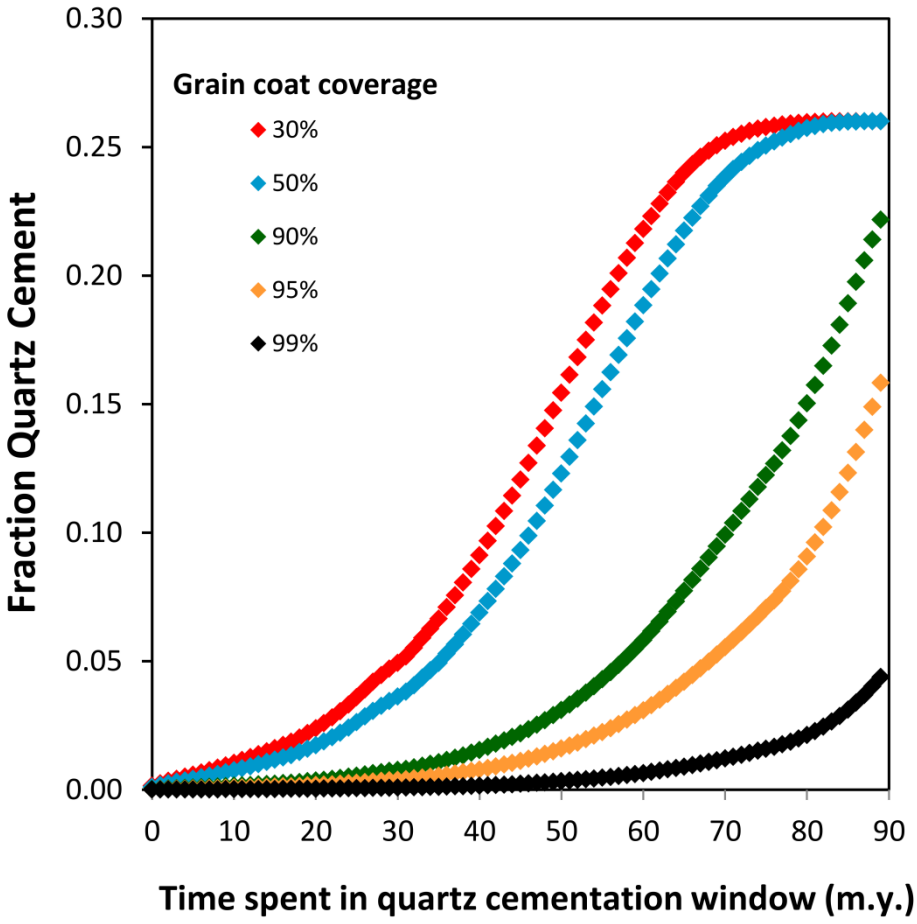

Figure 4.9. Quartz cementation model output for Upper Jurassic Fulmar Formation sandstones from Elgin field showing evolution of quartz cement through geologic time. Walderhaug's (1996) approach was applied to 1cm^3 volume of the studied sandstone using an 80°C threshold temperature for cementation and a starting porosity of 26%. Time-temperature history was generated using PetroMod version 2014.1. The model also tested different grain coat coverage scenarios ranging from 30 – 99%, and the outputs suggest that the studied sandstones would require around 99% grain coat coverage for their present average quartz cement volume (4.6%). In order to incorporate the grain coat data in the model, the initial quartz surface area was reduced using the estimated grain coatings coverage area

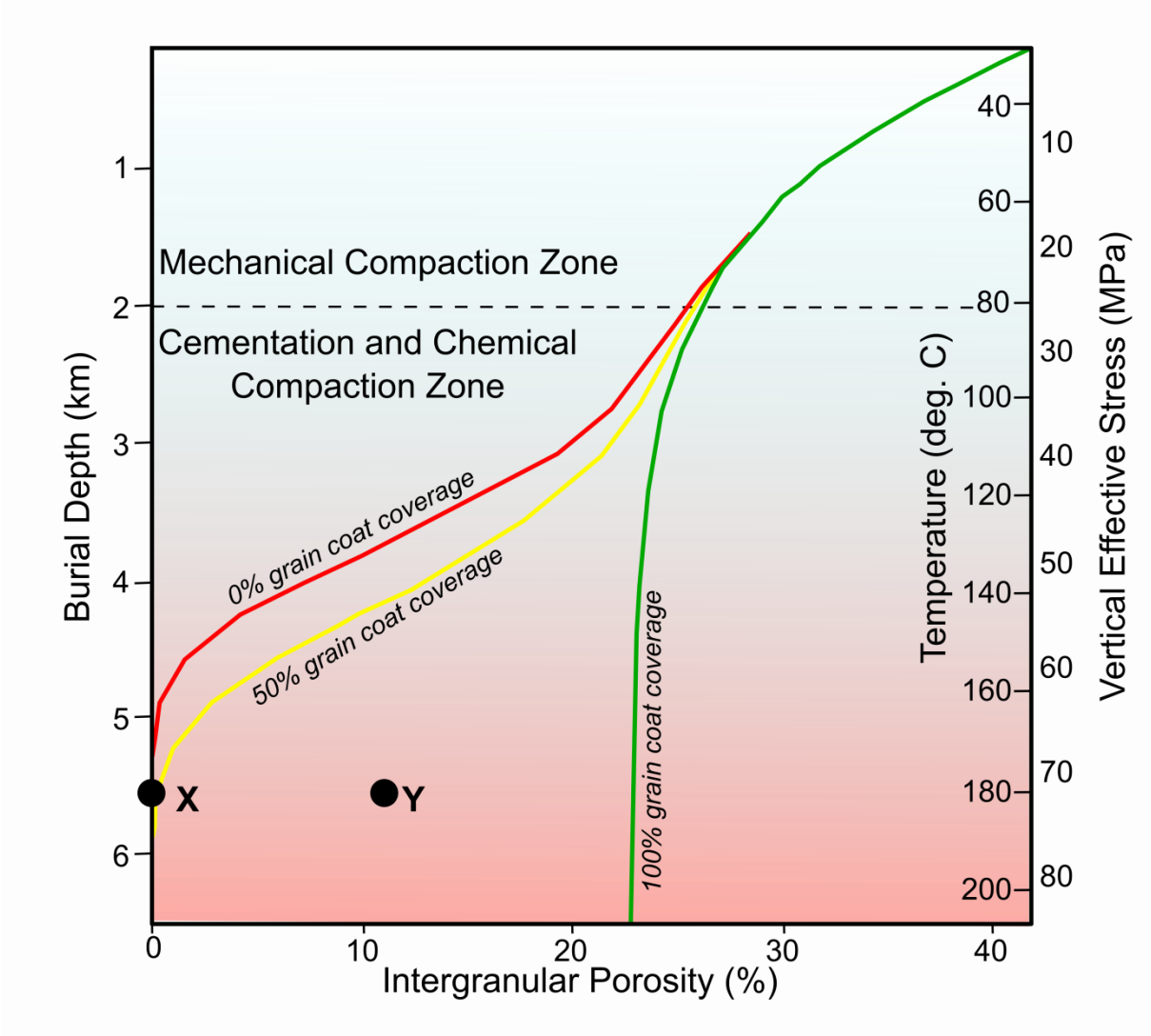

Figure 4.10. Modified hypothetical plot of porosity-depth trends with burial process and lithology based on Ajdukiewicz and Lander (2010). The well-sorted, fine-grained arkosic eolian sandstone assumed in this model has a simple burial history, variable grain coat coverage from shallow depth, and zero overpressure. Projection of the analysed Fulmar Formation sandstones on the plot based on burial depth, temperature, and average grain coat coverage (X) suggests that the sandstones should be completely cemented at Present-day. However, the measured average intergranular porosity in the sandstones (Y) is 11%.

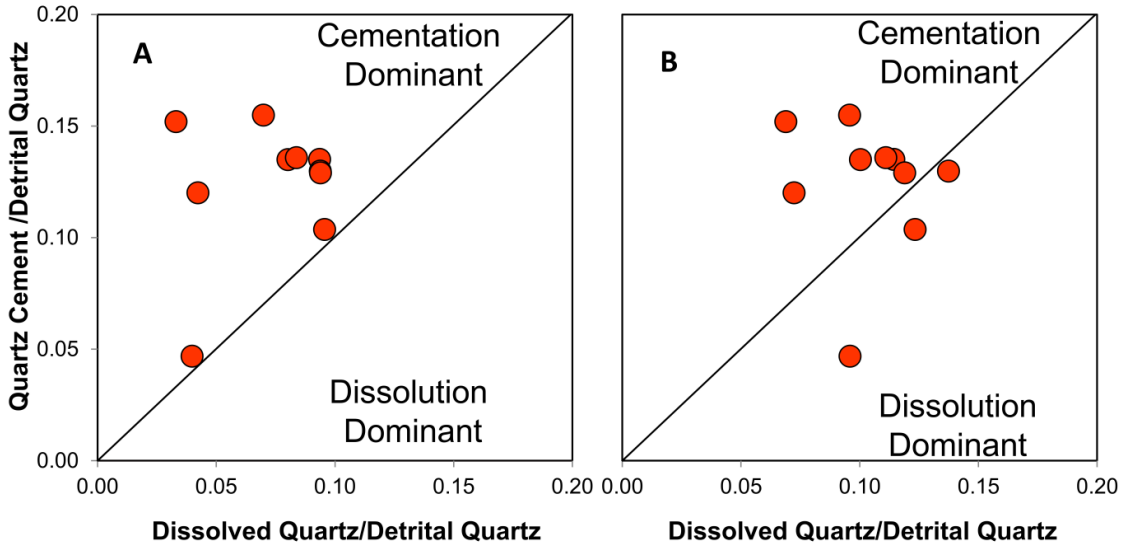

Figure 4.11. Plot of Elgin Field Fulmar Formation sandstones silica budget generated from petrographic data. All data have been normalised to detrital quartz content. A) Quantified pressure dissolution, represented by overlap quartz, supplied around 60% of the silica for precipitation of quartz cement. B) The incorporation of silica generated from feldspar dissolution into the budget analysis suggests feldspar dissolution and intergranular pressure dissolution can supply most or all the silica for quartz cementation from local sources.

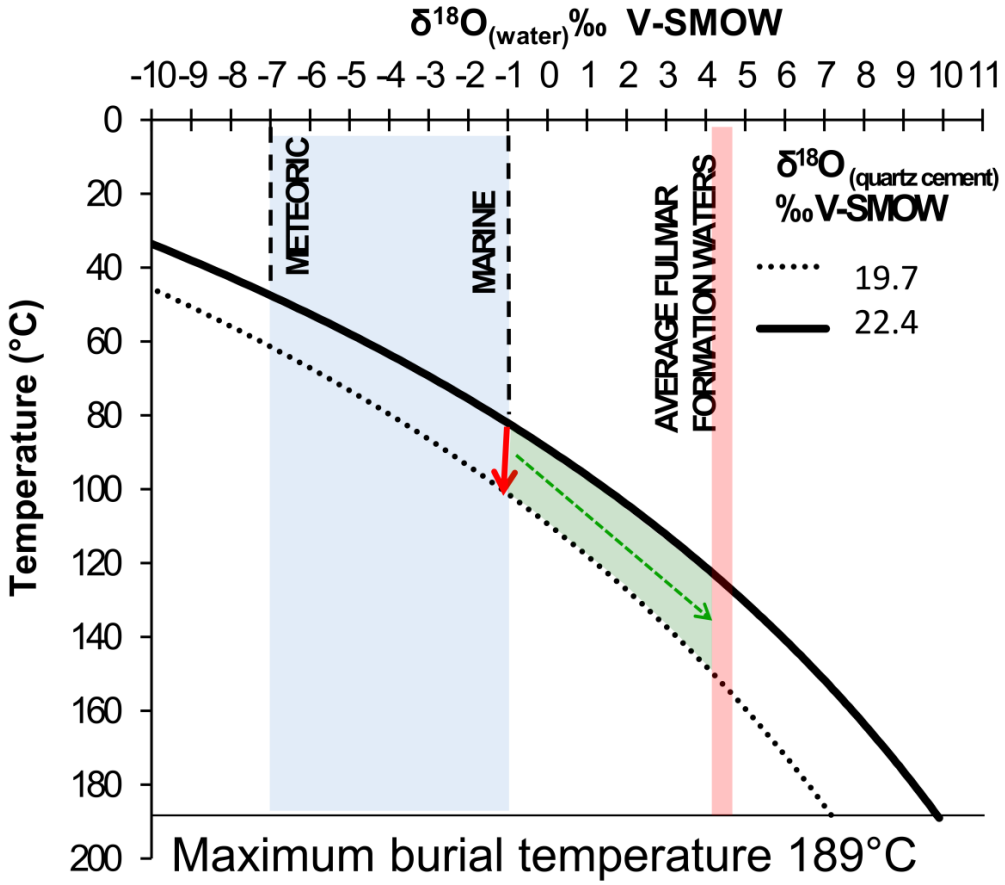

Figure 4.12. Plot of $\delta^{18}O_{(water)}$ in equilibrium with $\delta^{18}O_{(quartz\ cement)}$ as a function of temperature (Clayton et al., 1972). $\delta^{18}O_{(quartz\ cement)}$ contours 19.7 and 22.4 ‰ VSMOW defines the $\delta^{18}O$ range from early to late quartz cement. The red arrow represents an unlikely pathway for quartz cement precipitation, since $\delta^{18}O_{(water)}$ evolved to Present-day Formation water values (~ 4.5 ‰) in the Fulmar Formation reservoir (green arrow)

4.8. Conclusions

Fulmar Formation sandstones buried to 190 °C in the Elgin field have very low volumes of quartz cement.which contrasts with other deeply buried sandstones in the world where large volumes of quartz cements are present at high temperatures. Neither grain-coating microquartz nor illite can account for the low volume of quartz cement. Charge history reconstruction shows that hydrocarbons arrived at a temperature at which significant quartz cement would have already formed, so that hydrocarbon emplacement cannot be the cause of the low volume of quartz cement. Since basin modelling suggests that vertical effective stress was low throughout the burial history of these sands, I suggest that the rate of intergranular pressure dissolution was restricted by the continuously low vertical effective stress; it is therefore the rate of silica supply from intergranular pressure dissolution, not the rate of precipitation, which is the main control of quartz cementation. This is supported by *in situ* oxygen isotope analyses across individual quartz overgrowths which suggest that quartz cement formed over 100 Ma at an exceptionally slow rate, between 80 and 150 °C.

5. The Relative Importance of Vertical Effective Stress and Temperature on Quartz Cementation in Sandstone Reservoirs

5.1. Summary

I test the hypothesis that it is the rate of supply of silica from intergranular pressure dissolution rather than the rate of precipitation of silica, that is a key control on the rate of quartz cementation in sandstones. Two Paleocene-Eocene Wilcox Group sandstones from Texas and two Jurassic Fulmar Formation Sandstones from the Central North Sea have been studied, which have distinct histories of Vertical Effective Stress (VES) and temperature. We show that most or all the silica for quartz cement can be derived from intergranular pressure solution. The extent of intergranular pressure dissolution and related quartz cementation is strongly correlated with VES, and very poorly with temperature. High spatial resolution oxygen isotope analyses suggest temperature ranges for quartz cementation which demonstrate that the rate of quartz cementation is more strongly related to the history of VES rather than temperature. I suggest that it is the vertical effective stress history, rather than the temperature history, that exerts the greatest influence on quartz cementation.

5.2. Introduction

Quartz is the volumetrically most important diagenetic cement in quartz-rich sandstone that have been buried to depths greater than 2.5 km (McBride, 1989; Bjorlykke and Egeberg, 1993; Worden and Morad, 2000; Worden et al., 2018a). The process of quartz cementation and how it affects porosity and permeability in sandstones has been a subject of many diagenetic studies (McBride, 1989; Bjorlykke and Egeberg, 1993; Walderhaug, 1994a; Walderhaug, 1994b; Walderhaug, 1996; Walderhaug, 2000; Worden and Morad, 2000; Walderhaug and Bjørkum, 2003; Worden and Burley, 2003; Worden, 2004; Ajdukiewicz and Lander, 2010; Stricker et al., 2016b; Oye et al., 2018). Quartz cementation is the product of three serially-linked processes; silica supply from dissolution, transportation of silica through aqueous solution to precipitation sites, and precipitation of quartz cement (e.g. Worden and Morad, 2000; Bloch et al., 2002; Taylor et al., 2010). However, the dominant underlying process controlling the rate of quartz cementation remains a subject of ongoing debate in many diagenesis publications (e.g. Bjorlykke and Egeberg, 1993; Bjorkum, 1996; Walderhaug, 1996; Osborne and Swarbrick, 1999; Worden and Morad, 2000; Sheldon et al., 2003; Oye et al., 2018; Worden et al., 2018b). The currently favoured paradigm is that quartz cementation is controlled mainly by thermodynamically-driven processes; such that quartz precipitation initiates and the rate increases exponentially and predictably with temperature, once the precipitation kinetics barrier is exceeded around 70 – 80 °C (Walderhaug, 1994a; Walderhaug, 1996; Ajdukiewicz and Lander, 2010). These ideas have been incorporated into commonly-used models designed to predict quartz cementation and reservoir quality, allowing quartz cementation to be predicted as a function of temperature history (Lander and Walderhaug, 1999; Walderhaug, 2000).

The critical assumption in the temperature-based precipitation model is that silica supply is effectively infinite, so that for each silica molecule precipitated, another is released from a range of potential sources. The most commonly cited and observed silica source is from intergranular pressure dissolution (IPD) and related stylolitisation at quartz-quartz and quartz-sheet silicate interfaces (Waldschmidt, 1941; Pittman, 1972; Houseknecht, 1988; Osborne and Swarbrick, 1999; Worden and Morad, 2000). The zone of quartz cementation usually coincides with the realm of chemical compaction, where mineral grains undergo intergranular pressure dissolution (IPD) under the influence of vertical effective stress (VES) from an increasing overburden (Sheldon et al., 2003). Because the stress experienced by mineral grains at grain-to-grain contacts is

greater compared with the rest of the sandstone system, a persistent gradient in chemical potential is created that drives chemical compaction or intergranular pressure dissolution with subsequent release of silica for precipitation on free detrital quartz surfaces (De Boer et al., 1977; Tada and Siever, 1989; Dewers and Ortoleva, 1990; Elias and Hajash, 1992; Shimizu, 1995; Renard et al., 1997; Sheldon et al., 2003; Gratier et al., 2005; van Noort et al., 2008; Oye et al., 2018).

Because present-day VES might be significantly different to historical VES during basin history, the evolution of VES through time is pivotal to understanding how this mechanism influences intergranular pressure dissolution and eventual supply of silica for quartz cementation in sandstones (Osborne and Swarbrick, 1999; Bloch et al., 2002). Whle some studies (Oelkers et al., 1996; Walderhaug, 1996; Bjørkum et al., 1998; Lander and Walderhaug, 1999; Walderhaug, 2000) have suggested that intergranular pressure dissolution in sandstones is stress-insensitive and controlled mainly by temperature in the presence of sheet silicate catalysts, others (Elias and Hajash, 1992; Osborne and Swarbrick, 1999; Sheldon et al., 2003; van Noort et al., 2008; Oye et al., 2018) have demonstrated that the process is mainly a function of VES with a secondary influence of temperature.

There are other, local, influences on quartz cementation which can cloud the evaluation of the relative importance of silica supply or precipitation as master cementation variables. Many studies (Heald and Larese, 1974; Aase et al., 1996; Osborne and Swarbrick, 1999; Bloch et al., 2002; Ajdukiewicz et al., 2010; French et al., 2012; Stricker and Jones, 2016; Stricker et al., 2016b) have reported the presence of microquartz and/or clay coatings on detrital quartz surfaces as one of the potential controls on quartz cementation in sandstone This is because early development of robust clay and/or well developed micro quartz grain coats on quartz grains in deeply buried sandstones can inhibit quartz cementation by making potential quartz cement precipitation sites unavailable, thus preserving porosity and permeability.

There is also the contentious debate about the role of hydrocarbon as a potential control on quartz cementation in sandstones. While some, (Worden et al., 1998; Worden and Morad, 2000; Wilkinson and Haszeldine, 2011; Worden et al., 2018b) have related the observation of low volume of quartz cement in sandstone reservoirs to early hydrocarbon charge, others (e.g. Walderhaug, 1994a; Walderhaug, 1994b; Maast et al., 2011) suggested that quartz precipitation would proceed in the presence of hydrocarbon

as long as water remains the wetting phase in reservoir sandstones. However, emerging thoughts (Marchand et al., 2000; Marchand et al., 2001; Marchand et al., 2002; Maast et al., 2011; Sathar et al., 2012; Worden et al., 2018b) have indicated that the wetting state of grains and/or the level of tortuosity of diffusion pathways due to the degree of hydrocarbon saturation are important for hydrocarbon emplacement to effectively halt quartz cementation in sandstones.

In order to understand better the relative importance of (a) silica supply by intergranular pressure dissolution and (b) silica precipitation as controls on quartz cementation, I report the result of an investigation conducted on sandstones that have not only experienced varying VES and temperature regimes throughout their burial histories, but that also have different quartz cement volumes. These sandstones were chosen from four fields from two sedimentary basins (Figure 5.1); Upper Jurassic Fulmar Formation sandstones from Clyde and Elgin Fields in the Central North Sea (CNS), UK, and Paleocene-Eocene Wilcox Group sandstones from Rotherwood and Lake Creek Fields in the Gulf of Mexico (GOM), USA. The upper Jurassic Fulmar Formation and Paleocene-Eocene Wilcox Group sandstones pairs were chosen such that Elgin and Rotherwood samples have lower VES and higher temperatures than their equivalents from Clyde and Lake Creek at present-day (Table 5.1). The occurrence of lower quartz cement volumes in the lower VES and higher temperature sample sets suggests that the rate of quartz cementation might have been controlled by the effect of VES on the rate of silica supply from intergranular pressure dissolution. Because silica supply from intergranular pressure dissolution is not a one-off process, historical VES rather than present-day VES would be expected to be the main control. However, the effect of other potential controls on quartz cementation such as microquartz, clay coatings, and hydrocarbon charge must also be assessed.

I, therefore, integrate (a)detailed quantitative petrographic analysis, (b) basin modelling, (c) kinetic modelling of quartz cementation, and (d) high spatial resolution oxygen isotope analyses to test the hypothesis that it is the rate of supply of silica from IPD, rather than the rate of precipitation of silica, that controls the rate of quartz cementation. If the hypothesis is true, then it is the history of vertical effective stress, rather than temperature, which exerts the greatest influence on quartz cementation. Key questions to be answered are the following:

(a) What is the role of VES on quartz cementation in the Fulmar Formation and Wilcox Group sandstones?

(b) What is the effect of temperature on quartz cementation in the Fulmar Formation and Wilcox Group sandstones?

(c) Do grain-coating clays and microquartz have any effect on quartz cementation in the Fulmar Formation and Wilcox Group sandstones?

(d) What is the role of hydrocarbon on quartz cementation in the Fulmar Formation and Wilcox Group sandstones?

Table 5.1. Depth, Vertical Effective Stress and Temperature matrix for the studied Fulmar and Wilcox sandstones

Field	Basin	Group/Formation	Age	Depth (mssTVD)	Temp (°C)	VES (MPa)
Clyde	Central North Sea	Fulmar	Upper Jurassic	5410-5435	147.0	40.0
Elgin	Central North Sea	Fulmar	Upper Jurassic	3770-3790	189.0	12.3
Lake Creek	Gulf of Mexico	Wilcox	Early Eocene	3518.4	143.2	33.4
Rotherwood	Gulf of Mexico	Wilcox	Paleocene-Eocene	5063.3	185.4	23.9

5.3. Geological Settings

Samples were selected from four locations, two from the UK North Sea and two from the Texas Coast in the GoM, enabling us to examine the relative importance of both temperature and VES on quartz cementation (Table 5.1). For the chosen Formations, Elgin (North Sea) and Rotherwood (GoM) have temperatures of 185-189°C but different VES, and Clyde (North Sea) and Lake Creek (GoM) have temperatures of 143-147°C, again with different VES values.

Samples from Elgin and Clyde were taken from the syn-rift Upper Jurassic Fulmar Formation in the Central Graben area of the UK North Sea (Figure 5.1) The Central Graben is one of the main hydrocarbon producing habitats in the UK. The Central Graben was formed by two major east-west crustal extension events: the Permo-Triassic and the late Jurassic rifting events (Gowers and Sæbøe, 1985; Glennie, 2009). These periods were marked by the deposition of the Triassic and Jurassic siliciclastic syn-rift sediments, including the Fulmar Formation. The Late Jurassic rifting event also interplayed with salt withdrawal (halokinesis) at depth to give the Central Graben its complex structure (Roberts et al., 1990; Gowland, 1996). The deposition of thick successions of chalk, clay and silt in the Cretaceous to Cenozoic times post-dated the late Jurassic rifting event, and ensured that the graben experienced an intense sagging phase which probably initiated and maintained high formation pressures in the area (Darby et al., 1996). The Upper Jurassic Fulmar Formation is one of the principal hydrocarbon reservoir in many oil fields in the Central Graben, including Clyde, Elgin and Fulmar fields (e.g. Stevens and Wallis, 1991; Gowland, 1996; Lasocki et al., 1999; Osborne and Swarbrick, 1999; Kuhn et al., 2003; Gilham et al., 2005; Wilkinson et al., 2006; Wilkinson and Haszeldine, 2011). The Fulmar Formation was probably sourced from the Triassic sediment of the Western Platform in the Central North Sea, with some contributions from intrabasinal highs such as: Forties – Montrose High and Josephine ridge (Gowland, 1996). The formation is shallow marine in origin, intensely bioturbated, and typically occurs as a coarsening–upward succession grading from siltstones into very fine – medium grained arkosic sandstone (Gowland, 1996; Lasocki et al., 1999; Hendry et al., 2000). The Fulmar formation is mainly Oxfordian to Kimmeridgian in age, but the diachronous nature of this formation resulted in the occurrence of localised formations with younger ages that extend to the Ryazanian times (Figure 5.2). The presence of abundant *Rhaxella* sponge spicules has been reported within some intervals locally (Gowland, 1996).

Samples from the upper Texas Gulf Coast were taken from the Late Paleocene to Early Eocene, fluvio-deltaic Wilcox Group (Figure 5.1 and Figure 5.3). The upper Texas Gulf Coast is part of the GOM basin. The formation of the GOM basin, as described by (Buffler and Sawyer, 1985), can be broadly divided into two phases separated by the mid-Cretaceous unconformity (MCU); the pre-MCU and the post-MCU phases. The pre-MCU phase set the scene and provided the framework for the post-MCU clastic sediment infilling of the GOM basin in Late Cretaceous to Early Cenozoic (Buffler and Sawyer, 1985). Deposition of the Fluvio-deltaic Wilcox Group sediment in the upper Texas Gulf Coast area (north-western GOM), is the first in the Cenozoic, and span from Late Paleocene to Early Eocene (Galloway et al., 2000; Dutton and Loucks, 2010). The group formed as series of sands, silts and shales intercalations (Figure 5.3), and have been extensively studied by several researchers (e.g. Fisher and McGowen, 1967; Dutton and Loucks, 2010). The sediments that make up these sandstones were likely sourced from the Laramide uplands area in the southern Rocky Mountains, and have been petrographically-described as lithic arkoses to feldspathic litharenites (Dutton and Loucks, 2010). Because geothermal gradients vary in the Texas coast area, ranging from 24 to 43°C, the Wilcox sandstones exhibit varying temperature regimes across different localities as evidenced from well data (Dutton and Loucks, 2010). The occurrence of Wilcox sandstones extend from onshore to the deep offshore, and their economic significance as hydrocarbon bearing intervals have been identified in the onshore areas (Dutton and Loucks, 2010).

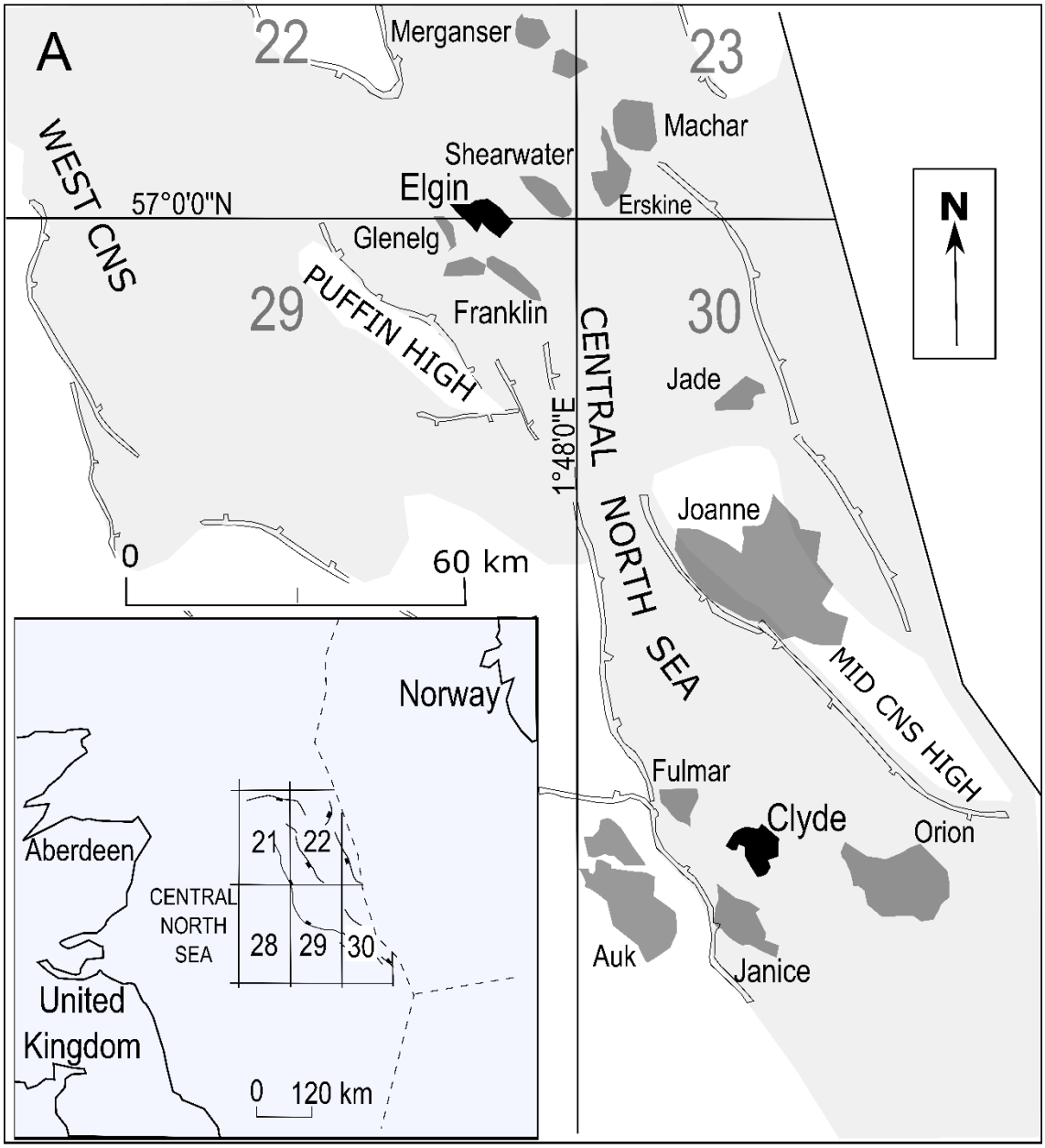
A
22
23
Merganser
Machar
Shearwater
Elgin
Erskine
57°0'0"N
WEST CNS
Glenelg
29
PUFFIN HIGH
Franklin
30
CENTRAL NORTH SEA
1°48'0"E
Jade
Joanne
N
0
60 km
Norway
MID CNS HIGH
Fulmar
Clyde
Orion
Aberdeen
21
22
CENTRAL NORTH SEA
28
29
30
Auk
Janice
United Kingdom
0 120 km

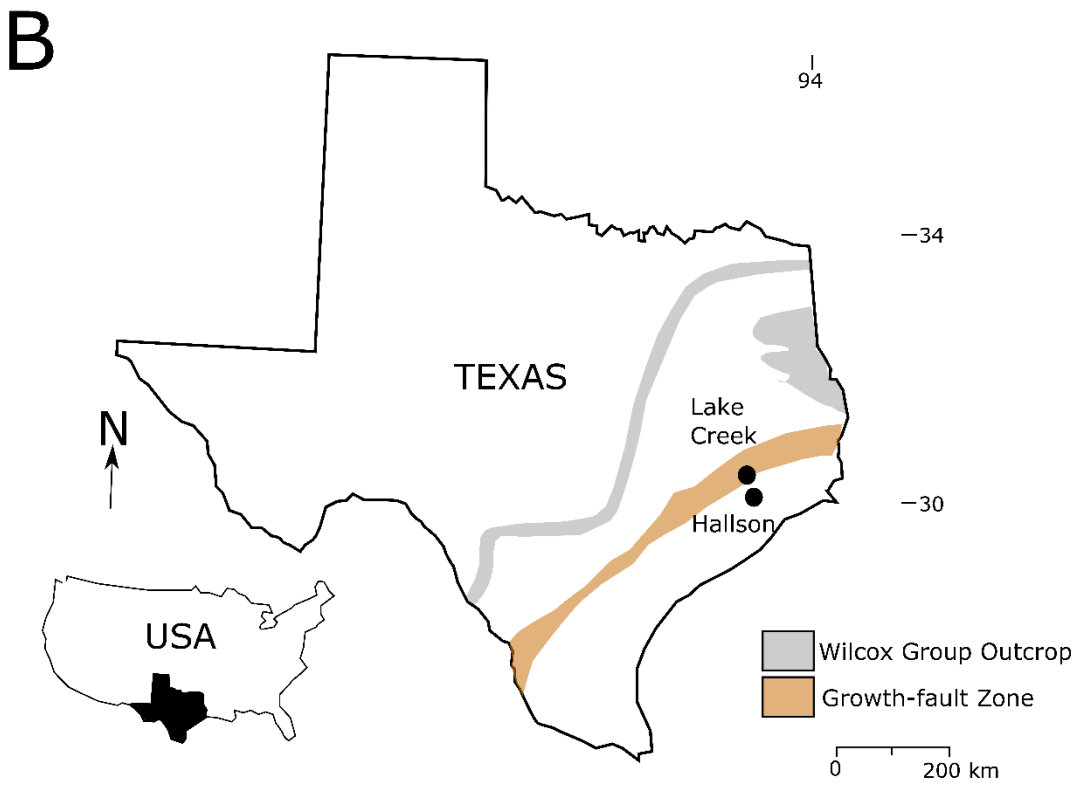

Figure 5.1. Maps of study locations; A) UK Central North Sea (CNS) showing Clyde, Elgin and other surrounding fields: B) Texas showing Lake Creek in Montgomery County and Rotherwood in Harris County (Adapted from Fisher and Land (1986) and Day-Stirrat et al. (2010))

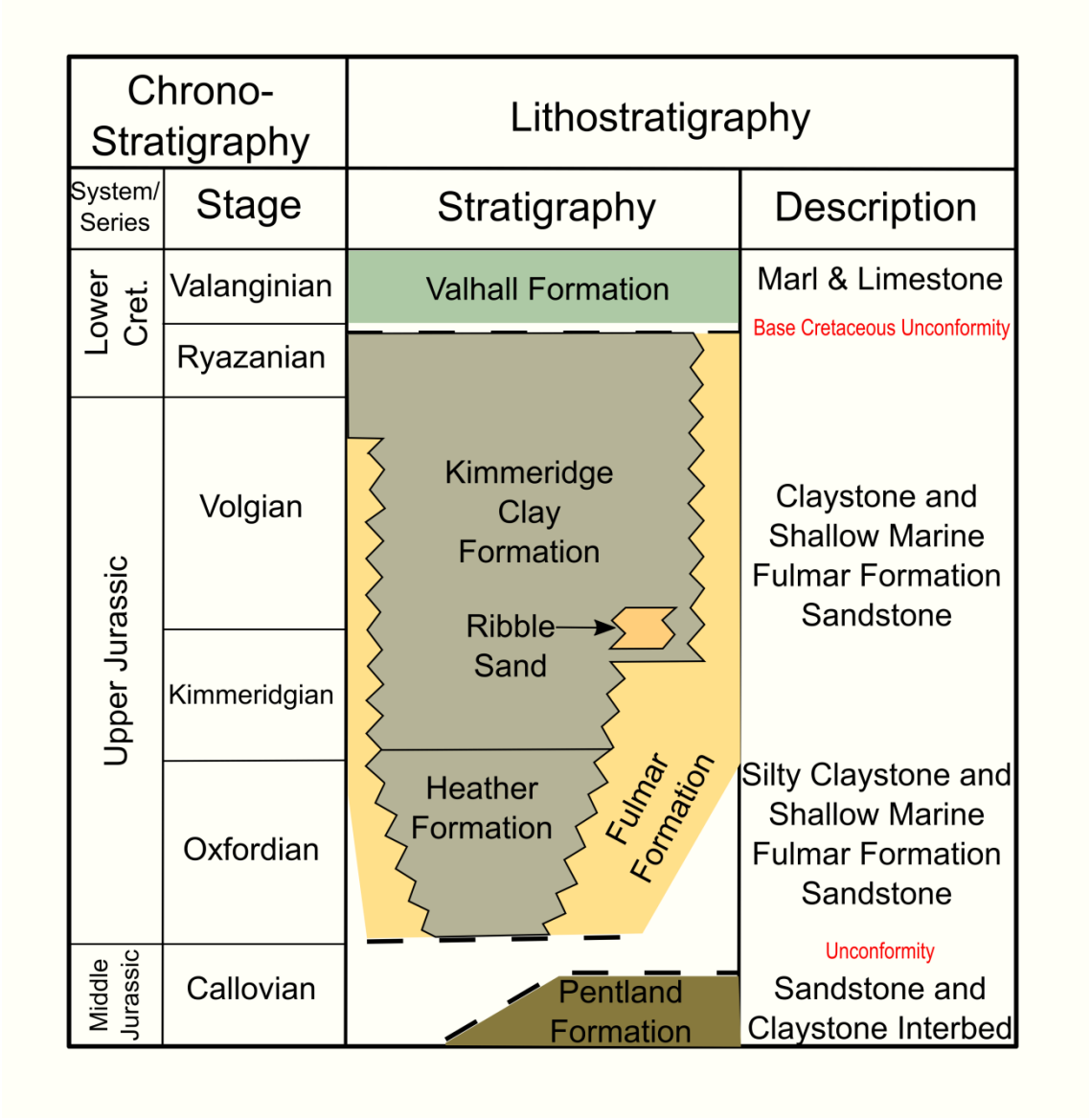

Figure 5.2. Regional Stratigraphy of the Central North Sea from Middle Jurassic to Lower Cretaceous. Shallow Marine Fulmar Formation was investigated in this study (adapted from Graham et al., 2003)

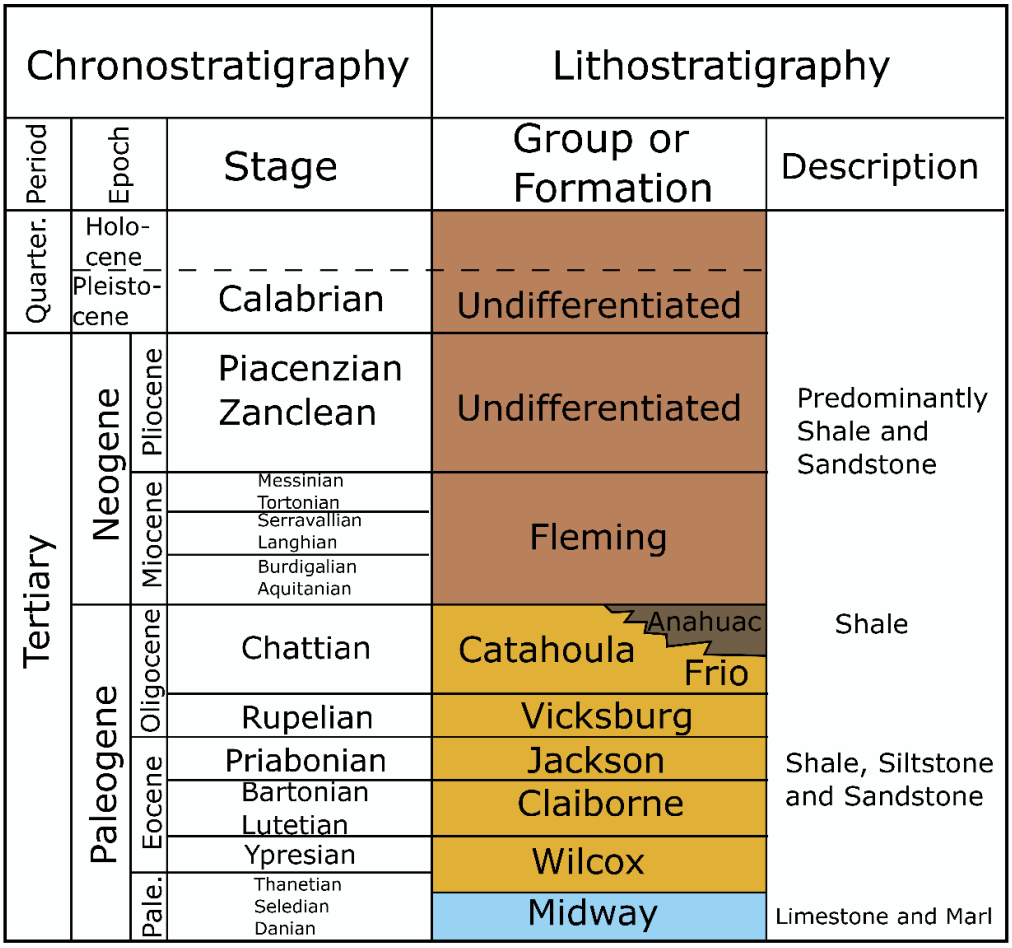

Figure 5.3. Generalised stratigraphy of the Gulf Coast Tertiary and Quarternary section showing the Paleocene-Eocene Wilcox Group and other Lithologies (adapted from Pitman and Rowan, 2012)

5.4. Method

5.4.1. Sampling Strategy

Fulmar Formation samples were obtained from wells 30/17B-2 and 22/30C-G4 in Clyde and Elgin respectively (Figure 5.1), from clean, clay-poor intervals (Table 5.1). A similar strategy was adopted for the Wilcox sandstones: two wells that penetrated the Wilcox sandstones were selected from Lake Creek Field, Montgomery County and Rotherwood Field, Harris County in the Gulf of Mexico. All the sandstones are at or close to their maximum burial depth. Sample depths, temperatures and VES are given in Table 5.1.

5.4.2. Petrography

All petrographic data for the Wilcox sandstones were obtained from Harwood (2011), except intergranular pressure dissolution data which was determined in this study. In the case of the Fulmar Formation sandstones, two types of quantitative petrographic analysis,standard and cathodoluminescence (SEM-CL) petrography, were used to characterise the samples. Thin sections produced from Fulmar sandstone samples were subjected to modal analysis using standard petrographic microscope. Proportions of bulk compositions including grain types, matrix and cement contents were calculated by making not less than 300 point count in thin sections. Twenty samples (ten from each field) representing all range of quartz cements in the analysed sandstones were subsequently selected for CL petrography. The CL petrography involved the acquisition of Si element and CL maps over the same areas (3mm x 3mm) for each of the twenty thin sections using energy dispersive x-ray (EDX) and SEM-CL. A grid of 1600 (40x40) square boxes was superimposed on the CL map, while the EDX map was used as a control for the identification of mineral grains. Modal analysis was then performed by manual point-counting of both detrital quartz, overlap quartz and authigenic quartz using the grids to generate 1600 data points per thin section.

5.4.3. Effective Stress and Temperature Histories

One-dimensional basin modelling was used in this study to reconstruct the effective stress and temperature histories for both Fulmar Formation and Wilcox Group sandstones using Schlumberger's PetroMod Petroleum Systems modelling software (Version 2014.1).

Present-day stratigraphic data from composite logs, geological well reports, core analysis, and core description reports were used to build the models (Table 5.2, Table

5.3 and Table 5.4). Heat flow models were built after Allen and Allen (2005), with an average of 62 and 64 mW/m^2 for Elgin and Clyde fields throughout their burial histories. The heat flow values at the peak of Permo-Triassic and Upper Jurassic paleo-rifting events were 70 and 90 mW/m^2 respectively for both Elgin and Clyde fields. Heat flow, however, averages ~57 mW/m^2 (range 50 - 78 mW/m^2) for the GOM fields (Smith et al., 1981; Nunn and Sassen, 1986). Vitrinite reflectance data, where available, were used as palaeothermometer data and combined with present-day temperature data to constrain thermal models and reconstruct temperature evolution pathways.

Compaction was modelled using formation porosities for the individual sandstones. PetroMod's default lithologies were also modified to match those observed in core. Default chalk and shale permeabilities in PetroMod were modified after Swarbrick et al. (2000), lowering permeabilities for the Chalk Group and the Pre-Cretaceous shale units until a good fit was achieved between modelled and observed pore pressures/VES. The Chalk Group were assigned typical shale permeability values because they are extensively cemented (Swarbrick et al., 2010). Similar adjustments were made for Rotherwood and Lake Creek fields, where permeability values for the Claiborne and Wilcox shales were modified to lower values until modelled pore pressures matched field data.

Although temperature histories can be quite accurately modelled in 1D, the same is not necessarily true for pore pressure and VES, since one-dimensional modelling packages are limited by their inability to model lateral fluid flow. It transpires that this is critical for the Clyde field, where regional pore pressure data within the Fulmar Formation show that pore fluid pressures have decreased substantially in the last *ca*. 0.5 million years as a result of lateral drainage (Swarbrick et al., 2005). These data strongly suggest that VES has increased from *ca*. 19 MPa around 0.5 million years ago, to 40 MPa at the present-day. This is critical for the present study, given its focus on unravelling the relative importance of temperature and effective stress on quartz cementation.

5.4.4.Kinetic modelling of Quartz cementation

Quartz precipitation kinetic models for the Fulmar Formation and Wilcox Group sandstones were built using Walderhaug's (1996) approach. This method simulates quartz cementation based on logarithmic function of temperature (Walderhaug, 1996; Walderhaug, 2000). Arrhenius equation based commercial cementation modelling software packages that allows variation of activation energy have also been developed

(e.g.Walderhaug, 2000; Walderhaug et al., 2009), but were not available for this study. However, Arrhenius and logarithm based methods yielded similar results for some Jurassic Brent Group sandstones from the North Sea (Walderhaug, 2000), suggesting that the simpler approach is valid. The empirical model is mathematically expressed as:

$$Vq_2 = \phi_0 - (\phi_0 - Vq_1)exp\frac{-MaA_0}{\rho\phi_0 bc \ln 10}(10^{bT_2} - 10^{bT_1}) \qquad (5.1)$$

Where M and ρ are molar mass (60.09 g/mol) and density (2.65g/cm^3) of quartz, c is the heating rate (°C/s) calculated from time-temperature history, ϕ_0 is the porosity at the onset of precipitation, Vq_1 is the volume (cm^3) of quartz cement present at time T_1 (s), Vq_2 is the volume (cm^3) of quartz cement precipitated in 1 cm^3 of sandstone from time T_1 and T_2 (s), A_0 is initial quartz surface area (cm^2) in 1 cm^3 of sandstone, and a (moles/cm^{2}s) and b (°C^{-1}) are the precipitation kinetic constants (Walderhaug, 1996).

The model incorporates grain size, mineralogy, and available quartz surface area, all of which were quantified in this study. The model assumes that compaction terminates at the onset of quartz cementation and stabilization of framework grains. Time-temperature histories generated from PetroMod (version 2014.1) were used to calculate the heating rates incorporated in the cementation models. The model also used 1cm^3 sandstone, 80°C threshold temperature, 26% porosity at the onset of quartz cementation, grain sizes estimates from CL petrography, and Walderhaug (1994b) kinetic constants a (1.98×10^{-22} moles/cm^{2}s) and b (0.022°C^{-1}). Fractions of detrital quartz in the bulk rock were obtained from CL petrographic data. Quantitative petrographic data of grain coat coverage were also incorporated in the model using a method similar to Walderhaug's (1996) and (2000) approach, for a better constraint of the available quartz surface area. Quantification of grain coatings coverage was done through visual inspection and manual point counting using CL, BSE, and silica maps generated over same area (Oye et al., 2018). While BSE eased the identification of microquartz and clay coatings in thin section, CL and silica maps helped identify and discriminate quartz grains and their phases.

5.4.5. Oxygen Isotope Analysis

The isotopic fractionation of oxygen between quartz and water can provide information about diagenetic temperatures and fluid composition, especially when analysed at appropriate scale and high spatial resolution (e.g. Pollington et al., 2011; Harwood et

al., 2013). Harwood et al. (2013) were the first to use secondary ion mass Spectrometry (SIMS) to create profiles of oxygen isotope ratios ($\delta^{18}O$) on quartz overgrowths in sandstones using 2µm spot sizes. Similar analysis was performed on two Fulmar Formation samples at the WiscSIMS Laboratory in the University of Wisconsin-Madison using a CAMECA ims-1280 ion microprobe (Kita et al., 2009). Each of these samples was selected from Clyde and Elgin fields sample sets. Six distinct overgrowths, three from each sandstone sample, with thicknesses between 40 and 100 µm were chosen for *in situ* oxygen isotope analysis. Linear profiles of $\delta^{18}O$ were measured across each overgrowth using a 3µm spot diameter on the ion microprobe. Individual samples were embedded in polished epoxy mount alongside grains of University of Wisconsin quartz standard UWQ-1 (Kita et al., 2009). Bracketing analyses were performed on the quartz standards grains within each mount to enable correction of measured $\delta^{18}O$ values to the Vienna Standard Mean Ocean Water (VSMOW) scale to monitor instrumental drift and to calculate external reproducibility for sample analyses (Kita et al., 2009; Valley and Kita, 2009). The average spot to spot reproducibility of $\delta^{18}O$ in the bracketing UWQ1 analyses was 0.7‰ (2 SD). Ion microprobe analysis of individual quartz overgrowths in Wilcox sandstones have been previously conducted and documented by Harwood (2011). The SIMS analytical procedure used for the Fulmar sandstones are similar to those adopted for the Wilcox sandstones, except that measurements were done using 12µm spot sizes (Harwood, 2011), and $^{16}OH^-$ was measured simultaneously during $\delta^{18}O$ analysis of the Fulmar samples. Ratios of $^{16}OH^-/^{16}O^-$ were background corrected by subtraction of ratios measured on nominally anhydrous UWQ-1 analyses that bracket the sample data. Four analyses representing outlying data points after $^{16}OH^-/^{16}O^-$ correction was discarded (Appendix 3). A more detailed ion microprobe analytical procedure is described in (Page et al., 2007; Kita et al., 2009; Valley and Kita, 2009; Pollington et al., 2011; Oye et al., 2018). All Fulmar Formation and Wilcox Group data are reported in Appendix 3 and Harwood (2011).

Table 5.2. Formation thicknesses and lithotypes used for Clyde and Elgin burial history modelling. Percentage values show mix ratio for interbedded formations

System	Series	Group	Age (Ma)	Formation	Elgin Lithology	Thick-ness(m)	Clyde Lithology	Thick-ness (m)
Neogene	Miocene - Pleistocene	Nordland Group (Undiff.)	13	Nordland Group (Undiff.)	Shale	1416	Shale (organic lean, typical)	1441
Paleogene	Eocene – Miocene	Hordaland Group (undiff.)	54	Hordaland Group (undiff.)	Shale	1579	Shale 70% Silt 30%	1375
Paleogene	Eocene	Rogaland	54.3	Balder Fm	Silty Shale 95%_tuff 5%	30	Shale 70% Silt 30%	14
Paleogene	Paleocene	Rogaland	56	Sele Fm	Shale 65%_Sandstone 35%	48	Shale70% Silt 30%	45
Paleogene	Paleocene	Montrose	57.8	Lista Fm	Shale	79		
Paleogene	Paleocene	Montrose	58.3	Lista Fm (Andrew Member)	Shale 65%_Limestone 35%	63	Shale 70% Sand 30%	109
Paleogene	Paleocene	Montrose	62.5	Maureen Fm	Shaly Limestone 90%_Marl 10%	130	Marl 85% silt 10% Clay 5%	23
Paleogene	Paleocene	Chalk	65	Ekofisk Fm	Chalk 85% Silt 5%_Clay 5%_Marl 5%	102	Chalk 80% Clay 10% Limestone 10%	67
Cretaceous	Upper	Chalk	72	Tor Fm	Chalk	502	Chalk 90% Silt 5% Clay 5%	327
Cretaceous	Upper	Chalk	91	Hod Fm	Chalk 90%_Marl 10%	718	Chalk 85% Silt 5% Clay 5% Marl 5%	120
Cretaceous	Upper	Chalk	93	Herring Fm	Chalk	144	Missed	
Cretaceous	Upper	Chalk	94	Plenus Marl Fm	Shale	2	Missed	
Cretaceous	Upper	Chalk	99	Hidra Fm	Chalk	85	Missed	
Cretaceous	Lower	Cromer Knoll	107	Rodby Fm	Shale 65%_Limestone 30%_Marl 5%	15	Missed	
Cretaceous	Lower	Cromer Knoll	128.5	Valhall	Shale 60%_Marl 40%	49	Marl	5
Jurassic	Upper	Humber	153	Kimmeridge C. Fm.	Shale (black)	103	Shale (8% TOC) 80% Silt 20%	68
Jurassic	Upper	Humber	156	Heather Fm	Shale (organic rich, typical)	334	Missed	
Jurassic	Upper	Humber	158.4	Fulmar Sands	Sandstone (arkose, quartz rich)	160	Sandstone (arkose, quartz rich)	217
Jurassic	Middle	Fladen	166	Pentland Sand	Sandstone (clay rich)	164	Missed	
Jurassic	Middle	Fladen	170	Pentland Shale	Shale (organic rich, typical)	110	Missed	
Triassic	Lower	Heron	248.2	Smith Bank Fm	Missed		Shale (organic lean, sandy)	81

Table 5.3 Layer thicknesses and lithotypes used for Rotherwood burial history modelling. Percentage values show mix ratio for interbedded formations.

Rotherwood					
System	Series	Layer	Age (Ma)	Lithology	Thickness (m)
Neogene	Oligocene - Miocene	Miocene	24.0	Shale 50% Sand 50%_1	780
Paleogene	Oligocene	Frio	31.2	Sandstone 55% Shale 40% Silt 5%	560
Paleogene	Eocene - Oligocene	Jackson	36.0	Shale 95% Sandy Shale 5%_1	515
Paleogene	Eocene	Yegua	39.4	Sandstone 50% Shale 45% Sand 5%_1	335
Paleogene	Eocene	Lower Claiborne	49.4	Shale 85% Silt 10% Sand 5%	680
Paleogene	Eocene	Upper Wilcox	53.7	Shale 55% Sand 45%	1040
Paleogene	Paleocene - Eocene	Lower Wilcox	59.2	Shale 57% Sand 33% Silt 10%	1190

Table 5.4. Layer thicknesses and lithotypes used for Lake Creek burial history modelling. Percentage values show mix ratio for interbedded formations.

Lake Creek					
System	Series	Layer	Age (Ma)	Lithology	Thickness (m)
Neogene	Oligocene - Holocene	Miocene	28.2	Shale 50% Sand 50%	970
Paleogene	Oligocene	Frio	33.9	Shale 50% Sand 50%	240
Paleogene	Eocene - Oligocene	Jackson	40.3	Shale 95% Sandy Shale 5%	390
Paleogene	Eocene	Yegua	45.0	Shale 50% Sand 50%	460
Paleogene	Eocene	Clairborne	49.0	Shale (organic lean, sandy)	570
Paleogene	Eocene	Wilcox A	49.1	Shale 50% Sand 45% Silt 5%	120
Paleogene	Eocene	Wilcox Formation 1	51.0	Shale 50% Sand 45% Silt 5%	780
Paleogene	Eocene	Wilcox Formation 2	53.0	Sandstone 50% Shale 45% Sand 5%	1000

5.5. Results

5.5.1. Burial, Temperature and VES Histories

Burial histories are shown in Figure 5.4, and both temperature and VES histories in Figure 5.5. Temperature histories for Clyde and Elgin are broadly similar, with higher temperatures in Elgin as a result of a more rapid early phase of burial (Figure 5.5). Temperature histories for Rotherwood and Lake Creek are also like each other, with higher temperatures in Rotherwood due to greater burial in the Eocene-Oligocene (Figure 5.5).

Wilcox Group sandstones from Rotherwood and Lake Creek fields experienced simple burial histories. However, temperature and VES histories differ moderately between Rotherwood and Lake Creek fields. Deposition of the Wilcox sandstone in Rotherwood and Lake Creek was initiated in the Late Paleocene and Early Eocene respectively, and burial was rapid from onset through until the end of the Miocene (Figure 5.5). However, Rotherwood field experienced more rapid burial (~ 96 m/Myr) which led to 0.6km more burial compare to Lake Creek's ~ 95 m/Myr. The rapid burial in both fields led to significant temperature and pore fluid pressure increase. A sustained period of overpressuring was also initiated that influenced the evolution of VES in both fields. However, greater rate of burial in Rotherwood field ensured higher overpressure and lower VES compare with Lake Creek. While VES in Figure 5.5. Rotherwood field increased sharply to ~24MPa in Early Eocene and remained constant to present-day (), Lake Creek sands experienced rapid increase of VES to ~30MPa in Late Eocene, and peaked at a present-day maximum of 33.4MPa (Figure 5.5). The more rapid burial in Rotherwood field also ensured that temperature increased steadily to above 180°C at the end of Miocene compared to the ~145°C in Lake Creek (Table 5.1). The last 6 Myrs in both fields is characterised by period of limited deposition that maintained the prevailing temperatures and VES until Present-day.

Fulmar Formation sands from Elgin experienced an early 1km rapid burial in the Upper Jurassic prior to a period of limited deposition that spanned almost the whole Lower Cretaceous (Figure 5.4). A second phase of burial was initiated at the end of Lower Cretaceous with a burial rate of ~ 42 m/Myrs that spanned until Present-day, with the last 12 Myrs typified by a period of more rapid burial with a sedimentation rate of ~ 70 m/Myrs. In Clyde, the Fulmar Formation sands experienced around 0.5km of rapid burial in the Late Jurassic before passing into a period of limited deposition spanning

the whole of Lower Cretaceous to early part of Upper Cretaceous (Figure 5.4). This was followed by a second phase of burial that lasted till Present-day, with the characteristic last 12 Myrs of burial with a sedimentation rate of ~ 70m/Myrs also typifying the Fulmar Formation sands in this field (Figure 5.4). However, greater rate of burial was experienced in Elgin than Clyde during the two later phases of burial. Since the burial history at Clyde is broadly like that at Elgin, the evolution of VES should be like that at Elgin, perhaps with slightly higher VES due to a lower burial rate and thus the greater possibility of pore pressure dissipation by fluid flow. However, the present-day VES is much higher than that at Elgin, 40 MPa rather than 12 MPa (Table 5.1). As discussed earlier, regional pore pressure studies of the Fulmar Formation in the Clyde area show pore pressure distributions which indicate regional depressurisation of the Fulmar sands through a leak off point to the west of Clyde (Swarbrick et al., 2005). The regional pore pressure data are best interpreted as depressurisation occurring over the last 0.5 million years, increasing the VES at Clyde from 19 MPa to 40 MPa (Swarbrick et al., 2005). VES at Clyde is likely to have been low, no more than 19 MPa, throughout all its burial history bar the last 0.5 Ma.

5.5.2. Petrographic Observations

Petrographic description of the Wilcox Group sandstones is based on the observation reported by Harwood (2011). The two Wilcox sandstone samples from Rotherwood and Lake Creek are clean, fine grained, lithic subarkose sandstones, with higher plagioclase fraction than their Fulmar Formation counterparts (Figure 5.6; Table 5.5 and Table 5.6). Average porosities in the examined samples are 6.8% for Rotherwood and 11.8% for Lake Creek (Table 5.6). The feldspars in these sandstones have experienced large scale albitisation and dissolution (Dutton and Loucks, 2010). Their clay fractions, illite and chlorite, are generally less than 4%. Other minor components of these sandstones are berthierine, titania, and micas. Pore-occluding ankerite cement was observed only in the sample from high-temperature Rotherwood field (Figure 5.6 E and F).

The Upper Jurassic Fulmar Formation sandstones investigated in this study were selected from clay-starved upper shoreface facies in Clyde and Elgin Fields. Analysis shows that these sandstones are fine grained, with sub-angular to sub-rounded grain shape, and arkosic mineralogical composition. Illite, the main clay type observed in the analysed Fulmar Formation sandstones, is generally less than 3% of bulk composition in all thin sections (Table 5.5). These clays are partly a product of feldspar dissolution and are found as grain-coats or pore- filling matrices. The illite grain coats in Elgin are also

found coating authigenic quartz, and the matrixes are frequently impregnated with bitumen (Figure 5.7). Partially or completely dissolved feldspars with initial shape preserved as hollow clay rims are common features in the Elgin field, but infrequently observed in Clyde. Intragranular porosity, which is the measure of dissolved feldspars in the analysed thin sections, averages 0.9% in Clyde and 3.3% in Elgin (Figure 5.7E and F; Table 5.5). Intragranular porosity from feldspar dissolution was probably underestimated in Clyde samples as oversized intergranular pore spaces which most likely are sites of dissolved grains which are present in the samples. Petrographic observation shows carbonate cements are ~9% in the Fulmar sandstone sample from both fields (Table 5.5). These carbonates are typically found occluding available pore spaces or destroying porosity locally. Some carbonates were also found as replacive cement in Elgin sample sets, where they either partially assimilate adjacent grains or completely replace dissolved mineral grains. Mineralogically, these carbonate cements occur as discrete dolomite, ferroan dolomite, and zoned species (dolomite core in ferroan dolomite). In addition to dolomite and ferroan dolomites, syntaxial ankerite rims on dolomite nuclei were commonly observed only in Elgin samples. Lithic fragments, micas and pyrite are the other minor components common to samples from both fields, with glauconite observed only in Clyde.

1.5.1.1 Quartz Cementation

Two types of quartz cements, macroquartz and microquartz, were observed during qualitative petrographic analysis (Figure 5.7, Figure 5.8 and Figure 5.9). The macroquartz cements occur as syntaxial and blocky overgrowths and are optically continuous with their detrital quartz nuclei under transmitted light. Different CL zoning patterns can be observed within some of the macroquartz overgrowths at high resolution (Figure 5.8). In contrast, microquartz overgrowths are thin, randomly oriented, polycrystalline quartz overgrowths; with lengths usually ranging from 1 to 10 µm (Aase et al., 1996; French and Worden, 2013).

Quantitative CL petrographic data from the CNS samples (Table 5.5) show sandstones from Elgin have more volume of macroquartz cement (4.6 %) than samples from Clyde (4.4 %). However, normalization of macroquartz cement volume to detrital quartz content indicate that Clyde samples have 20% more macroquartz cement than Elgin samples (Table 5.5). Assessment of the GOM samples show an average macroquartz cement content of 18.8 % in Wilcox Group sandstone from Lake Creek is more than the 12.3 % in high temperature Rotherwood field sample. Even after normalisation to

detrital quartz content, Lake Creek sample still has 37% more macroquartz cement than samples from Rotherwood (Table 5.6). Petrographic data also show that the Wilcox samples generally have at least 40 % more macroquartz cement than the Fulmar Formation samples at equivalent temperatures. Comparison of measured data from CL petrography with modelled values from quartz cementation models suggests that the current macroquartz cement volume in the studied sandstones is low for their present-day temperatures (Table 5.7).

Microquartz were frequently observed within certain intervals in the Clyde samples where they occur as well developed, and sometimes, pore occluding overgrowths, but are almost absent in Elgin samples (Figure 5.7 and Figure 5.9). No microquartz was observed in the Wilcox sandstones, as for previous studies (e.g. McBride et al., 1991; Grigsby et al., 1992; Dutton and Loucks, 2010).

1.5.1.2 Intergranular Pressure Dissolution

Estimation of pressure dissolution along grain contacts was performed on the samples using Sibley and Blatt's (1976b) and Houseknecht's (1991) quantitative approach (Figure 5.8 A). Quantitative results from CL petrography suggest that the average volume of silica released by intergranular pressure dissolution is 2.7% in Clyde, 2.7% in Elgin, 11.7% in Rotherwood, and 19.7% in Lake Creek. Subsequent normalisation of values to detrital quartz content *(see* Houseknecht, 1984; Houseknecht, 1988; Houseknecht, 1991) shows ~ 20% more silica is released by intergranular pressure dissolution in the Fulmar Formation samples from Clyde than in higher temperature, low VES Elgin samples (Table 5.5). Similar observation were made for the Wilcox Group samples where ~ 40% more silica is released in the sandstones from Lake Creek than high temperature, low VES Rotherwood (Table 5.6). Inter-basinal comparison of the normalised data also shows that, at equivalent temperatures, ≥ 45% more silica was released by intergranular pressure dissolution in the Wilcox Group sandstones than their Fulmar Formation counterparts.

In summary, the data in Table 5.8 show that there is:

a) A strong positive correlation between the extent of intergranular pressure dissolution and VES
b) A strong positive correlation between the extent of intergranular pressure dissolution and the amount of quartz cement
c) No correlation between the amount of quartz cement and temperature.

1.5.1.3 Oxygen Isotope

High resolution SIMS analysis has proven to be a valuable tool for reconstructing cementation history of diagenetic quartz cement, by measuring $\delta^{18}O$ profiles across individual macroquartz overgrowth (e.g. Pollington et al., 2011; Harwood et al., 2013).

Seventy-two $\delta^{18}O$ measurements were made by ion microprobe on six different overgrowths from two sandstones from Clyde and Elgin samples. All $\delta^{18}O_{(quartz\ cement)}$ are shown as a function of the distance from their detrital grain boundary in (Figure 5.11). The $\delta^{18}O_{(quartz\ cement)}$ of the Fulmar sandstone sample from Clyde show a 4.1‰ range from +22.7 to +26.8‰ V-SMOW, while Elgin sample fall within a 2.7 ‰ range, from +19.7 to +22.4‰ V-SMOW (Figure 5.11).

Seventy-nine $\delta^{18}O$ measurements were also made by ion microprobe on ten different overgrowths from the two Wilcox sandstone samples from Lake Creek and Rotherwood fields (Harwood, 2011). $\delta^{18}O_{(quartz\ cement)}$ of analysed overgrowths in the Wilcox sample show a 6.1‰ range from +18.6 to +24.7‰ V-SMOW for Lake Creek, and a 5.5‰ range from +18.3 to +23.8‰ V-SMOW for Rotherwood. The $\delta^{18}O_{(quartz\ cement)}$ values from all analysed overgrowths in each sandstone sample overlap and there is no trend from grain boundary to cement edge.

The analyses compromised by the occurrence of fluid inclusions or which fell within cracks or included detrital quartz were discarded (e.g. Figure 5.10). Apart from Elgin overgrowths, the $\delta^{18}O_{(quartz\ cement)}$ for all sandstones decrease from heavier values in the earliest formed cement to lighter values in latest formed cement (Figure 5.11). Also, the $\delta^{18}O_{(quartz\ cement)}$ versus distance plots (Figure 5.11) do not show smooth trends from the detrital boundary to the edge of the overgrowth. The observed fluctuations, when combined with the varied CL zoning pattern seen in the overgrowths during petrographic studies (e.g. Figure 5.8), demonstrate that the development of quartz cement is more complex than a simple concentric growth pattern.

5.5.3. Temperature-controlled Quartz Cementation Models

Results of the quartz cementation modelling are shown in Figure 5.12 and predict that, except for Clyde, all the sandstones in this study have experienced sufficient levels of thermal stress to be completely cemented with quartz. However, there is a very poor agreement between modelled and measured quartz cement volumes (Table 5.7). The models overpredict quartz cement volumes by 50 and 80 % in sandstones from the high temperature Rotherwood and Elgin Fields respectively (Figure 5.12 and Table 5.7).

Similarly, the model overpredicts quartz cement volumes by 30 and 70 % for the sandstones from Lake Creek and Clyde Fields respectively (Figure 5.12 and Table 5.7).

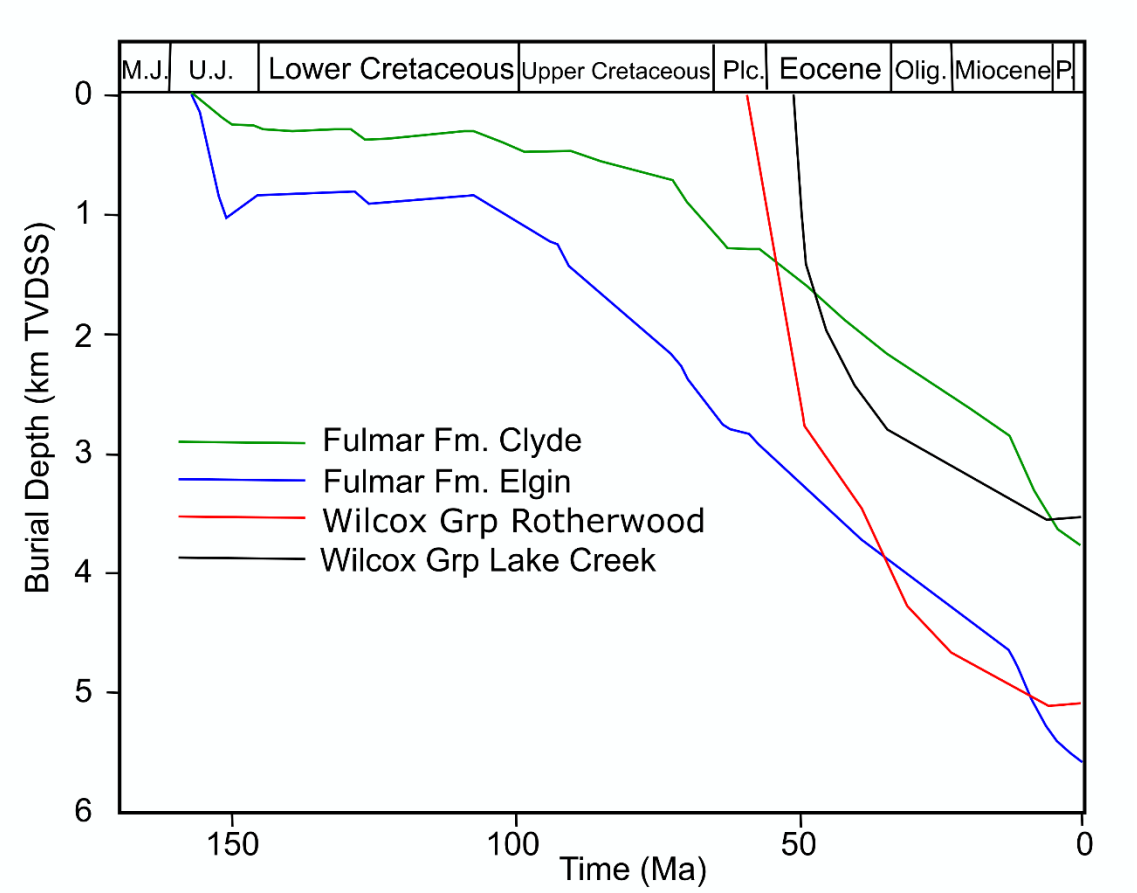

Figure 5.4. Burial history reconstruction for the Central North Sea Fulmar Formation sandstones from Clyde and Elgin Fields, and the onshore Gulf of Mexico Wilcox Group sandstones from Rotherwood and Lake Creek Fields. These models were constructed by using a forward modelling approach on PetroMod 1D version 2014.1. Fulmar Formation sandstones are 100Myrs older than the Wilcox Group sandstones. M.J – Middle Jurassic, U.J – Upper Jurassic, Plc – Paleocene, Olig. – Oligocene, P. – Pliocene, TVDSS – True vertical depth subsea.

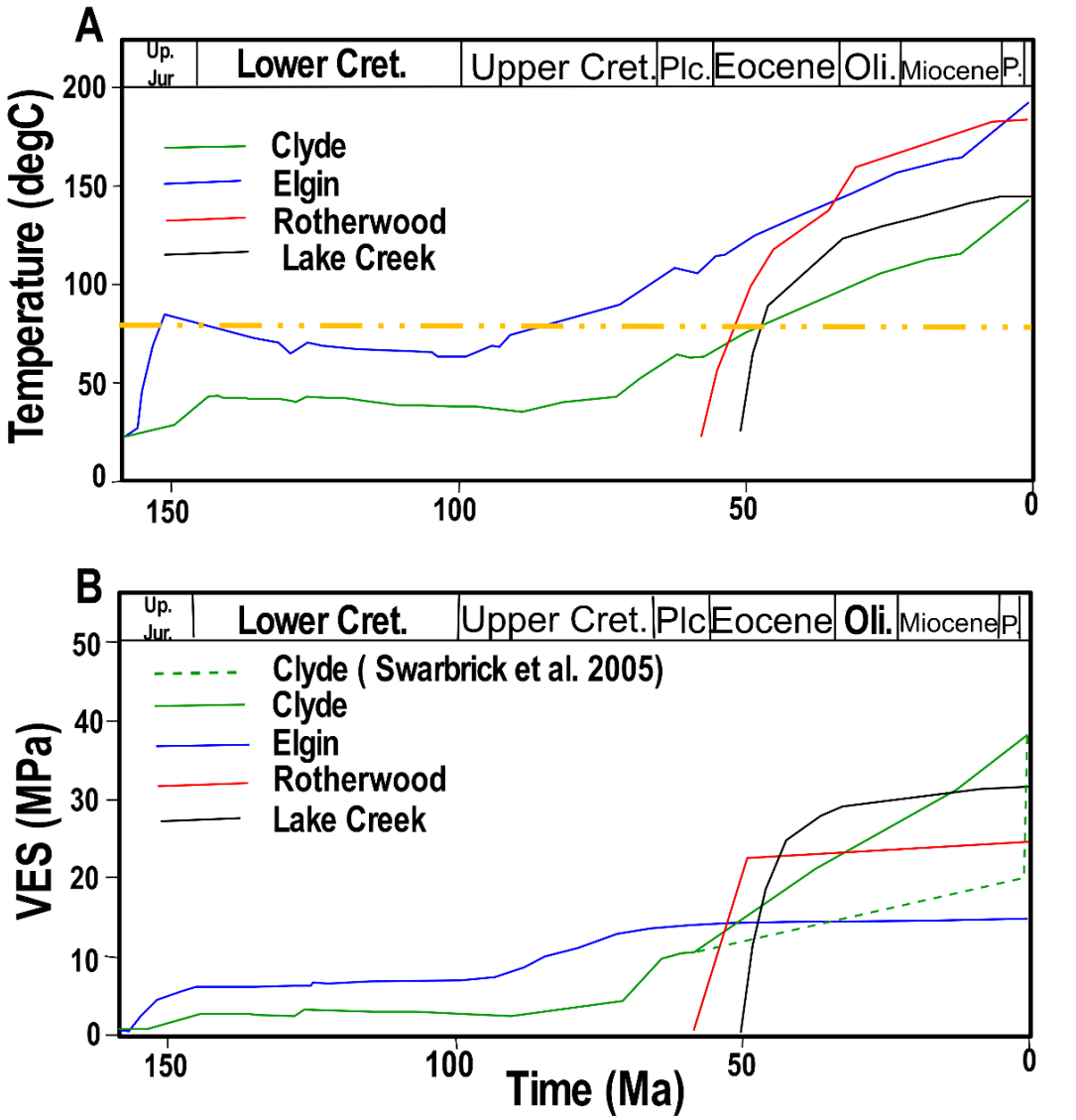

Figure 5.5. Modelled temperature (A) and vertical effective stress (B) histories for Central North Sea Fulmar Formation from Clyde and Elgin fields, and Gulf of Mexico Wilcox sandstones from Rotherwood and Lake Creek. The yellow dashed-line in A is the 80ºC isotherm. These models were constructed by using a forward modelling approach on PetroMod 1D version 2014.1. Upper Jurassic Fulmar Formation sandstones are 100Ma older than the Paleocene-Eocene Wilcox Group sandstones. Green dashed line represents the most likely evolution pathway for Fulmar Formation VES history in Clyde Field based on Swarbrick et al. (2005) Fulmar Formation sandstones experienced low vertical effective stress (VES) for most of their burial histories compared to Wilcox Group sandstones

Table 5.5. Petrographic data of the Upper Jurassic Fulmar Formation sandstones from Clyde and Elgin fields, Central North Sea. Number of analysed samples is the same for the two fields. More detailed data are reported in Appendix 1

	Number of samples	Clyde Mean	Clyde Standard deviation	Clyde Minimum	Clyde Maximum	Elgin Mean	Elgin Standard deviation	Elgin Minimum	Elgin Maximum
Detrital grain size (mm)	10	0.18	0.06	0.06	0.41	0.16	0.05	0.06	0.36
Quartz (%)	19	38.1	3.9	30.3	44.3	44.2	5.6	32.3	55.7
Feldspar (%)	19	27.3	3.3	19.7	32.7	23.5	3.4	17.3	29.7
Lithic Fragments (%)	19	1.2	0.5	0.0	2.3	1.1	0.7	0.0	2.7
Quartz cement - standard petrography (%)	19	3.6	1.6	0.7	7.0	2.0	1.4	0.3	6.3
Quartz cement - CL petrography (%)	10	4.4	1.1	2.7	5.9	4.6	1.2	2.1	6.4
Intergranular Pressure Dissolution - CL petrography (%)	10	2.7	1.0	1.1	3.8	2.7	0.8	1.4	3.8
Quartz cement normalised to detrital quartz	10	0.15	0.03	0.10	0.20	0.12	0.03	0.05	0.15
Intergranular Pressure Dissolution normalised to detrital quartz	10	0.09	0.03	0.04	0.13	0.07	0.02	0.04	0.10
Carbonate cement (%)	19	8.7	5.1	1.3	21	9.4	12.3	0.0	40
Intergranular porosity (%)	19	12.9	2.7	7.3	17.0	11.0	4.6	1.7	20.7
Intragranular porosity (%)	19	0.9	1.0	0.0	3.0	3.3	1.5	1.0	8.0
Core Porosity (%)	33	24.4	2.1	17.2	29.4	22.0	5.2	8.5	27.9
Clay (%)	19	2.3	1.4	0.3	5.3	2.8	2.3	0.7	9.3

Table 5.6. Petrographic data of the studied Wilcox group sandstones (source: Harwood 2011) Bt = berthierine, M/I = mica/illite, K-F = K-feldspar, Na-F = Na-feldspar, Ch = chlorite, An = ankerite.

Field	Sample size	Average quartz cement (%)	Average detrital quartz (%)	QC/DQ	Non-quartz minerals (%)	Porosity (%)	Average grain size (mm)
Lake Creek	1	18.8	53.4	0.35	M/I, Bt, K-F (16%)	11.8	0.17
Rotherwood	1	12.3	56.9	0.22	Ch, M/I, Bt, Na-F, An (24%)	6.8	0.16

Table 5.7. Comparison of modelled and measured quartz cement volumes for sandstones from all the study locations Rotherwood and Lake Creek data were obtained from Harwood (2011).

	Clyde	Elgin	Rotherwood	Lake Creek
Temperature (°C)	147	189	185	143
Modelled Quartz Cement (%)	16.4	26.0	27.9	19.2
Measured Quartz Cement (%)	4.4	4.6	12.3	18.8

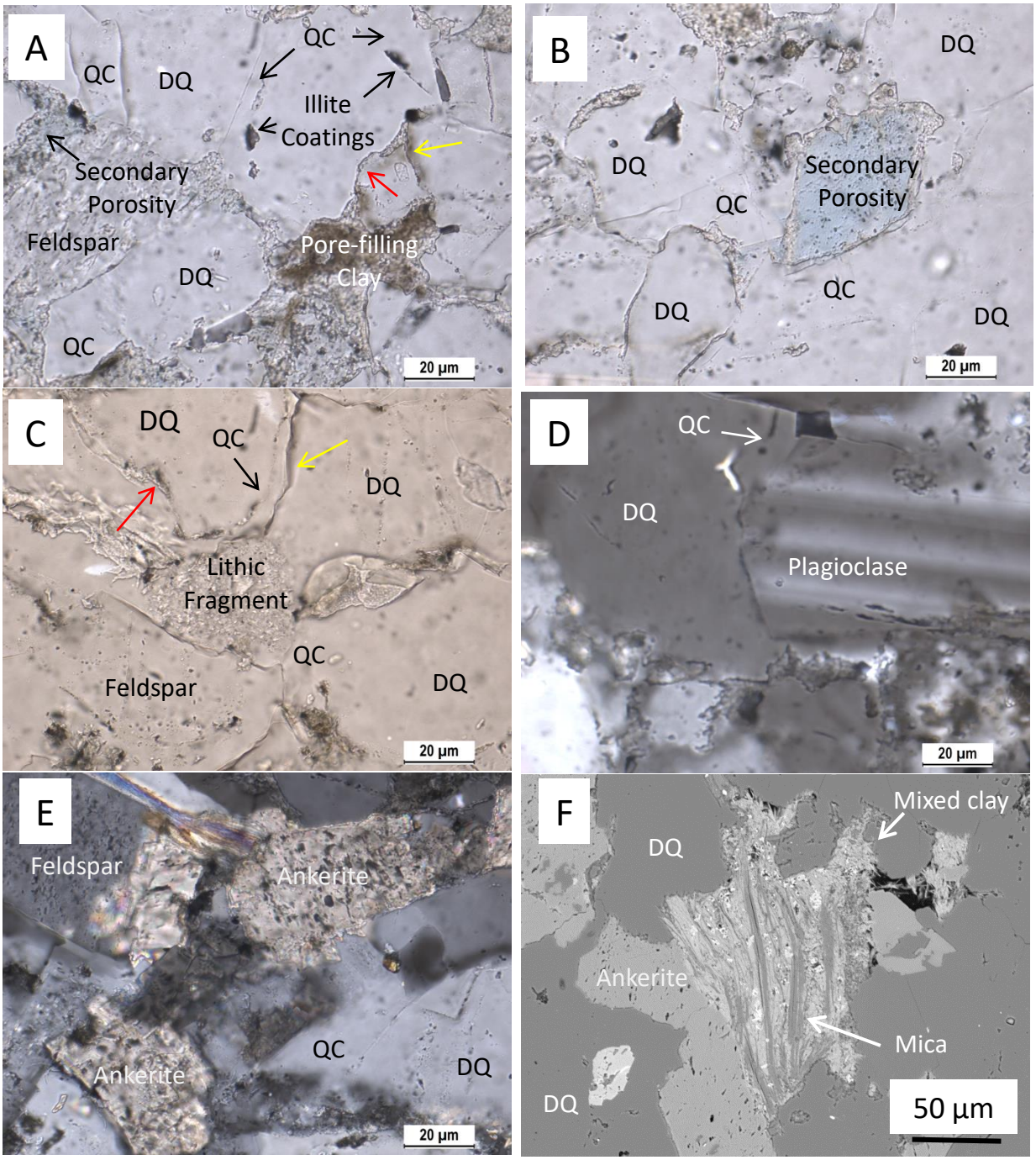

Figure 5.6. Photomicrographs of Wilcox Group sandstones from the Gulf of Mexico. The mineral grains in the samples are interlocked, and evidences of pressure dissolution are visibly indicated by the red (concavo-convex contacts) and yellow (long contacts) arrows. Slides A and B are Lake Creek field samples showing secondary porosity from dissolved feldspars, pore-filling illite, and grain-coating illite engulfed by quartz cement (QC). Lithic fragment (C) and plagioclase feldspars are more common in Wilcox Group sandstones than their Fulmar Formation counterparts. Ankerite cements occluding intergranular porosity in sandstones from Rotherwood field are visible in cross polarised light image (E) and back scatter image (F). Detrital quartz is represented by DQ.

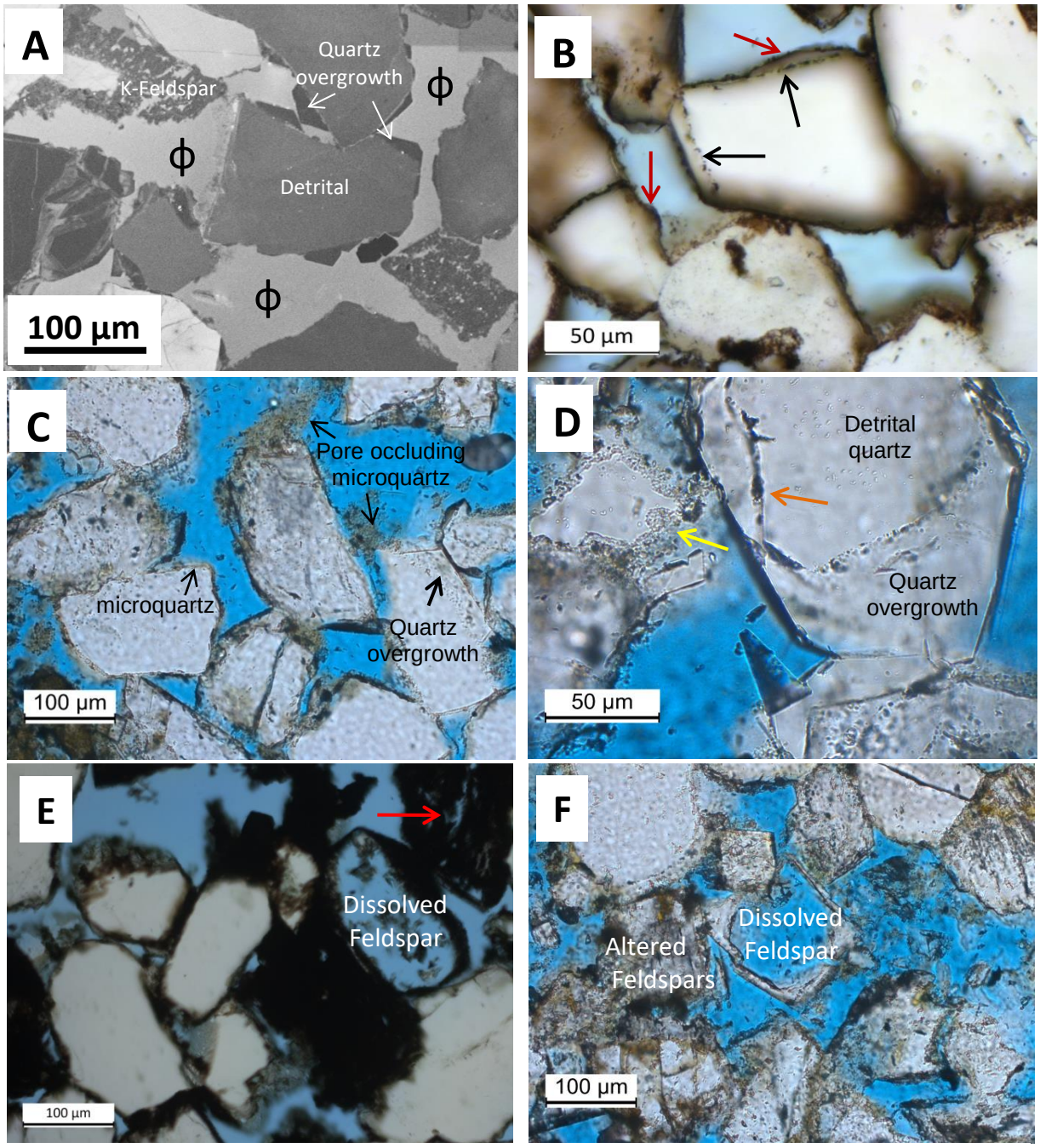

Figure 5.7. Photomicrographs of Upper Jurassic Fulmar sandstone samples from the Central North Sea. The blue areas represent porosity. A) Elgin field sample CL image showing partially dissolved feldspar, quartz cement and detrital quartz. Quartz overgrowths have stunted growth despite significant porosity and the very high present-day temperature (~190 °C). B) Elgin field sample with bitumen impregnated authigenic illite (red arrows) coating already precipitated macroquartz cement surfaces. Macroquartz cements completely engulfed grain-coating illite (black arrow). C) Clyde field sample micrograph showing detrital grains with macroquartz and microquartz overgrowths. Pore-occluding microquartz cements are also present. D) Clyde field sample showing the coexistence of adjacent detrital grains completely enveloped by either microquartz or macroquartz overgrowths. The orange arrow points to pooly developed clay coat on the detrital quartz with thick macroquartz overgrowth. The yellow arrow points at the well-developed grain-coating microquartz completely coating available surface area on the other detrital quartz grain. E) Elgin field sample showing bitumen impregnated clay rim preserving the shape of completely dissolved feldspar and the red arrow point at partially dissolved feldspar impregnated with bitumen. F) Clyde field sample showing altered feldspars, and preserved K-feldspar overgrowth outlining the shape of dissolved detrital K-feldspar.

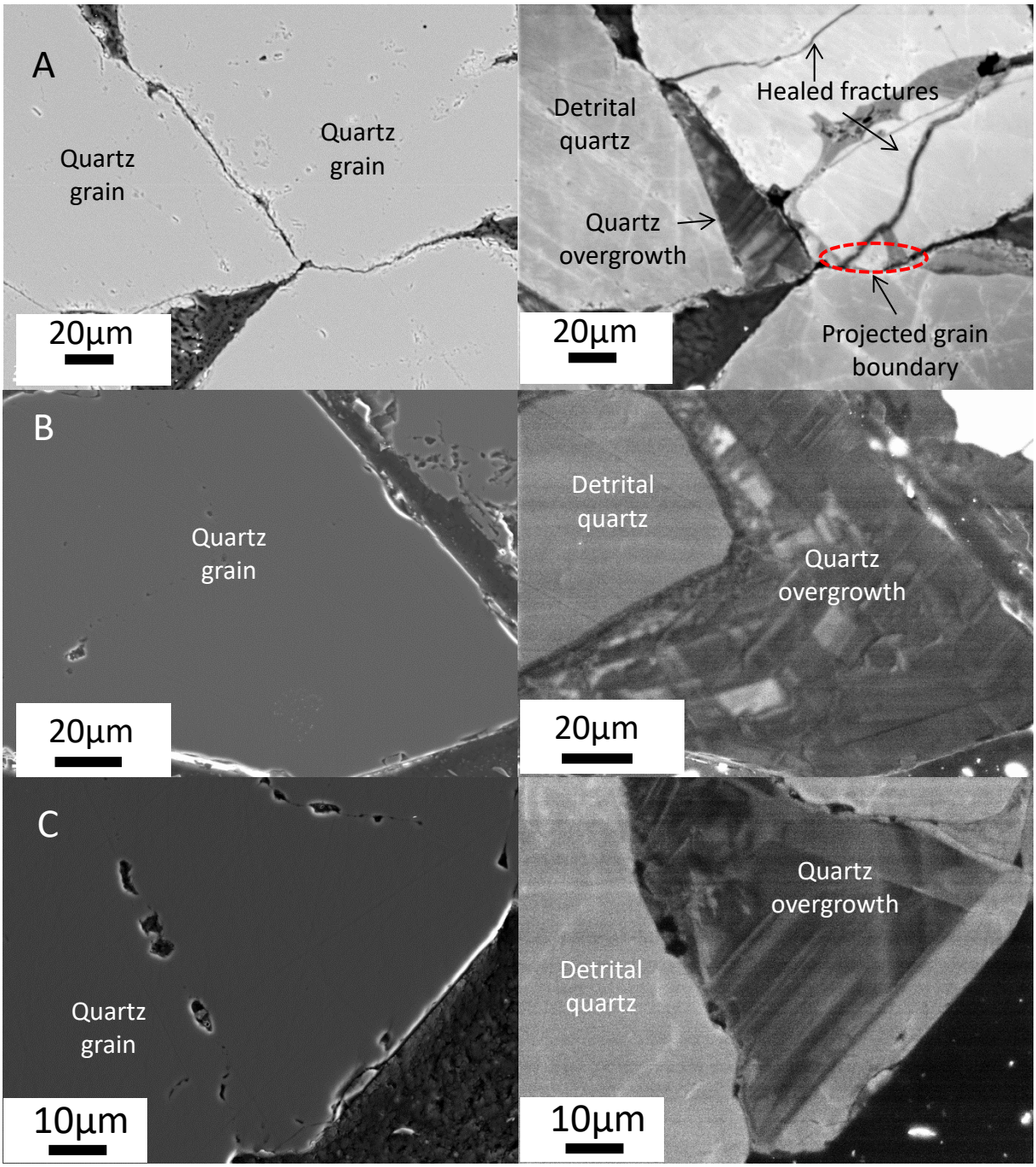

Figure 5.8.Backscattered electron (BSE) and equivalent cathodoluminescence (CL) images of Upper Jurassic Fulmar sandstones showing A) sample projected grain boundary(after Sibley and Blatt (1976b) and Houseknecht (1991)) used to define and quantify pressure dissolution, and healed grain fractures; B) quartz grain from Clyde sample set with very thick syntaxial overgrowth typified by mosaic-type CL zoning; C) quartz grain from Elgin sample set with syntaxial overgrowth showing angular CL zonation. These zoning patterns show that the idea of a overgrowth nucleating concentrically on detrital quartz, as assumed in quartz cementation model, is not always the case. Generally, overgrowth thicknesses are up to 60µm in Elgin samples, and 100µm in Clyde samples.

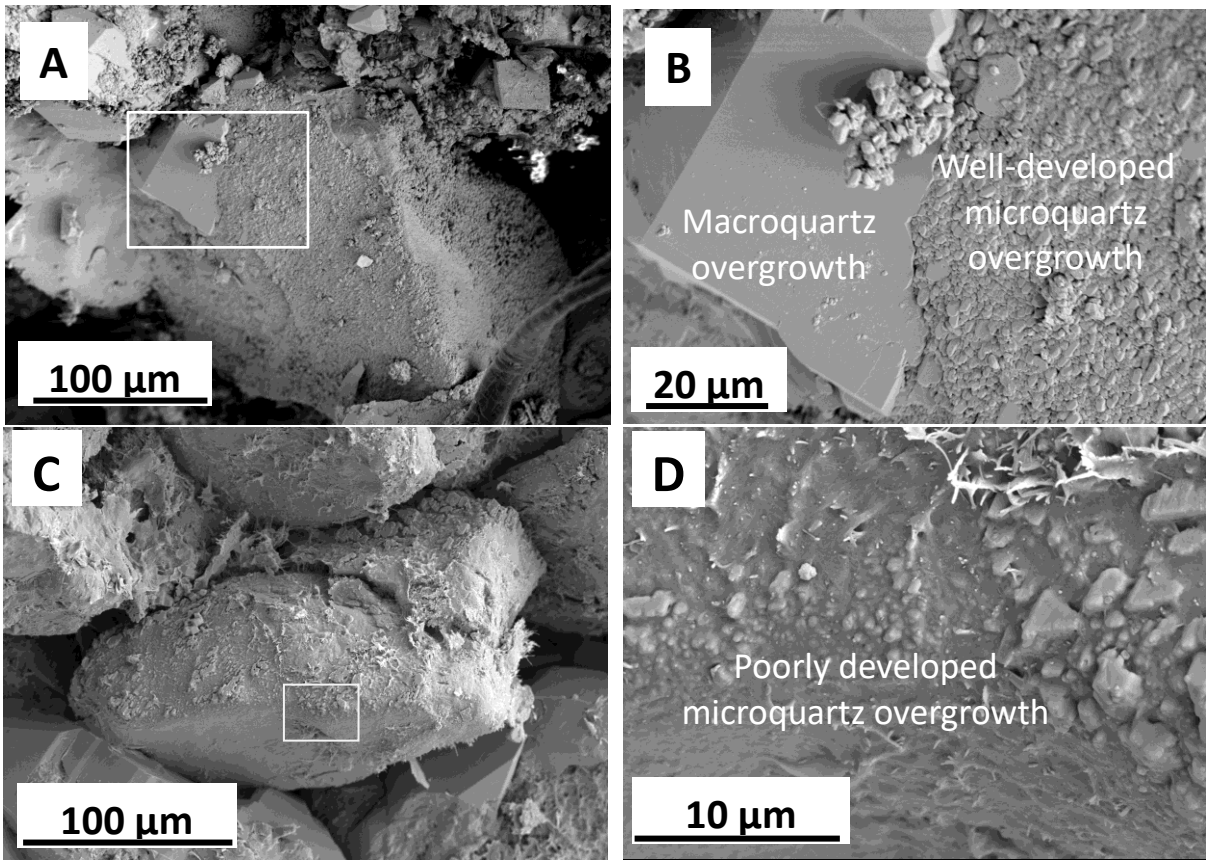

Figure 5.9. Micrographs of Upper Jurassic Fulmar Formation sandstones from Clyde and Elgin fields A) Secondary electron (SE) image of Clyde sample showing macroquartz and microquartz overgrowths nucleated on the same detrital quartz. B) Higher magnification view equivalent to the box in panel A. C) Secondary electron (SE) image of Elgin sample showing quartz grain surface with poorly developed microquartz overgrowth and clay coats. D) Higher magnification of the box in panel C. Microquartz overgrowth is almost absent and poorly-developed in the Elgin samples

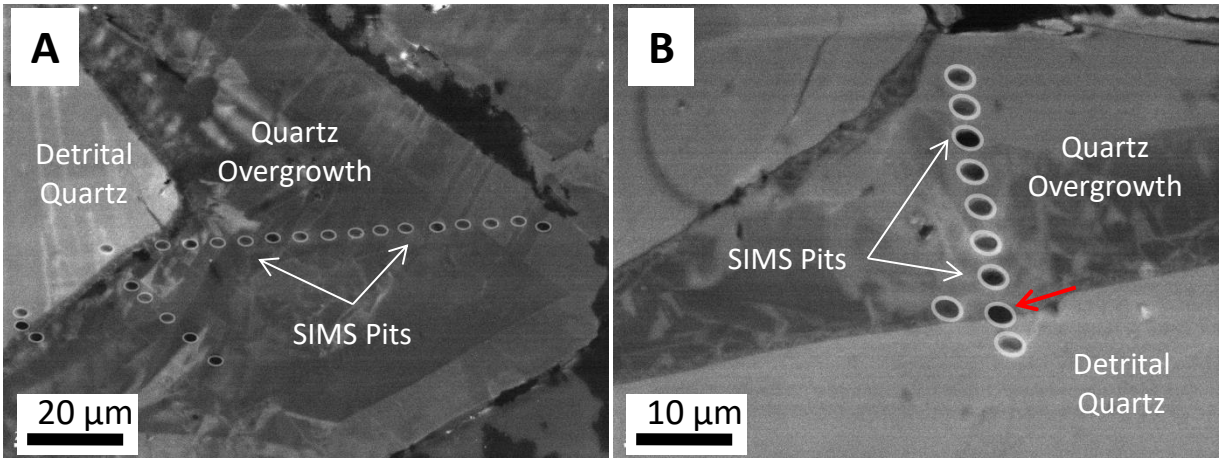

Figure 5.10. Cathodoluminescence (CL) images of Upper Jurassic Fulmar sandstone sections from showing boundaries between detrital quartz and quartz overgrowths, and 3µm diameter SIMS pits generated during oxygen isotope analysis. The CL zonation seen in the quartz overgrowths on the two panels presented only subtle variation in SIMS data. The red arrow in panel B indicates a compromised SIMS pit that included detrital and authigenic quartz

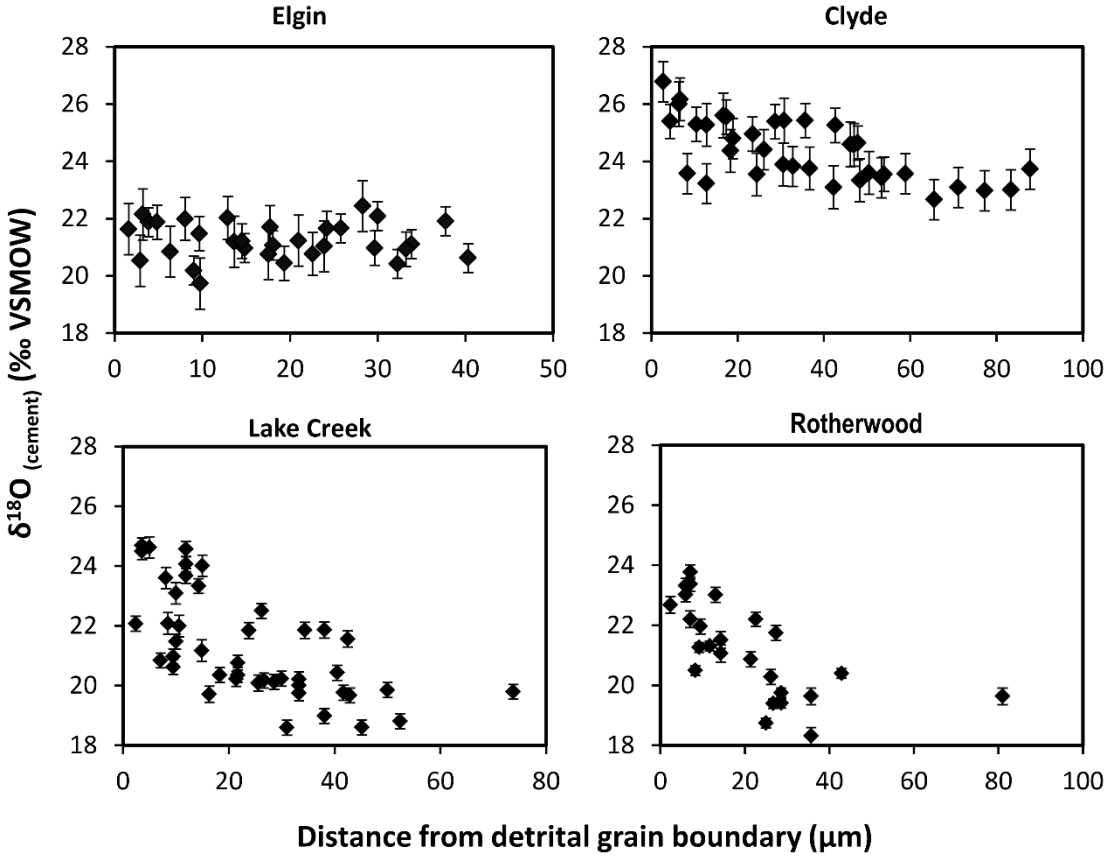

Figure 5.11. Plot of $\delta^{18}O_{(quartz\ cement)}$ against distance in microns from detrital grain boundaries. Distance axis is limited to 50µm in Elgin, 80µm in Lake Creek, and 100µm in Clyde and Rotherwood. Clyde and Elgin data were acquired from three overgrowths each using 3µm SIMS spot sizes. Lake Creek and Rotherwood data were acquired from six and four overgrowths respectively using 12µm SIMS spot sizes. All $\delta^{18}O_{(quartz\ cement)}$ decrease from heavier values close to detrital grain boundary to lighter values at the outermost edge of the overgrowths with the exception of Elgin samples

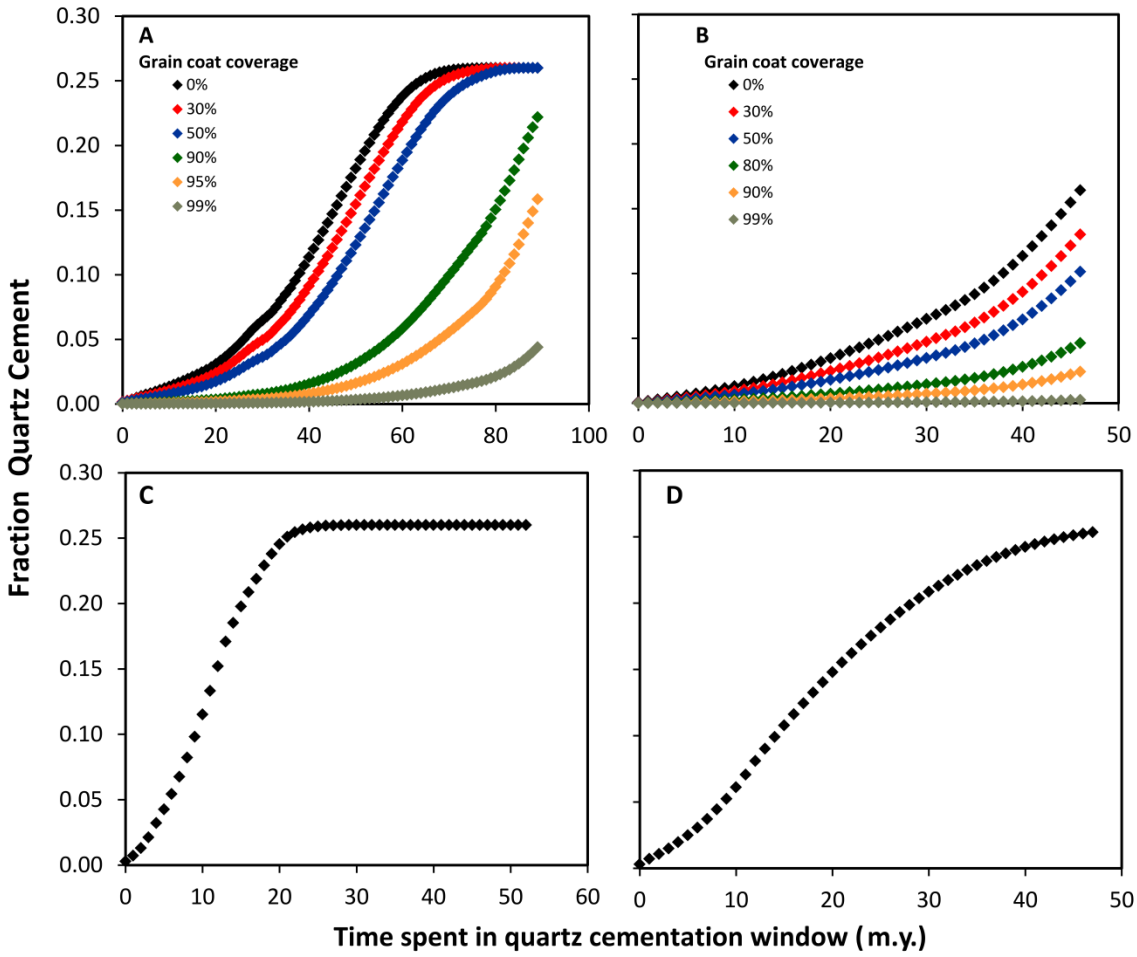

Figure 5.12. Model plots showing quartz precipitation through geologic time for Fulmar Formation from Elgin (A) and Clyde (B) fields, and Wilcox Group sandstones from Rotherwood (C) and Lake Creek (D) fields. Walderhaug's (1996) approach was applied to 1cm^3 volume of the studied sandstones using an 80°C threshold temperature for cementation and a starting porosity of 26%. Time-temperature history was generated using PetroMod version 2014.1. Average grain coatings coverage in Clyde and Elgin samples sets is below 50%. The variation of grain coat coverage for these models suggests that grain coat coverage of 80 and 99% is required for the present average quartz cement volume of 4.3% in Clyde samples and 4.6% in Elgin samples. Grain coatings are rare in the Wilcox Group sandstones.

Table 5.8. Table showing normalized quartz cement contents for the Fulmar Formation and Wilcox Group sandstones. VES = Vertical Effective Stress (VES); $\delta^{18}O_{(qc)}$ is the oxygen isotope composition of quartz cement. VES in Clyde is the proposed VES 0.5 Ma ago, prior to depressurising via lateral fluid flow (Swarbrick et al., 2005). Present VES is 40 MPa. Temp. Range is the temperature range over which quartz cement is suggested to form, based on oxygen isotope composition.

Field	Quartz Cement/ Detrital Quartz	IPD/Detrital Quartz	Temp. (°C)	VES (MPa)	δ18O(qc) range	Temp. Range (°C)
Elgin	0.12	0.07	189	12.5	2.7	80-150
Clyde	0.15	0.09	147	19.2	4.1	55-125
Rotherwood	0.22	0.21	185	23.2	5.5	75-160
Lake Creek	0.35	0.37	143	33.7	6.1	65-145

5.6. Discussion

5.6.1. Quartz Cementation Histories

In situ oxygen isotope profiles were obtained across selected overgrowths within the studied sandstones to reveal information about their quartz cementation histories (Figure 5.11). $\delta^{18}O_{(quartz\ cement)}$ ranges for all sample sets correlate positively with normalised intergranular pressure dissolution and quartz cement data (Table 5.8). For example, Fulmar Formation samples from high temperature Elgin have a narrower range of $\delta^{18}O_{(quartz\ cement)}$, lower volume of quartz cement, and lower degree of intergranular pressure dissolution than the Clyde samples. Similar observation were made for the Wilcox Group where high temperature Rotherwood sample set has slightly narrower range of $\delta^{18}O_{(quartz\ cement)}$ than Lake Creek sample set (Figure 5.11 and Table 5.8).

In order to understand the implication of the oxygen isotope data, I evaluated the $\delta^{18}O_{(quartz\ cement)}$ data acquired for all sample sets. Although $\delta^{18}O_{(quartz\ cement)}$ cannot provide a unique temperature of quartz precipitation because the oxygen isotope composition of quartz is a product of the dual function of temperature and $\delta^{18}O_{(water)}$ (Clayton et al., 1972). The data can, however, be interpreted to make the most geologically realistic deductions. I, therefore, integrated the $\delta^{18}O_{(quartz\ cement)}$ data with that of $\delta^{18}O$ of water in the Fulmar Formation and Wilcox Group sandstones (Figure 5.13). Present-day $\delta^{18}O_{(water)}$ in the Fulmar Formation sandstone is ~+4.5 ‰ (Hendry et al., 2000), and measurements more positive than this value are unusual for Jurassic reservoirs in the Central North Sea (Warren et al., 1994). If quartz precipitation started with $\delta^{18}O_{(quartz\ cement)}$ of +26.8 ‰ in Clyde and +22.4 ‰ in Elgin from fluid similar to Jurassic marine water (-1 ‰), then all cementation would have occurred in $\delta^{18}O_{(water)}$ that evolved from -1 to +4.5 ‰ at present-day. This correspond to a temperature window of 55 to 125 ˚C in Clyde and 80 to 150 ˚C in Elgin (Figure 5.13A).

For the Wilcox Group sandstones Land and Fisher (1987) reported present-day $\delta^{18}O_{(water)}$ ranging from +3.5 to +5.8 ‰ measured over a wide range of temperature for Wilcox Group sandstones from fields adjacent to the study areas (Figure 5.13B). If quartz precipitation started with $\delta^{18}O_{(quartz\ cement)}$ of +24.69 ‰ in Lake Creek and +23.77 ‰ in Rotherwood from fluid similar to Eocene Texas marine water (-1 ‰), all quartz cementation could have occurred in $\delta^{18}O_{(water)}$ that evolved from -1 to +3.5 ‰ at present-day, which would give a temperature window of 65 to 145 ˚C in Lake Creek

and 74 – 160 ˚C in Rotherwood (Figure 5.13B). The lack of very late quartz cement or isotopic record for higher temperatures in Clyde, Elgin and Rotherwood samples is due to either hydrocarbon charge or slower rate of cementation at the outer edge of analysed overgrowths that was not picked up by SIMS analysis (Figure 5.10B) . The latter is more valid and would imply that quartz cementation continued to more recent geologic times or present-day in the studied sandstones.

These $\delta^{18}O$ data interpretations indicate that:

(a) Quartz precipitation rate was slower in the Fulmar Formation sandstones than the Wilcox Group sandstones

(b) Quartz precipitation rate is slower in the Fulmar Formation and Wilcox Group sandstones from high temperature Elgin and Rotherwood than their corresponding low temperature counterparts from Clyde and Lake Creek Fields and

(c) Quartz precipitation rates across all sample sets increased with the degree of intergranular pressure dissolution and not with temperature.

I suggest that this is the explanation for the positive correlation that the $\delta^{18}O_{(quartz\ cement)}$ ranges for all sample sets is showing with normalised intergranular pressure dissolution and quartz cement data (Table 5.8).

5.6.2.Silica Supply and Quartz Cementation

Upper Jurassic Fulmar Formation sandstones from Elgin field at 189 °C at present-day have 20% less volume of quartz cement compared with those from Clyde field at 147°C. Similar observation were made for the Paleocene-Eocene Wilcox Group sandstones from the Gulf of Mexico where the Rotherwood field sample set, at 185 °C, has 35% less volume of quartz cement than Lake Creek sample set at 143 °C. Another key observation is the presence of more quartz cement (≥ 45 %) in the Wilcox Group sandstones than the Fulmar Formation sandstones at equivalent temperatures.

While there appears to be no relationship between quartz cement volumes and temperature in the studied sandstones, normalised quantitative petrographic data reveal a positive correlation between intergranular pressure dissolution and quartz cement volumes (Table 5.8). This observation suggests that pressure dissolution along grain-grain contacts is the main source of the silica for quartz cementation in the studied sandstones. This “source-sink” relationship between pressure dissolution and quartz

cementation is well-documented in many geological studies (De Boer et al., 1977; Tada et al., 1987; McBride, 1989; Tada and Siever, 1989; Dewers and Ortoleva, 1990; Giles et al., 2000; Worden and Morad, 2000; van Noort et al., 2008). Intergranular pressure dissolution supplied between 95 - 115 % of silica in the Wilcox Group sandstones, and 60% of silica in the Fulmar Formation (Table 5.8). The remaining silica could have come from feldspar dissolution, clay mineral reactions and/or adjacent mudrock reactions (Worden and Morad, 2000) .

Presence of dissolved feldspars in the Fulmar Formation and Wilcox Group sandstones (Figure 5.6A and B, Figure 5.7E and F) suggests that part of the silica for quartz cementation in these sample sets was sourced from feldspar dissolution. Unlike the Wilcox Group sandstones, where feldspar dissolution started at shallow depth, when the sandstones were still in contact with meteoric water (Dutton and Loucks, 2010), feldspar dissolution featured during mid-late diagenesis in the Fulmar Formation (Haszeldine et al., 1999; Lasocki et al., 1999; Wilkinson and Haszeldine, 2011). Since this diagenetic stage coincides with the time when Fulmar Formation sandstones are already fully within the quartz cementation window, it is rational that all the feldspar-dissolution-sourced silica would be available for quartz cementation in these sandstones. Oye et al. (2018) already made a case for the Fulmar Formation sandstones where apart from intergranular pressure dissolution, mass balance calculation suggests that feldspar dissolution supplied the remaining silica for their observed quartz cement volumes.

5.6.3. VES or Temperature as the Main Control on Quartz Cementation

Sandstone reservoirs at depth are subjected to pressure exerted by weight of overlying sediment called lithostatic stress. Part of the lithostatic stress is offset by pore fluid pressure and the resultant stress is called vertical effective stress (VES). Many studies (Thomson, 1959; Weyl, 1959; Rutter and Elliott, 1976; De Boer et al., 1977; Robin, 1978; Tada et al., 1987; Tada and Siever, 1989; Dewers and Ortoleva, 1990; Dewers and Ortoleva, 1991; Elias and Hajash, 1992; Shimizu, 1995; Renard et al., 1997; Renard et al., 1999; Sheldon et al., 2003; Gratier et al., 2005; van Noort et al., 2008; Nenna and Aydin, 2011) have shown that pressure dissolution at intergranular contacts and stylolitic bands in sandstones is driven by VES. Pressure dissolution, otherwise known as chemical compaction, results due to anisotropic stress within sandstone systems; such that, the chemical potential at grain contacts is higher than that within the remaining part of the system (Tada and Siever, 1989; Elias and Hajash, 1992; Sheldon et al., 2003;

van Noort et al., 2008). Pressure dissolution at intergranular and stylolitic contacts in sandstones is a silica-releasing process, and is accepted to be common sources of silica for quartz cementation in sandstones(De Boer et al., 1977; Tada et al., 1987; McBride, 1989; Tada and Siever, 1989; Oelkers et al., 1996; Giles et al., 2000; Worden and Morad, 2000). The presence of high pore fluid pressure could reduce or completely offset the overall VES experienced by sandstones (Osborne and Swarbrick, 1999; Stricker et al., 2016a), thus resulting in corresponding reduction, or complete cut-off, of silica supply from pressure dissolution. Since quartz cementation is a product of three consecutively linked processes of source-transportation-precipitation, any changes on the source would definitely affect the other processes (Sheldon et al., 2003). For example, a truncated supply process would inhibit the entire quartz cementation process regardless of the prevalent temperature regime (Oye et al., 2018).

Based on the current paradigm, the rate of quartz cementation is supposed to increase exponentially with temperature once precipitation kinetics barrier is broken around 70-80°C (e.g.Walderhaug, 1994a; Walderhaug, 1996; Ajdukiewicz and Lander, 2010). However, the measured volumes of quartz cement are lower than those predicted by temperature-controlled precipitation kinetic model for all the studied sandstones (Figure 5.12 and Table 5.7). Similarly, Fulmar Formation and Wilcox Group sandstones from higher temperature Elgin and Rotherwood Fields have lower quartz cement contents than their lower temperature counterparts from Clyde and Lake Creek Fields (Table 5.8). Inter-basinal comparison of the Fulmar Formation and Wilcox Group sandstones at equivalent temperatures also revealed that quartz cement volumes are much higher in the Wilcox (Table 5.8). These observations call to question the role of temperature as the main driver of quartz cementation in reservoir sandstones.

The quartz cementation phenomenon can be explained if the effect of VES on pressure dissolution and by extension, quartz cementation, is considered. I have argued earlier that intergranular pressure dissolution can supply most, or all the silica required for quartz cementation in the studied sandstones. However, historical VES is very important for understanding how VES influences pressure dissolution and quartz cementation (Osborne and Swarbrick, 1999; Bloch et al., 2002). Present-day VES of ~ 12.5 MPa in Elgin is lower than the 40 MPa in Clyde. One-dimensional basin model output revealed that Elgin VES was not above 12.5 MPa throughout geologic history (Figure 5.5). In the case of Clyde, Swarbrick et al. (2005) indicated that temporal VES

was low in the geological past as the Fulmar Formation reservoir in this field forms part of the Fulmar-Halley overpressured compartment in the Central North Sea that became depressurised by lateral flow starting from about 0.5Ma when VES was around 19.2MPa. This interpretation is corroborated by the low degree of pressure dissolution observed in the sample set during petrographic analysis (Figure 5.5). Hence, present-day VES of 40 MPa in Clyde is a recent development that has had little or no effect on the reservoir sandstone. Similarly, temporal and present-day VES is lower for the Wilcox Group sandstones from Rotherwood compare to Lake Creek. While temporal VES in Rotherwood has never exceeded the present–day value of 24 MPa, VES increased steadily in Lake Creek to present-day maximum of ~ 33 MPa.

Qualitative cementation rates, derived from the temperature range over which quartz is inferred to form, based on oxygen isotope data, are more strongly correlated to VES than temperature (Table 5.8). These data suggest that effective stress is the main control on the rate of quartz cementation, and not temperature-related precipitation kinetics. Whilst a control by VES on quartz cementation has been suggested previously (Elias and Hajash, 1992; Osborne and Swarbrick, 1999; Sheldon et al., 2003; van Noort et al., 2008; Oye et al., 2018), the dataset presented here, supporting that suggestion, is the most comprehensive to date.

Overall assessment of the data shows that the magnitude of historical VES experienced by sandstone systems is important for ensuring the continuous supply of silica from intergranular pressure dissolution for quartz cementation. Although temperature may be a key for precipitation kinetics, the rate of quartz cementation would still be largely determined by the amount of silica available for precipitation. Beyond the scope of this study, a critical predictive next step would be to quantify the rate of IPD as a function of VES and temperature. van Noort et al. (2008) has presented such a model, based on higher temperature laboratory experiments, but it has never been tested against data in sandstones in sedimentary basins. Some initial insights can be gleaned from this study, in that VES in Clyde has increased from 19 to 40 MPa in the last 0.5 million years, but has quartz cement volumes which are qualitatively consistent with the lower VES value. This suggests that the kinetics of IPD are such that greater timescales are required for the results of IPD to be observed as quartz cement.

5.6.4. Can the pattern of quartz cementation be explained by other factors?

5.6.4.1. Grain-coating Microquartz

The occurrence of grain-coating microquartz in reservoir sandstones has been linked to sponge spicules precursors (Aase et al., 1996; Gowland, 1996; Osborne and Swarbrick, 1999; Taylor et al., 2015). When sponge spicule undergo dissolution during burial, they produce biogenic silica that has higher solubility than silica produced from intergranular pressure dissolution and/or stylolites (Aase et al., 1996). The resultant enrichment and preferential supersaturation of pore water with biogenic silica would inhibit dissolution at quartz grain-grain contacts and stylolites, thus limiting the amount of silica available for macroquartz cementation (Aase et al., 1996; Osborne and Swarbrick, 1999; Aase and Walderhaug, 2005). The biogenic silica would re-precipitate on free detrital quartz grain surfaces as microcrystalline quartz overgrowths, thus reducing or completely blocking the quartz surface area available for macroquartz cementation (Aase et al., 1996; Osborne and Swarbrick, 1999). Other researchers (French et al., 2012; Worden et al., 2012; French and Worden, 2013) also reported that an amorphous silica layer is present between microquartz overgrowths and their host grains, and that this layer shields the host from macroquartz precipitation and give microquartz overgrowths their random orientation.

Because the distribution of microquartz in sandstone reservoirs are often non-uniform, their occurrence may be restricted to specific intervals (Osborne and Swarbrick, 1999). Previous studies (Aase et al., 1996; Gowland, 1996; Osborne and Swarbrick, 1999) have reported the occurrence of grain-coating microquartz within certain stratigraphic intervals in some Jurassic sandstones in the Central North Sea. Grain-coating microquartz was observed in variable abundance in the Clyde sample set examined in this study. Although samples with the most grain-coating microquartz overgrowths have the least quartz cement contents, quantitative CL petrography revealed that other samples with little or no microquartz also had very low volume of quartz cement compared to the volume predicted by a quartz cementation model (Figure 5.12 and Table 5.5). Grain coating microquartz is deemed to have no effect on quartz cementation in the Fulmar Formation sandstones from Elgin as they were effectively absent in these samples.

Grain-coating microquartz was not observed in the sandstones from Rotherwood and Lake Creek, and no such occurrence has been reported in previous studies (e.g. Loucks

et al., 1984; Johnston and Johnson, 1987; Grigsby et al., 1992; Dutton and Loucks, 2010)on the Wilcox Group sandstones from other localities.

5.6.4.2. Grain-coating Clays

Grain-coating clays are very effective inhibitors of quartz cementation when they are pervasive and well developed within sandstone reservoirs (Berger et al., 2009; Ajdukiewicz and Lander, 2010; Morad et al., 2010; Taylor et al., 2010; Nguyen et al., 2013; Taylor et al., 2015; Dutton et al., 2016; Stricker et al., 2016b). Grain-coating clays inhibit quartz cementation by making detrital quartz surface area unavailable for quartz precipitation. Grain-coating clays are not only rare in the studied Wilcox Group sandstones, the few observed have mostly been engulfed by quartz cement (Figure 5.6). The dearth of grain-coating clays observed in the studied Wilcox Group sandstones is consistent with the study of Dutton and Loucks (2010). However, other studies (Johnston and Johnson, 1987; Dutton et al., 2016) have reported the inhibition of quartz cementation by robust grain-coating chlorite in the Wilcox Group sandstones from other locations.

Several studies (Wilkinson and Haszeldine, 1996; Wilkinson et al., 1997; Osborne and Swarbrick, 1999; Wilkinson and Haszeldine, 2011; Taylor et al., 2015) have shown that illite clays are the most important in the Upper Jurassic Fulmar Formation. The studied Fulmar Formation sandstones are upper shoreface facies with generally low volume of illite clays (< 3%). The origin of these illite clays, detrital or authigenic, is not easily discernible as the entire detrital fraction has undergone recrystallization under the influence of temperature (Wilkinson and Haszeldine, 2011). The grain-coating illite from authigenic sources is not likely to have any inhibitive effect on quartz cementation within the Fulmar Formation sandstones, because quartz cement would have precipitated on free detrital quartz prior to their release from dissolved feldspars (Oye et al., 2018). Petrographic evidence from Figure 5.7 confirms this assertion, as authigenic illite coating the surfaces of some macroquartz overgrowths suggests macroquartz cementation predates authigenic illite formation from dissolved feldspars.

Illite from detrital origin usually forms early on detrital grains and is likely to possess more inhibitive effect on quartz cementation. However, petrographic observation of the Fulmar Formation sandstones shows that some of these grain coatings have been completely engulfed by quartz cement due to poor development (Figure 5.7). Quantitative analysis shows that average grain coat coverage (combined clay and

microquartz) is less than 40% in the Fulmar Formation samples from Clyde and Elgin Fields (Figure 5.14). Quartz cementation modelling performed on the Fulmar Formation sandstones were tested with varying grain-coat coverage values (Figure 5.14). The outputs (Figure 5.12 A and B) suggest that each detrital quartz grain must have grain-coat coverage of around 80% in Clyde, and 99% in Elgin, to limit the observed average quartz cement volumes in both fields to their current values of 4.4 and 4.6%. The required coating coverage is thus much higher than those observed.

5.6.4.3. Hydrocarbon emplacement

The possible role of hydrocarbon emplacement as an inhibitor of quartz cementation in sandstone reservoirs has been discussed in many studies (e.g. Dixon et al., 1989; Saigal et al., 1992; Emery et al., 1993; Gluyas et al., 1993; Aase et al., 1996; Worden et al., 1998; Marchand et al., 2000; Marchand et al., 2002; Aase and Walderhaug, 2005; Molenaar et al., 2008; Wilkinson and Haszeldine, 2011; Worden et al., 2018a; Worden et al., 2018b). In this study, basin modelling suggests that all the studied sandstones were charged with hydrocarbons from the Miocene, except for the Elgin reservoir that was charged from the Eocene. These timings are similar to those estimated in previous studies of the Fulmar Formation and Wilcox Group sandstones (Stevens and Wallis, 1991; Rudkiewicz et al., 2000; Pitman and Rowan, 2012). Comparison of the charge histories with modelled and actual cementation histories estimated from oxygen isotope data, indicate that the effect of hydrocarbon emplacement on quartz cementation in the studied sandstones is negligible. Firstly, temperature-based quartz precipitation models predict that substantial quartz cement should have precipitated prior to hydrocarbon emplacement and secondly, quartz cementation histories from *in situ* oxygen isotope analysis suggest that cementation continued beyond the time of hydrocarbon emplacement, potentially to the present-day. These results suggest that hydrocarbon emplacement has not played a significant role on quartz cementation in the studied sandstones.

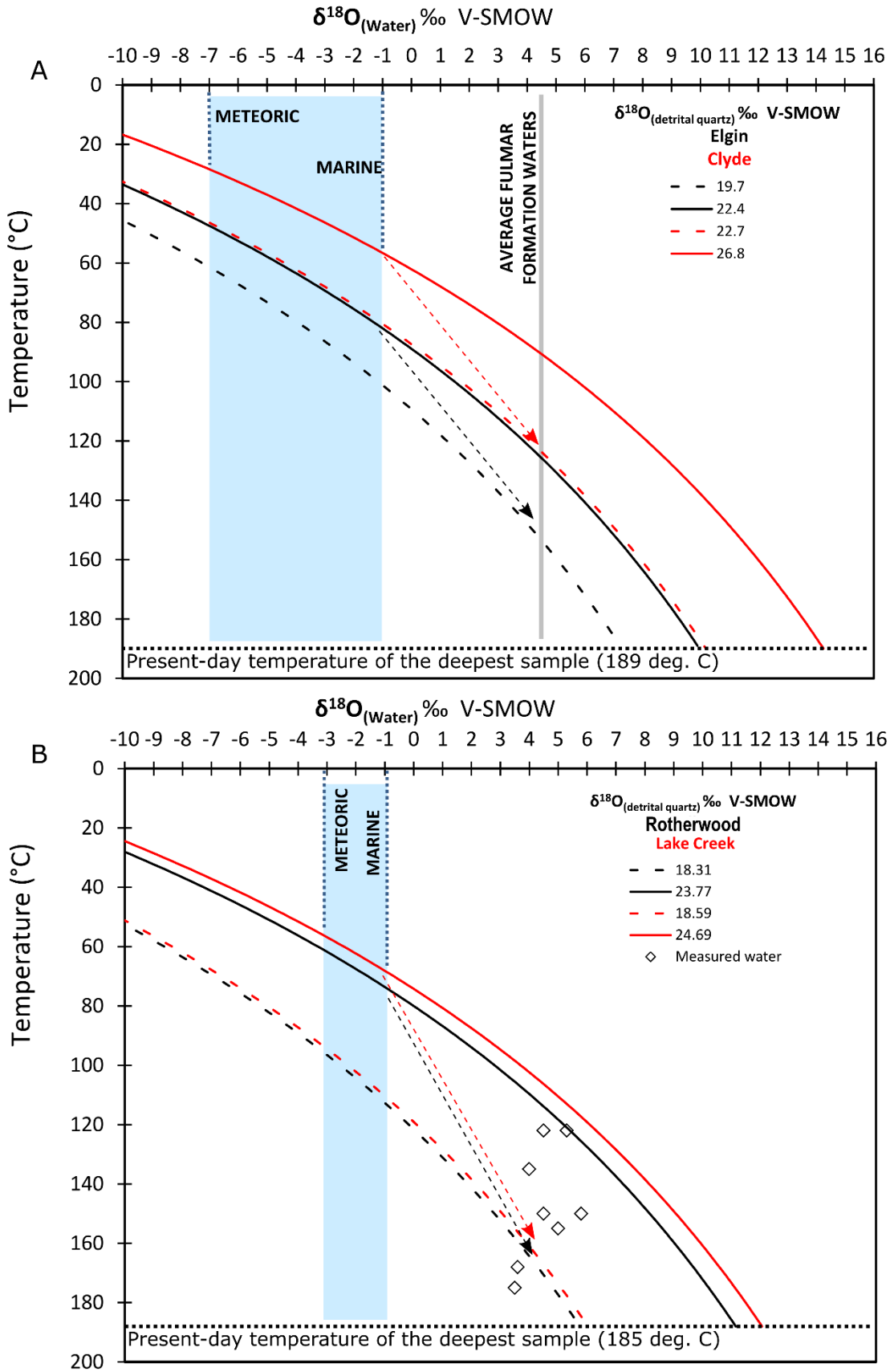
A
δ18O(Water) ‰ V-SMOW
-10 -9 -8 -7 -6 -5 -4 -3 -2 -1 0 1 2 3 4 5 6 7 8 9 10 11 12 13 14 15 16
Temperature (°C)
0 20 40 60 80 100 120 140 160 180 200
METEORIC
MARINE
AVERAGE FULMAR FORMATION WATERS
δ18O(detrital quartz) ‰ V-SMOW
Elgin
Clyde
19.7
22.4
22.7
26.8
Present-day temperature of the deepest sample (189 deg. C)
B
δ18O(Water) ‰ V-SMOW
-10 -9 -8 -7 -6 -5 -4 -3 -2 -1 0 1 2 3 4 5 6 7 8 9 10 11 12 13 14 15 16
Temperature (°C)
0 20 40 60 80 100 120 140 160 180 200
METEORIC
MARINE
δ18O(detrital quartz) ‰ V-SMOW
Rotherwood
Lake Creek
18.31
23.77
18.59
24.69
Measured water
Present-day temperature of the deepest sample (185 deg. C)

Figure 5.13. Plot showing $\delta^{18}O_{(water)}$ in equilibrium with $\delta^{18}O_{(quartz\ cement)}$ as a function of temperature(Matsuhisa et al., 1979). (A) Red and Black $\delta^{18}O_{(quartz\ cement)}$ VSMOW contours represent the $\delta^{18}O$ range from early to late quartz cement in Clyde and Elgin. $\delta^{18}O_{(water)}$ likely evolved from Jurassic marine water to present-day formation water (~ 4.5 ‰) in the Fulmar reservoirs in Clyde and Elgin fields. (B) Red and Black $\delta^{18}O_{(quartz\ cement)}$ VSMOW contours represent $\delta^{18}O$ range from early to late quartz cement in Lake Creek and Rotherwood fields. $\delta^{18}O_{(water)}$ likely evolved from Tertiary marine water to present-day formation water (+3.5 to + 5.8 ‰) in Lake Creek and in Rotherwood. These $\delta^{18}O_{(water)}$ are based on measured data from Wilcox Group sandstones from adjacent fields in the onshore Gulf Coast region (Land and Fisher, 1987). Evolution paths in graphs A and B are depicted by red (Clyde and Lake Creek) and black (Elgin and Rotherwood) arrows

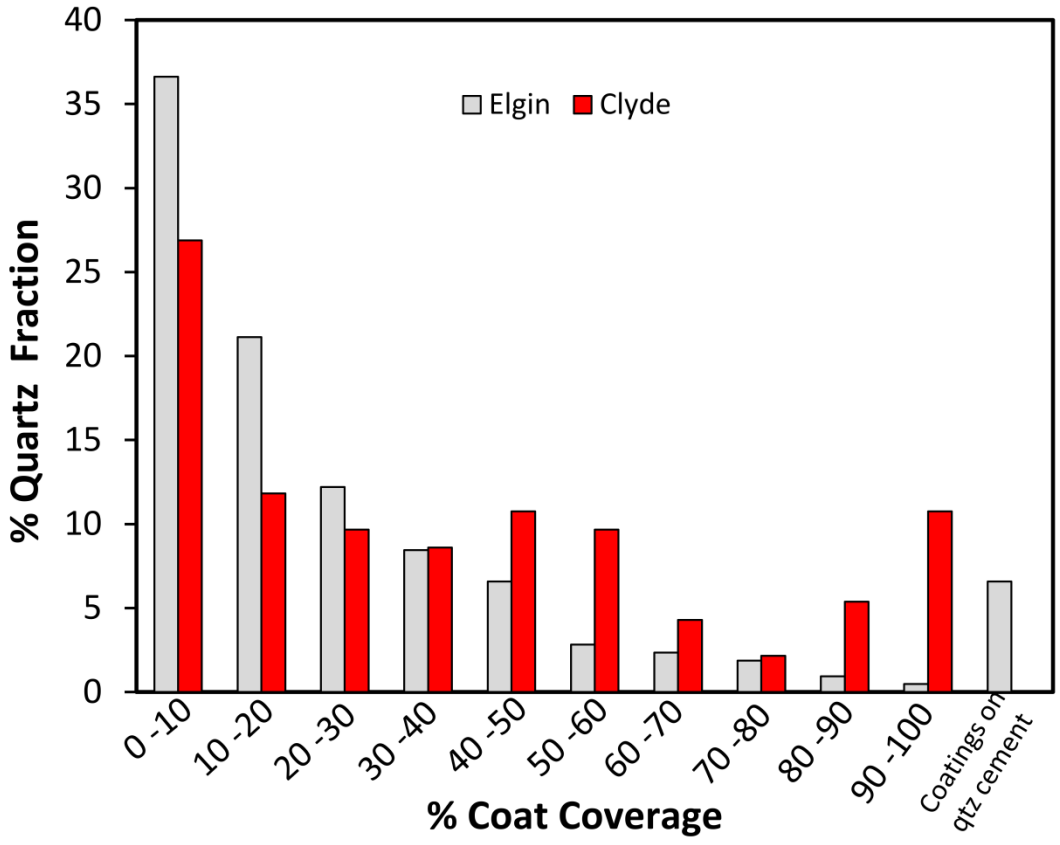

Figure 5.14. Graph showing percentage of detrital quartz fraction in the analysed Upper Jurassic Fulmar Formation sandstones from Clyde and Elgin fields, and their corresponding percentage grain coat coverage. The graph suggests that the average grain coat coverage in both Clyde and Elgin field is less than 40%. The analysed grain coatings in Clyde include clays and microquartz.

5.7. Conclusions

Fulmar Formation Sandstones from Clyde and Elgin fields and the Wilcox sandstone from Rotherwood field generally have low volume of macroquartz cement compared to that predicted by commonly-used models based on temperature-controlled precipitation kinetics. Fulmar Formation sandstones from Clyde field at 147°C have 20% more macroquartz cement, post-normalization with detrital quartz, than their counterpart from low VES Elgin field at 189°C, despite the presence of grain-coating microquartz in Clyde reservoir. A similar observation was made in the Wilcox sandstones where Lake Creek sample at 143°C has ~ 40 % more macroquartz cement than Rotherwood field sample at 185°C. This quartz cementation phenomenon cannot be explained by grain-coating microquartz or clays, or by hydrocarbon charge. Most or all the silica for quartz cement in these sandstones can be sourced locally from intergranular pressure dissolution, with additional silica from feldspar dissolution. The extent of intergranular pressure dissolution and related quartz cementation is strongly correlated with VES, and poorly correlated with temperature. Inferred time-temperature histories for quartz cementation demonstrate that the rate of quartz cementation is more strongly related to the history of VES than the history of temperature. I suggest that it is the vertical effective stress history, rather than the temperature history, that exerts the greatest influence on quartz cementation. An important next step is to quantify the rate of IPD as a function of VES and temperature. In our Clyde case study, VES has increased from 19 to 40 MPa in the last 0.5 million years but sandstones have quartz cement volumes which are qualitatively consistent with the lower VES value. This suggests that the kinetics of IPD are slow on a sub-million-year timescale.

6. Temperature and Vertical Effective Stress Regime Variation in Sandstones: Consequences for Quartz Cementation

6.1. Introduction

The understanding of the main processes that control quartz cementation in reservoir sandstones is very important for reservoir quality prediction. The existing paradigm is that the precipitation of quartz cement increases exponentially with temperature once precipitation kinetic barriers are exceeded around 70-80°C (Walderhaug, 1996; Lander and Walderhaug, 1999; Walderhaug, 2000). However, some high temperature sandstone reservoirs have been observed to have very low volume of quartz cements and excellent reservoir quality due to low VES (e.g. Osborne and Swarbrick, 1999; Stricker et al., 2016b).

Based on the concept introduced by Terzaghi (1925), VES and related intergranular pressure dissolution is reduced when high pore fluid pressure develops in a sandstone system. Whilst few studies (e.g. Osborne and Swarbrick, 1999; Sheldon and Wheeler, 2003) have tried to appraise the role of VES on quartz cementation in sandstone reservoirs, others (e.g. Walderhaug, 1996; Lander and Walderhaug, 1999; Walderhaug, 2000; Taylor et al., 2015) have advocated that the effect of VES is minimal or negligible. This study was carried out to determine the relative importance of VES and temperature as controls on quartz cementation in sandstones by investigating Upper Jurassic Fulmar Formation sandstones from the Central North Sea, UK and Paleocene-Eocene Wilcox Group sandstones from the Gulf Coast, USA. These sandstones were selected from geological environments with varying temperature and VES regimes. The multidisciplinary approach adopted for the study combines petrography, SEM, basin modelling, high precision SIMS analysis, and kinetic modelling of quartz cementation. The aim of this chapter is to compare the results in this study to those of (Taylor et al., 2015), and to synthesise the key findings to evaluate the effect of temperature and the role played by VES on quartz cementation in sandstone reservoirs.

6.2. Comparison of the results from the analysis of the Fulmar Formation sandstones in this study with those of Taylor et al. (2015)

This study examined the Fulmar Formation sandstones from three fields (Clyde, Elgin and Fulmar) in the UK Central North Sea (CNS). The Fulmar Formation sandstones examined by Taylor et al. (2015) were also from the CNS, except that samples were chosen from the Martha, Juno and Shearwater Fields. The comparison of results from this study with those of Taylor et al. (2015) is deemed necessary because the Fulmar Formation is fairly homogenous in character across several locations within the CNS. Indeed, this study and Taylor et al. (2015) made similar observation about the Fulmar Formation. However, the similarities and differences in the interpretation of results will be highlighted and discussed in this section.

6.2.1. Feldspar Dissolution

Taylor et al. (2015) observed abundant partially or completely dissolved feldspars with initial shape preserved as mouldic pore (6.1% for Juno, 6.6% for Martha, and 5.5% for Shearwater) within the Fulmar Formation. Similar observation was made in this study, especially in the samples from Elgin Field. Petrographic data from modal analysis of thin sections reveals intragranular porosity from feldspar dissolution makes up about 3.3 % of bulk rock volume in the analysed samples. It was noted that the volume of porosity from feldspar dissolution does not translate into net porosity gain as part of the porosities are offset by products of the reaction: such as newly formed illite which may be deposited in adjacent intergranular pores (Giles, 1987; Taylor et al., 2015), and silica (Osborne and Swarbrick, 1999; Worden and Morad, 2000) which may precipitate as macroquartz cements on detrital host grain.

6.2.2. Grain-coating Microquartz

This study also observed that grain-coating microquartz occurs in variable abundance in the Fulmar samples from the Clyde and Fulmar Fields but was effectively absent in the samples from Elgin Field. Taylor et al. (2015) reported the occurrence of grain-coating microquartz in variable abundance in the Fulmar Formation from Martha, Juno, and Shearwater, and that samples from Shearwater have sparse and incomplete microquartz coatings. This non-uniformity in the distribution of microquartz in the Fulmar Formation was also reported byOsborne and Swarbrick (1999). Even though samples with the most grain-coating microquartz have the least quartz cement contents, other samples with little or no microquartz also had very low volume of quartz cement compared to the volume predicted by a quartz cementation model (Figure 5.12 and

Table 5.5). This result shows that grain-coating microquartz cements cannot be the main reason for the low volume of macroquartz cement in the Fulmar Formation.

6.2.3. Grain-coating Clay

Taylor et al. (2015) reported that detrital and authigenic clay coats contributed significantly to inhibition of quartz cementation, and that authigenic illitic clay coats on quartz grains are most common directly adjacent to dissolved feldspar grains. Since feldspar dissolution in the Upper Jurassic Fulmar Formation occurred during middle - late diagenesis (Haszeldine et al., 1999; Lasocki et al., 1999; Wilkinson and Haszeldine, 2011), it means dissolution-sourced authigenic illite first developed around same period. Because macroquartz cementation threshold is around 80 °C (e.g. Walderhaug, 1994a), some macroquartz cement would have precipitated on free detrital quartz surfaces in the Fulmar Formation prior to authigenic illite formation. Petrographic analysis (Figure 4.6A and F) confirms this assertion, as authigenic illite seen coating the surfaces of some macroquartz overgrowths suggests quartz cementation predates authigenic illite formation.

Taylor et al. (2015) reported that clay coatings, presumably of detrital origin, completely coat many framework grains within bioturbated intervals, but did not provide any quantitative data to support this claim. Taylor et al. (2015) showed that quartz overgrowths are almost always present on detrital quartz that lacks continuous grain coatings. Similar observation was made in this study, where macroquartz cement was often found on host detrital quartz that has poorly-developed grain-coats in the samples from Elgin Field (Figure 4.5C and D, Figure 4.6). Quantitative data showed that the clay-coatings (illite) commonly coats around 30% of quartz surfaces (Figure 4.8). Quartz cements also engulf some of the grain-coating illite (Figure 4.6A). The implication is that discontinuous coats are not a very effective brake on quartz cementation.

6.2.4. Vertical Effective Stress

Whilst few dispute the role of intergranular pressure dissolution as a source of silica and thus of macroquartz cement in sandstones, the strong, current consensus is that the rate of macroquartz cementation in sandstones is a primary function of temperature-controlled quartz precipitation kinetics (Walderhaug, 1994b; Bjorkum, 1996; Taylor et al., 2015). Osborne and Swarbrick (1999) contrarily indicated that the rates of

intergranular pressure dissolution were influenced by vertical effective stress, and the data in this study support that assertion.

The volume of macroquartz overgrowth cement reported by Taylor et al. (2015) for the Fulmar Formation (3.9 % for Martha, 4.6 % for Juno and 5.1 % for Shearwater) are similar to those reported in this study (4.4% for Clyde, 4.6% for Elgin and 3.7% for Fulmar). Taylor et al. (2015) cited the lack of correlation between macroquartz cement volume and intergranular pressure dissolution was as evidence for non-suppression of macroquartz cementation by high fluid pressure/low vertical effective stress, without providing any quantitative data. This study used quantitative petrographic data (Table 3.1, Table 5.5 and Table 6.1) to show that intergranular pressure dissolution and the abundant dissolved feldspars observed in the Fulmar Formation can supply most, or all the silica required for their macroquartz cement contents.

6.3. Effect of Temperature on Quartz Cementation

The studied Upper Jurassic Fulmar Formation sandstones from the Central North Sea generally have low volumes of quartz cement for their present-day temperatures. The amounts of quartz cement make up less than 30% of the expected quartz cement volume predicted for these sandstones by quartz kinetic modelling (Figure 5.12 and Table 5.7). Despite the high thermal stress experienced by sandstones from Elgin Field (Figure 6.1), their quartz cement volume is comparable to that of Fulmar Field and lower than that of Clyde Field, all in the same basin. The inter-basinal comparison of the Fulmar Formation and Wilcox Group sandstones from equivalent temperature regimes shows that the Wilcox Group sandstones contains > 40% more volume of quartz cement, in spite of the fact that the Fulmar Formation sandstones are 100 Myrs older (Figure 6.1).

Quartz cementatiin as a product of three interlinked processes of supply-transport-precipitation and is reported to be controlled mainly by the rate of precipitation which is in turn dependent on temperature (Walderhaug, 1994a; Walderhaug, 1994b; Walderhaug, 1996; Lander and Walderhaug, 1999). Current computer-based models of quartz cementation are predicated mainly on temperature-controlled rate of quartz precipitation (e.g.Lander and Walderhaug, 1999; Walderhaug, 2000). Based on these models, the rate of quartz precipitation is expected to increase exponentially with temperature once the precipitation kinetic barriers are overcome around 70 - 80°C (Walderhaug, 1994a; Walderhaug, 1994b; Walderhaug, 1996). According to this model, sandstone reservoirs that have experienced greater thermal stresses should have more volumes of quartz cement than others.

This research has revealed that the rate of quartz cementation is not mainly controlled by temperature-controlled rate of quartz precipitation. Also, the quartz cementation phenomenon in the analysed sandstones is not strictly related to unavailability of precipitation sites. Grain-coating clays and microquartz are known to inhibit quartz cementation by making precipitation sites unavailable (Heald and Larese, 1974; Aase et al., 1996; Bloch et al., 2002; Storvoll et al., 2002; Berger et al., 2009; Stricker et al., 2016b). Quartz cementation may also be hindered by the activity of highly soluble biogenic silica which is a precursor to the formation of grain-coating microquartz (Aase et al., 1996). Notably, the poor development of grain-coating clays observed in the Fulmar Formation sandstones limits their potential effect on quartz cementation. Also, intervals that lack grain-coating microquartz in Clyde and Fulmar field sandstones still

did have low volume of quartz cement. Grain-coating clay and microquartz are absent in the studied Wilcox Group sandstones.

In summary, the observations in this study defy the concept suggested in common sandstone reservoir quality studies (e.g. Walderhaug, 1994a; Walderhaug, 1994b; Walderhaug, 1996; Lander and Walderhaug, 1999; Walderhaug, 2000) that temperature-controlled rate of quartz precipitation is the main control on quartz cementation. The research shows that the dearth of quartz cements in the analysed sandstones is due mainly to inadequate silica supply. For example, the studied Fulmar Formation sandstones have experienced enough historical thermal stress to precipitate large volume of quartz cement. Because the supply of silica is the first stage in the process of quartz cementation, any changes affecting the rate of supply would undoubtedly be carried through to the precipitation stage. Although temperature may be the kinetic driver for quartz precipitation, silica must first be supplied before quartz can precipitate.

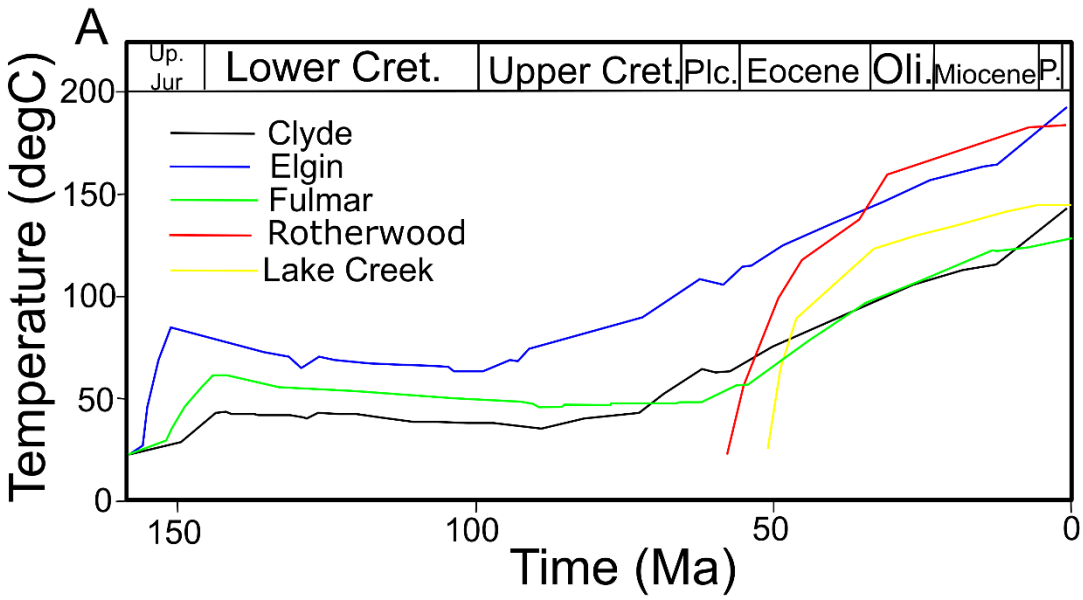

Figure 6.1. Modelled 1D temperature histories for Fulmar Formation (Clyde, Elgin, and Fulmar fields), and Wilcox Group sandstones (Rotherwood and Lake Creek fields). The Upper Jurassic Fulmar Formation sandstones are 100Ma older than the Paleocene-Eocene Wilcox Group sandstones.

6.4. The Role of Vertical Effective Stress on Quartz Cementation

This research revealed that VES, and related intergranular pressure dissolution, is an important control on quartz cementation in sandstones. Intergranular pressure dissolution is commonly regarded as a ubiquitous source of silica for quartz cementation in sandstones (Sibley and Blatt, 1976a; McBride, 1989; Evans et al., 1994; Worden and Morad, 2000). The bulk of silica for quartz cementation (around 60 %) in the studied Fulmar Formation sandstones was supplied locally by intergranular pressure dissolution. Similar observation made for the Wilcox Group sandstones revealed that > 90% of silica was supplied by intergranular pressure dissolution.

VES drives intergranular pressure dissolution that, in turn, supplies silica locally for quartz cementation in sandstones (De Boer et al., 1977; Tada and Siever, 1989; Dewers and Ortoleva, 1990; Elias and Hajash, 1992; Shimizu, 1995; Renard et al., 1997; Sheldon et al., 2003; Gratier et al., 2005; van Noort et al., 2008). This study recognized that the development of low VES in sandstone systems due to high pore fluid pressure. This process retards intergranular pressure dissolution and related silica supply. Previous studies (Osborne and Swarbrick, 1999; Stricker et al., 2016b) have observed similar phenomenon in some Upper Jurassic sandstones from the Central North Sea.

It was also established from this study that the history of VES rather than present-day VES that is the main control on the rate of intergranular pressure dissolution, and thus the rate of silica supply. This is strengthened by the fact that intergranular pressure dissolution and related quartz cementation correlated strongly with VES and very poorly with temperature in the studied sandstones (Table 6.1). The elevated quartz cement contents observed in the Wilcox Group sandstones from Rotherwood (0.22) and Lake Creek (0.35) fields have been identified as products of prolonged high VES experienced throughout history by these sandstones (Figure 6.2). Similarly, the protractedly low historical VES (Figure 6.2) experienced by the Fulmar Formation sandstones from the HPHT Elgin field has been recognized as the reason for their very low quartz cement volumes (0.12). Fulmar sandstones from Clyde and Fulmar fields also have quartz cement volumes (0.15 and 0.11) which are qualitatively consistent with lower VES values. Regional pore pressure data show that VES increased from 19 to 40 MPa in Clyde and 10 to 31 MPa in Fulmar in the last *ca*. 0.5 million years (Figure 6.3), when pore fluid pressures within the Fulmar Formation decreased substantially as a result of lateral drainage (Swarbrick et al., 2005). This interpretation suggests that the

kinetics of IPD are such that great timescales are required for the results of IPD to be observed as quartz cement.

In summary, VES controls the rate of silica supply from intergranular pressure dissolution and, by extension, the volume of silica available for the precipitation of quartz cement. Hence, the source of silica is the most important control on quartz cementation in sandstone.

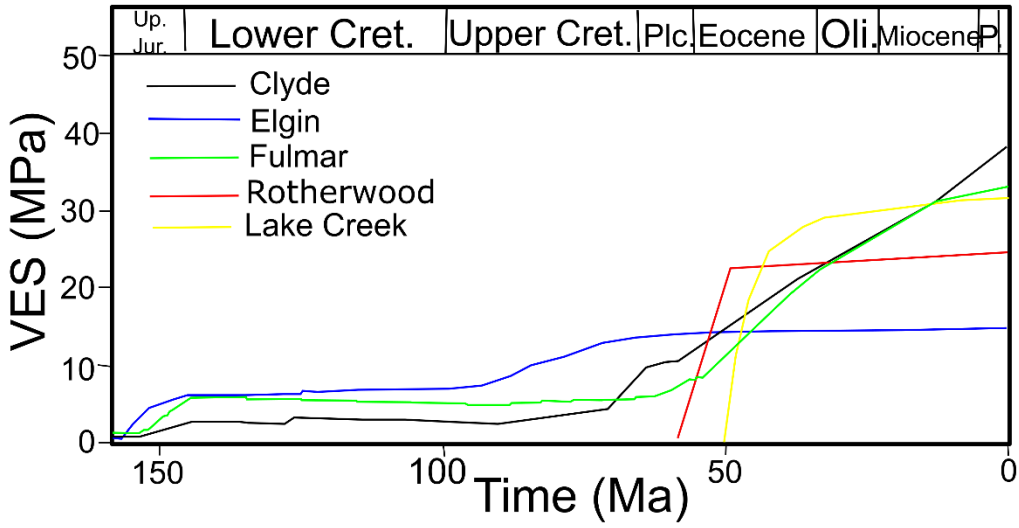

Figure 6.2. Modelled 1D VES histories for Fulmar Formation (Clyde, Elgin, and Fulmar fields), and Wilcox Group sandstones (Rotherwood and Lake Creek fields).

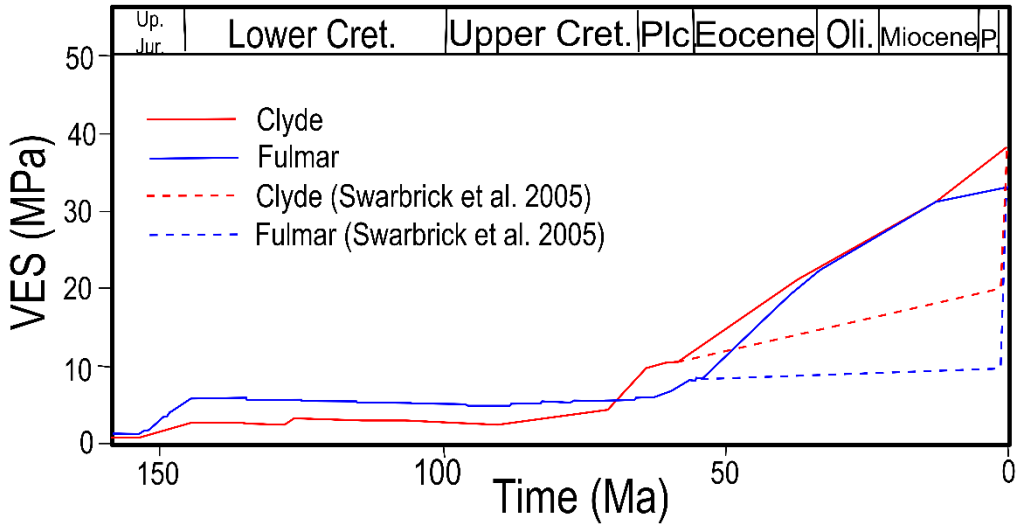

Figure 6.3. Vertical effective stress (VES) histories of the Fulmar Formation from Clyde and Fulmar fields. Red and Blue dashed lines represent the most likely VES evolution pathway based on Swarbrick et al. (2005)

Table 6.1. Table showing normalized quartz cement contents for the Fulmar Formation and Wilcox Group sandstones. VES is vertical effective stress; $\delta^{18}O_{(qc)}$ is the oxygen isotope composition of quartz cement. VES in Clyde and Fulmar is the proposed VES 0.5 Ma ago, prior to depressurising via lateral fluid flow (Swarbrick et al., 2005). Present –day VES in Clyde and Fulmar are 40 and 31 MPa. Temp. Range is the temperature range over which quartz cement is suggested to form, based on oxygen isotope composition.

Field	Quartz Cement/ Detrital Quartz	IPD/Detrital Quartz	Temp. (°C)	VES (MPa)	δ18O(qc) range	Temp. Range (°C)
Fulmar	0.11	0.04	127	10.1	3.7	50-110
Elgin	0.12	0.07	189	12.5	2.7	80-150
Clyde	0.15	0.09	147	19.2	4.1	55-125
Rotherwood	0.22	0.21	185	23.2	5.5	75-160
Lake Creek	0.35	0.37	143	33.7	6.1	65-145

6.5. Implications for Deep Hydrocarbon Exploration and Production

The pre-drill prediction of economic reservoir quality (porosity and permeability) in reservoir sandstones is pivotal for the success of hydrocarbon exploration and production. Since the search for hydrocarbon is increasingly being focused on deeper targets that are usually characterised by extreme temperature and VES conditions, reservoir quality risk assessments of such reservoir sandstones is important for supporting commercial development and maximizing the return on investment (Taylor et al., 2010; Worden et al., 2018a).

Porosity and permeability are the most important properties of sandstone reservoirs. While porosity determines the volume of hydrocarbon that can be preserved, permeability directly impacts the rate of hydrocarbon recovery from the reservoir (Worden and Morad, 2000; Worden et al., 2018a). Because quartz cement is the most common porosity (and permeability) degrading cement in sandstone reservoirs, predicting its occurrence and distribution would aid prospect evaluation, reservoir management and rate of production (Worden and Morad, 2000).

Elevated temperatures are known to be favourable for quartz cement precipitation, and predictive models have been developed that is premised on temperature-driven precipitation kinetics. This study shows that the development of prolonged low VES conditions during the burial history of deeply buried sandstone reservoirs can halt or significantly reduce quartz cementation regardless of the prevalent temperature regime. Hence, VES histories should be incorporated in quartz cementation models for more accurate prediction. Low VES conditions develop in sandstone reservoirs due to the introduction of high pore fluid pressure. The early development of these conditions is helpful for reservoir quality preservation in deeply buried sandstones, and such reservoirs would provide excellent potential as deep hydrocarbon targets.

6.6. Conclusions

The studied Fulmar Formation sandstones from Clyde, Elgin, and Fulmar fields and the Wilcox Group sandstone from Rotherwood field generally have low volume of macroquartz cement compared to that predicted by commonly-used models based on temperature-controlled precipitation kinetics.

Fulmar Formation sandstones from Clyde field at 147°C has 20% more macroquartz cement post-normalization with detrital quartz than their counterpart from low VES Elgin field at 189°C, despite the presence of grain-coating microquartz in Clyde reservoir. Similar observations were made in the Wilcox sandstones where Lake Creek sample at 143°C has ~ 40 % more macroquartz cement than Rotherwood field sample at 185°C.

Also, inter-basinal comparison of the tudied CNS Fulmar Formation sandstones and the GOM Wilcox Group sandstones at equivalent temperatures revealed that the GOM samples have at least 40% more quartz cement. This quartz cementation phenomenon cannot be significantly explained by grain-coating microquartz or clays, or by hydrocarbon charge.

Most of the silica for quartz cementation in the studied Fulmar Formation sandstones is supplied by intergranular pressure dissolution at quartz-quartz grain boundaries, and this is also the case for the Wilcox Group sandstones. Intergranular pressure dissolution and related quartz cementation also showed strong correlation with VES and poor correlation with temperature. I, therefore, conclude that the rate of intergranular pressure dissolution, which is due to the magnitude of VES experienced through time, is the main control on the rate of quartz cementation in these sandstones, and not temperature-controlled precipitation kinetics.

The conclusion is supported by the positive correlation of total range of $\delta^{18}O$ from *in situ* oxygen isotope analyses with VES and volume of quartz cement in the studied sandstones. Quartz cementation models should therefore incorporate VES histories for more accurate reservoir quality prediction. Since the development of low VES/ high pore fluid pressure would suppress chemical compaction and quartz cementation, HPHT sandstones which have been subjected to low VES throughout burial history provide good potential as deep hydrocarbon targets

6.7. Future Work

6.7.1. Quantification of the rate of IPD as a function of VES and temperature

This study has shown that VES is an important control on quartz cementation in sandstones. a critical predictive next step would be to quantify the rate of IPD as a function of VES and temperature. van Noort et al. (2008) have presented such a model, based on higher temperature laboratory experiments, but it has never been tested against data in sandstones in sedimentary basins.

6.7.2. Accurate reconstruction of VES histories using 2D/3D models

The use of one-dimensional (1D) model for reconstruction of VES histories appears to be partly problematic for the Clyde and Fulmar study locations. VES is a function of the degree of pore fluid pressure experienced by a system. Apart from disequilibrium compaction, other high pore fluid pressure controlling mechanism in sandstone reservoirs (e.g. Osborne and Swarbrick, 1997b) cannot be incorporated in 1D models. For example, the accurate reconstruction of VES histories for the depressurised Fulmar Formation reservoirs in the Fulmar-Clyde area would require a 2D or 3D model to account for the effect of lateral flow (Swarbrick et al., 2005).

6.7.3. Investigation of the role of effective stress on quartz cementation in other HPHT settings

This study and many others (e.g. Stricker et al., 2016a; Stricker et al., 2016b) have investigated sandstones in settings where effective stress is acting vertically. However, other HPHT settings where compressive forces led to the development of horizontally-acting effective stress have been identified (e.g. Borneo Basin). The study of the role of effective stress on the rate of quartz cementation in geological domain where lateral effective stress is dominant would further broaden our understanding and also aid the development of better reservoir quality predictive tools.

6.7.4. Integration of fluid inclusion micro-thermometry and SIMS analysis

While fluid inclusion micro-thermometry is a commonly used technique for investigation of quartz overgrowth in sandstones, the use of high precision, high accuracy, high spatial resolution secondary ion mass spectrometry (SIMS) analysis is still relatively new. Although fluid inclusions can determine unique temperatures, they are problematic because they are usually restricted to regions close to the boundary between detrital quartz grains and overgrowths. On the other hand; SIMS can generate $\delta^{18}O$ profiles (temperature proxies) across quartz overgrowths but cannot generate unique temperatures of quartz precipitation. These limitations can be overcome if high

spatial SIMS analysis is integrated with fluid inclusion micro-thermometry for petrographic studies. Such combination would help constrain precipitation temperatures more accurately and aid better evaluation of quartz cementation histories in sandstones.

Appendix 1

Raw Petrographic Data

Fulmar Field (30/16-7) data from Optical Microscopy

TVDss (m)	Depth (m)	Depth (ft)	Quartz (%)	Poly Quartz (%)	K-Feldspar (%)	K-Feldspar overgrowth (%)	Dissolved K-Feld (%)	plagioclase (%)	Intergranular Porosity (%)	Intragranular Porosity (%)	Quartz Cement (%)	Carbonate cement (%)	Matrix (%)	Lithic Fragment (%)	Mica (%)	Coating (%)	Bitumen (%)	Glauconite (%)	Kaolinite (%)	Pyrite (%)	Replacive Minerals (%)
3245.3	3269.1	10725.3	36.3	0.3	32.0	2.0	0.0	1.3	19.3	0.0	2.7	0.3	0.3	0.7	0.7	3.7	0.0	0.0	0.0	0.3	0.0
3246.4	3270.1	10728.8	39.0	0.3	31.7	1.3	0.0	0.3	17.3	0.0	1.3	1.3	1.3	1.0	0.0	4.7	0.0	0.0	0.0	0.0	0.3
3247.0	3270.8	10730.9	39.0	0.0	31.3	0.7	0.0	0.7	20.3	0.0	3.3	0.0	1.3	1.3	0.0	2.0	0.0	0.0	0.0	0.0	0.0
3247.6	3271.4	10733.0	42.7	0.3	30.7	0.7	0.0	0.3	16.3	0.3	5.3	0.0	1.0	1.0	0.0	1.3	0.0	0.0	0.0	0.0	0.0
3248.7	3272.5	10736.5	40.3	0.0	29.3	3.7	0.0	0.7	15.0	0.0	6.3	0.3	0.7	2.0	0.3	1.0	0.0	0.0	0.0	0.3	0.0
3249.2	3273.0	10738.1	42.3	0.0	27.3	2.7	0.0	0.0	15.0	0.0	5.7	0.0	0.7	1.7	0.0	3.7	0.0	0.0	0.0	1.0	0.0
3249.7	3273.5	10739.8	35.3	0.7	33.0	1.0	0.0	0.3	15.7	0.3	4.3	0.3	2.0	0.0	0.0	6.7	0.0	0.0	0.0	0.3	0.0
3260.7	3284.5	10775.9	40.7	0.0	35.0	2.7	0.0	0.0	14.7	0.0	3.7	1.0	0.3	0.7	0.0	1.0	0.0	0.0	0.0	0.3	0.0
3261.4	3285.1	10778.0	43.7	0.0	31.3	2.0	0.0	0.0	16.0	0.3	3.3	1.0	0.3	0.7	0.0	1.3	0.0	0.0	0.0	0.0	0.0
3262.0	3285.7	10780.0	41.0	0.7	27.3	2.3	0.0	0.7	18.0	0.0	3.3	0.3	1.7	2.7	0.0	1.0	0.0	0.0	0.0	1.0	0.0
3262.6	3286.4	10782.0	39.3	0.7	29.7	1.3	0.0	0.3	20.0	0.3	2.3	1.0	1.3	1.0	0.0	2.3	0.0	0.0	0.0	0.3	0.0
3264.1	3287.9	10787.0	43.3	0.0	24.3	0.3	0.0	1.3	21.7	0.3	1.7	1.3	1.3	0.7	0.0	3.3	0.0	0.0	0.0	0.3	0.0
3264.4	3288.2	10788.1	46.7	0.0	29.0	2.3	0.0	0.7	16.3	0.0	2.3	0.0	0.7	1.0	0.3	0.7	0.0	0.0	0.0	0.0	0.0
3268.8	3292.6	10802.5	34.3	0.3	36.7	3.3	0.0	0.0	20.0	0.0	2.3	0.3	1.3	1.3	0.0	0.0	0.0	0.0	0.0	0.3	0.3
3270.1	3293.9	10806.6	36.7	0.3	31.3	4.0	0.0	0.0	13.3	0.0	4.3	1.7	4.3	2.3	0.3	0.7	0.0	0.0	0.0	0.0	0.0
3270.7	3294.5	10808.7	39.7	0.0	33.0	3.0	0.0	0.3	18.3	0.0	2.3	0.0	1.3	0.7	0.3	1.0	0.0	0.0	0.0	0.3	0.0
3271.2	3294.9	10810.1	42.7	0.0	27.7	3.7	0.0	0.0	20.3	0.0	1.3	1.3	1.7	0.3	0.0	0.3	0.0	0.3	0.0	0.0	0.0
3272.4	3296.2	10814.3	44.7	1.0	24.7	4.0	0.0	0.7	19.7	0.0	1.0	0.7	1.7	1.0	0.7	0.0	0.0	0.3	0.0	0.0	0.0
3273.1	3296.8	10816.4	43.3	0.3	23.3	5.7	0.0	0.3	22.0	0.0	0.7	0.7	1.3	1.7	0.0	0.7	0.0	0.0	0.0	0.3	0.0
3274.8	3298.5	10822.0	36.7	0.0	25.7	3.0	0.0	0.3	26.7	0.0	0.0	1.7	2.0	1.0	0.3	2.3	0.0	0.0	0.0	0.0	0.3
3275.7	3299.5	10825.1	36.0	0.7	25.7	3.0	0.0	0.0	23.7	0.0	0.7	1.7	2.7	1.3	1.3	2.3	0.0	0.7	0.0	0.3	0.3
3276.2	3300.0	10826.7	41.0	0.0	30.0	3.0	0.0	0.7	0.0	17.3	0.0	0.0	0.0	0.3	1.7	1.3	1.3	0.7	2.0	0.0	0.0

Clyde Field (30/17B-2) data from Optical Microscopy

TVDSS (m)	Depth (m)	Depth	Quartz	Poly Quartz	K-Feldspar	K-Feldspar overgrowth	plagioclase	Intergranular Porosity (%)	Intragranular Porosity (%)	Quartz Cement	Carbonate cement	Matrix	Lithic Fragment	Mica	Coatings (%)	Glauconite	Pyrite	Replacive Mineral
3770.751	3795.751	12453.25	31.0	0.0	24.7	1.3	0.7	10.7	1.3	5.3	11.0	5.0	0.7	0.0	5.3	0.0	3.0	0.0
3772.174	3797.174	12457.92	40.3	0.3	19.3	2.3	0.3	8.0	3.0	2.3	15.0	2.7	1.0	0.0	4.3	0.0	1.0	0.0
3773.037	3798.037	12460.75	39.7	1.0	24.3	1.7	0.0	16.7	1.0	5.0	6.7	2.3	1.0	0.3	0.3	0.0	0.0	0.0
3773.671	3798.671	12462.83	40.3	0.3	22.0	3.3	0.0	17.0	0.0	1.0	7.3	5.3	2.0	0.3	0.7	0.0	0.3	0.0
3774.536	3799.536	12465.67	35.0	0.0	27.0	3.0	0.0	14.7	1.3	3.3	5.3	4.3	1.3	1.3	2.0	0.3	1.0	0.0
3776.414	3801.414	12471.83	30.0	0.3	24.3	1.7	0.7	12.3	0.0	3.7	19.0	4.0	0.7	1.0	1.3	0.0	1.0	0.0
3777.432	3802.432	12475.17	35.3	0.0	24.0	2.7	0.3	7.3	0.0	2.3	21.0	3.0	2.3	0.0	0.7	0.0	0.7	0.3
3778.243	3803.243	12477.83	38.3	0.3	28.7	0.7	0.3	15.0	1.7	4.0	3.3	1.7	1.3	0.3	4.0	0.0	0.0	0.3
3778.956	3803.956	12480.17	34.0	0.3	31.3	2.0	0.3	16.7	3.0	0.7	6.7	1.3	0.0	0.3	1.7	0.0	0.3	0.3
3780.508	3805.508	12485.5	41.3	0.0	31.0	1.3	0.0	12.7	0.0	3.7	3.0	0.3	1.7	0.3	3.3	0.7	0.7	0.0
3781.114	3806.114	12487.25	41.0	0.0	27.7	0.3	0.0	14.3	1.7	7.0	1.3	1.7	0.7	0.0	3.0	0.7	0.7	0.0
3781.808	3806.808	12489.5	41.0	0.3	27.3	1.0	0.3	12.3	0.0	5.0	6.0	1.0	1.0	0.3	3.7	0.0	0.7	0.0
3782.918	3807.918	12493.17	38.3	0.0	24.7	1.0	0.3	13.0	1.7	3.0	12.3	2.7	0.0	0.3	1.7	0.0	1.0	0.0
3783.604	3808.604	12495.42	32.0	0.0	29.7	1.3	0.3	16.3	0.0	5.7	9.0	1.0	1.0	0.0	3.0	0.0	0.7	0.0
3784.238	3809.238	12497.5	40.3	0.3	30.0	2.7	0.3	12.7	0.0	4.3	5.3	1.3	0.7	0.0	2.0	0.0	0.0	0.0
3785.052	3810.052	12500.17	39.7	0.0	28.3	3.7	0.7	12.3	0.0	3.3	7.3	1.7	0.3	0.7	2.0	0.0	0.0	0.0
3785.686	3810.686	12502.25	37.7	0.0	32.3	1.3	0.3	11.7	2.0	2.3	7.3	0.7	0.0	0.7	1.0	0.3	1.0	0.0
3786.295	3811.295	12504.25	40.3	0.0	30.0	1.0	0.0	10.7	0.0	2.0	12.0	1.0	1.7	0.0	1.0	0.3	0.0	0.0
3787.49	3812.49	12508.17	44.3	0.0	26.3	0.3	0.0	10.3	0.0	4.0	5.3	2.0	1.7	0.3	4.7	0.3	0.0	0.3

Elgin Field (22/30C-G4) data from Optical Microscopy

TVDss (m)	Depth (m)	Depth (ft)	Quartz (%)	Poly Quartz (%)	K-Feldspar (%)	K-Feldspar Overgrowth (%)	Plagioclase (%)	Intergranular Porosity (%)	Intragranular Porosity (%)	Quartz Cement (%)	Carbonate Cement (%)	Matrix (%)	Lithic Fragment (%)	Mica (%)	Coatings (%)	Bitumen (%)	Pyrite (%)
5413.3	5602.4	18380.6	31.0	1.3	26.3	0.0	1.3	6.0	3.0	0.3	25.0	0.7	1.3	1.0	1.3	0.0	1.3
5414.3	5603.4	18383.9	33.7	0.0	18.7	0.0	0.0	1.7	2.7	0.7	40.0	0.7	1.0	0.0	0.7	0.0	0.3
5415.5	5604.6	18387.8	46.7	0.0	23.3	0.0	0.0	20.7	4.3	1.0	0.3	1.3	0.0	0.3	0.0	0.0	2.0
5416.0	5605.1	18389.4	47.3	0.7	21.0	0.0	0.0	12.3	8.0	3.7	0.0	3.0	1.0	0.0	2.0	0.0	1.0
5417.1	5606.2	18392.9	54.3	1.3	23.0	0.0	0.0	11.7	2.7	1.3	1.3	1.7	1.3	0.3	1.0	0.0	0.0
5418.4	5607.5	18397.3	42.3	0.3	17.3	0.0	0.0	10.7	1.7	2.0	21.0	1.3	0.7	0.7	1.0	0.0	1.0
5418.9	5608.0	18399.0	37.0	0.7	18.7	0.0	0.3	5.0	2.0	1.0	31.3	1.3	2.3	0.3	0.0	0.0	0.0
5420.5	5609.6	18404.2	50.3	0.3	19.7	0.0	0.0	5.0	1.0	1.7	15.3	3.0	0.7	0.0	2.0	0.0	1.0
5422.4	5611.5	18410.4	47.3	0.3	26.3	0.3	0.0	13.3	4.7	1.7	0.7	0.3	1.3	0.3	2.7	0.0	0.7
5424.8	5613.9	18418.3	46.3	1.0	29.0	0.0	0.7	7.7	3.3	1.3	1.3	3.7	1.3	0.7	1.3	0.0	2.3
5427.2	5616.3	18426.2	44.0	0.0	23.7	0.0	0.0	19.3	3.3	1.0	1.0	2.7	0.3	0.7	2.7	0.3	1.0
5428.6	5617.7	18430.8	50.7	0.7	20.0	0.3	0.0	13.7	4.7	3.3	0.3	1.3	1.7	0.0	2.0	0.0	1.3
5429.3	5618.4	18433.1	42.3	0.0	25.0	0.3	0.0	15.7	5.0	6.3	0.3	2.0	1.0	0.7	0.7	0.0	0.7
5430.3	5619.4	18436.2	42.0	0.3	27.3	0.0	0.0	10.3	2.3	3.0	1.3	9.3	1.7	0.3	1.3	0.0	0.7
5431.5	5620.6	18440.1	40.0	0.3	26.3	0.0	0.0	13.0	2.7	2.7	2.0	7.3	2.0	0.3	2.0	0.3	1.0
5432.2	5621.3	18442.6	43.3	0.0	25.7	0.0	0.3	11.7	2.7	2.7	2.0	5.0	2.0	1.3	2.7	0.3	0.3
5433.1	5622.2	18445.5	43.0	0.7	25.7	0.3	0.0	13.0	2.7	2.7	4.0	2.3	2.0	0.0	3.0	0.0	0.7
5434.6	5623.7	18450.5	42.0	0.7	22.0	0.0	0.0	8.3	2.7	1.3	19.7	0.7	1.3	0.3	0.7	0.0	0.3
5435.3	5624.4	18452.8	48.0	0.3	25.7	0.3	0.0	11.0	3.0	1.0	2.3	4.7	0.0	1.7	1.3	0.0	0.7

Fulmar Field (30/16-7) CL petrographic data

Depth (m)	TVDSS (m)	Quartz (%)	Quartz Cement (%)	Dissolved Quartz (%)	Quartz Cement/Detrital Quartz	Dissolved Quartz/Detrital Quartz
3269.06	3245.29	30.50	2.19	1.44	0.07	0.05
3272.49	3248.72	33.65	5.84	1.33	0.16	0.04
3272.97	3249.20	39.06	4.75	0.75	0.13	0.02
3284.50	3260.73	31.58	5.58	1.07	0.09	0.03
3285.13	3261.97	32.06	4.75	2.38	0.08	0.07
3288.21	3264.44	39.31	3.44	1.63	0.05	0.04
3293.85	3270.08	33.00	6.88	2.00	0.12	0.06
3294.92	3271.15	32.44	1.56	0.81	0.03	0.03
3296.20	3272.43	29.91	0.88	0.44	0.02	0.01
3299.98	3276.21	30.81	1.25	1.19	0.01	0.04

Clyde Field (30/17B-2) CL petrographic data

Depth (m)	TVDSS (m)	Quartz (%)	Quartz Cement (%)	Dissolved Quartz (%)	Quartz Cement/Detrital Quartz	Dissolved Quartz/Detrital Quartz
3798.04	3773.04	28.13	3.52	1.28	0.13	0.05
3799.54	3774.54	30.06	5.25	1.63	0.17	0.05
3803.24	3778.24	28.44	4.44	2.13	0.16	0.07
3803.96	3778.96	28.53	2.75	1.04	0.10	0.04
3805.58	3780.58	30.81	4.75	2.44	0.15	0.08
3806.11	3781.11	29.38	5.94	2.31	0.20	0.08
3806.80	3781.80	29.50	5.50	2.19	0.19	0.07
3809.24	3784.24	26.78	3.22	1.58	0.12	0.06
3810.05	3785.05	25.19	3.52	1.11	0.14	0.04
3812.49	3787.49	32.19	5.44	3.94	0.17	0.12

Elgin Field (22/30C-G4) CL petrographic data

Depth (m)	TVDSS (m)	Quartz (%)	Quartz Cement (%)	Dissolved Quartz (%)	Quartz Cement/Detrital Quartz	Dissolved Quartz/Detrital Quartz
5605.1	5416.03	45.50	2.13	1.81	0.05	0.04
5606.15	5417.08	40.75	5.50	3.81	0.13	0.09
5613.9	5424.83	35.44	4.25	1.50	0.12	0.04
5616.3	5427.23	41.14	6.37	2.87	0.15	0.07
5617.7	5428.63	41.56	6.31	1.38	0.15	0.03
5618.4	5429.33	36.63	4.75	3.44	0.13	0.09
5619.35	5430.28	37.02	4.99	2.97	0.13	0.08
5620.55	5431.48	33.94	4.38	3.19	0.13	0.09
5622.2	5433.13	31.31	4.25	2.63	0.14	0.08
5624.4	5435.33	34.57	3.58	3.31	0.10	0.10

Core porosity data for Fulmar Formation samples from Clyde, Elgin and Fulmar fields

Elgin TVDss (m)	Elgin Depth (m)	Elgin Core Porosity (%)	Clyde TVDss (m)	Clyde Depth (m)	Clyde Core Porosity (%)	Fulmar TVDSS (m)	Fulmar Depth (m)	Fulmar Core Porosity (%)
5412.9	5602.0	26.0	3770.7	3795.7	27.4	3245.7	3269.4	30.4
5413.2	5602.3	25.7	3771.9	3796.9	21.7	3246.5	3270.2	29.3
5413.4	5602.5	16.8	3772.8	3797.8	25.0	3247.3	3271.1	28.0
5413.9	5603.0	15.2	3773.1	3798.1	24.7	3248.4	3272.1	25.8
5414.2	5603.3	19.5	3773.4	3798.4	25.6	3249.0	3272.7	27.3
5414.4	5603.5	8.5	3773.7	3798.7	24.0	3249.9	3273.7	27.8
5415.2	5604.3	24.8	3774.6	3799.6	25.5	3256.1	3279.9	28.7
5415.4	5604.5	24.1	3775.9	3800.9	23.8	3257.8	3281.6	33.5
5415.6	5604.7	25.2	3776.2	3801.2	24.6	3258.6	3282.4	27.4
5415.8	5604.9	24.9	3777.1	3802.1	17.2	3261.5	3285.3	27.7
5415.8	5604.9	25.4	3777.4	3802.4	19.4	3262.3	3286.1	30.5
5416.2	5605.3	24.8	3778.0	3803.0	26.0	3262.9	3286.7	31.0
5416.4	5605.5	27.9	3778.3	3803.3	29.4	3263.6	3287.4	28.1
5416.9	5606.0	25.3	3778.9	3803.9	25.7	3264.5	3288.3	27.7
5417.2	5606.3	23.8	3779.2	3804.2	25.3	3268.4	3292.1	26.0
5417.4	5606.5	24.0	3780.4	3805.4	26.1	3270.5	3294.3	30.9
5418.4	5607.5	18.3	3780.7	3805.7	25.0	3271.5	3295.3	32.5
5418.9	5608.0	11.0	3781.0	3806.0	24.4	3273.7	3297.5	32.0
5420.4	5609.5	9.3	3781.3	3806.3	25.1	3274.0	3297.8	34.4
5420.7	5609.8	14.2	3781.6	3806.6	25.5	3274.9	3298.6	35.3
5422.5	5611.5	25.1	3782.0	3807.0	23.1	3277.4	3301.2	33.7
5423.6	5612.5	24.4	3782.9	3807.9	24.8	3278.3	3302.1	32.6
5423.8	5612.8	24.7	3783.2	3808.2	22.7	3279.9	3303.7	29.8
5427.2	5616.3	26.0	3783.5	3808.5	24.7	0.0	0.0	0.0
5428.4	5617.5	25.7	3783.8	3808.8	25.5	0.0	0.0	0.0
5428.7	5617.8	26.1	3784.1	3809.1	24.5	0.0	0.0	0.0
5429.2	5618.2	24.6	3784.4	3809.4	22.5	0.0	0.0	0.0
5430.4	5619.5	22.7	3785.0	3810.0	25.8	0.0	0.0	0.0
5431.4	5620.5	25.2	3785.3	3810.3	24.5	0.0	0.0	0.0
5432.4	5621.5	22.7	3785.6	3810.6	24.4	0.0	0.0	0.0
5433.2	5622.3	25.0	3785.9	3810.9	24.4	0.0	0.0	0.0
5434.7	5623.8	16.5	3786.2	3811.2	24.1	0.0	0.0	0.0
5435.4	5624.5	21.3	3786.5	3811.5	22.1	0.0	0.0	0.0
0.0	0.0	0.0	3787.4	3812.4	24.0	0.0	0.0	0.0

Appendix 2

Photomicrographs and EDX analysis

Clyde Field

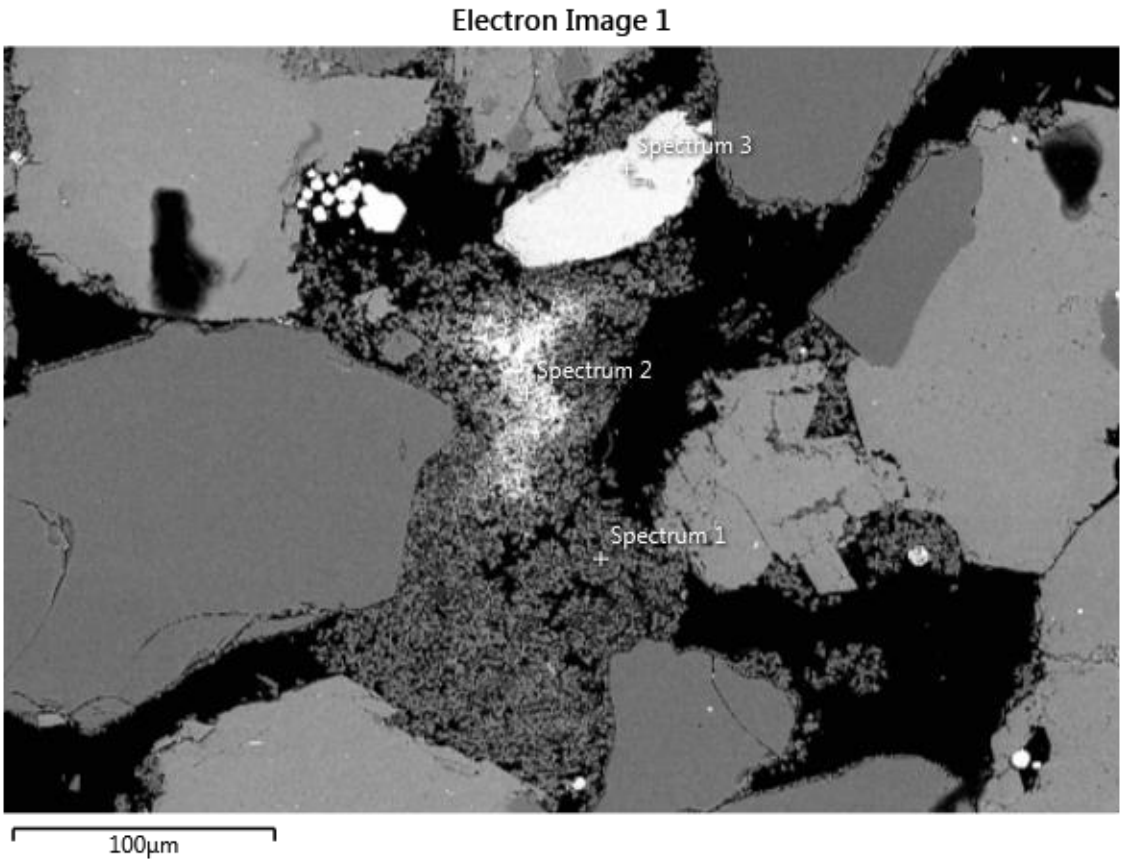
Electron Image 1
Spectrum 3
Spectrum 2
Spectrum 1
100µm

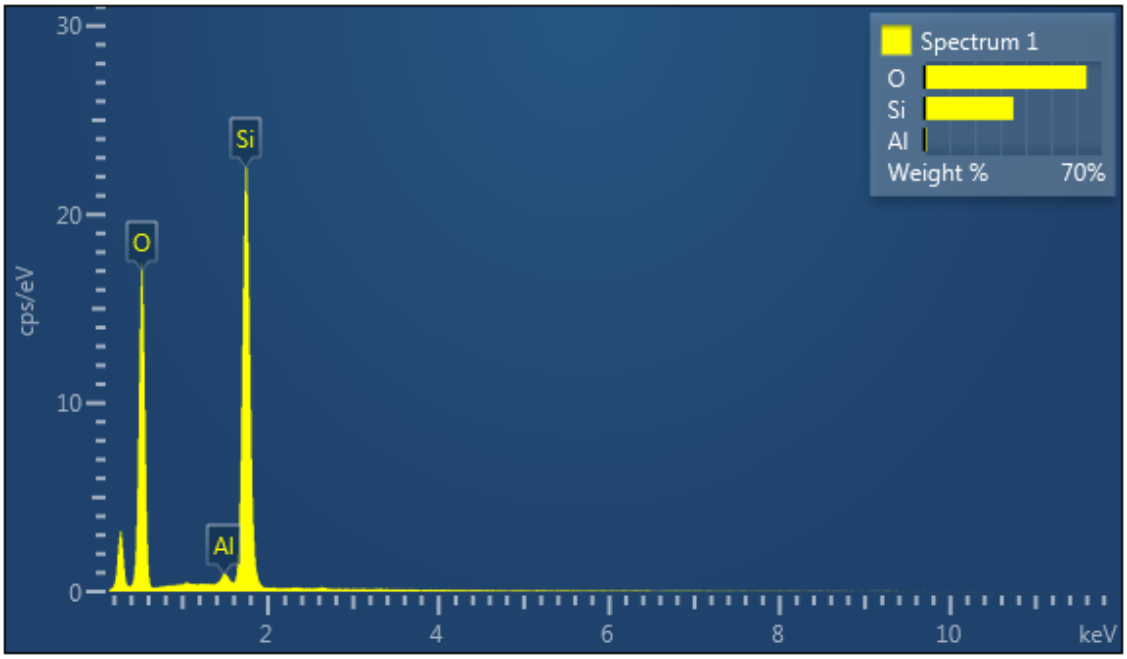
Spectrum 1
O
Si
Al
Weight %
70%
30
20
10
0
cps/eV
O
Si
Al
2
4
6
8
10
keV

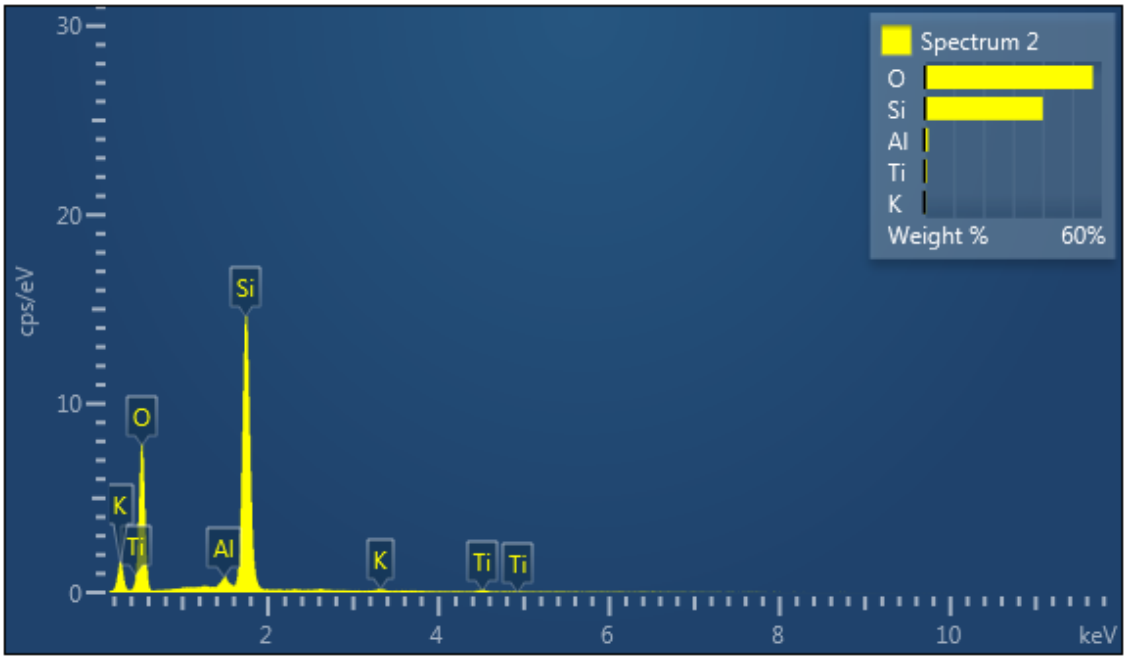
Spectrum 2
O
Si
Al
Ti
K
Weight %
60%
cps/eV
30
20
10
0
O
K
Ti
Al
Si
K
Ti
Ti
2
4
6
8
10
keV

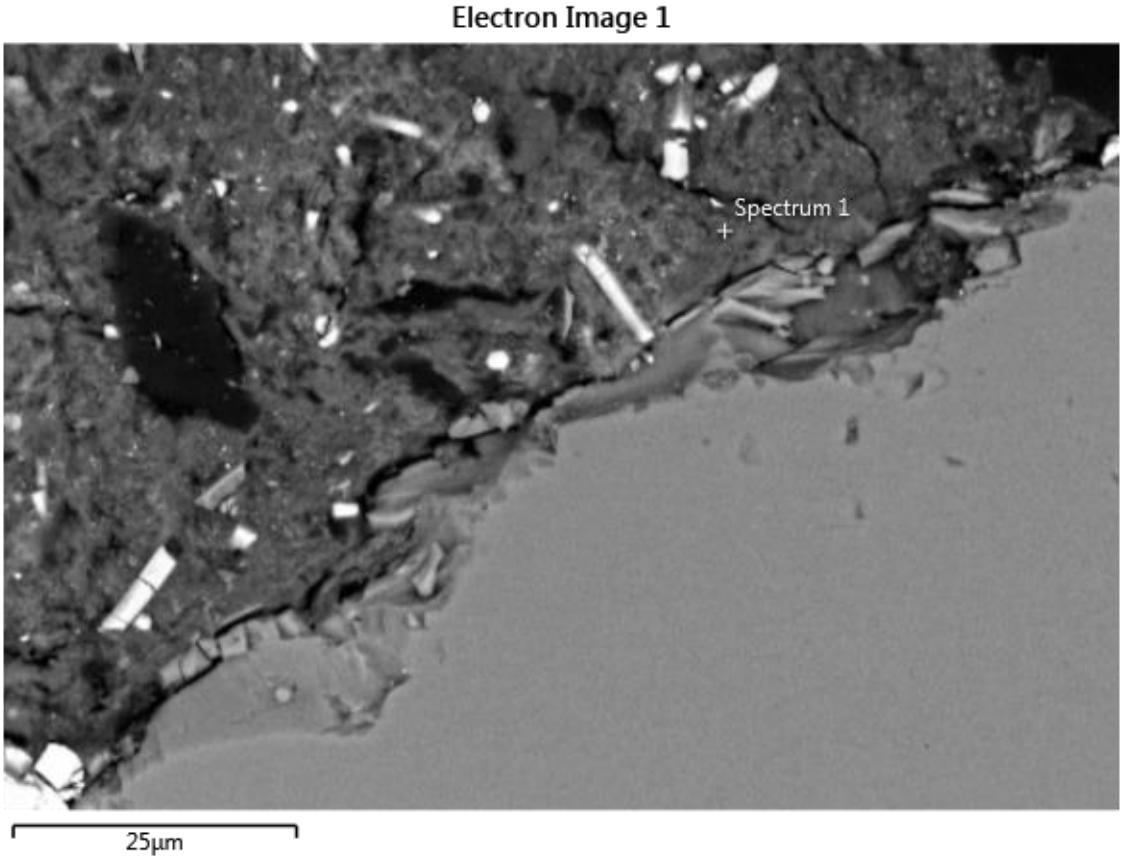
Electron Image 1
Spectrum 1
25µm

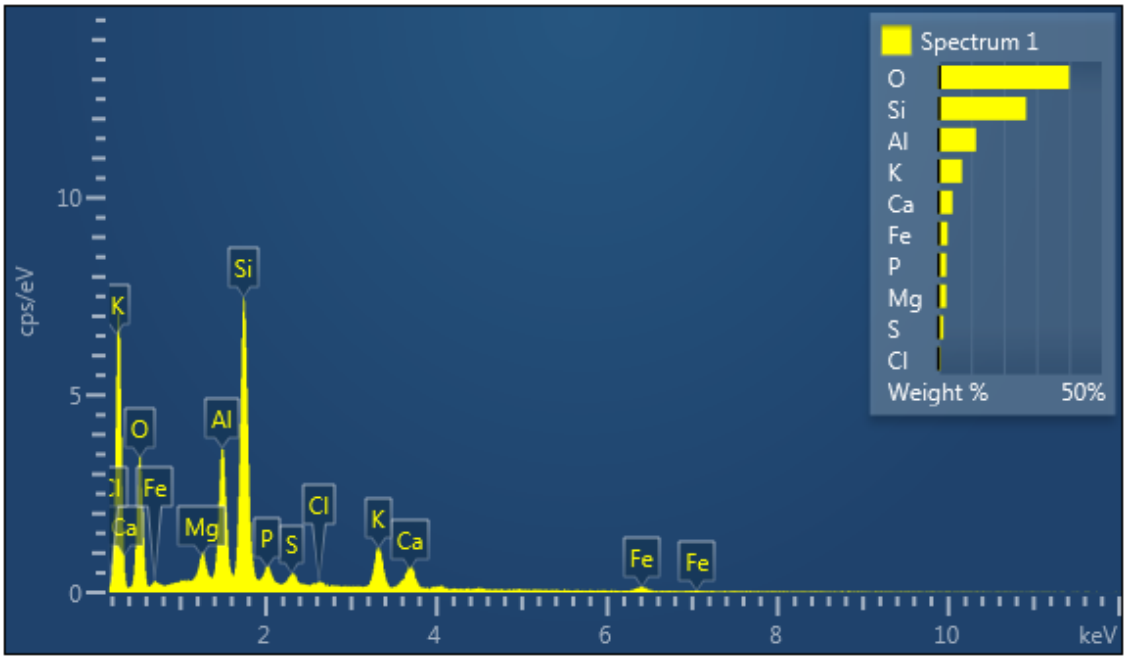
Spectrum 1
O
Si
Al
K
Ca
Fe
P
Mg
S
Cl
Weight %
50%
cps/eV
10
5
0
K
O
Si
Al
Cl
Fe
Ca
Mg
P
S
Cl
K
Ca
Fe
Fe
2
4
6
8
10
keV

Elgin Field

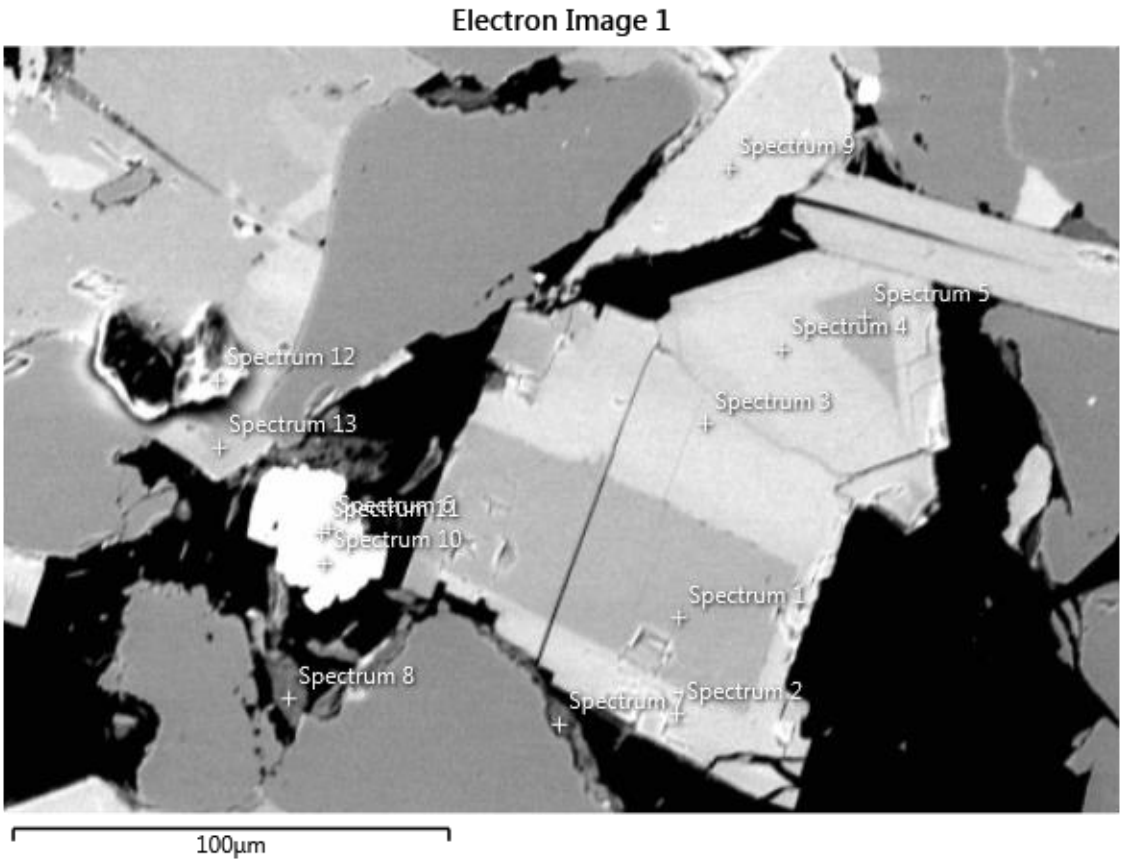
Electron Image 1
Spectrum 9
Spectrum 5
Spectrum 4
Spectrum 12
Spectrum 3
Spectrum 13
Spectrum 11
Spectrum 10
Spectrum 1
Spectrum 8
Spectrum 7
Spectrum 2
100µm

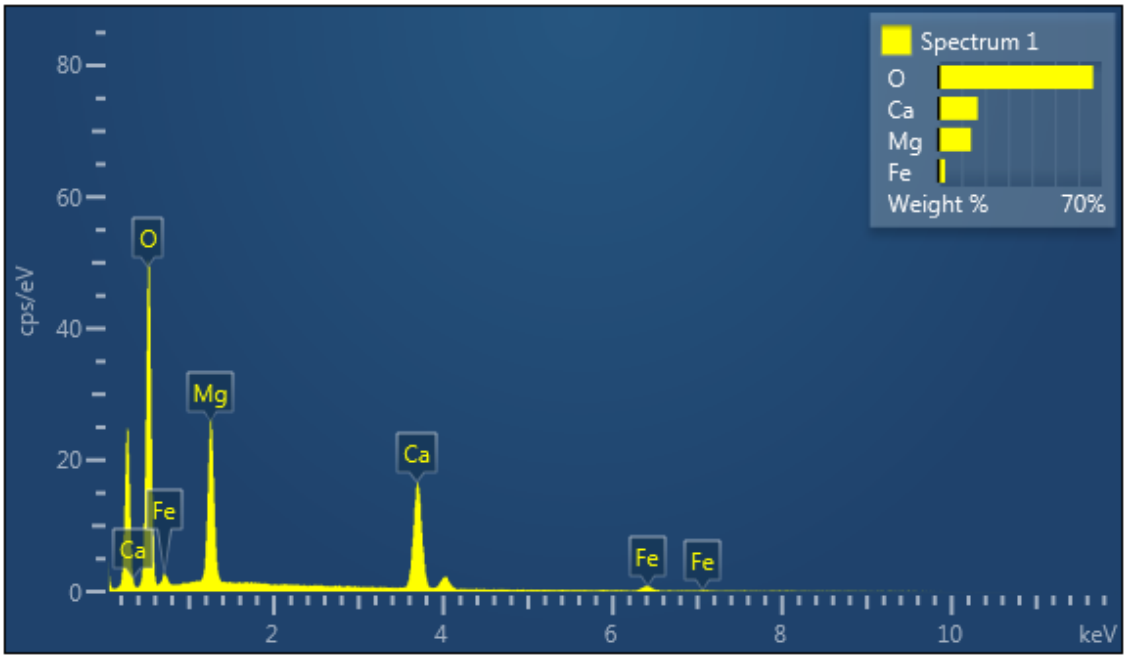
Spectrum 1
O
Ca
Mg
Fe
Weight %
70%
cps/eV
80
60
40
20
0
O
Mg
Ca
Fe
Ca
Fe
Fe
2
4
6
8
10
keV

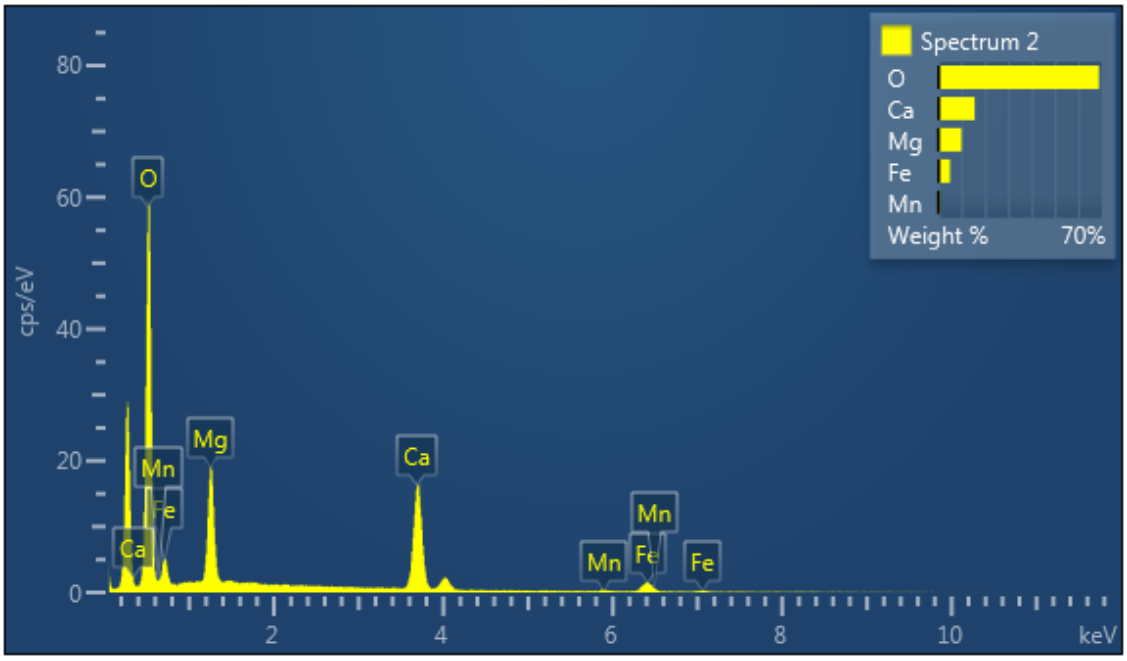
Spectrum 2
O
Ca
Mg
Fe
Mn
Weight %
70%
cps/eV
keV
O
Mg
Mn
Fe
Ca
Mn
Fe
Mn
Fe

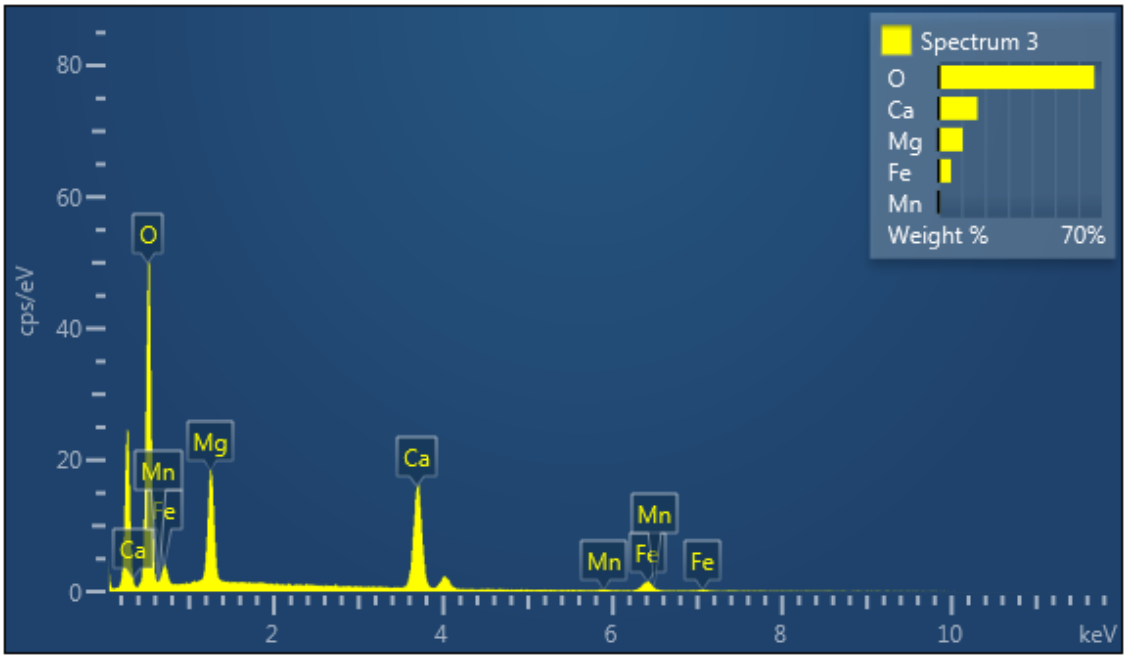
Spectrum 3
O
Ca
Mg
Fe
Mn
Weight %
70%
cps/eV
keV
O
Mg
Mn
Fe
Ca
Mn
Fe
Mn
Fe

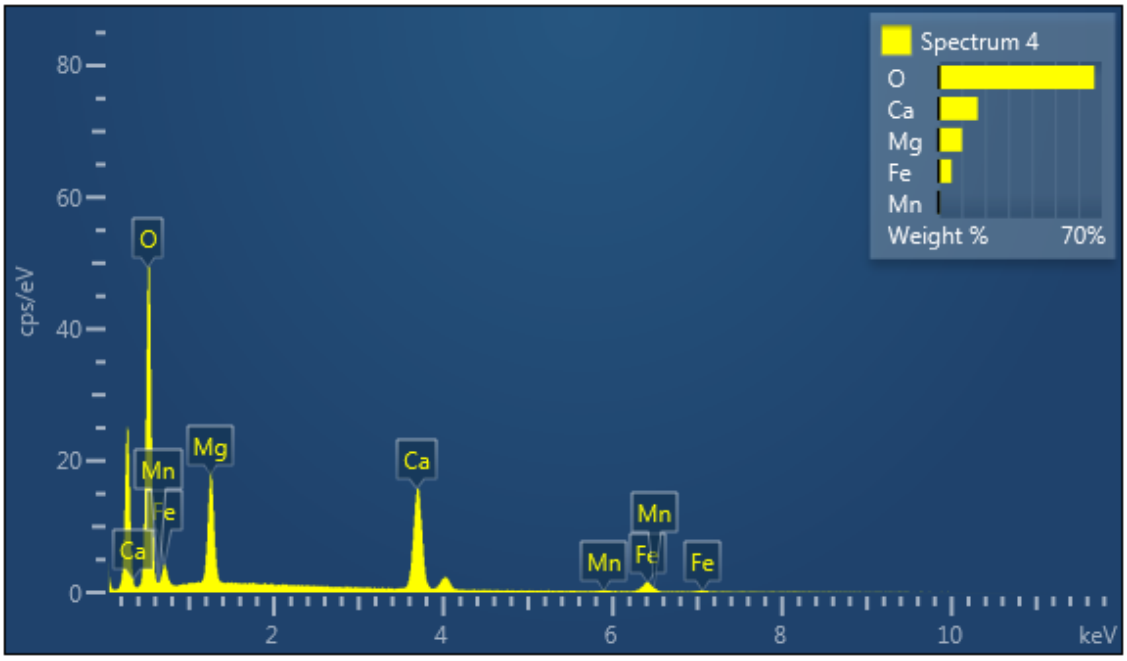
Spectrum 4
O
Ca
Mg
Fe
Mn
Weight %
70%
cps/eV
80
60
40
20
0
O
Mn
Mg
Fe
Ca
Mn
Mn
Fe
Fe
2
4
6
8
10
keV

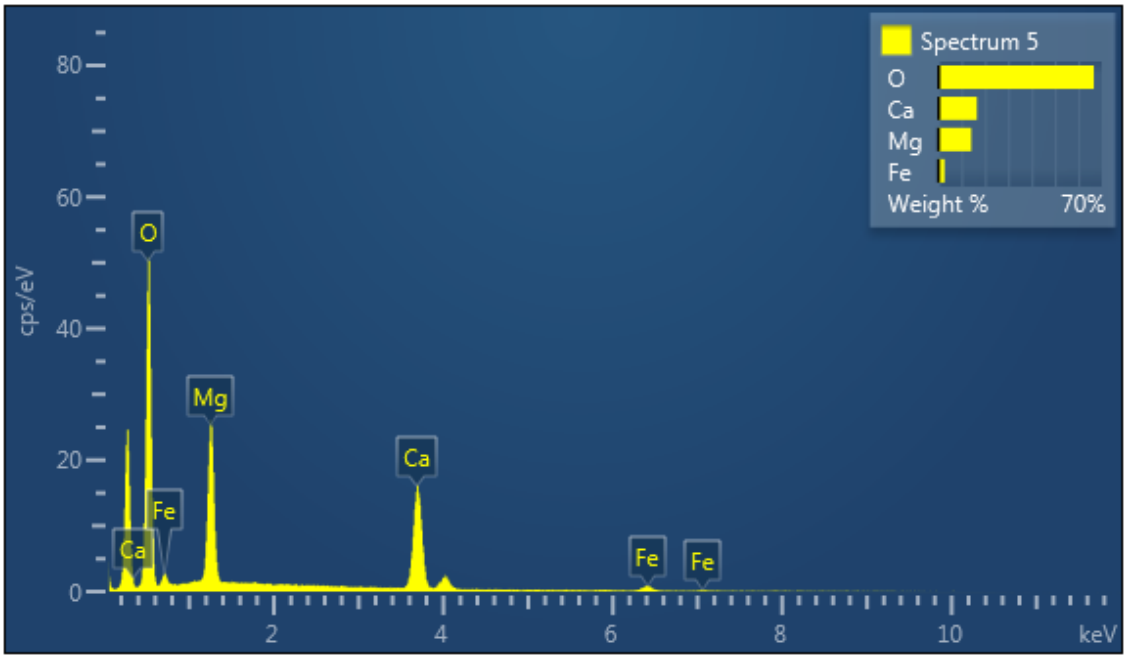
Spectrum 5
O
Ca
Mg
Fe
Weight %
70%
cps/eV
80
60
40
20
0
O
Mg
Ca
Fe
Ca
Fe
Fe
2
4
6
8
10
keV

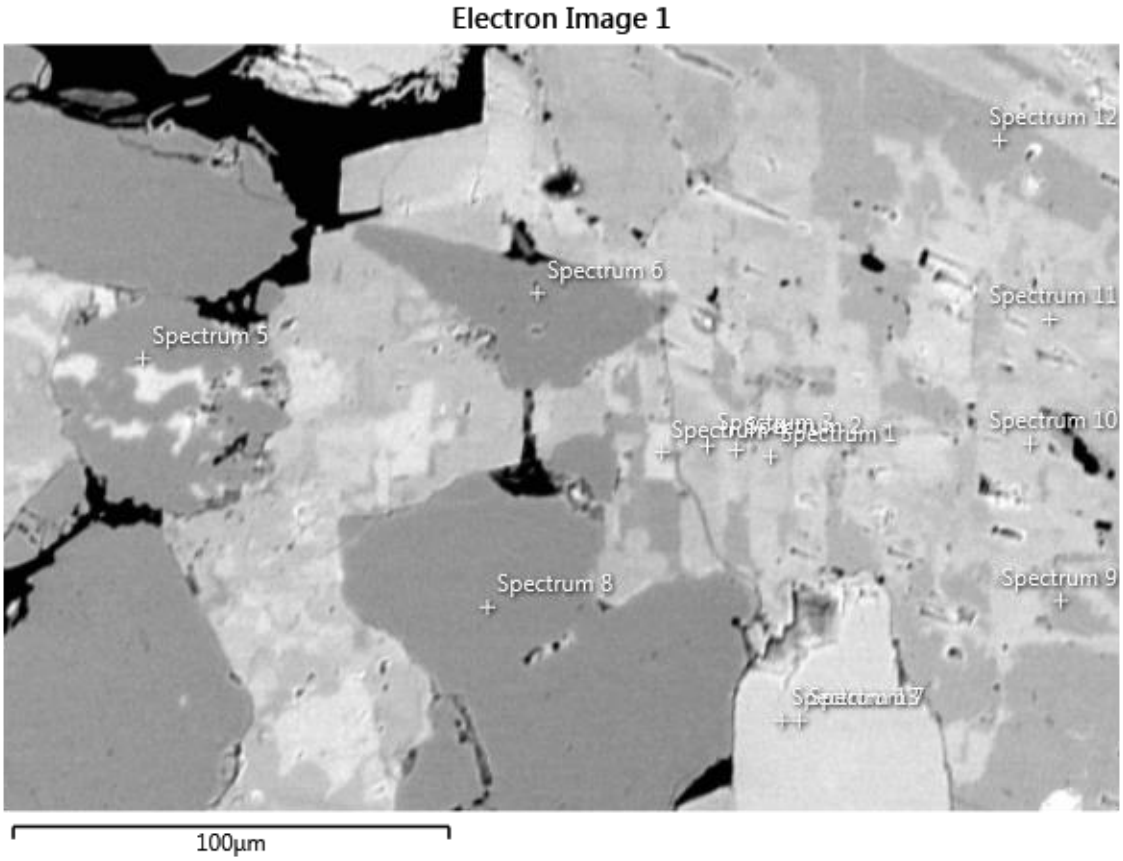
Electron Image 1
Spectrum 12
Spectrum 6
Spectrum 11
Spectrum 5
Spectrum 10
Spectrum 8
Spectrum 9
100µm

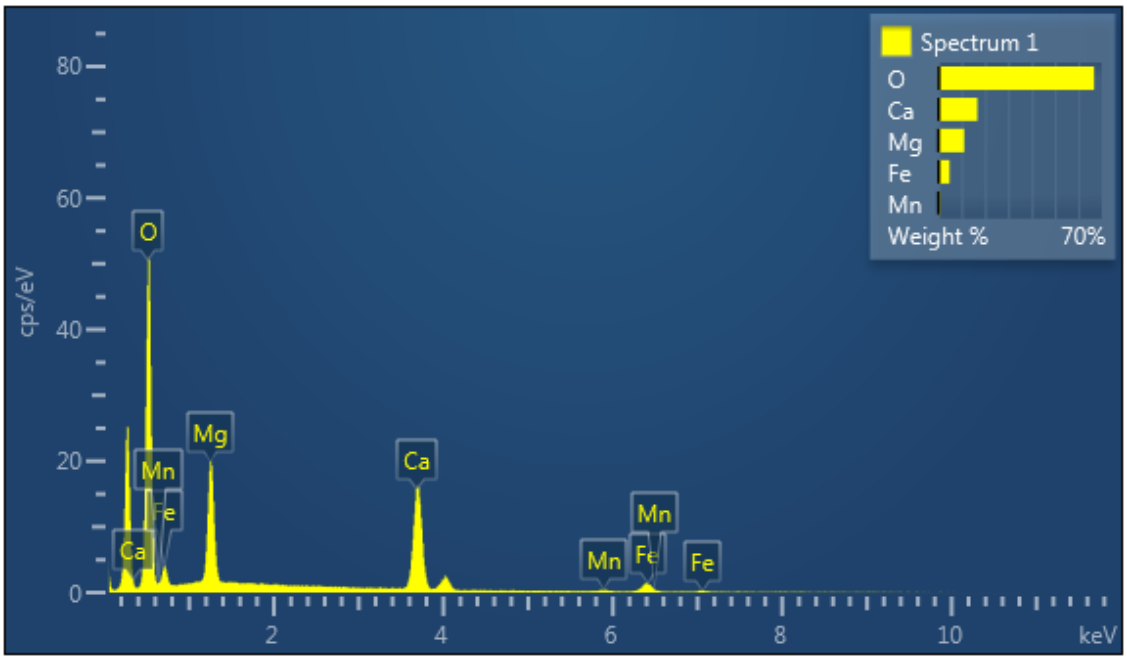
Spectrum 1
O
Ca
Mg
Fe
Mn
Weight %
70%
cps/eV
80
60
40
20
0
O
Mg
Mn
Fe
Ca
Ca
Mn
Mn
Fe
Fe
2
4
6
8
10
keV

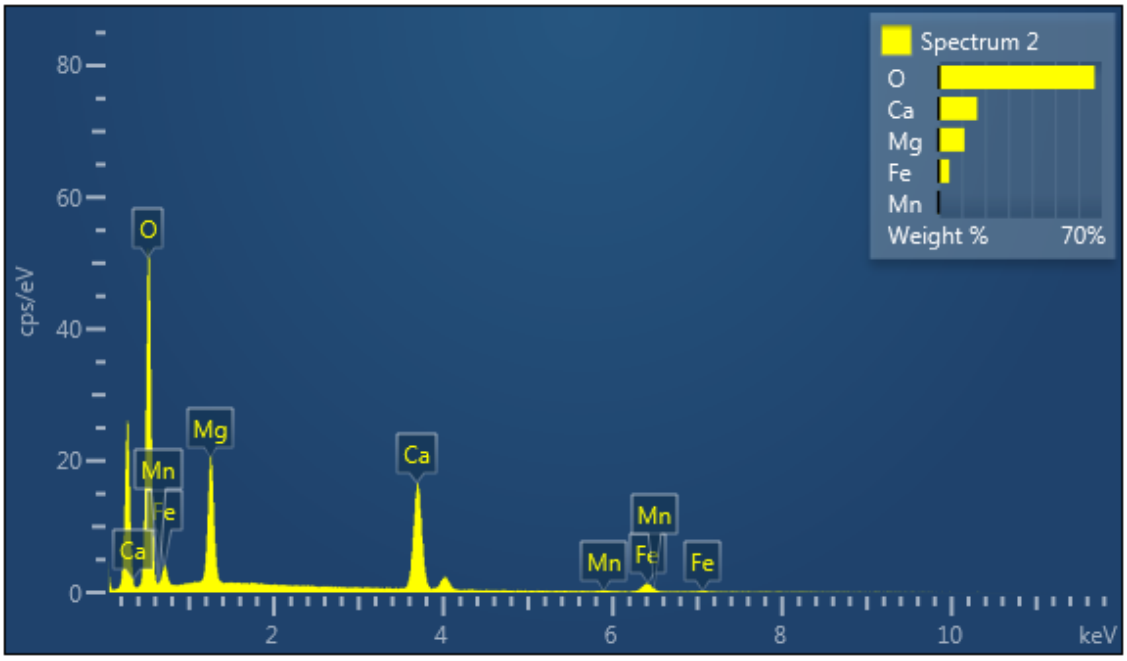
Spectrum 2
O
Ca
Mg
Fe
Mn
Weight %
70%
cps/eV
keV
O
Mg
Mn
Fe
Ca
Mn
Fe
Mn
Fe
Ca
0
20
40
60
80
2
4
6
8
10

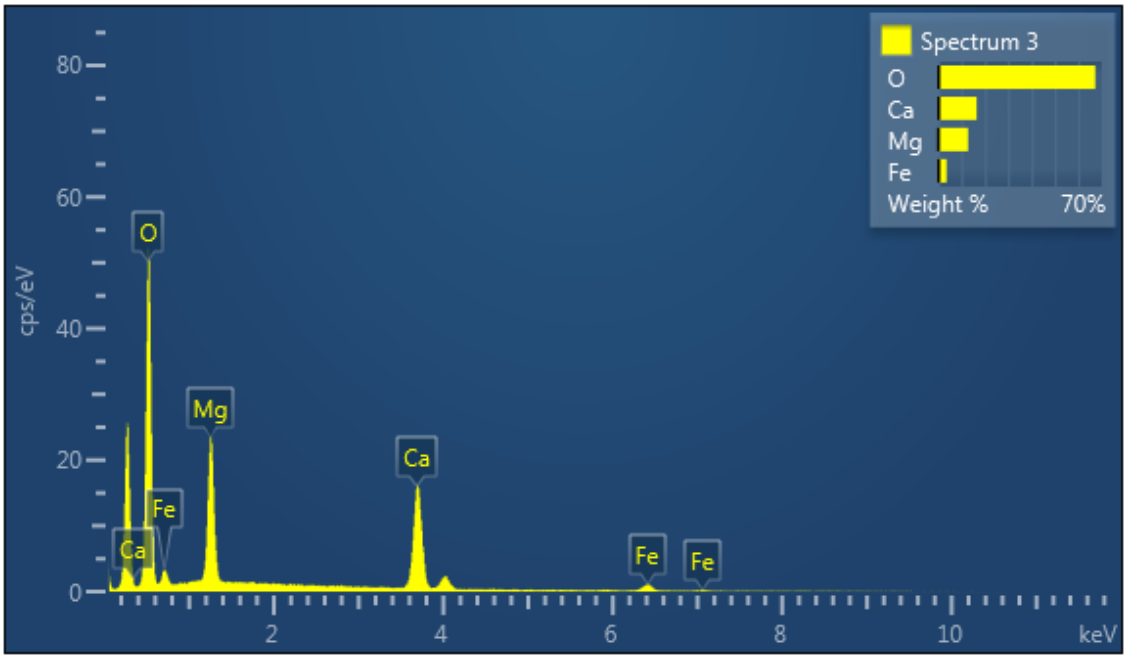
Spectrum 3
O
Ca
Mg
Fe
Weight %
70%
cps/eV
keV
O
Mg
Ca
Fe
Ca
Fe
Fe
0
20
40
60
80
2
4
6
8
10

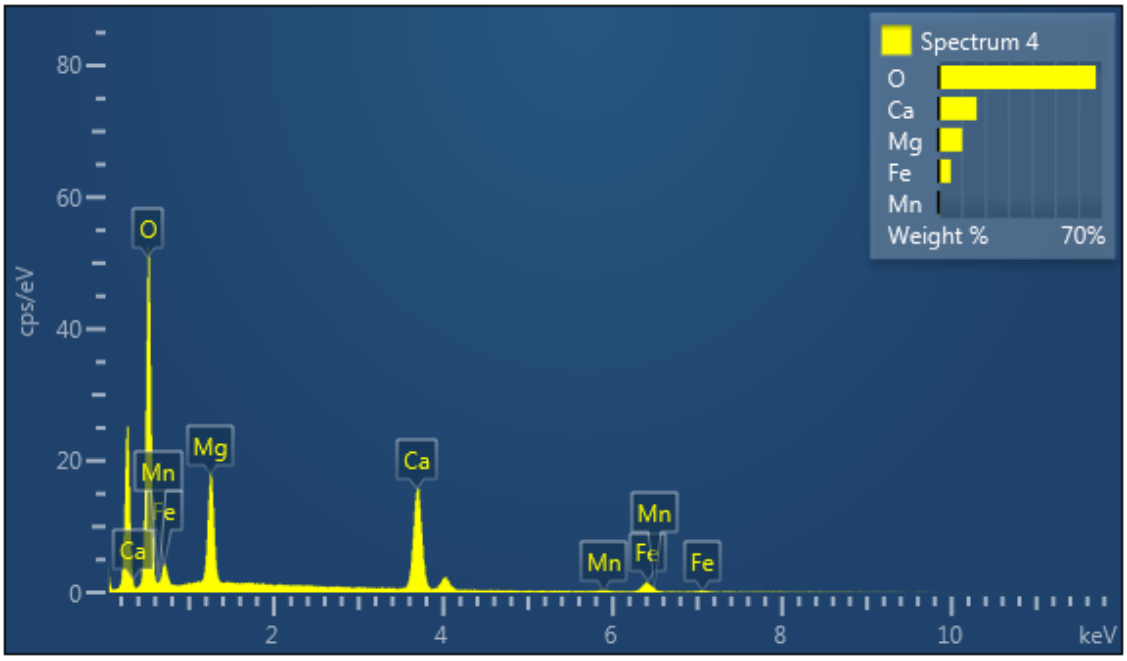

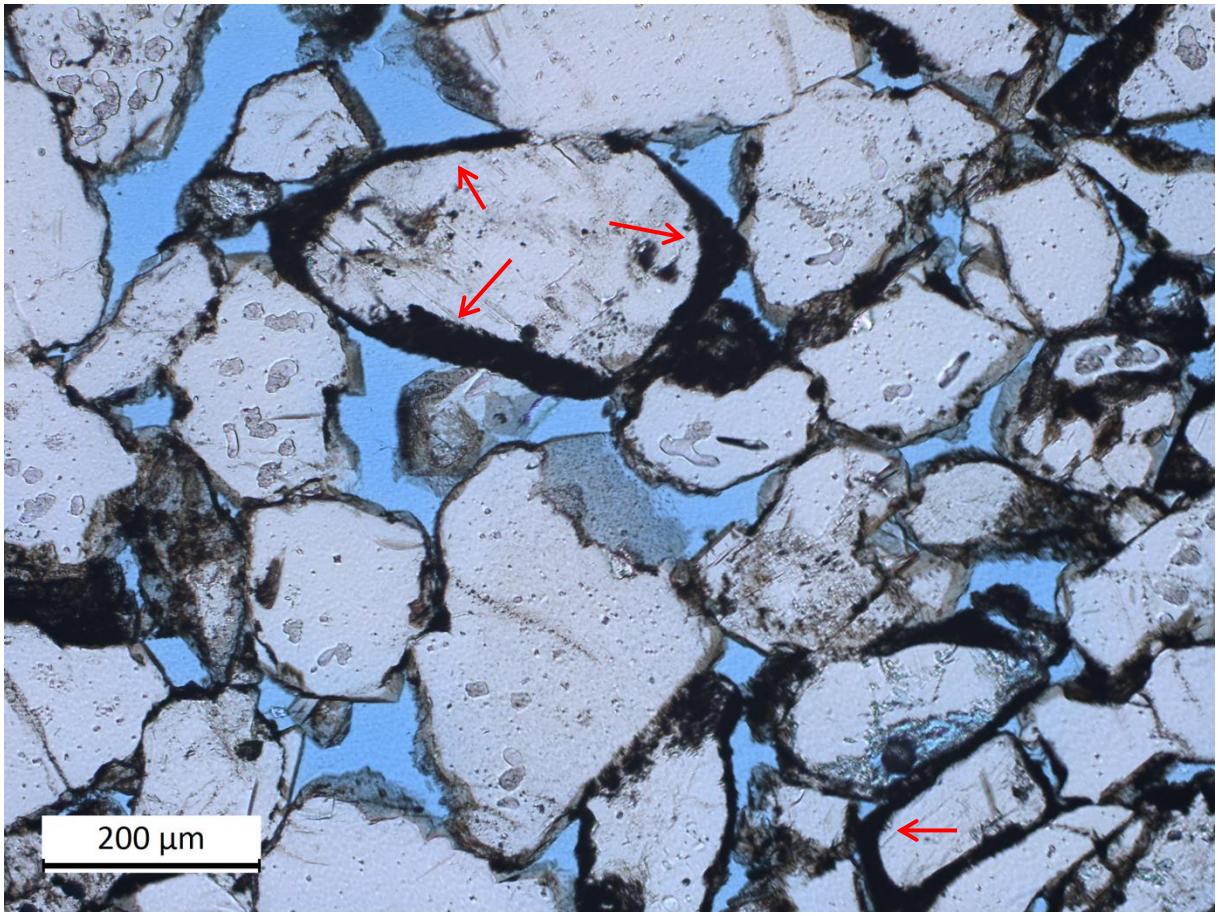

Photomicrograph of Fulmar Formation sandstones from Elgin Field. Red arrows indicate altered feldspar overgrowths

Fulmar field

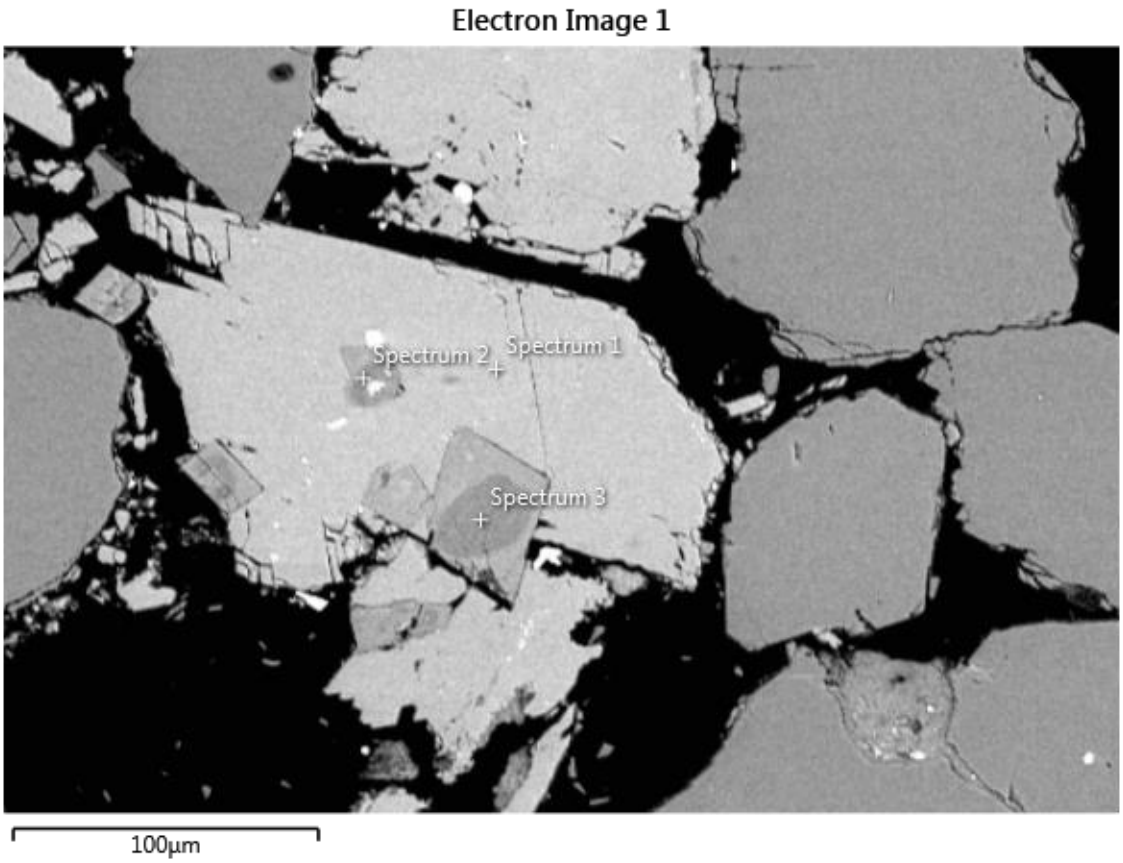

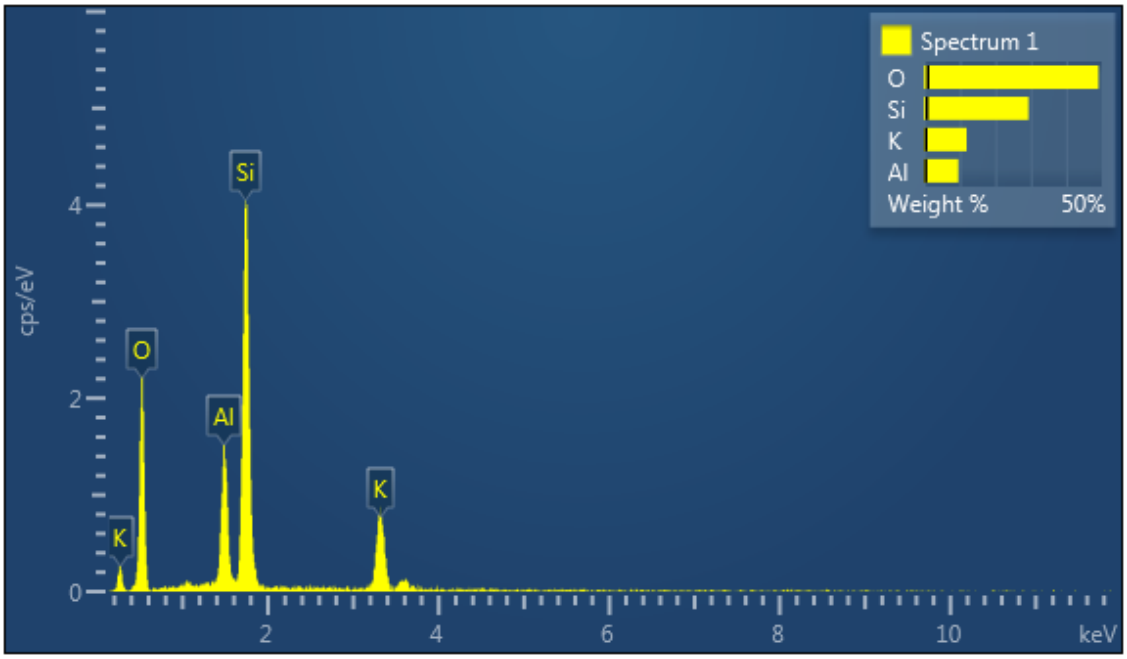

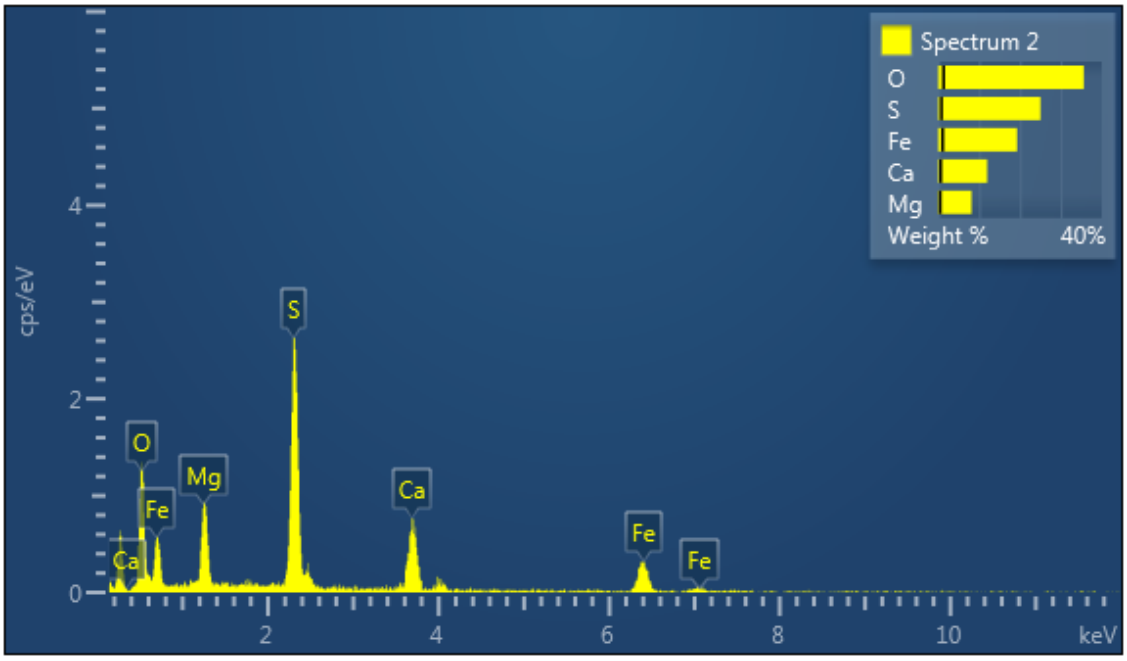
Spectrum 2
O
S
Fe
Ca
Mg
Weight %
40%
cps/eV
keV
O
Mg
Fe
Ca
S
Ca
Fe
Fe

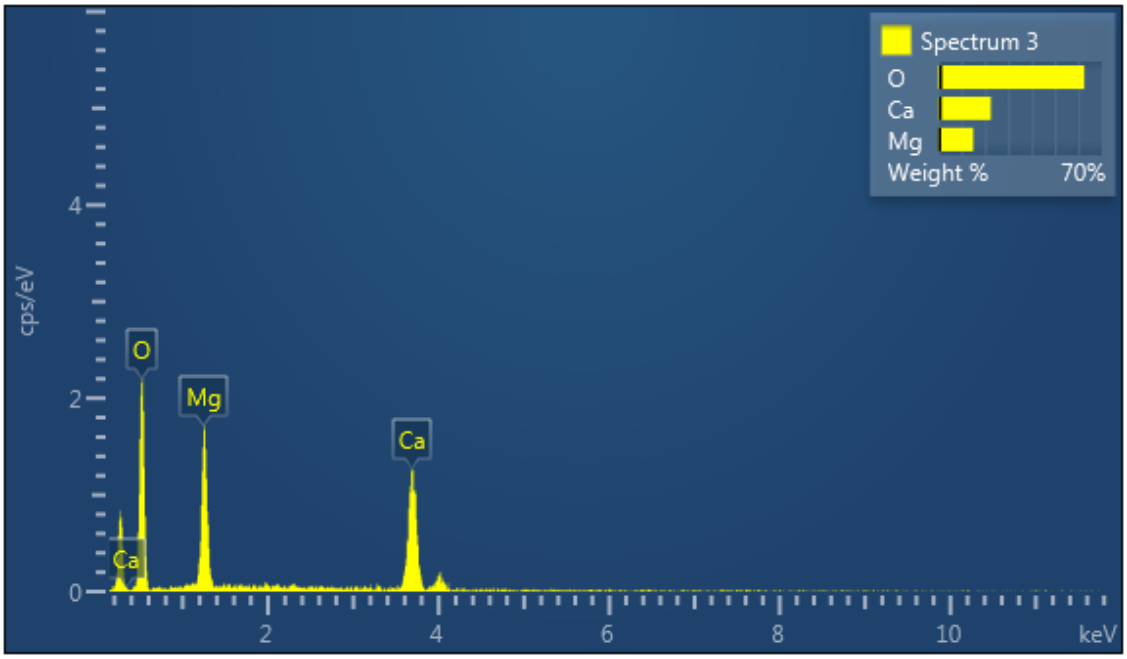
Spectrum 3
O
Ca
Mg
Weight %
70%
cps/eV
keV
O
Mg
Ca
Ca

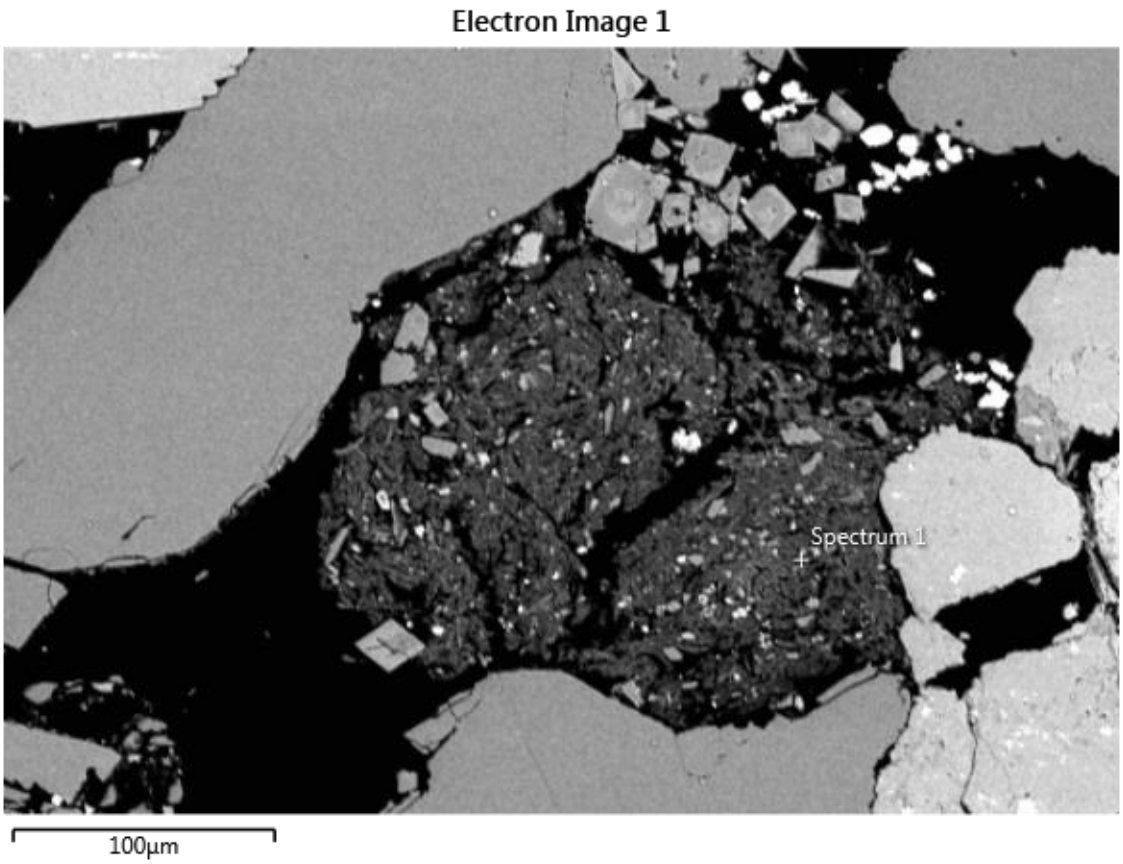
Electron Image 1
Spectrum 1
100µm

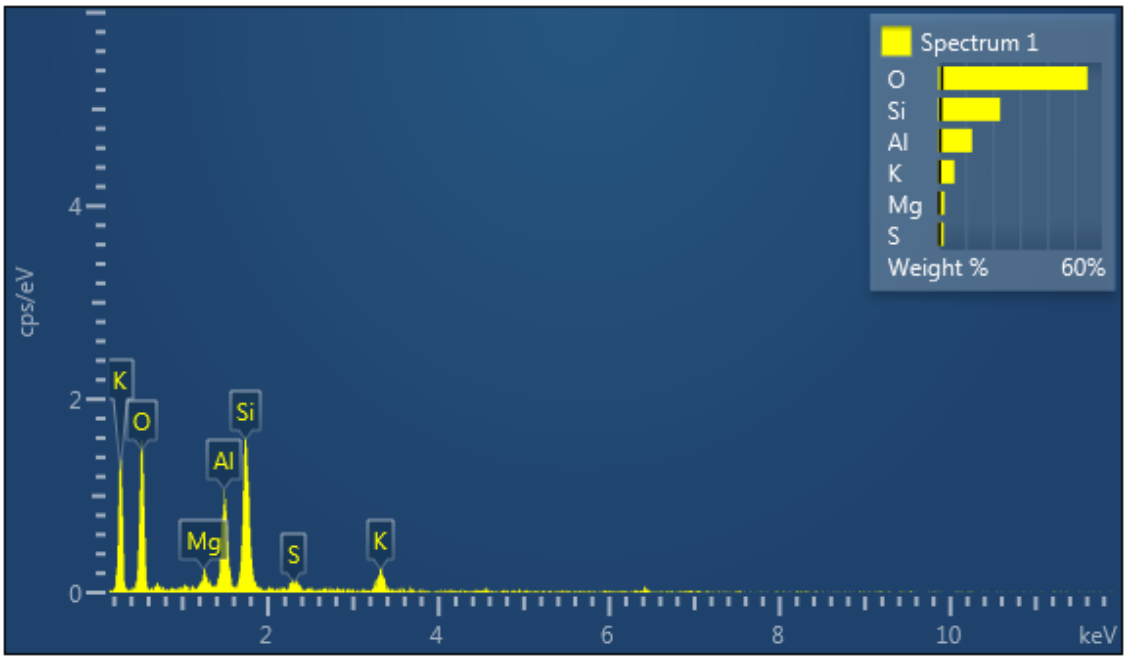
Spectrum 1
O
Si
Al
K
Mg
S
Weight %
60%
cps/eV
K
O
Si
Al
Mg
S
K
keV

Appendix 3

Oxygen Isotope (SIMS) Analysis Data

Clyde field sample large area BSE map

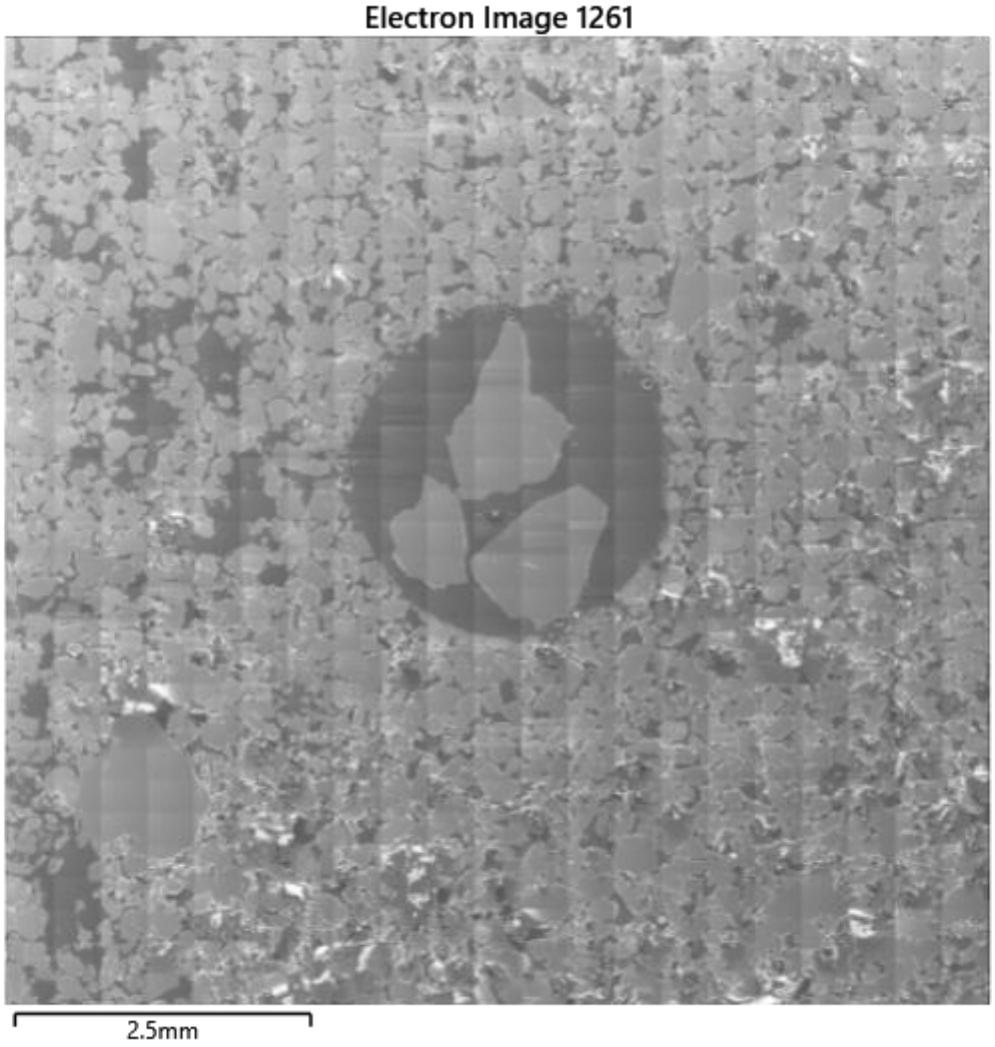

Clyde field sample large area CL map

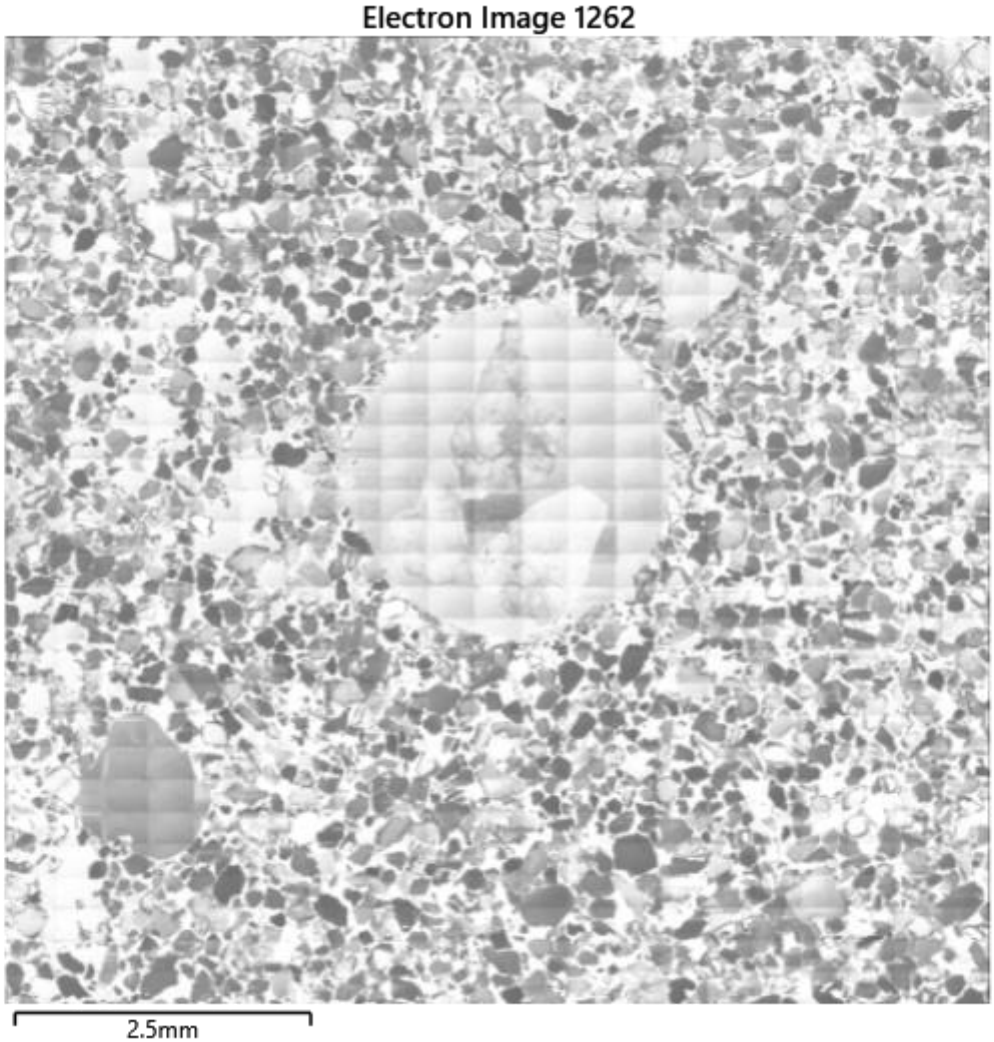

Elgin field sample large area BSE map

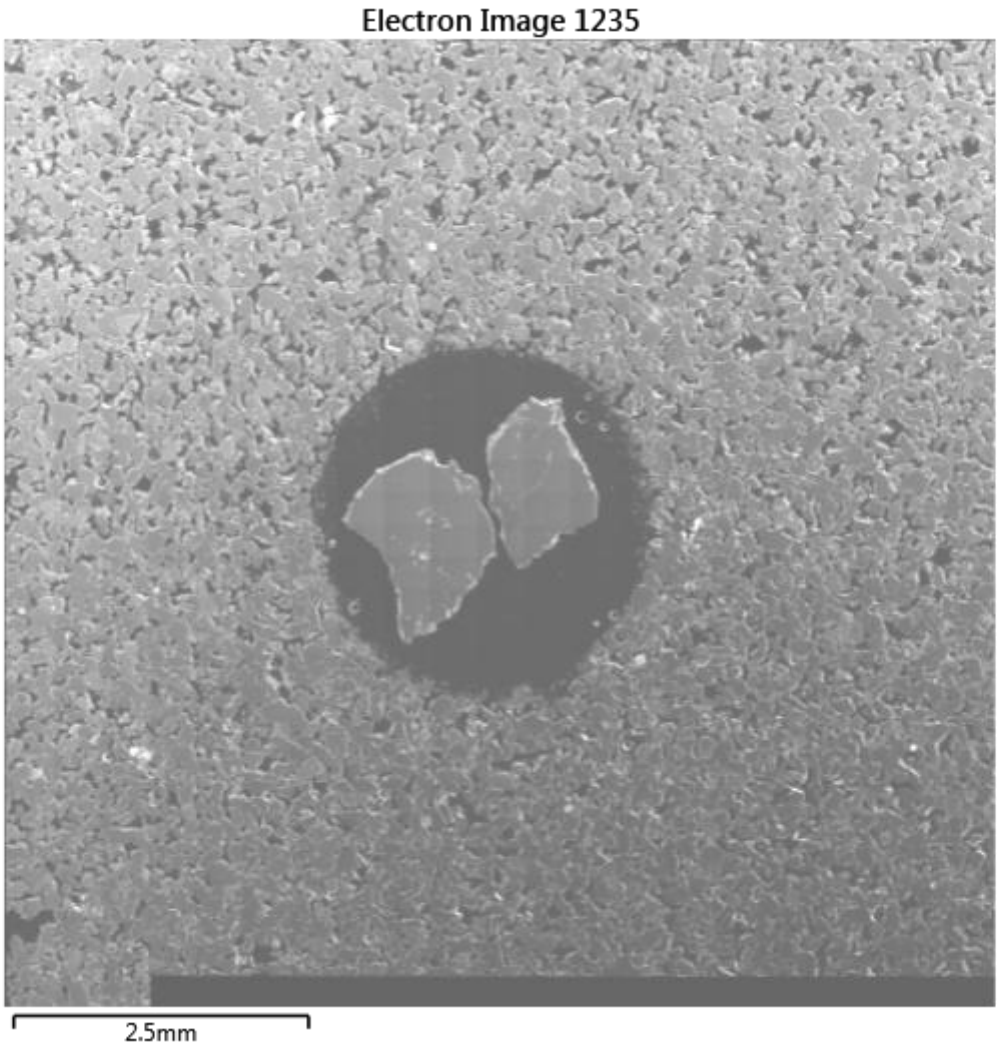

Elgin field sample large area CL map

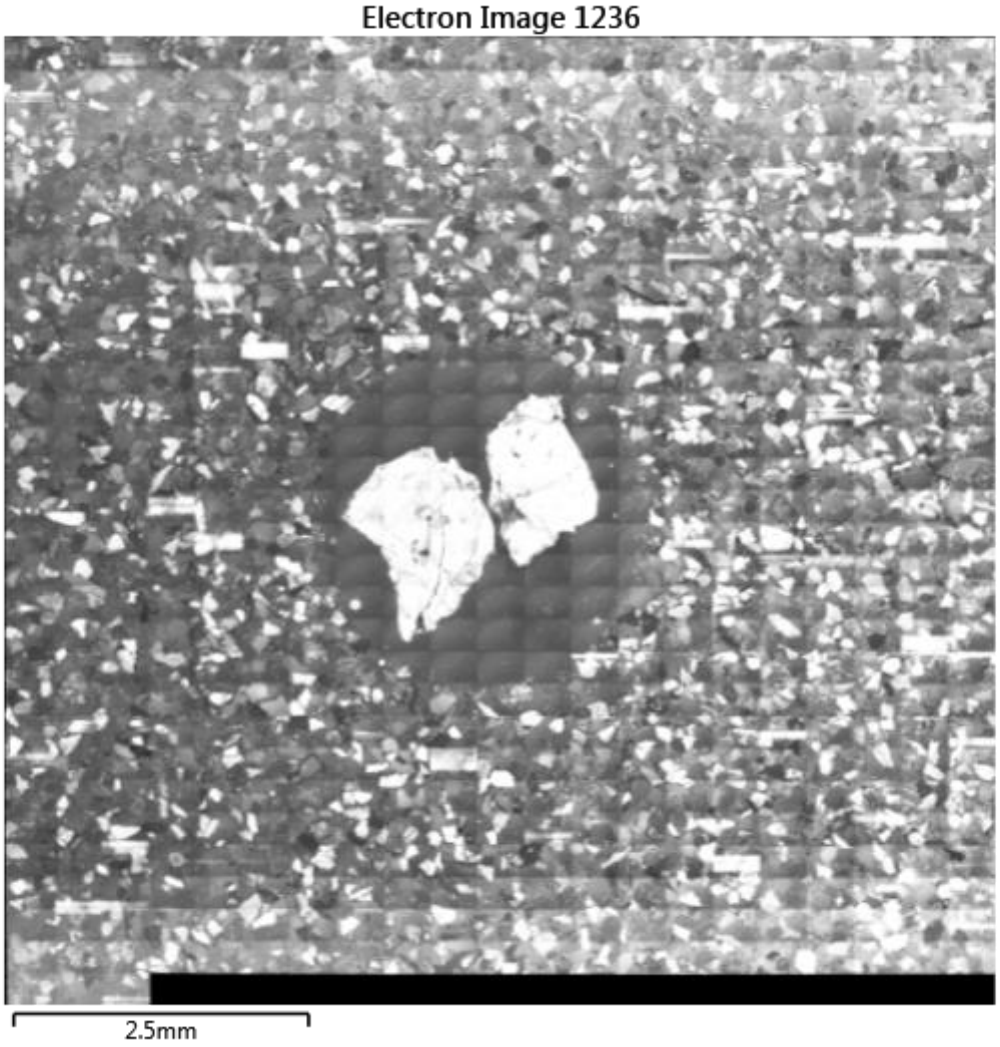

Fulmar field sample large area BSE map

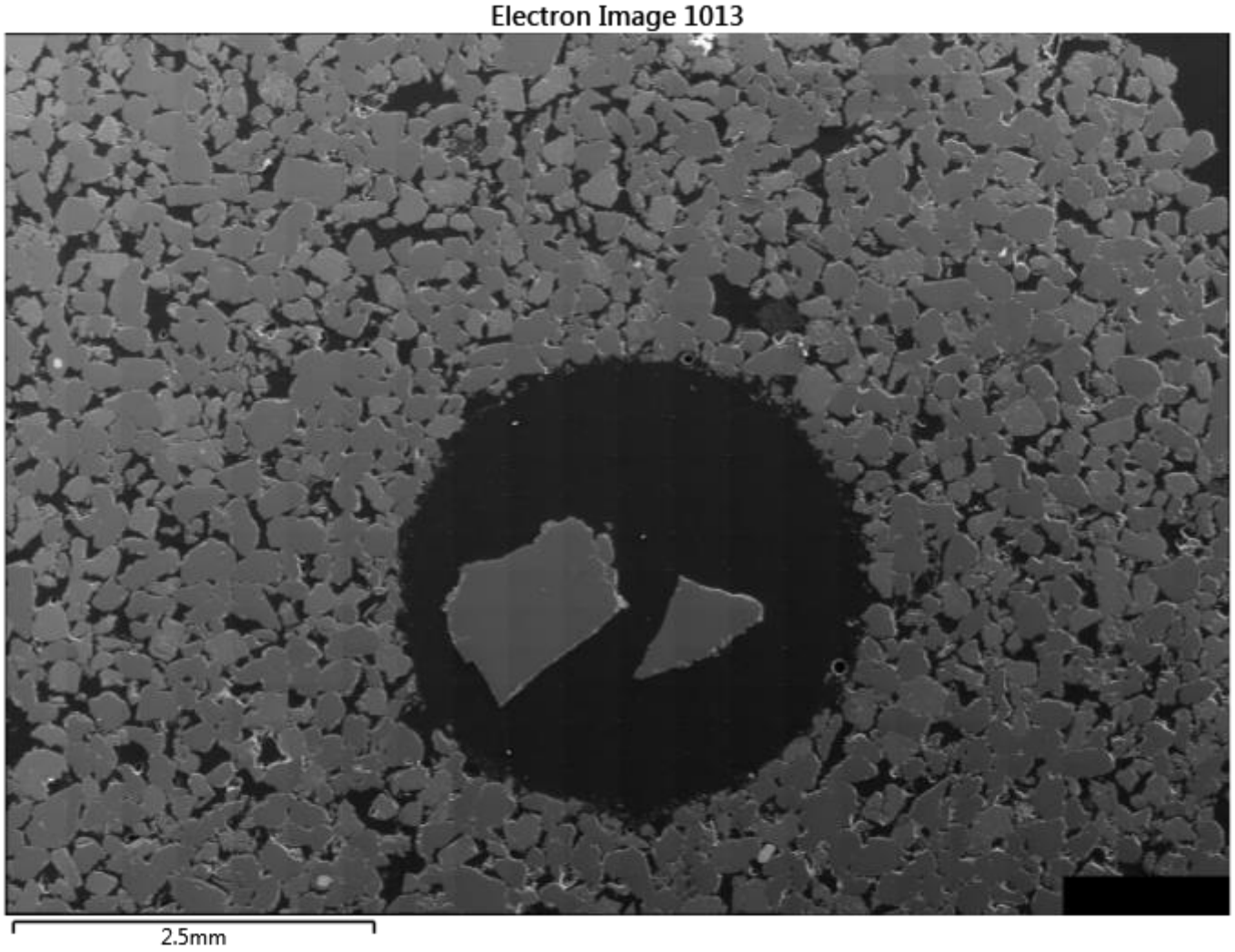

Fulmar field sample large area CL map

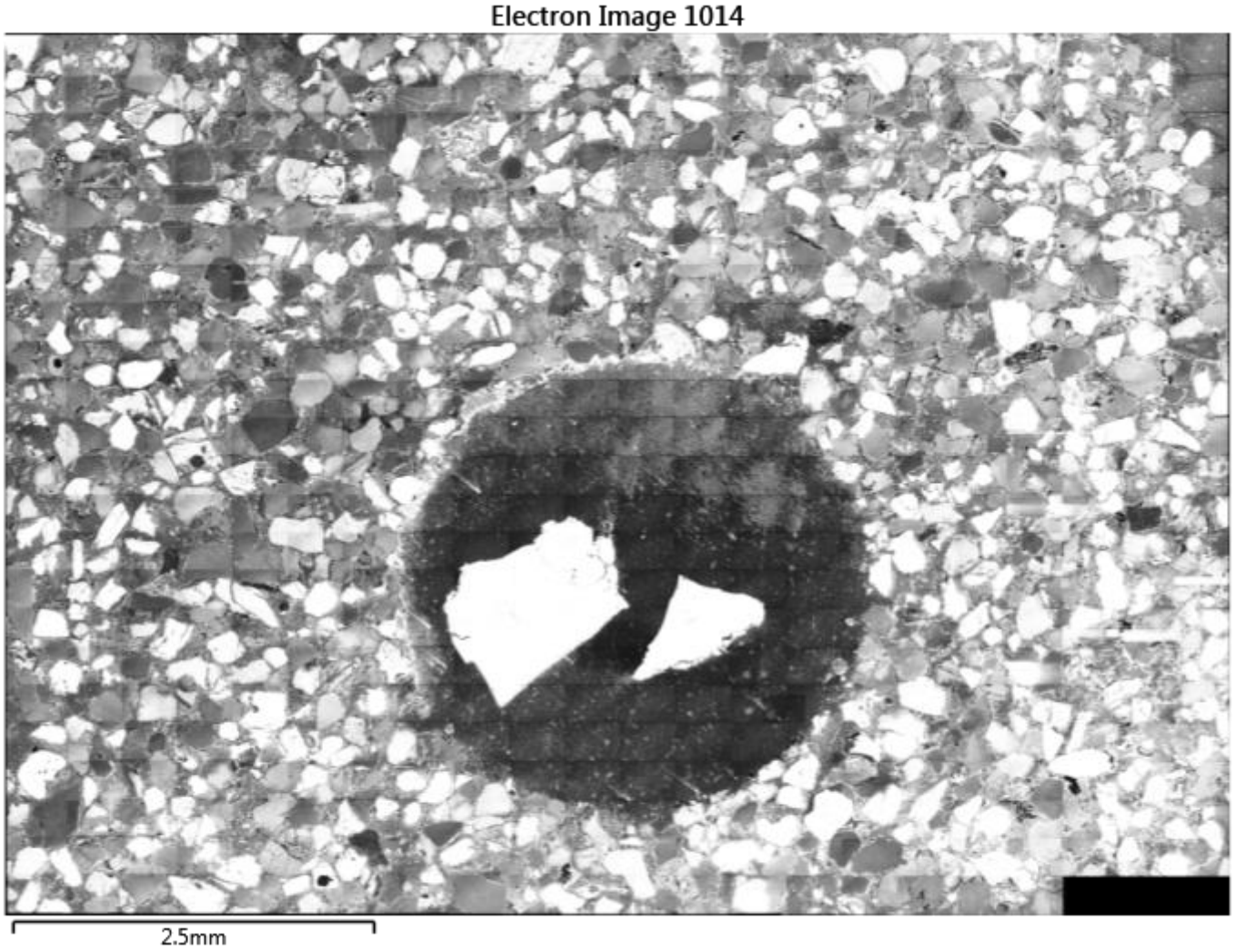

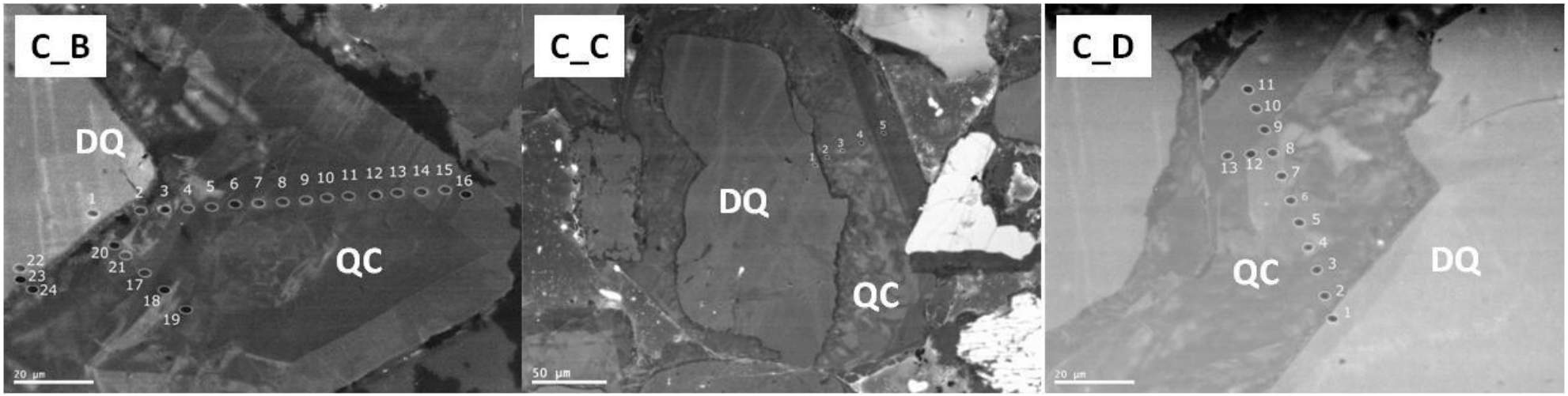

Post-SIMS examination CL images of SIMS pits of analysed quartz grains from the Upper Jurassic Fulmar Formation sandstones from Clyde field (QC – quartz cement, DQ - detrital quartz)..

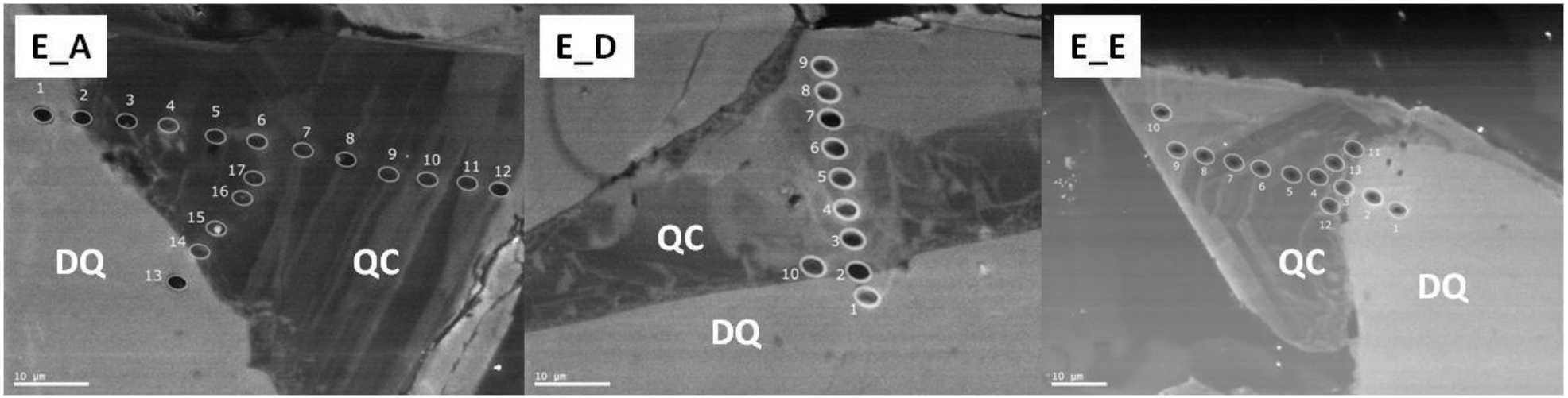

Post-SIMS examination CL images of SIMS pits of analysed quartz grains from the Upper Jurassic Fulmar Formation sandstones from Elgin field (QC – quartz cement, DQ - detrital quartz)..

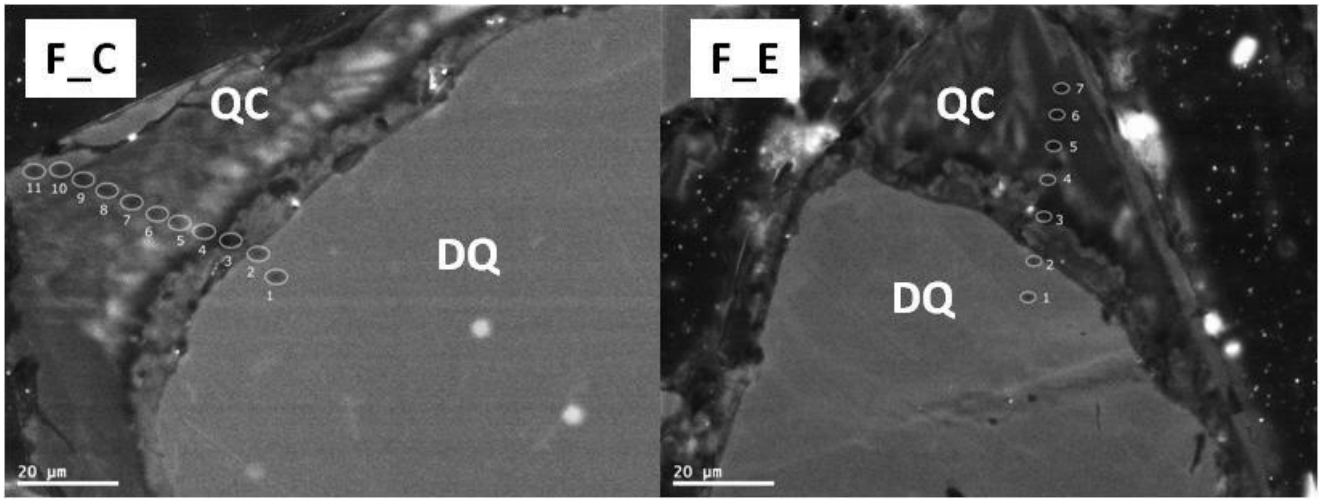

Post-SIMS examination CL images of SIMS pits of analysed quartz grains from the Upper Jurassic Fulmar Formation sandstones from Fulmar field (QC – quartz cement, DQ - detrital quartz)..

Analytical details of SIMS analyses on quartz grains (detrital and overgrowth). Outliers that are excluded from the plots and interpretations are included here (orange and red font colours). External precision (2SD reproducibility) is reported for each bracket.

Sample ID	^{16}O (Mcps)	$\delta^{18}O$ ‰ measured	2SE (int.)	Mass Bias (‰)	$\delta^{18}O$ ‰ VSMOW	2SD (ext.)	$^{16}OH/^{16}O$	$^{16}OH/^{16}O$ corrected	Relative Yield	X (µm)	Y (µm)	Comment
UWQ-1					**12.33**							
WI-STD-80 UWQ1 G1	30.756	-20.169	0.606				4.56E-04			403	1734	
WI-STD-80 UWQ1 G1	33.107	-20.417	0.743				4.85E-04			413	1737	
WI-STD-80 UWQ1 G1	33.137	-20.412	0.644				4.54E-04			417	1745	
WI-STD-80 UWQ1 G1	33.129	-8.870	0.708				4.13E-04			420	1756	
WI-STD-80 UWQ1 G1	32.696	-8.883	0.473				4.57E-04			423	1762	
WI-STD-80 UWQ1 G1	32.857	-8.861	0.721				4.20E-04			426	1772	
WI-STD-80 UWQ1 G1	32.809	-8.143	0.520				4.79E-04			9980	550	
average and 2SD		**-8.69**				**0.73**						
3µm beam, 22 pA intensity												
Mass calibration												
Analysis day: 4/6/2017												
Sample: C												
UWQ1 G1	34.160	-8.008	0.534				5.02E-04			-412	-384	Good
UWQ1 G1	34.546	-8.143	0.688				6.85E-04			-422	-389	Good
UWQ1 G1	34.136	-8.798	0.519				7.35E-04			-431	-379	Good
UWQ1 G1	34.112	-8.373	0.654				1.03E-03			-432	-389	Good
average and 2SD	**34.239**	**-8.331**	**0.692**				**0.0007**					
C_D-001	32.668	-10.741	0.611		9.91	0.60	3.71E-04	-3.41E-04	0.952648	1433	1759	Detrital
C_D-002	32.320	4.435	0.639		25.40	0.60	5.15E-04	-1.98E-04	0.98535	1428	1768	Good
C_D-003	32.414	4.328	0.418		25.29	0.60	4.75E-04	-2.37E-04	0.988221	1426	1775	Good
C_D-004	32.207	4.583	0.683		25.55	0.60	4.95E-04	-2.17E-04	0.981903	1424	1781	Good
C_D-005	32.107	4.001	0.596		24.95	0.60	4.72E-04	-2.41E-04	0.978851	1422	1787	Good

Sample ID	^{16}O (Mcps)	$\delta^{18}O$ ‰ measured	2SE (int.)	Mass Bias (‰)	$\delta^{18}O$ ‰ VSMOW	2SD (ext.)	$^{16}OH/^{16}O$	$^{16}OH/^{16}O$ corrected	Relative Yield	X	Y	Comment
C_D-006	31.818	4.421	0.717		25.38	0.60	4.66E-04	-2.47E-04	0.970041	1420	1793	Good
C_D-007	31.452	4.463	0.669		25.43	0.60	5.06E-04	-2.06E-04	0.958896	1418	1799	Good
C_D-008	31.237	4.298	0.525		25.26	0.60	4.52E-04	-2.60E-04	0.997699	1416	1805	Good
C_D-009	30.627	3.695	0.637		24.64	0.60	5.05E-04	-2.07E-04	0.978195	1414	1811	Good
C_D-010	29.674	2.624	0.496		23.55	0.60	4.37E-04	-2.76E-04	0.94775	1412	1817	Good
UWQ1 G1	31.764	-8.314	0.563				8.30E-04			-405	-383	Good
UWQ1 G1	31.347	-8.420	0.522				7.73E-04			-402	-375	Good
UWQ1 G1; Cs res 165-167	33.008	-8.786	0.514				5.47E-04			-413	-361	Good
UWQ1 G1; Cs res 167-168	33.746	-8.083	0.466				5.98E-04			-424	-358	Good
average and 2SD	**32.466**	**-8.401**		**-20.48**		**0.586**	**0.0007**					
bracket average and 2SD	**33.352**	**-8.366**		**-20.44**		**0.598**	**0.0007**					
C_D-011	30.547	3.022	0.733		24.13	0.75	3.63E-04	-3.29E-04	0.922814	1411	1822	Good
C_D-012	32.924	3.466	0.533		24.58	0.75	6.75E-04	-1.75E-05	0.994621	1411	1802	Good
C_D-013	32.030	2.501	0.571		23.59	0.75	5.64E-04	-1.28E-04	0.96762	1405	1802	Good
C_B-001	32.988	-9.211	0.560		11.64	0.75	3.70E-04	-3.23E-04	0.996545	-171	-4093	Detrital
C_B-002	32.205	5.019	0.953		26.17	0.75	6.57E-04	-3.57E-05	0.972907	-159	-4093	Good
C_B-003	31.768	4.148	0.746		25.28	0.75	3.94E-04	-2.98E-04	0.959704	-153	-4093	Good
C_B-004	32.343	3.256	0.560		24.37	0.75	4.34E-04	-2.58E-04	0.97706	-147	-4093	Good
C_B-005	31.479	2.452	0.560		23.54	0.75	4.50E-04	-2.42E-04	0.95098	-141	-4093	Good
C_B-006	32.086	2.786	0.609		23.89	0.75	4.49E-04	-2.43E-04	0.969316	-135	-4093	Good
C_B-007	31.396	2.654	0.520		23.75	0.75	4.29E-04	-2.63E-04	0.993634	-129	-4093	Good
C_B-008	31.661	2.007	0.594		23.09	0.75	4.39E-04	-2.53E-04	1.002009	-123	-4093	Good
C_B-009	30.851	2.247	0.538		23.34	0.75	4.28E-04	-2.65E-04	0.976377	-117	-4093	Good
UWQ1 G1	31.963	-9.269	0.741				4.98E-04			-434	-352	Good
UWQ1 G1	32.061	-8.617	0.557				7.33E-04			-436	-359	Good
UWQ1 G1	31.785	-8.547	0.750				8.28E-04			-436	-367	Good
UWQ1 G1; Cs res 168-170	33.042	-8.218	0.673				7.30E-04			-448	-363	Good

Sample ID	^{16}O (Mcps)	$\delta^{18}O$ ‰ measured	2SE (int.)	Mass Bias (‰)	$\delta^{18}O$ ‰ VSMOW	2SD (ext.)	$^{16}OH/^{16}O$	$^{16}OH/^{16}O$ corrected	Relative Yield	X	Y	Comment
average and 2SD	**32.213**	**-8.663**		**-20.74**		**0.880**	**0.0007**					
bracket average and 2SD	**32.339**	**-8.532**		**-20.61**		**0.747**	**0.0007**					
C_B-010	32.755	2.375	0.571		23.43	0.00	3.61E-04	-3.81E-04	0.98818	-112	-4091	Good
C_B-011	32.429	2.508	0.603		23.57	0.00	4.09E-04	-3.32E-04	0.978362	-106	-4091	Good
C_B-012	32.591	1.622	0.476		22.66	0.00	4.06E-04	-3.36E-04	0.983237	-100	-4091	Good
C_B-013	32.318	2.045	0.521		23.09	0.00	4.19E-04	-3.23E-04	0.975001	-94	-4091	Good
C_B-014	32.412	1.932	0.471		22.98	0.00	4.51E-04	-2.91E-04	0.97783	-88	-4091	Good
C_B-015	31.917	1.960	0.504		23.01	0.00	4.51E-04	-2.91E-04	0.962916	-82	-4091	Good
C_B-016	32.178	2.668	0.739		23.73	0.00	4.46E-04	-2.96E-04	0.970796	-78	-4095	Good
C_B-017	31.984	3.715	0.438		24.80	0.00	3.83E-04	-3.58E-04	0.964918	-169	-4100	Good
C_B-018	32.167	3.332	0.695		24.41	0.00	4.59E-04	-2.83E-04	1.016657	-164	-4105	Good
C_B-019	32.083	2.760	0.613		23.82	0.00	4.69E-04	-2.72E-04	1.013994	-159	-4110	Good
C_B-020	31.318	2.521	0.883		23.58	0.00	4.76E-04	-2.65E-04	0.989819	-154	-4115	Good
C_B-021	31.373	2.171	0.854		23.22	0.00	5.10E-04	-2.32E-04	0.991556	-149	-4120	Good
C_B-022	31.569	-7.972	0.542		12.87	0.00	3.52E-04	-3.89E-04	0.997751	-193	-4104	Detrital
C_B-023	31.244	-7.919	0.442		12.92	0.00	4.85E-04	-2.57E-04	0.987497	-190	-4110	Detrital
C_B-024	31.572	5.658	0.582		26.78	0.00	5.80E-04	-1.62E-04	0.997872	-187	-4112	Good
UWQ1 G1	31.655	-8.191	0.734				7.48E-04			-445	-374	Good
UWQ1 G1	31.527	-8.243	0.733				7.34E-04			-456	-376	Good
UWQ1 G1	31.323	-8.377	0.605				8.39E-04			-449	-383	Good
UWQ1 G1	31.265	-8.507	0.692				8.23E-04			-449	-390	Good
average and 2SD	**31.443**	**-8.330**		**-20.41**		**0.28**	**0.0008**					
bracket average and 2SD	**31.828**	**-8.496**		**-20.57**		0.70	**0.0007**					
Sample: E (User: Olakunle Oye, Asst: IO)												
UWQ1 G1	33.663	-8.843	0.558				6.42E-04			-403	361	Good
UWQ1 G1	33.481	-8.567	0.740				9.08E-04			-410	359	Good

Sample ID	^{16}O (Mcps)	$\delta^{18}O$ ‰ measured	2SE (int.)	Mass Bias (‰)	$\delta^{18}O$ ‰ VSMOW	2SD (ext.)	$^{16}OH/^{16}O$	$^{16}OH/^{16}O$ corrected	Relative Yield	X	Y	Comment
UWQ1 G1	33.601	-8.513	0.386				9.61E-04			-405	350	Good
UWQ1 G1	33.393	-8.481	0.550				1.00E-03			-396	352	Good
average and 2SD	**33.534**	**-8.601**		**-20.68**		**0.33**	**0.0009**					
E_E-001	33.603	-10.875	0.598		9.82	0.60	6.27E-04	-3.60E-04	1.018003	-265	-3380	Detrital
E_E-002	33.217	-11.173	0.502		9.52	0.60	8.86E-04	-1.02E-04	1.006319	-269	-3375	Detrital
E_E-003	32.847	-2.235	1.793		18.64	0.60	1.05E-03	5.98E-05	0.995093	-275	-3372	Compromised
E_E-004	32.809	0.929	0.445		21.87	0.60	1.06E-03	6.83E-05	0.993963	-279	-3369	Good
E_E-005	32.708	0.535	0.384		21.47	0.60	1.10E-03	1.10E-04	0.990905	-284	-3368	Good
E_E-006	33.031	0.279	0.590		21.21	0.60	1.10E-03	1.09E-04	1.000689	-289	-3366	Good
E_E-007	32.663	-0.477	0.590		20.44	0.60	1.12E-03	1.33E-04	0.989541	-294	-3364	Good
E_E-008	32.532	0.715	0.756		21.65	0.60	1.01E-03	2.73E-05	0.985568	-299	-3362	Good
E_E-009	32.210	0.044	0.598		20.97	0.60	9.32E-04	-5.55E-05	0.975798	-304	-3360	Good
E_E-010	32.160	0.010	0.593		20.93	0.60	8.53E-04	-1.35E-04	0.974284	-306	-3352	Good
E_E-011	32.064	7.957	0.951		29.05	0.60	1.42E-03	4.35E-04	1.017648	-272	-3367	Compromised
UWQ1 G1	31.856	-8.536	0.638				1.04E-03			-396	366	Good
UWQ1 G1	31.627	-7.864	0.495				1.00E-03			-387	361	Good
UWQ1 G1	31.560	-8.426	0.705				1.22E-03			-388	354	Good
UWQ1 G1; Cs 173-175	33.279	-8.112	0.650				1.13E-03			-386	346	Good
average and 2SD	**32.081**	**-8.235**		**-20.31**		**0.611**	**0.0011**					
bracket average and 2SD	**32.808**	**-8.418**		**-20.50**		**0.600**	**0.0010**					
E_A-001	33.018	-14.785	0.633		5.68	0.75	5.63E-04	-5.67E-04	0.994833	-1839	-3214	Detrital
E_A-002	32.975	-1.785	0.642		18.95	0.75	2.67E-03	**1.54E-03**	0.993545	-1831	-3218	Compromised
E_A-003	32.977	1.195	0.596		21.99	0.75	8.30E-04	-3.00E-04	0.99362	-1825	-3218	Good
E_A-004	33.627	1.226	0.552		22.02	0.75	8.30E-04	-3.00E-04	1.013189	-1821	-3218	Good
E_A-005	32.905	0.914	0.584		21.70	0.75	8.04E-04	-3.26E-04	0.991455	-1815	-3220	Good
E_A-006	33.002	-0.002	0.725		20.77	0.75	7.90E-04	-3.40E-04	0.994367	-1808	-3225	Good

Sample ID	^{16}O (Mcps)	$\delta^{18}O$ ‰ measured	2SE (int.)	Mass Bias (‰)	$\delta^{18}O$ ‰ VSMOW	2SD (ext.)	$^{16}OH/^{16}O$	$^{16}OH/^{16}O$ corrected	Relative Yield	X	Y	Comment
UWQ1 G1	33.087	-7.860	0.653				1.12E-03			-408	345	Good
UWQ1 G1	33.243	-8.021	0.462				1.19E-03			-417	342	Good
UWQ1 G1	33.219	-8.950	0.825				1.13E-03			-411	333	Good
UWQ1 G1	33.114	-8.356	0.581				1.22E-03			-403	334	Good
average and 2SD	**33.166**	**-8.297**		**-20.38**		**0.964**	**0.0012**					
bracket average and 2SD	**32.623**	**-8.266**		**-20.34**		**0.750**	**0.0011**					
3µm beam, 22 pA intensity												
Mass calibration												
Analysis day: 4/7/2017												
Sample: E												
UWQ1 G1; EMHV readjusted from 3449	33.388	-8.874	0.659				1.05E-03			-409	372	
UWQ1 G1	32.815	-9.408	0.614				1.15E-03			-399	372	Good
UWQ1 G1	32.456	-9.742	0.727				1.10E-03			-391	373	Good
UWQ1 G1	32.194	-9.229	0.593				9.46E-04			-382	373	Good
UWQ1 G1	31.938	-9.611	0.453				1.11E-03			-379	365	Good
average and 2SD	**32.351**	**-9.498**		**-21.56**		**0.451**	**0.0011**					
E_A007	30.908	-0.353	0.551		21.66	0.50	3.41E-04	-7.16E-04	1.00651	-1805	-3224	Good
E_A008	31.330	0.063	0.635		22.08	0.50	3.68E-04	-6.90E-04	0.973877	-1798	-3226	Good
E_A009	31.903	-1.569	0.651		20.42	0.50	3.88E-04	-6.69E-04	0.991694	-1791	-3229	Good
E_A010	31.702	-0.898	0.553		21.10	0.50	3.76E-04	-6.81E-04	0.985451	-1786	-3233	Good
E_A011	31.250	-0.107	0.627		21.91	0.50	3.41E-04	-7.17E-04	0.971409	-1781	-3232	Good
E_A012	30.966	-1.367	0.553		20.62	0.50	3.30E-04	-7.27E-04	0.962556	-1777	-3236	Good
E_A013	31.260	-15.610	0.516		6.07	0.50	3.18E-04	-7.40E-04	1.017966	-1826	-3241	Detrital
E_A014	31.255	-0.143	0.605		21.87	0.50	4.60E-04	-5.98E-04	0.971559	-1818	-3237	Good
E_A015	31.471	-1.796	0.833		20.18	0.50	5.08E-04	-5.49E-04	0.978258	-1815	-3233	Good

Sample ID	^{16}O (Mcps)	$\delta^{18}O$ ‰ measured	2SE (int.)	Mass Bias (‰)	$\delta^{18}O$ ‰ VSMOW	2SD (ext.)	$^{16}OH/^{16}O$	$^{16}OH/^{16}O$ corrected	Relative Yield	X	Y	Comment
E_A016	31.562	-1.031	0.619		20.97	0.50	5.09E-04	-5.49E-04	0.981105	-1811	-3230	Good
E_A017	31.272	-0.937	0.554		21.06	0.50	7.05E-04	-3.52E-04	0.972067	-1809	-3227	Good
UWQ1 G1	31.507	-9.071	0.573				1.01E-03			-405	382	Good
UWQ1 G1	31.566	-9.628	0.607				1.05E-03			-398	385	Good
UWQ1 G1; Cs 172-174	33.332	-9.781	0.614				1.04E-03			-391	386	Good
UWQ1 G1	32.931	-9.371	0.676				1.05E-03			-385	383	Good
average and 2SD	**32.334**	**-9.463**		**-21.53**		**0.622**	**0.0010**					
bracket average and 2SD	**32.342**	**-9.480**		**-21.54**		**0.505**	**0.0011**					
E_D-001	33.313	-11.690	0.524		9.75	0.89	3.76E-04	-6.98E-04	0.987948	-2327	-3092	Detrital
E_D-002	32.509	-6.954	**1.870**		14.58	0.89	1.59E-03	5.14E-04	0.923939	-2328	-3088	Compromised
E_D-003	33.756	-0.832	0.439		20.84	0.89	5.70E-04	-5.04E-04	1.001096	-2328	-3084	Good
E_D-004	32.780	-1.915	0.589		19.73	0.89	7.14E-04	-3.60E-04	1.016341	-2328	-3080	Good
E_D-005	31.520	-0.489	0.686		21.19	0.89	5.83E-04	-4.91E-04	0.97727	-2328	-3076	Good
E_D-006	31.175	-0.915	0.665		20.75	0.89	5.62E-04	-5.12E-04	1.012597	-2328	-3072	Good
E_D-007	30.860	-0.449	0.636		21.23	0.89	5.64E-04	-5.10E-04	1.002371	-2328	-3068	Good
E_D-008	30.313	-0.646	0.472		21.03	0.89	5.79E-04	-4.95E-04	0.984607	-2328	-3064	Good
E_D-009	29.717	0.730	0.577		22.44	0.89	5.22E-04	-5.52E-04	0.965249	-2328	-3060	Good
E_D-010	30.218	-1.139	0.661		20.53	0.89	9.72E-04	-1.02E-04	0.981504	-2334	-3089	Good
E_E-012	29.616	0.448	0.753		22.15	0.89	9.54E-04	-1.20E-04	1.010061	-270	-3374	Good
E_E-013	29.384	-0.063	0.876		21.62	0.89	1.03E-03	-4.33E-05	1.002142	-268	-3366	Good
UWQ1 G1; ebeam OFF	~~1.662~~	~~-4.197~~	~~3.134~~	-	-	-	~~1.46E-03~~	-	-	~~-421~~	~~383~~	-
UWQ1 G1	29.593	-8.933	0.580				9.17E-04			-414	388	Good
UWQ1 G1	29.836	-9.258	0.610				1.16E-03			-407	390	Good
UWQ1 G1	29.502	-8.839	0.612				1.37E-03			-401	391	Good
UWQ1 G1; ebeam OFF	~~1.787~~	~~-1.895~~	~~2.776~~				~~4.04E-03~~	-		~~-426~~	~~372~~	-
UWQ1 G1; Cs res 174-176	30.777	-8.404	0.497				1.01E-03			-393	394	Good

Sample ID	^{16}O (Mcps)	$\delta^{18}O$ ‰ measured	2SE (int.)	Mass Bias (‰)	$\delta^{18}O$ ‰ VSMOW	2SD (ext.)	$^{16}OH/^{16}O$	$^{16}OH/^{16}O$ corrected	Relative Yield	X	Y	Comment
average and 2SD	**29.927**	**-8.859**		**-20.93**		**0.704**	**0.0011**					
bracket average and 2SD	**31.131**	**-9.161**		**-21.23**		**0.892**	**0.0011**					
Sample: F												
UWQ1 G1; Cs res 176-178	30.575	-9.716	0.693				3.48E-04			-608	508	Good
UWQ1 G1	31.050	-9.583	0.759				4.46E-04			-617	504	Good
UWQ1 G1	31.213	-9.700	0.725				5.41E-04			-606	502	Good
UWQ1 G1	30.898	-9.157	0.761				4.41E-04			-614	494	Good
average and 2SD	**30.934**	**-9.539**		**-21.60**		**0.523**	**0.0004**					
F_E-001	29.312	-9.192	0.706		12.23	1.02	6.59E-04	2.74E-04	0.949708	1555	-1043	Detrital
F_E-002	29.398	-7.718	0.592		13.74	1.02	5.53E-04	1.68E-04	0.952511	1556	-1038	Detrital
F_E-003	27.739	7.133	0.746		28.91	1.02	1.05E-03	**6.68E-04**	0.898751	1558	-1034	Compromised
F_E-004	27.894	7.458	0.596		29.24	1.02	1.06E-03	**6.76E-04**	0.903781	1559	-1030	Compromised
F_E-005	26.815	7.442	0.775		29.23	1.02	9.19E-04	5.34E-04	0.868812	1559	-1029	Compromised
F_E-006	23.655	7.741	0.707		29.53	1.02	1.34E-03	**9.60E-04**	0.766436	1562	-1023	Compromised
F_E-007	21.855	7.895	0.828		29.69	1.02	1.65E-03	**1.26E-03**	0.708117	1563	-1022	Compromised
F_C-001	29.186	-9.859	0.760		11.55	1.02	2.36E-04	-1.49E-04	0.990675	-2854	2582	Detrital
F_C-002	29.827	-6.339	1.096		15.15	1.02	3.54E-04	-3.14E-05	1.012422	-2857	2586	Detrital
F_C-003	30.407	4.534	0.603		26.26	1.02	4.87E-04	1.01E-04	1.032106	-2861	2588	Good
F_C-004	29.566	5.463	0.727		27.21	1.02	5.68E-04	1.83E-04	1.003572	-2865	2590	Good
F_C-005	29.552	6.145	0.826		27.90	1.02	5.20E-04	1.35E-04	1.003093	-2869	2592	Good
UWQ1 G1	29.386	-8.516	0.734				2.96E-04			-606	487	Good
UWQ1 G1	29.918	-8.779	0.689				3.39E-04			-609	481	Good
UWQ1 G1	29.261	-8.596	0.678				3.29E-04			-619	474	Good
UWQ1 G1; Cs res 178-180	30.393	-8.741	0.652				3.42E-04			-606	470	Good
average and 2SD	**29.740**	**-8.658**		**-20.73**		**0.246**	**0.0003**					
bracket average and 2SD	**30.337**	**-9.099**		**-21.17**		**1.015**	**0.0004**					

Sample ID	^{16}O (Mcps)	$\delta^{18}O$ ‰ measured	2SE (int.)	Mass Bias (‰)	$\delta^{18}O$ ‰ VSMOW	2SD (ext.)	$^{16}OH/^{16}O$	$^{16}OH/^{16}O$ corrected	Relative Yield	X	Y	Comment
F_C-006	29.952	5.507	0.628		27.06	0.69	4.18E-04	9.35E-05	0.978143	-2882	2592	Good
F_C-007	29.928	4.721	0.668		26.26	0.69	3.79E-04	5.47E-05	0.977378	-2886	2594	Good
F_C-008	30.198	4.025	0.451		25.55	0.69	3.71E-04	4.66E-05	0.98618	-2890	2596	Good
F_C-009	30.318	3.530	0.603		25.04	0.69	3.60E-04	3.55E-05	0.990119	-2894	2598	Good
F_C-010	29.760	3.422	0.688		24.93	0.69	3.64E-04	3.92E-05	0.971893	-2898	2600	Good
F_C-011	29.911	2.772	0.675		24.27	0.69	3.77E-04	5.19E-05	0.976833	-2900	2598	Good
F_D-001	29.658	-14.753	0.553		6.37	0.69	2.78E-04	-4.67E-05	0.968556	-3994	191	Detrital
F_D-002	29.402	-14.497	0.655		6.63	0.69	2.65E-04	-5.94E-05	0.960186	-3996	196	Detrital
F_D-003	29.603	6.289	0.561		27.86	0.69	3.77E-04	5.25E-05	0.966749	-3998	201	Good
F_D-004	28.778	4.299	0.735		25.83	0.69	3.63E-04	3.82E-05	0.939826	-4000	206	Good
F_D-005	29.397	4.487	0.581		26.02	0.69	3.63E-04	3.86E-05	0.960034	-4002	211	Good
F_D-006	28.850	3.781	0.674		25.30	0.69	3.78E-04	5.32E-05	0.942165	-4004	216	Good
F_D-007	28.890	3.392	0.572		24.90	0.69	3.80E-04	5.55E-05	0.943476	-4006	221	Good
F_D-008	28.476	2.737	0.763		24.23	0.69	3.46E-04	2.09E-05	0.974237	-4008	226	Good
F_D-009	28.342	2.711	0.576		24.20	0.69	3.01E-04	-2.38E-05	0.96964	-4010	231	Good
UWQ1 G1	28.123	-9.143	0.593				2.76E-04			-575	482	Good
UWQ1 G1	28.860	-8.778	0.578				3.01E-04			-573	474	Good
UWQ1 G1	29.551	-9.446	0.756				3.85E-04			-583	471	Good
UWQ1 G1; Cs 180-182	31.136	-9.317	0.658				3.31E-04			-579	463	Good
average and 2SD	**29.417**	**-9.171**		**-21.24**		**0.580**	**0.0003**					
bracket average and 2SD	**29.579**	**-8.915**		**-20.99**		**0.686**	**0.0003**					
Sample: C												
UWQ1 G1; ebeam OFF	1.484	-4.240	2.851				7.88E-03			-463	-349	Good
UWQ1 G1	32.485	-9.590	0.595				3.31E-04			-446	-343	Good
UWQ1 G1	32.678	-9.450	0.349				3.76E-04			-443	-335	Good
UWQ1 G1	32.198	-8.767	0.589				3.60E-04			-433	-336	Good

Sample ID	^{16}O (Mcps)	$\delta^{18}O$ ‰ measured	2SE (int.)	Mass Bias (‰)	$\delta^{18}O$ ‰ VSMOW	2SD (ext.)	$^{16}OH/^{16}O$	$^{16}OH/^{16}O$ corrected	Relative Yield	X	Y	Comment
average and 2SD	**32.454**	**-9.269**	**0.881**	**-21.34**			**0.0004**					
C_C-001	31.580	-6.468	0.491		15.15	0.78	3.26E-04	-4.02E-05	0.978749	1465	-3999	Detrital
C_C-002	31.807	4.148	0.585		26.00	0.78	4.26E-04	6.01E-05	0.985793	1472	-3994	Good
C_C-003	31.218	3.759	0.606		25.60	0.78	3.84E-04	1.87E-05	0.967516	1482	-3989	Good
C_C-004	31.499	3.584	0.659		25.42	0.78	3.57E-04	-8.92E-06	0.976245	1493	-3983	Good
C_C-005	30.979	2.773	0.471		24.59	0.78	2.96E-04	-6.96E-05	0.960127	1507	-3976	Good
UWQ1 G1	32.082	-9.183	0.619				4.01E-04			-427	-324	Good
UWQ1 G1	32.044	-9.621	0.542				3.51E-04			-420	-317	Good
UWQ1 G1	32.108	-8.766	0.596				3.76E-04			-412	-319	Good
average and 2SD	**32.078**	**-9.190**		**-21.26**		**0.855**	**0.0004**					
bracket average and 2SD	**32.266**	**-9.230**		**-21.30**		**0.781**	**0.0004**					

Average 2SD for $\delta^{18}O$‰ VSMOW 0.73

Details of data excluded from further interpretations

Sample ID	Explanation
E_A-002	Influenced by detrital input and fluid inclusion
E_D-002	Influenced by detrital input and fluid inclusion
E_E-003	Influenced by detrital input
E_E-011	Influenced by fluid inclusion
F_E-003	Low yield or influence of fluid inclusion
F_E-004	Low yield or influence of fluid inclusion
F_E-005	Low yield or influence of fluid inclusion
F_E-006	Low yield or influence of fluid inclusion
F_E-007	Low yield or influence of fluid inclusion

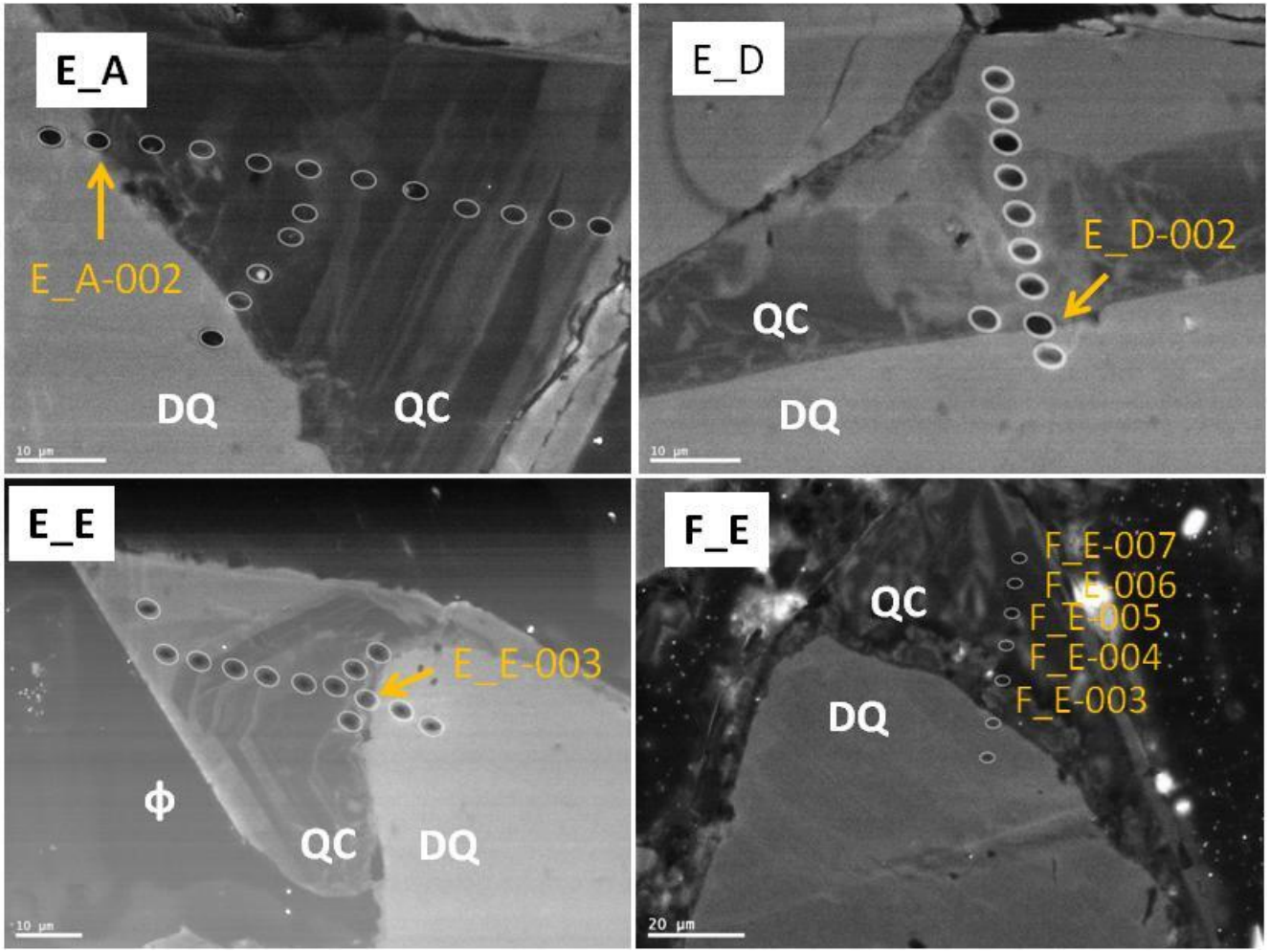

Post-SIMS analyses of CL images of analysed quartz grains from the Upper Jurassic Fulmar Formation sandstones from Elgin (E_A, E_D, and E_E) and Fulmar (F_E) fields. The yellow labels are compromised SIMS pits, and these data points were excluded from further interpretation (QC – quartz cement, DQ - detrital quartz).

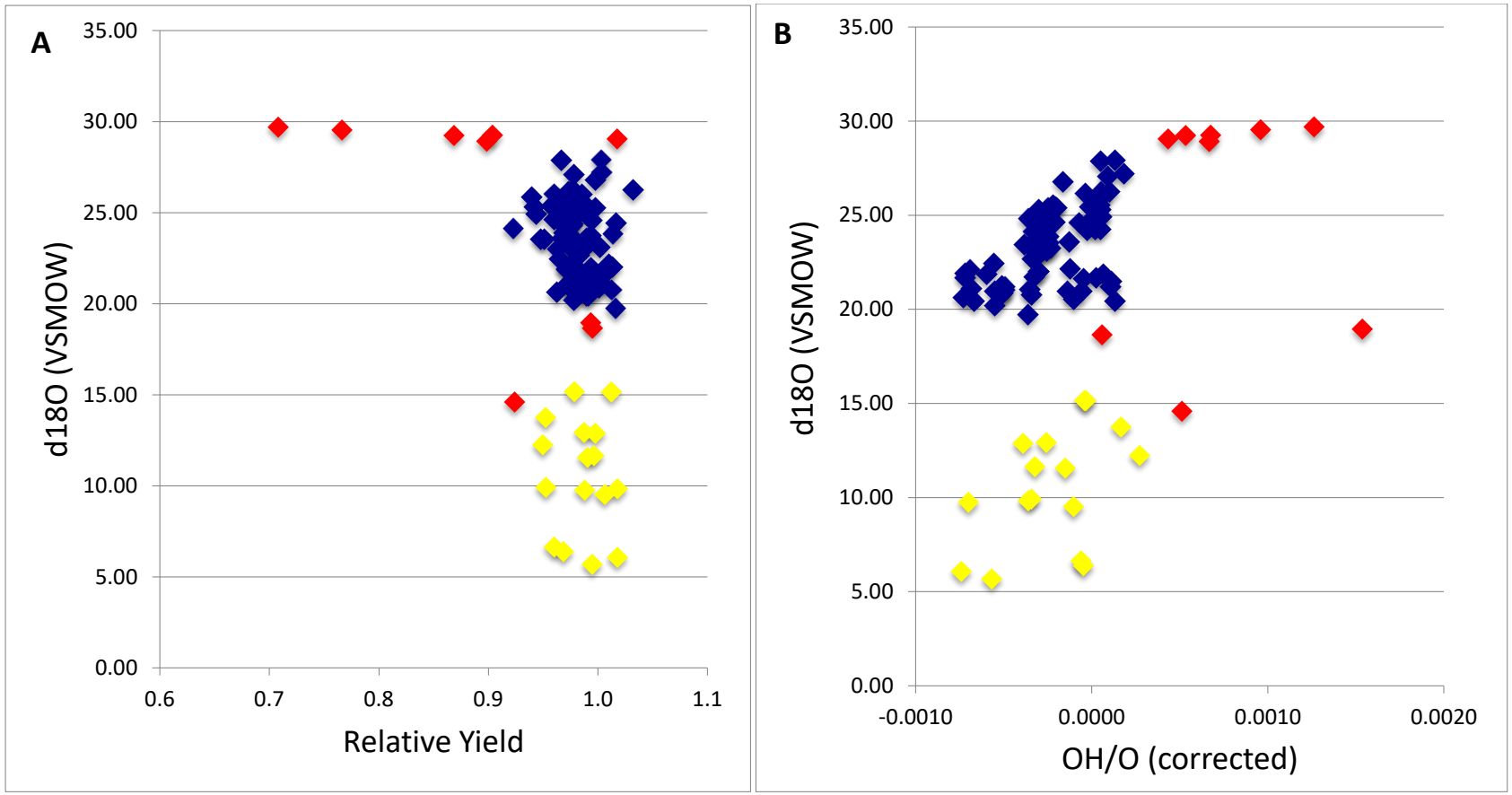

(A) Plot of $\delta^{18}O$ against relative yield. The detrital grains data points (yellow) stand out with lower $\delta^{18}O$ values. Outliers and compromised data are in red (B) Plot of $\delta^{18}O$ against (OH/O)-corrected. Detrital grains data points are highlighted yellow. Red data points represent those influenced by detrital input and combination of fluid inclusion and detrital input. The elevated OH/O indicates that these data points have been compromised.

REFERENCES

AAGAARD, P., JAHREN, J., HARSTAD, A., NILSEN, O. & RAMM, M. 2000. Formation of grain-coating chlorite in sandstones. Laboratory synthesized vs. natural occurrences. *Clay Minerals,* 35**,** 261-261.

AASE, N. E., BJORKUM, P. A. & NADEAU, P. H. 1996. The effect of grain-coating microquartz on preservation of reservoir porosity. *AAPG bulletin,* 80**,** 1654-1673.

AASE, N. E. & WALDERHAUG, O. 2005. The effect of hydrocarbons on quartz cementation: diagenesis in the Upper Jurassic sandstones of the Miller Field, North Sea, revisited. *Petroleum Geoscience,* 11**,** 215-223.

AJDUKIEWICZ, J., NICHOLSON, P. & ESCH, W. 2010. Prediction of deep reservoir quality using early diagenetic process models in the Jurassic Norphlet Formation, Gulf of Mexico. *AAPG bulletin,* 94**,** 1189-1227.

AJDUKIEWICZ, J. M. & LANDER, R. H. 2010. Sandstone reservoir quality prediction: The state of the art. *AAPG bulletin,* 94**,** 1083-1091.

ALLEN, P. A. & ALLEN, J. R. 2005. Basins due to lithospheric stretching. *Basin analysis: Principles and applications.* 2nd ed. Australia: Blackwell Publishing 63 - 115.

APLIN, A. C. & WARREN, E. A. 1994. Oxygen isotopic indications of the mechanisms of silica transport and quartz cementation in deeply buried sandstones. *Geology,* 22**,** 847-850.

BERGER, A., GIER, S. & KROIS, P. 2009. Porosity-preserving chlorite cements in shallow-marine volcaniclastic sandstones: Evidence from Cretaceous sandstones of the Sawan gas field, Pakistan. *AAPG bulletin,* 93**,** 595-615.

BERNER, R. A. 1970. Sedimentary pyrite formation. *American journal of science,* 268**,** 1-23.

BJORKUM, P. A. 1996. How important is pressure in causing dissolution of quartz in sandstones? *Journal of Sedimentary Research,* 66**,** 147-154.

BJØRKUM, P. A., OELKERS, E. H., NADEAU, P. H., WALDERHAUG, O. & MURPHY, W. M. 1998. Porosity prediction in quartzose sandstones as a function of time, temperature, depth, stylolite frequency, and hydrocarbon saturation. *AAPG bulletin,* 82**,** 637-648.

BJØRLYKKE, K. 2014. Relationships between depositional environments, burial history and rock properties. Some principal aspects of diagenetic process in sedimentary basins. *Sedimentary Geology,* 301**,** 1-14.

BJORLYKKE, K. & EGEBERG, P. 1993. Quartz cementation in sedimentary basins. *AAPG bulletin,* 77**,** 1538-1548.

BJØRLYKKE, K., ELVEKHØI, B. A. & MALM, A. 1979. Diagenesis in Mesozoic sandstones from Spitsbergen and the North Sea—a comparison. *Geologische Rundschau,* 68**,** 1152-1171.

BLOCH, S., LANDER, R. H. & BONNELL, L. 2002. Anomalously high porosity and permeability in deeply buried sandstone reservoirs: Origin and predictability. *AAPG bulletin,* 86**,** 301-328.

BUFFLER, R. T. & SAWYER, D. S. 1985. Distribution of crust and early history, Gulf of Mexico basin. *GCAGS Transactions,* 35**,** 333 - 344.

BURNS, F. E., BURLEY, S. D., GAWTHORPE, R. L. & POLLARD, J. E. 2005. Diagenetic signatures of stratal surfaces in the Upper Jurassic Fulmar Formation, central North Sea, UKCS. *Sedimentology,* 52**,** 1155-1185.

CLAYTON, R. N., O'NEIL, J. R. & MAYEDA, T. K. 1972. Oxygen isotope exchange between quartz and water. *Journal of Geophysical Research,* 77**,** 3057-3067.

DARBY, D., HASZELDINE, R. S. & COUPLES, G. D. 1996. Pressure cells and pressure seals in the UK Central Graben. *Marine and Petroleum Geology,* 13**,** 865-878.

DARBY, D., WILKINSON, M., FALLICK, A. & HASZELDINE, R. 1997. Illite dates record deep fluid movements in petroleum basins. *Petroleum Geoscience,* 3**,** 133-140.

DAY-STIRRAT, R. J., MILLIKEN, K. L., DUTTON, S. P., LOUCKS, R. G., HILLIER, S., APLIN, A. C. & SCHLEICHER, A. M. 2010. Open-system chemical behavior in deep Wilcox Group mudstones, Texas Gulf Coast, USA. *Marine and Petroleum Geology,* 27**,** 1804-1818.

DE BOER, R., NAGTEGAAL, P. & DUYVIS, E. 1977. Pressure solution experiments on quartz sand. *Geochimica et Cosmochimica acta,* 41**,** 257-264.

DEWERS, T. & ORTOLEVA, P. 1990. A coupled reaction/transport/mechanical model for intergranular pressure solution, stylolites, and differential compaction and cementation in clean sandstones. *Geochimica et Cosmochimica Acta,* 54**,** 1609-1625.

DEWERS, T. & ORTOLEVA, P. 1991. Influences of clay minerals on sandstone cementation and pressure solution. *Geology,* 19**,** 1045-1048.

DIXON, S., SUMMERS, D. & SURDAM, R. 1989. Diagenesis and preservation of porosity in Norphlet Formation (Upper Jurassic), southern Alabama. *AAPG Bulletin,* 73**,** 707-728.

DUTTON, S. P., AMBROSE, W. A. & LOUCKS, R. G. 2016. Diagenetic Controls on Reservoir Quality in Deep Upper Wilcox Sandstones of the Rio Grande Delta System, South Texas. *Gulf Coast Association of Geological Societies* 5**,** 95-110.

DUTTON, S. P. & LOUCKS, R. G. 2010. Diagenetic controls on evolution of porosity and permeability in lower Tertiary Wilcox sandstones from shallow to ultradeep (200–6700m) burial, Gulf of Mexico Basin, USA. *Marine and Petroleum Geology,* 27**,** 69-81.

EGEBERG, P. K. & AAGAARD, P. 1989. Origin and evolution of formation waters from oil fields on the Norwegian shelf. *Applied Geochemistry,* 4**,** 131-142.

EGGINK, J., RIEGSTRA, D. & SUZANNE, P. 1996. Using 3D seismic to understand the structural evolution of the UK Central North Sea. *Petroleum Geoscience,* 2**,** 83-96.

EHRENBERG, S. 1990. Relationship Between Diagenesis and Reservoir Quality in Sandstones of the Garn Formation, Haltenbanken, Mid-Norwegian Continental Shelf (1). *AAPG bulletin,* 74**,** 1538-1558.

EHRENBERG, S. 1993. Preservation of anomalously high porosity in deeply buried sandstones by grain-coating chlorite: examples from the Norwegian continental shelf. *AAPG Bulletin,* 77**,** 1260-1286.

EHRENBERG, S. N., NADEAU, P. H. & STEEN, O. 2008. A megascale view of reservoir quality in producing sandstones from the offshore Gulf of Mexico. *AAPG bulletin,* 92**,** 145-164.

ELIAS, B. P. & HAJASH, A. 1992. Changes in quartz solubility and porosity due to effective stress: An experimental investigation of pressure solution. *Geology,* 20**,** 451-454.

EMERY, D. & ROBINSON, A. 1993. Inorganic Geochemistry: Applications to Petroleum Geology. Blackwells. Oxford.

EMERY, D., SMALLEY, P., OXTOBY, N., RAGNARSDOTTIR, K., AAGAARD, P., HALLIDAY, A., COLEMAN, M. & PETROVICH, R. 1993. Synchronous oil migration and cementation in sandstone reservoirs demonstrated by quantitative description of diagenesis. *Philosophical Transactions of the Royal Society of London A: Mathematical, Physical and Engineering Sciences,* 344**,** 115-125.

ERRATT, D. Relationships between basement faulting, salt withdrawal and Late Jurassic rifting, UK Central North Sea. Geological Society, London, Petroleum Geology Conference series, 1993. Geological Society of London, 1211-1219.

EVANS, J., HOGG, A. J., HOPKINS, M. S. & HOWARTH, R. J. 1994. Quantification of quartz cements using combined SEM, CL, and image analysis. *Journal of Sedimentary Research,* 64**,** 334-338.

FISHER, Q., KNIPE, R. & WORDEN, R. 2009. Microstructures of deformed and non-deformed sandstones from the North Sea: implications for the origins of quartz cement in sandstones. *In:* WORDEN, R. & MORAD, S. (eds.) *Quartz cementation in sandstones.* John Wiley & Sons, 2009.

FISHER, R. S. & LAND, L. S. 1986. Diagenetic history of Eocene Wilcox sandstones, south-central Texas. *Geochimica et Cosmochimica Acta,* 50**,** 551-561.

FISHER, W. L. & MCGOWEN, J. 1967. Depositional Systems in the Wilcox Group of Texas and Their Relationship to Occurrence of Oil and Gas (1).

FRASER, S., ROBINSON, A., JOHNSON, H., UNDERHILL, J., KADOLSKY, D., CONNELL, R., JOHANNESSEN, P. & RAVNÅS, R. 2003. Upper Jurassic. *The Millennium Atlas: Petroleum Geology of the Central and Northern North Sea. Geological Society, London***,** 157-189.

FRENCH, M. W. & WORDEN, R. H. 2013. Orientation of microcrystalline quartz in the Fontainebleau Formation, Paris Basin and why it preserves porosity. *Sedimentary Geology,* 284**,** 149-158.

FRENCH, M. W., WORDEN, R. H., MARIANI, E., LARESE, R. E., MUELLER, R. R. & KLIEWER, C. E. 2012. Microcrystalline quartz generation and the preservation of porosity in sandstones: Evidence from the Upper Cretaceous of the Subhercynian Basin, Germany. *Journal of Sedimentary Research,* 82**,** 422-434.

GALLOWAY, W. E., GANEY-CURRY, P. E., LI, X. & BUFFLER, R. T. 2000. Cenozoic depositional history of the Gulf of Mexico basin. *AAPG bulletin,* 84**,** 1743-1774.

GENNARO, M. 2011. The chalk depositional system in the Central Graben–concepts of regional geology, sedimentology and stratigraphy. *3D seismic stratigraphy and reservoir characterization of the Chalk Group in the Norwegian Central Graben, North Sea*.

GIER, S., WORDEN, R. H., JOHNS, W. D. & KURZWEIL, H. 2008. Diagenesis and reservoir quality of Miocene sandstones in the Vienna Basin, Austria. *Marine and Petroleum Geology,* 25**,** 681-695.

GILES, M. 1987. Mass transfer and problems of secondary porosity creation in deeply buried hydrocarbon reservoirs. *Marine and Petroleum Geology,* 4**,** 188-204.

GILES, M., INDRELID, S., BEYNON, G. & AMTHOR, J. 2000. The Origin of Large-Scale Quartz Cementation: Evidence from Large Data Sets and Coupled Heat–Fluid Mass Transport Modelling. *In:* WORDEN, R. & MORAD, S. (eds.) *Quartz Cementation in Sandstones: Special Publication 29 of the IAS.* Oxford: Wiley-Blackwell, 21 -38.

GILES, M., STEVENSON, S., MARTIN, S., CANNON, S., HAMILTON, P., MARSHALL, J. & SAMWAYS, G. 1992. The reservoir properties and diagenesis of the Brent Group: a regional perspective. *Geological Society, London, Special Publications,* 61**,** 289-327.

GILES, M. R. & MARSHALL, J. D. 1986. Constraints on the development of secondary porosity in the subsurface: re-evaluation of processes. *Marine and Petroleum Geology,* 3**,** 243-255.

GILHAM, R., HERCUS, C., EVANS, A. & DE HAAS, W. Shearwater (UK Block 22/30b): managing changing uncertainties through field life. Geological Society, London, Petroleum Geology Conference series, 2005. Geological Society of London, 663-673.

GLENNIE, K. W. 2009. *Petroleum geology of the North Sea: basic concepts and recent advances*, John Wiley & Sons.

GLUYAS, J. & CADE, C. A. 1997. Prediction of porosity in compacted sands. *AAPG Memoir,* 69**,** 19 - 27.

GLUYAS, J., ROBINSON, A., EMERY, D., GRANT, S. & OXTOBY, N. The link between petroleum emplacement and sandstone cementation. Geological Society, London, Petroleum Geology Conference series, 1993. Geological Society of London, 1395-1402.

GLUYAS, J. G. & HICHENS, H. M. United Kingdom oil and gas fields: commemorative millennium volume. 2003. Geological Society of London, 41-44, 485-647.

GOWERS, M. B. & SÆBØE, A. 1985. On the structural evolution of the Central Trough in the Norwegian and Danish sectors of the North Sea. *Marine and Petroleum Geology,* 2**,** 298-318.

GOWLAND, S. 1996. Facies characteristics and depositional models of highly bioturbated shallow marine siliciclastic strata: an example from the Fulmar Formation (Late Jurassic), UK Central Graben. *Geological Society, London, Special Publications,* 114**,** 185-214.

GRAHAM, C., ARMOUR, A., BATHURST, P., EVANS, D. & PETROLEUMSFORENING, N. The millennium atlas: Petroleum geology of the central and northern North Sea. 2003. Geological Society of London, 27, 49, 157-173.

GRANT, N. T., MIDDLETON, A. J. & ARCHER, S. 2014. Porosity trends in the Skagerrak Formation, Central Graben, United Kingdom Continental Shelf: The role of compaction and pore pressure historyPorosity Trends in Skagerrak Formation. *AAPG bulletin,* 98**,** 1111-1143.

GRATIER, J.-P., MUQUET, L., HASSANI, R. & RENARD, F. 2005. Experimental microstylolites in quartz and modeled application to natural stylolitic structures. *Journal of Structural Geology,* 27**,** 89-100.

GRIGSBY, J. D., VIDAL, J. M., LUFFEL, D. L., HAWKINS, J. & MENDENHALL, J. M. 1992. Effects of fibrous illite on permeability measurements from preserved cores obtained in lower Wilcox Group gas sandstones, Lake Creek Field, Montgomery County, Texas. *Gulf Coast Association of Geological Societies Transactions,* 42**,** 161-172.

HARRIS, N. B. 2006. Low-porosity haloes at stylolites in the feldspathic Upper Jurassic Ula sandstone, Norwegian North Sea: an integrated petrographic and chemical mass-balance approach. *Journal of Sedimentary Research,* 76**,** 444-459.

HARWOOD, J. 2011. *The origin and timing of quartz cementation in reservoir sandstones: evidence from in-situ microanalysis of oxygen isotopes.* Doctor of Philosophy, Newcastle University.

HARWOOD, J., APLIN, A. C., FIALIPS, C. I., ILIFFE, J. E., KOZDON, R., USHIKUBO, T. & VALLEY, J. W. 2013. Quartz Cementation History of Sandstones Revealed By High-Resolution Sims Oxygen Isotope Analysis. *Journal of Sedimentary Research,* 83**,** 522-530.

HASZELDINE, R., WILKINSON, M., DARBY, D., MACAULAY, C., COUPLES, G., FALLICK, A., FLEMING, C., STEWART, R. & MCAULAY, G. Diagenetic porosity creation in an overpressured graben. Geological Society, London, Petroleum Geology Conference series, 1999. Geological Society of London, 1339-1350.

HASZELDINE, R. S., CAVANAGH, A. J. & ENGLAND, G. L. 2003. Effects of oil charge on illite dates and stopping quartz cement: calibration of basin models. *Journal of Geochemical Exploration,* 78**,** 373-376.

HEALD, M. & LARESE, R. 1974. Influence of coatings on quartz cementation. *Journal of Sedimentary Research,* 44**,** 1269-1274.

HENDRY, J. P., WILKINSON, M., FALLICK, A. E. & HASZELDINE, R. S. 2000. Ankerite cementation in deeply buried Jurassic sandstone reservoirs of the central North Sea. *Journal of Sedimentary Research,* 70**,** 227-239.

HOUSEKNECHT, D. W. 1984. Influence of grain size and temperature on intergranular pressure solution, quartz cementation, and porosity in a quartzose sandstone. *Journal of Sedimentary Research,* 54**,** 348-361.

HOUSEKNECHT, D. W. 1987. Assessing the relative importance of compaction processes and cementation to reduction of porosity in sandstones. *AAPG bulletin,* 71**,** 633-642.

HOUSEKNECHT, D. W. 1988. Intergranular pressure solution in four quartzose sandstones. *Journal of Sedimentary Research,* 58**,** 228-246.

HOUSEKNECHT, D. W. 1989. Assessing the relative importance of compaction processes and cementation to reduction of porosity in sandstones: reply. *AAPG Bulletin,* 73**,** 1277-1279.

HOUSEKNECHT, D. W. 1991. Use of cathodoluminescence petrography for understanding compaction, quartz cementation, and porosity in sandstones. *SEPM Special Publication,* SC25**,** 59-66.

HUTCHEON, I. & ABERCROMBIE, H. 1990. Carbon dioxide in clastic rocks and silicate hydrolysis. *Geology,* 18**,** 541-544.

ISAKSEN, G. H. 2004. Central North Sea hydrocarbon systems: Generation, migration, entrapment, and thermal degradation of oil and gas. *AAPG bulletin,* 88**,** 1545-1572.

JEANS, C. 1994. Clay diagenesis, overpressure and reservoir quality: an introduction. *Clay Minerals,* 29**,** 415-424.

JOHNSTON, D. D. & JOHNSON, R. J. 1987. Depositional and diagenetic controls on reservoir quality in First Wilcox Sandstone, Livingston Field, Louisiana. *AAPG Bulletin,* 71**,** 1152-1161.

KELLY, J. L., FU, B., KITA, N. T. & VALLEY, J. W. 2007. Optically continuous silcrete quartz cements of the St. Peter Sandstone: high precision oxygen isotope analysis by ion microprobe. *Geochimica et Cosmochimica Acta,* 71**,** 3812-3832.

KITA, N. T., USHIKUBO, T., FU, B. & VALLEY, J. W. 2009. High precision SIMS oxygen isotope analysis and the effect of sample topography. *Chemical Geology,* 264**,** 43-57.

KOZDON, R., USHIKUBO, T., KITA, N., SPICUZZA, M. & VALLEY, J. 2009. Intratest oxygen isotope variability in the planktonic foraminifer N. pachyderma: Real vs. apparent vital effects by ion microprobe. *Chemical Geology,* 258**,** 327-337.

KUHN, O., SMITH, S., VAN NOORT, K. & LOISEAU, B. 2003. The Fulmar Field, Blocks 30/16, 30/11b, UK North Sea. *Geological Society, London, Memoirs,* 20**,** 563-585.

LABEYRIE, L. 1974. New approach to surface seawater palaeotemperatures using 18O/16O ratios in silica of diatom frustules. *Nature,* 248**,** 40-42.

LAND, L. S. & FISHER, R. S. 1987. Wilcox sandstone diagenesis, Texas Gulf Coast: a regional isotopic comparison with the Frio Formation. *Geological Society, London, Special Publications,* 36**,** 219-235.

LANDER, R. H. & WALDERHAUG, O. 1999. Predicting porosity through simulating sandstone compaction and quartz cementation. *AAPG bulletin,* 83**,** 433-449.

LASAGA, A. C. 1984. Chemical kinetics of water-rock interactions. *Journal of geophysical research: solid earth,* 89**,** 4009-4025.

LASOCKI, J., GUEMENE, J., HEDAYATI, A., LEGORJUS, C. & PAGE, W. The Elgin and Franklin fields: UK Blocks 22/30c, 22/30b and 29/5b. Geological Society, London, Petroleum Geology Conference series, 1999. Geological Society of London, 1007-1020.

LEE, M. R. & PARSONS, I. 2003. Microtextures of authigenic Or-rich feldspar in the Upper Jurassic Humber Group, UK North Sea. *Sedimentology,* 50**,** 597-608.

LOUCKS, R. G., DODGE, M. M. & GALLOWAY, W. E. 1984. Regional controls on diagenesis and reservoir quality in lower Tertiary sandstones along the Texas Gulf Coast: Part 1. Concepts and principles. *In:* MCDONALD, D. A. & SURDAM, R. C. (eds.) *M 37: Clastic Diagenesis.* American Association of Petroleum Geologists.

LUNDEGARD, P. D. 1992. Sandstone porosity loss; a" big picture" view of the importance of compaction. *Journal of Sedimentary Research,* 62**,** 250-260.

MAAST, T. E., JAHREN, J. & BJORLYKKE, K. 2011. Diagenetic controls on reservoir quality in Middle to Upper Jurassic sandstones in the South Viking Graben, North Sea. *AAPG bulletin,* 95**,** 1937-1958.

MACKENZIE, F. T. & GEES, R. 1971. Quartz: synthesis at earth-surface conditions. *Science,* 173**,** 533-535.

MARCHAND, A., HASZELDINE, R., MACAULAY, C., SWENNEN, R. & FALLICK, A. 2000. Quartz cementation inhibited by crestal oil charge: Miller deep water sandstone, UK North Sea. *Clay Minerals,* 35**,** 201-201.

MARCHAND, A. M., HASZELDINE, R. S., SMALLEY, P. C., MACAULAY, C. I. & FALLICK, A. E. 2001. Evidence for reduced quartz-cementation rates in oil-filled sandstones. *Geology,* 29**,** 915-918.

MARCHAND, A. M., SMALLEY, P. C., HASZELDINE, R. S. & FALLICK, A. E. 2002. Note on the importance of hydrocarbon fill for reservoir quality prediction in sandstones. *AAPG bulletin,* 86**,** 1561-1572.

MATSUHISA, Y., GOLDSMITH, J. R. & CLAYTON, R. N. 1979. Oxygen isotopic fractionation in the system quartz-albite-anorthite-water. *Geochimica et Cosmochimica Acta,* 43**,** 1131-1140.

MCBRIDE, E., DIGGS, T. & WILSON, J. 1991. Compaction of Wilcox and Carrizo sandstones (Paleocene-Eocene) to 4420 M, Texas Gulf Coast. *Journal of Sedimentary Research,* 61**,** 93 - 85.

MCBRIDE, E. F. 1989. Quartz cement in sandstones: a review. *Earth-Science Reviews,* 26**,** 69-112.

MCKIE, T., JOLLEY, S. & KRISTENSEN, M. 2010. Stratigraphic and structural compartmentalization of dryland fluvial reservoirs: Triassic Heron Cluster, Central North Sea. *Geological Society, London, Special Publications,* 347**,** 165-198.

MEHENNI, M. & ROODENBURG, W. 1990. Fulmar field--UK south central graben, North Sea. *AAPG Special Volumes***,** p. 113 - 139.

MOLENAAR, N., CYZIENE, J., SLIAUPA, S. & CRAVEN, J. 2008. Lack of inhibiting effect of oil emplacement on quartz cementation: Evidence from Cambrian reservoir sandstones, Paleozoic Baltic Basin. *Geological society of America bulletin,* 120**,** 1280-1295.

MORAD, S., AL-RAMADAN, K., KETZER, J. M. & DE ROS, L. 2010. The impact of diagenesis on the heterogeneity of sandstone reservoirs: A review of the role of depositional facies and sequence stratigraphy. *AAPG bulletin,* 94**,** 1267-1309.

MORAD, S., KETZER, J. & DE ROS, L. F. 2000. Spatial and temporal distribution of diagenetic alterations in siliciclastic rocks: implications for mass transfer in sedimentary basins. *Sedimentology,* 47**,** 95-120.

MORAD, S., WORDEN, R. & KETZER, J. 2002. Oxygen and Hydrogen Isotopic Composition of Diagenetic Clay Minerals in Sandstones: A Review of the Data and Controls. *Clay Mineral Cements in Sandstones***,** 63-91.

NENNA, F. & AYDIN, A. 2011. The formation and growth of pressure solution seams in clastic rocks: A field and analytical study. *Journal of Structural Geology,* 33**,** 633-643.

NGUYEN, B. T., JONES, S. J., GOULTY, N. R., MIDDLETON, A. J., GRANT, N., FERGUSON, A. & BOWEN, L. 2013. The role of fluid pressure and diagenetic cements for porosity preservation in Triassic fluvial reservoirs of the Central Graben, North Sea. *AAPG bulletin,* 97**,** 1273-1302.

NICHOLS, G. 2009. *Sedimentology and stratigraphy,* John Wiley & Sons.

NIEMEIJER, A., SPIERS, C. & BOS, B. 2002. Compaction creep of quartz sand at 400–600 C: Experimental evidence for dissolution-controlled pressure solution. *Earth and Planetary Science Letters,* 195**,** 261-275.

NUNN, J. A. & SASSEN, R. 1986. The framework of hydrocarbon generation and migration, Gulf of Mexico continental slope. *Gulf Coast Association of Geological Societies Transactions,* 36**,** 257-262.

OELKERS, E. H., BJØRKUM, P. & MURPHY, W. M. 1996. A petrographic and computational investigation of quartz cementation and porosity reduction in North Sea sandstones. *American Journal of Science,* 296**,** 420-452.

OSBORNE, M. J. & SWARBRICK, R. E. 1997a. How Overpressure and Diagenesis Interact in Sedimentary Basins–Consequences for Porosity Preservation in HPHT Reservoir Sandstones. *Indonesian Petroleum Association***,** 947 - 954.

OSBORNE, M. J. & SWARBRICK, R. E. 1997b. Mechanisms for generating overpressure in sedimentary basins: a reevaluation. *AAPG bulletin,* 81**,** 1023-1041.

OSBORNE, M. J. & SWARBRICK, R. E. 1999. Diagenesis in North Sea HPHT clastic reservoirs—Consequences for porosity and overpressure prediction. *Marine and Petroleum Geology,* 16**,** 337-353.

OYE, O. J., APLIN, A. C., JONES, S. J., GLUYAS, J. G., BOWEN, L., ORLAND, I. J. & VALLEY, J. W. 2018. Vertical effective stress as a control on quartz cementation in sandstones. *Marine and Petroleum Geology,* 98**,** 640-652.

PAGE, F., USHIKUBO, T., KITA, N. T., RICIPUTI, L. & VALLEY, J. W. 2007. High-precision oxygen isotope analysis of picogram samples reveals 2 μm gradients and slow diffusion in zircon. *American Mineralogist,* 92**,** 1772-1775.

PAXTON, S., SZABO, J., AJDUKIEWICZ, J. & KLIMENTIDIS, R. 2002. Construction of an intergranular volume compaction curve for evaluating and predicting compaction and porosity loss in rigid-grain sandstone reservoirs. *AAPG bulletin,* 86**,** 2047-2067.

PITMAN, J. K. & ROWAN, E. R. 2012. Temperature and petroleum generation history of the Wilcox Formation, Louisiana. *Open-File Report.* Reston, VA: US Geological Survey.

PITTMAN, E. D. 1972. Diagenesis of quartz in sandstones as revealed by scanning electron microscopy. *Journal of Sedimentary Research,* 42**,** 507-519.

POLLINGTON, A. D., KOZDON, R. & VALLEY, J. W. 2011. Evolution of quartz cementation during burial of the Cambrian Mount Simon Sandstone, Illinois Basin: In situ microanalysis of δ18O. *Geology,* 39**,** 1119-1122.

PRIMMER, T. J., CADE, C. A., EVANS, J., GLUYAS, J. G., HOPKINS, M. S., OXTOBY, N. H., SMALLEY, P. C., WARREN, E. A. & WORDEN, R. H. 1997. Global patterns in sandstone diagenesis: their application to reservoir quality prediction for petroleum exploration. *AAPG Memoir 69***,** 61 - 77.

RAMM, M., FORSBERG, A. W. & JAHREN, J. S. 1997. Porosity--Depth Trends in Deeply Buried Upper Jurassic Reservoirs in the Norwegian Central Graben: An Example of Porosity Preservation Beneath the Normal Economic Basement by Grain-Coating Microquartz.

REED, R. M. & MILLIKEN, K. L. 2003. How to overcome imaging problems associated with carbonate minerals on SEM-based cathodoluminescence systems. *Journal of Sedimentary Research,* 73**,** 328-332.

RENARD, F., ORTOLEVA, P. & GRATIER, J. P. 1997. Pressure solution in sandstones: influence of clays and dependence on temperature and stress. *Tectonophysics,* 280**,** 257-266.

RENARD, F., PARK, A., ORTOLEVA, P. & GRATIER, J.-P. 1999. An integrated model for transitional pressure solution in sandstones. *Tectonophysics,* 312**,** 97-115.

ROBERTS, A. M., PRICE, J. D. & OLSEN, T. S. 1990. Late Jurassic half-graben control on the siting and structure of hydrocarbon accumulations: UK/Norwegian Central Graben. *Geological Society, London, Special Publications,* 55**,** 229-257.

ROBIN, P.-Y. F. 1978. Pressure solution at grain-to-grain contacts. *Geochimica et Cosmochimica Acta,* 42**,** 1383-1389.

RUDKIEWICZ, J., PENTEADO, H. D. B., VEAR, A., VANDENBROUCKE, M., BRIGAUD, F., WENDEBOURG, J. & DUPPENBECKER, S. 2000. Integrated Basin Modeling Helps to Decipher Petroleum Systems. *Petroleum systems of South Atlantic margins,* Memoir 73**,** 27-40.

RUTTER, E. & ELLIOTT, D. 1976. The kinetics of rock deformation by pressure solution. *Philosophical Transactions of the Royal Society of London A: Mathematical, Physical and Engineering Sciences,* 283**,** 203-219.

SAIGAL, G. C., BJORLYKKE, K. & LARTER, S. 1992. The Effects of Oil Emplacement on Diagenetic Processes: Examples from the Fulmar Reservoir Sandstones, Central North Sea: Geologic Note (1). *AAPG Bulletin,* 76**,** 1024-1033.

SATHAR, S. & JONES, S. 2016. Fluid overpressure as a control on sandstone reservoir quality in a mechanical compaction dominated setting: Magnolia Field, Gulf of Mexico. *Terra Nova,* 28**,** 155-162.

SATHAR, S., WORDEN, R. H., FAULKNER, D. R. & SMALLEY, P. C. 2012. The effect of oil saturation on the mechanism of compaction in granular materials: higher oil saturations lead to more grain fracturing and less pressure solution. *Journal of Sedimentary Research,* 82**,** 571-584.

SHELDON, H. A. & WHEELER, J. 2003. Influence of pore fluid chemistry on the state of stress in sedimentary basins. *Geology,* 31**,** 59-62.

SHELDON, H. A., WHEELER, J., WORDEN, R. H. & CHEADLE, M. J. 2003. An analysis of the roles of stress, temperature, and pH in chemical compaction of sandstones. *Journal of Sedimentary Research,* 73**,** 64-71.

SHIMIZU, I. 1995. Kinetics of pressure solution creep in quartz: theoretical considerations. *Tectonophysics,* 245**,** 121-134.

SIBLEY, D. F. & BLATT, H. 1976a. Intergranular pressure solution and cementation of the Tuscarora orthoquartzite. *Journal of Sedimentary Research,* 46**,** 881-896.

SIBLEY, D. F. & BLATT, H. 1976b. Intergranular pressure solution and cementation of the Tuscarora orthoquartzite. *Journal of Sedimentary Research,* 46.

SMITH, D. L., DEES, W. T. & HARRELSON, D. W. 1981. Geothermal conditions and their implications for basement tectonics in the Gulf Coast margin. *Gulf Coast Association of Geological Societies Transactions,* 31**,** 181-190.

SMITH, J. & EHRENBERG, S. 1989. Correlation of carbon dioxide abundance with temperature in clastic hydrocarbon reservoirs: relationship to inorganic chemical equilibrium. *Marine and Petroleum Geology,* 6**,** 129-135.

SPAAK, P., ALMOND, J., SALAHUDIN, S., SALLEH, Z. M. & TOSUN, O. Fulmar: a mature field revisited. Geological Society, London, Petroleum Geology Conference series, 1999. Geological Society of London, 1089-1100.

STEVENS, D. & WALLIS, R. 1991. The Clyde Field, Block 30/17b, UK North Sea. *Geological Society, London, Memoirs,* 14**,** 279-285.

STEWART, D. 1986. Diagenesis of the shallow marine Fulmar Formation in the central North Sea. *Clay Minerals,* 21**,** 537-564.

STOCKBRIDGE, C. & GRAY, D. 1991. The Fulmar Field, Blocks 30/16 & 30/llb, UK North Sea. *Geological Society, London, Memoirs,* 14**,** 309-316.

STORVOLL, V., BJØRLYKKE, K., KARLSEN, D. & SAIGAL, G. 2002. Porosity preservation in reservoir sandstones due to grain-coating illite: a study of the Jurassic Garn Formation from the Kristin and Lavrans fields, offshore Mid-Norway. *Marine and Petroleum Geology,* 19**,** 767-781.

STRICKER, S. & JONES, S. 2016. Enhanced porosity preservation by pore fluid overpressure and chlorite grain coatings in the Triassic Skagerrak, Central Graben, North Sea, UK. *Geological Society special publications.,* 435**,** 321-341.

STRICKER, S., JONES, S. J. & GRANT, N. T. 2016a. Importance of vertical effective stress for reservoir quality in the Skagerrak Formation, Central Graben, North Sea. *Marine and Petroleum Geology,* 78**,** 895-909.

STRICKER, S., JONES, S. J., SATHAR, S., BOWEN, L. & OXTOBY, N. 2016b. Exceptional reservoir quality in HPHT reservoir settings: Examples from the Skagerrak Formation of the Heron Cluster, North Sea, UK. *Marine and Petroleum Geology,* 77**,** 198-215.

SWARBRICK, R., OSBORNE, M., GRUNBERGER, D., YARDLEY, G., MACLEOD, G., APLIN, A., LARTER, S., KNIGHT, I. & AULD, H. 2000. Integrated study of the Judy Field (Block 30/7a)—an overpressured Central North Sea oil/gas field. *Marine and Petroleum Geology,* 17**,** 993-1010.

SWARBRICK, R., SELDON, B. & MALLON, A. 2005. Modelling the Central North Sea pressure history. *Geological Society, London, Petroleum Geology Conference series,* 6**,** 1237-1245.

SWARBRICK, R. E., LAHANN, R. W., O'CONNOR, S. A. & MALLON, A. J. 2010. Role of the Chalk in development of deep overpressure in the Central North Sea. *Geological Society, London, Petroleum Geology Conference series,* 7**,** 493-507.

TADA, R., MALIVA, R. & SIEVER, R. 1987. A new mechanism for pressure solution in porous quartzose sandstone. *Geochimica et Cosmochimica Acta,* 51**,** 2295-2301.

TADA, R. & SIEVER, R. 1989. Pressure Solution During Diagenesis. *Annual Review of Earth and Planetary Sciences,* 17**,** 89-118.

TAYLOR, A. & GAWTHORPE, R. Application of sequence stratigraphy and trace fossil analysis to reservoir description: examples from the Jurassic of the North Sea. Geological Society, London, Petroleum Geology Conference series, 1993. Geological Society of London, 317-335.

TAYLOR, T. R., GILES, M. R., HATHON, L. A., DIGGS, T. N., BRAUNSDORF, N. R., BIRBIGLIA, G. V., KITTRIDGE, M. G., MACAULAY, C. I. & ESPEJO, I. S. 2010. Sandstone diagenesis and reservoir quality prediction: Models, myths, and reality. *AAPG bulletin,* 94**,** 1093-1132.

TAYLOR, T. R., KITTRIDGE, M. G., WINEFIELD, P., BRYNDZIA, L. T. & BONNELL, L. M. 2015. Reservoir quality and rock properties modeling–Triassic and Jurassic sandstones, greater Shearwater area, UK Central North Sea. *Marine and Petroleum Geology,* 65**,** 1-21.

TAYLOR, T. R., STANCLIFFE, R., MACAULAY, C. & HATHON, L. 2004. High temperature quartz cementation and the timing of hydrocarbon accumulation in the Jurassic Norphlet Sandstone, offshore Gulf of Mexico, USA. *Geological Society, London, Special Publications,* 237**,** 257-278.

TERZAGHI, K. 1925. Principles of soil mechanics, IV—Settlement and consolidation of clay. *Engineering News-Record,* 95**,** 874-878.

THOMSON, A. 1959. Pressure solution and porosity. *Society of Economic Paleontologists and Mineralogists,* SP7**,** 92-110.

TIPSWORD, H., SETZER, F. & SMITH JR, F. L. 1966. Interpretation of depositional environment in Gulf Coast petroleum exploration from paleoecology and related stratigraphy. 50**,** 2321 - 2321.

TOBIN, R. C., MCCLAIN, T., LIEBER, R. B., OZKAN, A., BANFIELD, L. A., MARCHAND, A. M. & MCRAE, L. E. 2010. Reservoir quality modeling of tight-gas sands in Wamsutter field: Integration of diagenesis, petroleum systems, and production data. *AAPG bulletin,* 94**,** 1229-1266.

TURNER, P. Clyde: reappraisal of a producing field. Geological Society, London, Petroleum Geology Conference series, 1993. Geological Society of London, 1503-1512.

VAGLE, G. B., HURST, A. & DYPVIK, H. 1994. Origin of quartz cements in some sandstones from the Jurassic of the Inner Moray Firth (UK). *Sedimentology,* 41**,** 363-377.

VALLEY, J. W. & KITA, N. T. 2009. In situ oxygen isotope geochemistry by ion microprobe. *MAC short course: secondary ion mass spectrometry in the earth sciences,* 41**,** 19-63.

VAN NOORT, R., SPIERS, C. J. & PENNOCK, G. M. 2008. Compaction of granular quartz under hydrothermal conditions: Controlling mechanisms and grain boundary processes. *Journal of Geophysical Research: Solid Earth,* 113**,** 1-23.

WALDERHAUG, O. 1994a. Temperatures of quartz cementation in Jurassic sandstones from the Norwegian continental shelf--evidence from fluid inclusions. *Journal of Sedimentary Research,* 64**,** 311-323.

WALDERHAUG, O. 1994b. Precipitation rates for quartz cement in sandstones determined by fluid-inclusion microthermometry and temperature-history modeling. *Journal of Sedimentary Research,* 64**,** 324-333.

WALDERHAUG, O. 1996. Kinetic modeling of quartz cementation and porosity loss in deeply buried sandstone reservoirs. *AAPG bulletin,* 80**,** 731-745.

WALDERHAUG, O. 2000. Modeling quartz cementation and porosity in Middle Jurassic Brent Group sandstones of the Kvitebjørn field, northern North Sea. *AAPG bulletin,* 84**,** 1325-1339.

WALDERHAUG, O. & BJØRKUM, P. A. 2003. The effect of stylolite spacing on quartz cementation in the Lower Jurassic Stø Formation, southern Barents Sea. *Journal of Sedimentary Research,* 73**,** 146-156.

WALDERHAUG, O., LANDER, R., BJØRKUM, P., OELKERS, E., BJØRLYKKE, K. & NADEAU, P. 2009. Modelling quartz cementation and porosity in reservoir sandstones: examples from the Norwegian continental shelf. *Quartz cementation in sandstones***,** 39-49.

WALDSCHMIDT, W. A. 1941. Cementing materials in sandstones and their probable influence on migration and accumulation of oil and gas. *AAPG Bulletin,* 25**,** 1839-1879.

WARREN, E., SMALLEY, P. & HOWARTH, R. 1994. Compositional variations of North Sea formation waters. *North Sea formation waters atlas***,** 119-140.

WEYL, P. K. 1959. Pressure solution and the force of crystallization: a phenomenological theory. *Journal of geophysical research,* 64**,** 2001-2025.

WHITE, N. & LATIN, D. 1993. Subsidence analyses from the North Sea 'triple-junction'. *Journal of the Geological Society,* 150**,** 473-488.

WILKINSON, M., DARBY, D., HASZELDINE, R. S. & COUPLES, G. D. 1997. Secondary porosity generation during deep burial associated with overpressure leak-off: Fulmar Formation, United Kingdom Central Graben. *AAPG bulletin,* 81**,** 803-813.

WILKINSON, M. & HASZELDINE, R. S. 1996. Aluminium loss during sandstone diagenesis. *Journal of the Geological Society,* 153**,** 657-660.

WILKINSON, M. & HASZELDINE, R. S. 2011. Oil charge preserves exceptional porosity in deeply buried, overpressured, sandstones: Central North Sea, UK. *Journal of the Geological Society,* 168**,** 1285-1295.

WILKINSON, M., HASZELDINE, R. S. & FALLICK, A. E. 2006. Hydrocarbon filling and leakage history of a deep geopressured sandstone, Fulmar Formation, United Kingdom North Sea. *AAPG bulletin,* 90**,** 1945-1961.

WORDEN, R. H. Quartz Cementation in Sandstones: Reappraising the Controls. AAPG Hedberg Conference, 2004. 8-11.

WORDEN, R. H., ARMITAGE, P., BUTCHER, A., CHURCHILL, J., CSOMA, A., HOLLIS, C., LANDER, R. & OMMA, J. 2018a. Petroleum reservoir quality prediction: overview and contrasting approaches from sandstone and carbonate communities. *Geological Society, London, Special Publications,* 435**,** SP435. 21.

WORDEN, R. H., BUKAR, M. & SHELL, P. 2018b. The effect of oil emplacement on quartz cementation in a deeply buried sandstone reservoir. *AAPG Bulletin,* 102**,** 49-75.

WORDEN, R. H. & BURLEY, S. 2003. Sandstone diagenesis: the evolution of sand to stone. *Sandstone Diagenesis: Recent and Ancient,* 4**,** 3-44.

WORDEN, R. H., FRENCH, M. W. & MARIANI, E. 2012. Amorphous silica nanofilms result in growth of misoriented microcrystalline quartz cement maintaining porosity in deeply buried sandstones. *Geology,* 40**,** 179-182.

WORDEN, R. H. & MORAD, S. 2000. Quartz cementation in oil field sandstones: a review of the key controversies. *Quartz cementation in sandstones, Special publications of international association of sedimentologists,* 29**,** 1-20.

WORDEN, R. H., OXTOBY, N. H. & SMALLEY, P. C. 1998. Can oil emplacement prevent quartz cementation in sandstones? *Petroleum Geoscience,* 4**,** 129-137.